Coevolution (Or Not) of Supermassive Black Holes and Host Galaxies

John Kormendy[1] and Luis C. Ho[2]

[1]Department of Astronomy, University of Texas at Austin,
2515 Speedway C1400, Austin, TX 78712-1205; email: kormendy@astro.as.utexas.edu

[2]The Observatories of the Carnegie Institution for Science,
813 Santa Barbara Street, Pasadena, CA 91101; email: lho@obs.carnegiescience.edu

Abstract

Supermassive black holes (BHs) have been found in 87 galaxies by dynamical modeling of spatially resolved kinematics. The *Hubble Space Telescope* revolutionized BH research by advancing the subject from its proof-of-concept phase into quantitative studies of BH demographics. Most influential was the discovery of a tight correlation between BH mass $M_\bullet$ and the velocity dispersion σ of the bulge component of the host galaxy. Together with similar correlations with bulge luminosity and mass, this led to the widespread belief that BHs and bulges coevolve by regulating each other's growth. Conclusions based on one set of correlations from $M_\bullet \sim 10^{9.5}\ M_\odot$ in brightest cluster ellipticals to $M_\bullet \sim 10^6\ M_\odot$ in the smallest galaxies dominated BH work for more than a decade.

New results are now replacing this simple story with a richer and more plausible picture in which BHs correlate differently with different galaxy components. A reasonable aim is to use this progress to refine our understanding of BH – galaxy coevolution. BHs with masses of $10^5 - 10^6\ M_\odot$ are found in many bulgeless galaxies. Therefore, classical (elliptical-galaxy-like) bulges are not necessary for BH formation. On the other hand, while they live in galaxy disks, BHs do not correlate with galaxy disks. Also, any $M_\bullet$ correlations with the properties of disk-grown pseudobulges and dark matter halos are weak enough to imply no close coevolution.

The above and other correlations of host galaxy parameters with each other and with $M_\bullet$ suggest that there are four regimes of BH feedback. (1) Local, secular, episodic, and stochastic feeding of small BHs in largely bulgeless galaxies involves too little energy to result in coevolution. (2) Global feeding in major, wet galaxy mergers rapidly grows giant BHs in short-duration, quasar-like events whose energy feedback does affect galaxy evolution. The resulting hosts are classical bulges and coreless-rotating-disky ellipticals. (3) After these AGN phases and at the highest galaxy masses, maintenance-mode BH feedback into X-ray-emitting gas has the primarily negative effect of helping to keep baryons locked up in hot gas and thereby keeping galaxy formation from going to completion. This happens in giant, core-nonrotating-boxy ellipticals. Their properties, including their tight correlations between $M_\bullet$ and core parameters, support the conclusion that core ellipticals form by dissipationless major mergers. They inherit coevolution effects from smaller progenitor galaxies. Also, (4) independent of any feedback physics, in BH growth modes (2) and (3), the averaging that results from successive mergers plays a major role in decreasing the scatter in $M_\bullet$ correlations from the large values observed in bulgeless and pseudobulge galaxies to the small values observed in giant elliptical galaxies.

1. INTRODUCTION

Coevolution (or not) of supermassive black holes (BHs) and host galaxies is the central theme of this review. The heyday of this activity was the first half of the history of the universe, 7 – 12 Gyr ago. Conditions were different then than they are now. Lemaître (1931) captured this challenge elegantly and accurately: "The evolution of the universe can be likened to a display of fireworks that has just ended: some few red wisps, ashes, and smoke. Standing on a well-chilled cinder, we see the fading of the suns and try to recall the vanished brilliance of the origin of the worlds."

This paper reviews the archaeology of supermassive cinders. For more than a decade, the most important tool for this research was the *Hubble Space Telescope* (HST). Now, as HST nears the end of its life and begins to be replaced by other tools that have different capabilities, BH work is branching out in new directions. It is an appropriate time to review what we have learned.

If an iconic event can be said to have started work on BHs, it was the discovery (Schmidt 1963) that the 13$^{\rm th}$ magnitude, starlike object identified with the powerful radio source 3C 273 had the shockingly high redshift (for such a bright object) of $z = 0.158$. Assuming that the redshift was due to the Hubble expansion of the Universe, 3C 273 was the second-most-distant object then known. 3C 273 is $\sim$10 times more luminous than the brightest galaxies. The first quasar discovery was quickly followed by many others. Rapid variability implied tiny sizes. After a Darwinian struggle between competing theories, the idea that quasars and other, less luminous active galactic nuclei (AGNs) are powered by accretion onto supermassive BHs (Hoyle & Fowler 1963; Salpeter 1964; Zel'dovich 1964; Lynden-Bell 1969, 1978; Lynden-Bell & Rees 1971) quickly gained acceptance. Decades of productive work based on this idea followed. However, there was no dynamical evidence that BHs with the required masses, $M_\bullet \sim 10^6 - 10^9\,{\rm M}_\odot$, actually exist. At the same time, it was clear that quasars were much more numerous at $z \gtrsim 2$ than they are now. After they stop accreting, dark BH remnants should live essentially forever. So dead quasar engines should hide in many nearby galaxies. Finding them became one of the "holy grails" of astronomy.

However, the above masses are only $\sim$0.1 % of the stellar masses of the host galaxies. So BHs are expected to dominate the local gravity and to lead to observable dynamical consequences only inside a sphere-of-influence radius $r_{\rm infl} \equiv GM_\bullet/\sigma^2 \sim 1$ to 100 pc. At distances $D = 1$ to 20 Mpc for nearby galaxies, this corresponds to $\sim 0\farcs1$ to $1''$. Thus it was inevitable that dynamical evidence for BHs would be hard to find. In fact, the first stellar-dynamical BH detections followed as soon as they became feasible, i. e., in the mid- to late-1980s, when CCDs became available on spectrographs. A "proof-of-concept" phase followed, when the emphasis was on finding out whether ground-based observations could provide convincing evidence for BHs. Given our expectations about $r_{\rm infl}$, work at optical wavelengths required the excellent seeing of observatories like Palomar and Mauna Kea. This period is reviewed in Kormendy & Richstone (1995, hereafter KR95). The foundations of the BH search are laid out there. Here, we bring the story up-to-date through 2013 February.

G: gravitational constant
σ: velocity dispersion of the galaxy

1.1 Road Map

This paper has two parts. Sections 2 and 3 review the history of dynamical BH detections. We concentrate on improvements in spatial resolution, modeling machinery, and numbers of detections. Our confidence that we are finding supermassive black holes is discussed here. On the other hand, readers who are mainly interested in BH–host-galaxy correlations and the physics of coevolution can skip directly to Sections 4 (the distinction between classical and pseudo bulges), 5 (BH database), 6 and 7 (BH demographics), and 8 (BH–host-galaxy coevolution). Section 9 sums up.

Our picture of BH demographics divides itself naturally into two phases, one dominated by many HST BH detections and a post-HST phase when qualitatively new results emerge largely from ground-based, AO-assisted and maser BH detections that target a broader range of galaxy types. We begin (Section 1.2) by introducing these phases.

1.2 HST and the Two Phases of BH Demographic Studies

HST helped to complete the proof-of-concept phase by confirming ground-based BH detections with higher spatial resolution. Also, by delivering five-times-better resolution than ground-based, optical spectroscopy, HST made it possible to find BHs in many more galaxies. Thus, it could search statistically fair galaxy samples. This led to the convincing conclusion that BHs are present in essentially every galaxy that has a bulge component. By opening the floodgates of discovery, HST advanced the study of supermassive BHs into a new era in which we could study BH demographics.

Some results have been in place almost from the beginning of this subject. Most important is the agreement between the global volume density of BH mass that is predicted by AGN energetics and what we observe (Sołtan 1982; Yu & Tremaine 2002; Marconi et al. 2004). But most work in this subject has concentrated on correlations between $M_\bullet$ and properties of host galaxies.

We differentiate between two phases of this work:

Sections 6.1 and 6.2: From the early 1990s until recently, we believed that BH masses satisfy one correlation each with the luminosity, mass, and velocity dispersion of the host galaxy. Even during this period, we knew that these correlations apply to bulges and ellipticals but not to disks. Still, work to explain the correlations ignored component structure. The emphasis was on using the the potential well depth of the galaxy as measured by σ – and nothing else – to engineer coevolution.

Sections 6.3 – 6.14 and 7: In contrast, we are now starting to realize that BHs correlate in different ways with different components of galaxies. This is "low-hanging fruit": it reveals new connections between galaxy and BH growth. This phase of BH work is still in its early stages.

1.3 The Scope of this Review

Sections 2 – 3 discuss the robustness of BH detections and $M_\bullet$ estimates via optical absorption- and emission-line spectroscopy and radio-wavelength maser spectroscopy. AGN $M_\bullet$ estimates via reverberation mapping and single-epoch spectroscopy are discussed in Supplemental Information.

Section 4 briefly reviews the difference between classical and pseudo bulges of disk galaxies.

Section 5 is the $M_\bullet$ and host galaxy database for BHs detected via spatially resolved dynamics.

Sections 6 – 7 discuss correlations (or not) of $M_\bullet$ with host galaxy bulges, pseudobulges, disks, nuclear star clusters, core properties, globular cluster systems, and dark matter halos. Section 6.15 lists but does not discuss possible correlations that we do not confirm. Section 8 reviews coevolution.

BHs are now too big a subject for a single ARA&A review. We must omit many topics, including ones that are of great current interest. In particular, the theory of BH – host-galaxy coevolution is too large a topic for this paper. It has been the subject of whole conferences and deserves a review of its own. We concentrate on observed BH correlations and their implications. This includes a preliminary look at the evolution of these correlations with cosmological lookback time and what we learn from that evolution (Section 8.6).

Many reviews preceed ours. Rees (1984) and Begelman, Blandford & Rees (1984) review early theory work; KR95, Richstone et al. (1998), Ho (1999a), and Kormendy & Gebhardt (2001) review observations; Melia & Falcke (2001), Melia (2007), and Genzel, Eisenhauer & Gillessen (2010) discuss the Galactic center; Ferrarese & Ford (2005), Peterson (2008), and Marziani & Sulentic (2012) review the connection with AGN research; Ho (2008) reviews BHs in low-luminosity AGNs; Miller & Colbert (2004) is about intermediate-mass BHs; Volonteri (2010) and Greene (2012) are on BH seeds and early growth; Merritt & Milosavljević (2005) discuss the evolution of BH binaries; Centrella et al. (2010) is on general relativistic effects in BH binaries; Ho (2004a) and Cattaneo et al. (2009) summarize conferences on BH-galaxy coevolution; McNamara & Nulsen (2007; 2012), Alexander & Hickox (2012), Schawinski (2012), and Fabian (2012) review AGN feedback, and Fabian (2013) reviews BH spins. A short summary of the present paper is Kormendy (2013).

1.4 Terminology

To avoid confusion, we explain some terminology used in this review:

Supermassive black holes (BHs) are associated with the centers of galaxies that contain bulges or pseudobulges. "Supermassive" as opposed to what? Answer: supermassive as opposed to ordinary-mass BHs of $\sim 10\,M_\bullet$ that are end products of stellar evolution. A "gray area" involves the several-hundred-solar-mass BHs that may be the end products of the evolution of zero-metallicity stars (Bond et al. 1984; Fryer, Woosley & Heger 2001; Heger et al. 2003). They are plausible seeds of supermassive BHs (Larson 2000; Madau & Rees 2001; Volonteri, Haardt & Madau 2003; Volonteri & Rees 2005; Volonteri & Natarajan 2009; Volonteri 2010). We call BHs that are remnants of stellar evolution without additional growth **stellar-mass BHs**. If some BHs get ejected from galaxies as a consequence of the evolution of BH triples, we do not invent a new name for them.

Intermediate-mass black holes (IMBHs) here refers only to BHs that may live in the centers of globular clusters and in the nuclear star clusters (**nuclei**) of bulgeless, late-type, and spheroidal galaxies. The mass functions of BHs and IMBHs overlap (Section 7).

Classical bulges are defined purely by observational criteria: they are indistinguishable from elliptical galaxies, except that they are embedded in disks (Renzini 1999). Classification criteria are summarized in the Supplementary Information. E. g., classical bulges satisfy the fundamental plane correlations for ellipticals (Kormendy et al. 2009, hereafter KFCB; Fisher & Drory 2010; Kormendy & Bender 2011). Underlying the practical definition is the assumption that we use in interpretations, which is that classical bulges form as ellipticals do, in major galaxy mergers.

Pseudobulges: Kormendy & Kennicutt (2004) and Kormendy (2012) review observations which show that some central galaxy components that we used to identify as classical bulges have properties that are more disk-like than those of classical bulges and are, we infer, made not by galaxy mergers but by slow ("secular") evolution internal to isolated galaxy disks. Pseudobulges may be augmented by minor mergers; this is not an issue here. The difference between classical and pseudo bulges is important, because we find that they do not correlate in the same way with BHs. The above papers, Kormendy & Bender (2013b), and the Supplementary Information here summarize classification criteria. We emphasize that they are purely observational; they do not depend on interpretation. For reliable classification, it is important to use as many classification criteria as possible. All classifications in **Table 3** are based on at least two and in some cases as many as five independent criteria. Section 4 discusses this subject in more detail.

(Pseudo)bulge refers either to a classical bulge or to a pseudobulge, without prejudice.

Spheroidal galaxies (Sphs) are morphologically like ellipticals and are called "dwarf ellipticals" by many authors (e. g., Binggeli, Sandage, & Tarenghi 1984; Binggeli, Sandage, & Tammann 1985, 1988; Binggeli, Tammann, & Sandage 1987; Sandage & Binggeli 1984; Sandage, Binggeli, & Tammann 1985). But they are robustly different from ellipticals when examined quantitatively in terms of effective radii r_e that contain half of the total light and effective brightnesses μ_e at r_e. Whereas ellipticals satisfy fundamental plane parameter correlations such that less luminous ellipticals have higher effective brightnesses, Sphs define a parameter sequence that is roughly perpendicular to that of ellipticals such that less luminous Sphs have lower effective brightnesses (Wirth & Gallagher 1984; Kormendy 1985, 1987, 2009; Binggeli & Cameron 1991; Bender, Burstein & Faber 1992; KFCB; Kormendy & Bender 2012). The sequences overlap over a factor of at least 10 in luminosity. It is important to note that Sandage & Binggeli (1984) and Sandage, Binggeli, & Tammann (1985) distinguish between elliptical and dwarf elliptical galaxies over this whole luminosity range. This is testament to their different properties. Kormendy (1985, 1987, 2009), Kormendy et al. (2009), and Kormendy & Bender (2012) show that the $\mu_e - r_e$ – luminosity sequence of Sphs is closely similar to that of Sd – Im galaxies. They conclude that Sphs are defunct late-type

galaxies that have been transformed by a variety of internal and environmental gas removal processes. Physically, spheroidal galaxies are equivalent to bulgeless S0 galaxies (Kormendy & Bender 2012). Local Group dwarf spheroidals include Draco, Sculptor, and Fornax; brighter examples are NGC 147, NGC 185, and NGC 205. The Virgo cluster contains spheroidals up to $M_V \simeq -18$. At still higher luminosities, Sph-like galaxies contain bulges and so are called S0s.

The importance of distinguishing E and Sph galaxies is this: So-far scanty data imply that Sphs and pure-disk galaxies play similar roles in hosting BHs (Section 7.2). The luminosity function of Sph galaxies rises steeply at low luminosities; in the Virgo cluster, $\phi \propto L^{-1.35}$ (Binggeli, Sandage, & Tammann 1988). In contrast, the luminosity function of ellipticals has a maximum at $M_V \sim -18 \pm 2$ and then drops steeply at higher and lower L (Binggeli, Sandage, & Tammann 1988, Fig. 1). Classical bulges are similar. So the luminosity and mass functions of the components that correlate closely enough with $M_\bullet$ to imply coevolution are bounded at low masses. Understanding coevolution is easier if we do not have to face the prospect that it still happens in dwarf galaxies.

AGNs are active galactic nuclei that emit largely nonthermal radiation from BH accretion disks.

Nuclei have a specific meaning, different from any generic use to refer to the centers of galaxies. Nuclei are compact central clusters of stars that are distinct from – i. e., smaller and denser than – the galaxy components in which they are embedded (see Kormendy & McClure 1993; Lauer et al. 1998 for the Local Group example in M 33, Böker et al. 2002, 2004; Côté et al. 2006 for properties of more distant examples, and Böker 2010 for a brief review). They are similar to globular clusters; their structural parameters r_e and μ_e extend the correlations shown by globular clusters to higher luminosities L (see the above papers; Carollo 1999; Hopkins et al. 2009a). Therefore nuclei are not small bulges. Some "globular clusters" in our Galaxy and others may be defunct nuclei of galaxies whose main bodies have been stripped away by tidal forces (Section 7.4). Nuclei are found at virtually all Hubble types but are especially common in late-type and spheroidal galaxies. The relationship between nuclei and BHs is discussed in Section 6.11.

Black holes correlate with [some component in galaxies] means more than just that this component frequently contains a BH. By using this phrase, we mean that $M_\bullet$ is observed to correlate with parameters of the host component, usually mass, luminosity, and velocity dispersion.

Tight correlations are ones in which the observed scatter is closely similar to the parameter measurement errors. These correlations are particularly important because they are the ones that are suggestive of coevolution. We will see (Section 6) that $M_\bullet$ correlates tightly with the velocity dispersions, K-band luminosities, and stellar masses of classical bulges and ellipticals but little or not at all with any property of pseudobulges and disks.

Coevolution of BHs and galaxies happens differently in different galaxies. At its weakest, it must happen to all supermassive black holes that live in galaxies. They must evolve together. But they do not have to influence each other. A weak form of coevolution is (1) that galaxies affect how BHs grow because they control BH feeding and merging via global, galaxy-wide processes. A stronger form is (2) that BHs may control galaxy properties via energy and momentum feedback into the galaxy evolution process. When people interpret tight BH–host-galaxy correlations as implying coevolution, they usually mean the strong version when both of the above happen. This is what we mean when we use "coevolution" without qualification. We argue in Section 8 that this strong coevolution is less prevalent than the galaxy formation literature suggests. When only (1) applies but largely not (2), we still use the term "coevolution", but we make the distinction clear. In contrast, when BH feeding involves local (not galaxy-wide) processes and when the resulting AGNs have little noticeable effect on their hosts, then we say that no coevolution takes place, even though the BHs are, of course, still growing inside galaxies. Thus Section 8 discusses four regimes of AGN feedback that range from no coevolution to strong coevolution in the above senses.

2. PROGRESS IN BH DETECTION TECHNOLOGY. I. IMPROVEMENTS IN SPATIAL RESOLUTION

Figure 1 shows the history of $M_\bullet$ measurements for all galaxies that have BH detections based on observations of spatially resolved dynamics. Multiple measurements for each galaxy are joined by straight line segments to show how the available spatial resolution has improved with time. For BHs found with HST, only the discovery observations are shown; these have not been superseded. The individual measurements for our Galaxy, M 31, and M 32 are listed in **Table 1**. Spatial resolution is parametrized by the ratio of the radius $r_{\rm infl}$ of the sphere of influence of the BH to the effective Gaussian dispersion radius σ_* of the point-spread function (see notes to **Table 1**).

2.1 Early Ground-Based BH Discoveries

KR95 reviews the seven ground-based BH detections (and one based on HST) available in 1995.

The first dynamical BH discovery was in M 32 (Tonry 1984, 1987). It was made with barely enough resolution to be reasonably secure (Kormendy 2004; §§ 2.2.1 here). It is typical of a subject with urgent expectations and much at stake that the first discovery is made as soon as it becomes barely feasible and at a time when the result still has only modest significance. These early papers are successful if the discovery gets more secure as it gets tested with better technology. This has happened for M 31, M 32, NGC 3115, NGC 3377, and NGC 4594. M 32 has the most accurate $M_\bullet$ measurement based on absorption-line spectra of unresolved stellar populations.

Other pre-HST BH detections based on optical, absorption-line spectroscopy were those in M 31 (Dressler & Richstone 1988; Kormendy 1988a), NGC 4594 (Sombrero galaxy, Kormendy 1988b), NGC 3115 (Kormendy & Richstone 1992), and NGC 3377 (Kormendy 1992a, b; KR95; Kormendy et al. 1998). A ground-based BH detection in NGC 4486B was reported in the HST era (Kormendy et al. 1997). All these have been confirmed with HST except NGC 4486B (HST data are available but not yet modeled). These results are reviewed in Section 2.2.

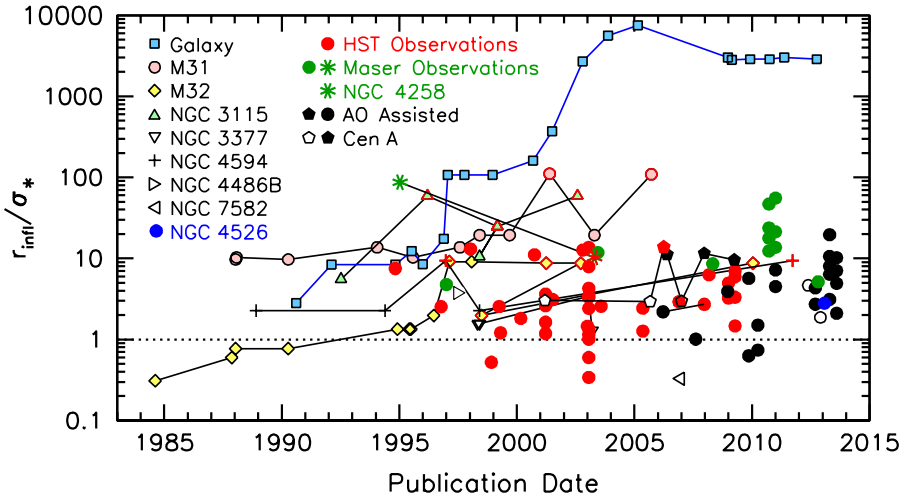

Figure 1

Spectroscopic spatial resolutions for BH discoveries (**Tables 1 – 3**) and histories of improvements in resolution. AO-assisted resolutions are approximate. The maser discoveries at 2010.9 ± 0.2 and the AO discoveries at 2013.4 ± 0.2 have been spread out enough so that they can be distinguished. Note that most pre-HST, ground-based BH discoveries were made at similar or higher $r_{\rm infl}/\sigma_*$ than most HST BH discoveries. But HST has 5 – 10 times better spatial resolution (absent adaptive optics), so it is used to discover smaller BHs in more distant galaxies. Updated from Kormendy (2004).

Table 1 Mass measurements of supermassive black holes in our Galaxy, M 31, and M 32

Galaxy	D (Mpc)	σ_e (km s^{-1})	$M_\bullet$ ($M_{\rm low}, M_{\rm high}$) ($M_\odot$)	$r_{\rm infl}$ (arcsec)	σ_* (arcsec)	$r_{\rm infl}/\sigma_*$	Reference
(1)	(2)	(3)	(4)	(5)	(6)	(7)	(8)
Galaxy			4.41(3.98 – 4.84) e6		0.0146	2868.	Meyer et al. 2012
Galaxy			4.2 (3.9 – 4.6) e6		0.0139	3013.	Yelda et al. 2011
Galaxy	0.00828	105	4.30(3.94 – 4.66) e6	41.9	0.0146	2868.	Genzel, Eisenhauer & Gillessen 2010
Galaxy	0.00828	105	4.30(3.94 – 4.66) e6	41.9	0.0146	2868.	Gillessen et al. 2009a
Galaxy			4.09(3.74 – 4.43) e6		0.0148	2829.	Gillessen et al. 2009b
Galaxy			4.25(3.44 – 4.79) e6		0.0139	3013.	Ghez et al. 2008
Galaxy			3.80(3.60 – 4.00) e6		0.0056	7478.	Ghez et al. 2005
Galaxy			3.7 (3.3 – 4.1) e6		0.0075	5583.	Ghez et al. 2003
Galaxy			3.8 (2.3 – 5.4) e6		0.0155	2702.	Schödel et al. 2002
Galaxy			2.1 (1.3 – 2.8) e6		0.113	371.	Chakrabarty & Saha 2001
Galaxy			3.1 (2.6 – 3.6) e6		0.26	161.	Genzel et al. 2000
Galaxy			2.7 (2.5 – 2.9) e6		0.39	107.	Ghez et al. 1998
Galaxy			2.70(2.31 – 3.09) e6		0.39	107.	Genzel et al. 1997
Galaxy			2.55(2.12 – 2.95) e6		0.39	107.	Eckart & Genzel 1997
Galaxy			2.8 (2.5 – 3.1) e6		2.4	17.4	Genzel et al. 1996
Galaxy			2.0 (0.9 – 2.9) e6		4.9	8.5	Haller et al. 1996
Galaxy			2.9 (2.0 – 3.9) e6		3.4	12.3	Krabbe et al. 1995
Galaxy			2. e6		5	8.4	Evans & de Zeeuw 1994
Galaxy			3. e6		5	8.4	Kent 1992
Galaxy			5.4 (3.9 – 6.8) e6		15	2.8	Sellgren et al. 1990
M 31	0.774	169	1.4 (1.1 – 2.3) e8	5.75	0.053	109.	Bender et al. 2005
M 31			1.0 e8		0.297	19.4	Peiris & Tremaine 2003
M 31			6.1 (3.6 – 8.7) e7		0.052	111.	Bacon et al. 2001
M 31			3.3 (1.5 – 4.5) e7		0.297	19.4	Kormendy & Bender 1999
M 31			6.0 (5.8 – 6.2) e7		0.297	19.4	Magorrian et al. 1998
M 31			9.5 (7 – 10) e7		0.42	13.7	Emsellem & Combes 1997
M 31			7.5 e7		0.56	10.3	Tremaine 1995
M 31			8.0 e7		0.42	13.7	Bacon et al. 1994
M 31			5 (4.5 – 5.6) e7		0.59	9.7	Richstone, Bower & Dressler 1990
M 31			3.8 (1.1 – 11) e7		0.56	10.3	Kormendy 1988a
M 31			5.6 (3.4 – 7.8) e7		0.59	9.7	Dressler & Richstone 1988
M 32	0.805	77	2.45(1.4 – 3.5) e6	0.46	0.052	8.76	van den Bosch & de Zeeuw 2010
M 32			2.9 (2.7 – 3.1) e6		0.052	8.76	Verolme et al. 2002
M 32			3.5 (2.3 – 4.6) e6		0.052	8.76	Joseph et al. 2001
M 32			2.4 (2.2 – 2.6) e6		0.23	1.98	Magorrian et al. 1998
M 32			3.9 (3.1 – 4.7) e6		0.050	9.11	van der Marel et al. 1998a
M 32			3.9 (3.3 – 4.5) e6		0.050	9.11	van der Marel et al. 1997a, 1997b
M 32			3.2 (2.6 – 3.7) e6		0.23	1.98	Bender, Kormendy & Dehnen 1996
M 32			2.1 (1.8 – 2.3) e6		0.34	1.34	Dehnen 1995
M 32			2.1 e6		0.34	1.34	Qian et al. 1995
M 32			2.1 (1.7 – 2.4) e6		0.34	1.34	van der Marel et al. 1994a
M 32			2.2 (0.8 – 3.5) e6		0.59	0.77	Richstone, Bower & Dressler 1990
M 32			9.3 e6		0.59	0.77	Dressler & Richstone 1988
M 32			7.5 (3.5–11.5) e6		0.76	0.60	Tonry 1987
M 32			5.8 e6		1.49	0.31	Tonry 1984

Lines based on HST spectroscopy are in red. Column 2 is the assumed distance. Column 3 is the stellar velocity dispersion inside the "effective radius" that encompasses half of the light of the bulge. Column 4 is the measured BH mass with the one-sigma range that includes 68 % of the probability in parentheses. Only the top four $M_\bullet$ values for the Galaxy include distance uncertainties in the error bars. Column 5 is the radius of the sphere of influence of the BH; the line that lists $r_{\rm infl}$ contains the adopted $M_\bullet$. Column 6 is the effective resolution of the spectroscopy, estimated as in Kormendy (2004). It is a radius that measures the blurring effects of the telescope point-spread function or "PSF," the slit width or aperture size, and the pixel size. The contribution of the telescope is estimated by the dispersion $\sigma_{*\rm tel}$ of a Gaussian fitted to the core of the average radial brightness profile of the PSF. In particular, the HST PSF has $\sigma_{*\rm tel} \simeq 0\farcs036$ from a single-Gaussian fit to the PSF model in van der Marel, de Zeeuw & Rix (1997a). Then the resolutions in the directions parallel and perpendicular to the slit are $\sigma_{*\|}$, the sum in quadrature of $\sigma_{*\rm tel}$ and 1/2 of the pixel size, and $\sigma_{*\perp}$, the sum in quadrature of $\sigma_{*\rm tel}$ and 1/2 of the slit width. Finally, the effective σ_* is the geometric mean of $\sigma_{*\|}$ and $\sigma_{*\perp}$. The top 7 lines for the Galaxy use a proxy σ_* equal to the smallest pericenter radius for the stellar orbits that were included in the derivation; usually this is for star S2, but for lines 6 and 7, it is star S16. Note: σ_* measures a PSF radius; for readers who prefer a PSF diameter, FWHM $\equiv 2.35\,\sigma_*$. Column 7 is the effective measure of the degree to which the observations reach inside the sphere of influence and reliably see the BH. Column 8 lists the reference. Updated from Kormendy (2004).

Some early authors worried that $r_{\rm infl}$ is too small for ground-based BH detection (e. g., Rix 1993; Emsellem, Bacon, & Monnet 1995). This was never the problem: the initial, ground-based $r_{\rm infl}/\sigma_*$ was equal to or better than the median for HST discoveries (*red points* in **Figure 1**) for our Galaxy, M 31, NGC 4594, NGC 3115, and NGC 4486B. That is, the easiest cases were found from the ground with $r_{\rm infl}/\sigma_* \sim 5$ to 10 before HST had a chance to discover them at higher $r_{\rm infl}/\sigma_*$.

Instead, there were two dangers:

First was the danger that $M_\bullet$ would be overestimated if $r_{\rm infl}$ was not well enough resolved. This happened slightly in Magorrian et al. (1998, see Kormendy 2004), which mostly used ground-based data that were not obtained with high spatial resolution for the BH search. Magorrian et al. (1998) derived a BH-to-bulge mass ratio of $0.0052^{+0.0014}_{-0.0011}$, higher than previous and subsequent values based on the same galaxies and physical assumptions. Ironically, the present, improved BH masses that give greater emphasis to giant, core ellipticals give (Section 6.6.1) the same BH mass fraction that Magorrian got. In any case, the ground-based BH detections reviewed in KR95 were obtained with sufficient resolution, and their $M_\bullet$ estimates (**Table 1**) were not systematically too high.

Second was the danger that ground-based work would succeed only for a biased sample with larger-than-average $M_\bullet$. But KR95 already got a mean BH-to-bulge mass ratio of $0.0022^{+0.0016}_{-0.0009}$. Later values based on larger HST samples range from $0.0013^{+0.0023}_{-0.0008}$ (Merritt & Ferrarese 2001; cf. McLure & Dunlop 2002) to $0.0023^{+0.0020}_{-0.0011}$ (Marconi & Hunt 2003). Modern searches with improved modeling machinery can measure $M_\bullet$ properly even when $r_{\rm infl}/\sigma_* \sim 0.3$–$0.5$ (§ 3.1.1). Concerns about sample biases have not vanished. But other effects prove to be more important. As discussed in Sections 3 and 6, improvements in $M_\bullet$ measurement technology (e. g., omission of $M_\bullet$ values based on gas dynamics when broad emission-line widths were not taken into account and inclusion of dark matter in stellar dynamical models) have revised typical BH masses upward and now lead (Section 6.61) to a substantially larger BH-to-bulge mass fraction.

The strongest BH cases—the ones in our Galaxy (§§ 2.3) and in NGC 4258 (§ 3.3) – come entirely from ground-based work. The maser galaxy NGC 4258 has been observed with HST, but only to check our modeling machinery (Pastorini et al. 2007; Siopis et al. 2009).

2.2 HST confirmed ground-based BH detections at high resolution

Conceptually (but not chronologically), the first important contribution from HST was to confirm the ground-based BH detections at ~ 5 times higher spatial resolution. Early detections were viewed with varying degrees of skepticism. The subject had a shaky history. KR95 emphasized the problem: "It is easy to believe that we have proved what we expect to find." Some kinds of evidence, e. g., finding cuspy brightness profiles (Young et al. 1978; Lauer et al. 1992, 1993, 1995; Crane et al. 1993) that look similar to the cusps expected from BHs (Peebles 1972; Bahcall & Wolf 1976; Young 1980) were interpreted as revealing BHs (Young et al. 1978) but proved not to be evidence for BHs at all (KR95). The authors of early stellar dynamical BH papers did their best to be careful, but detections were bound to be more secure – and mass estimates were bound to be more accurate – when verified with higher spatial resolution. Improvements in modeling machinery were under way in parallel. Early papers made simplifying assumptions (e. g., spherical symmetry, isotropic velocity dispersion tensors) that were quickly superseded. We discuss spatial resolution in the present section and improvements in modeling in § 3.1.

Our Galaxy, M 32, and M 31 have the most detailed histories of observational and modeling improvements in measurements of $M_\bullet$. **Table 1** lists all measurements of $M_\bullet$ in these galaxies, using $r_{\rm infl}/\sigma_*$ as a measure of how well they resolve the BH sphere of influence. They are ordered by publication date (updated from Kormendy 2004, which also lists such data for other galaxies). **Figure 2** illustrates this record for M 32.

2.2.1. M 32. **Figure 2** illustrates our point that the BH in M 32 was discovered as early as our technology allowed. With $r_{\rm infl}/\sigma_* < 1$, Tonry (1984) overestimated $M_\bullet$, although not significantly with respect to the uncertainties. Ten years were needed to achieve $r_{\rm infl}/\sigma_* > 1$ (van der Marel et al. 1994b; Dehnen 1995; Qian et al. 1995). By then, σ_* had improved by a factor of 4 from Tonry's data, and $M_\bullet$ had converged to its present value. Observations with the Canada-France-Hawaii telescope improved σ_* by an additional factor of 1.5 and further confirmed $M_\bullet$ (Bender, Kormendy & Dehnen 1996). Soon afterward, HST spectra with 5 times better resolution became available and resoundingly confirmed that stellar dynamical $M_\bullet$ measurements were working. The total improvement in resolution since Tonry (1984) is a factor of 30. But $M_\bullet$ estimates have stayed stable through 20 years of improvements in resolution and modeling. This is an example of a general result: constrained by formation physics, galaxies do not use their freedom to indulge in perverse orbit structures that would cause simple models to provide wrong masses. The above successful history has been critically important to our confidence in BH detections.

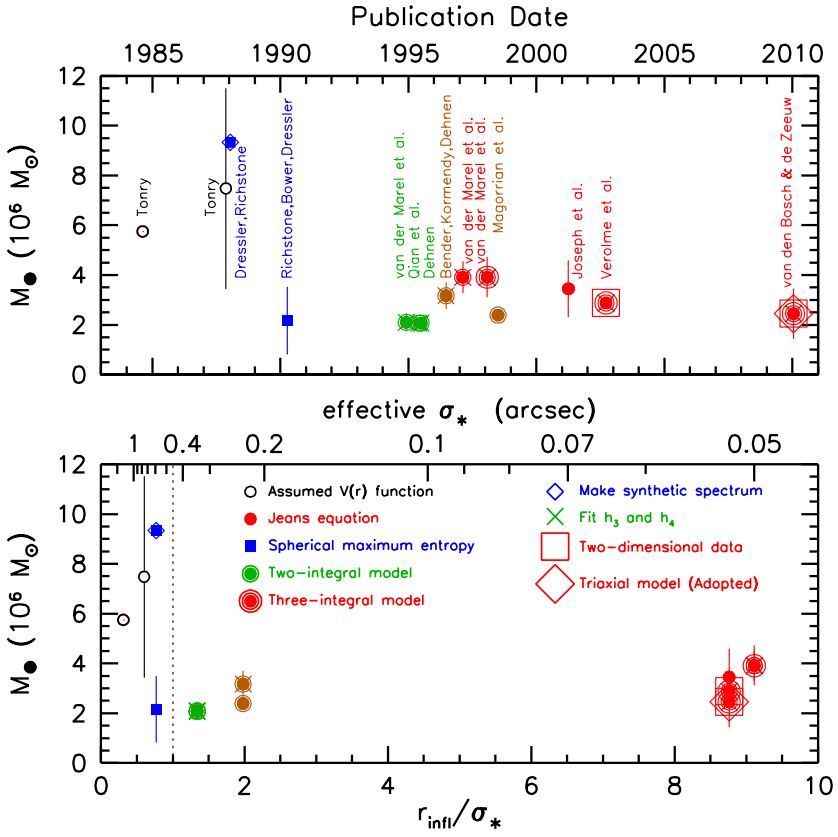

Figure 2

History of stellar-dynamical measurements of $M_\bullet$ in M 32 (updated from Kormendy 2004). Derived BH mass is shown as a function of (*top*) publication date and (*bottom*) spectroscopic spatial resolution. Resolution is measured by the effective Gaussian dispersion radius σ_* of the PSF. More relevant physically is the ratio of the radius of the BH sphere of influence, $r_{\rm infl} = GM_\bullet/\sigma^2$, to σ_*. If $r_{\rm infl}/\sigma_* \lesssim 1$, velocities are dominated by the mass distribution of the stars even in the central pixel and BH detection is difficult. If $r_{\rm infl}/\sigma_* \gg 1$, we resolve the region where velocities are controlled by the BH. Symbol shapes encode improvements in observations, in kinematic analysis, and in dynamical modeling techniques (see § 3.1). HST measurements are shown in red.

2.2.2. NGC 3115, NGC 3377, and NGC 4594. Similar improvements in $r_{\rm infl}/\sigma_*$ of a factor of 11 for NGC 3115 (from Kormendy & Richstone 1992 to Kormendy et al. 1996b; Emsellem, Dejonghe & Bacon 1999), a factor of 4.1 for NGC 4594 (Kormendy 1988b to Kormendy et al. 1996a; Jardel et al. 2011), and a factor of 2.2 for NGC 3377 (Kormendy et al. 1998 to Gebhardt et al. 2003) also improved confidence as the earlier $M_\bullet$ estimates were confirmed (Table 1.1 in Kormendy 2004).

2.2.3. M 31. Improvements in $r_{\rm infl}/\sigma_*$ of a factor of 11 from Dressler & Richstone (1988) and Kormendy (1988a) to Bender et al. (2005) have been especially important to our confidence in BH detection. M 31 was in some ways easy, because $r_{\rm infl}/\sigma_* \simeq 10$ already in the 1988 papers. But Lauer et al. (1993) discovered that the galaxy has an asymmetric double nucleus of red stars, P1 and P2 (**Figure 3**). The good news was that P1+P2 are rotation-dominated; this reduces uncertainties caused by poorly known velocity anisotropy. The bad news was that the asymmetry was at first not understood. It caused some authors to worry that the nucleus is not in equilibrium and that $M_\bullet$ can not be derived (Bacon et al. 1994; van der Marel 1995; Ferrarese & Ford 2005). The explanation of the double nucleus as an eccentric disk (Tremaine 1995; Peiris & Tremaine 2003) whose signature kinematic asymmetries are well confirmed at CFHT and HST resolution (Kormendy & Bender 1999; Bender et al. 2005) removes this uncertainty. In any case, these complications are now moot. CFHT observations by Kormendy & Bender (1999) showed that the BH lives in a third, tinier nucleus ("P3") of blue stars embedded in P2 (**Figure 3**). The highest-resolution BH mass measurement is now based entirely on the dynamics of P3, as follows (Bender et al. 2005).

CFHT: Canada-France-Hawaii Telescope

Figure 4 shows the rotation curve and velocity dispersion profile of P3 as measured with HST. The Keplerian rotation curve of a cold, razor-thin disk (*top panel*) fits the measurements well after PSF convolution and pixel sampling (*bottom two panels of plots*). PSF-convolved surface brightnesses, line-of-sight velocity dispersions, and mean velocities are shown at right in **Figure 4**. Note that the apparent dispersion is entirely caused by rotational line broadening. Orbit-superposition, maximum entropy models also were fitted to the data; the conclusion is that $M_\bullet = 1.4 \times 10^8\ M_\odot$ with a 1 sigma confidence range of (1.1 – 2.3) $\times 10^8\ M_\odot$. This larger $M_\bullet$ estimate is consistent with the error bars in earlier measurements from dynamical models of P1 and P2 but is more reliable. Thus the BH mass in M 31 has now been confirmed in a series of studies that greatly improved both the spatial resolution and the accuracy of modeling assumptions.

Figure 3

Nyquist-sampled color image of the triple nucleus of M 31 made from V-, B-, and 3000-Å-band images obtained with the HST Advanced Camera for Surveys (Lauer et al. 2012). The High Resolution Camera scale, $0\farcs028 \times 0\farcs025$, does not adequately sample the PSF. Dithered exposures were therefore obtained in a 2×2 square pattern of 0.5-pixel steps and combined using the Fourier image reconstruction technique of Lauer (1999). The final, PSF-deconvolved image has a scale of $0\farcs0114$ pixel^{-1}, a resolution FWHM of $0\farcs030 = 0.11$ pc, and a field of view of $3'' \times 3''$. North is up and east is at left. The upper-left brightness peak is P1; the lower-right peak is P2. The brightest blue source at the center is P3. The BH lives in P3.

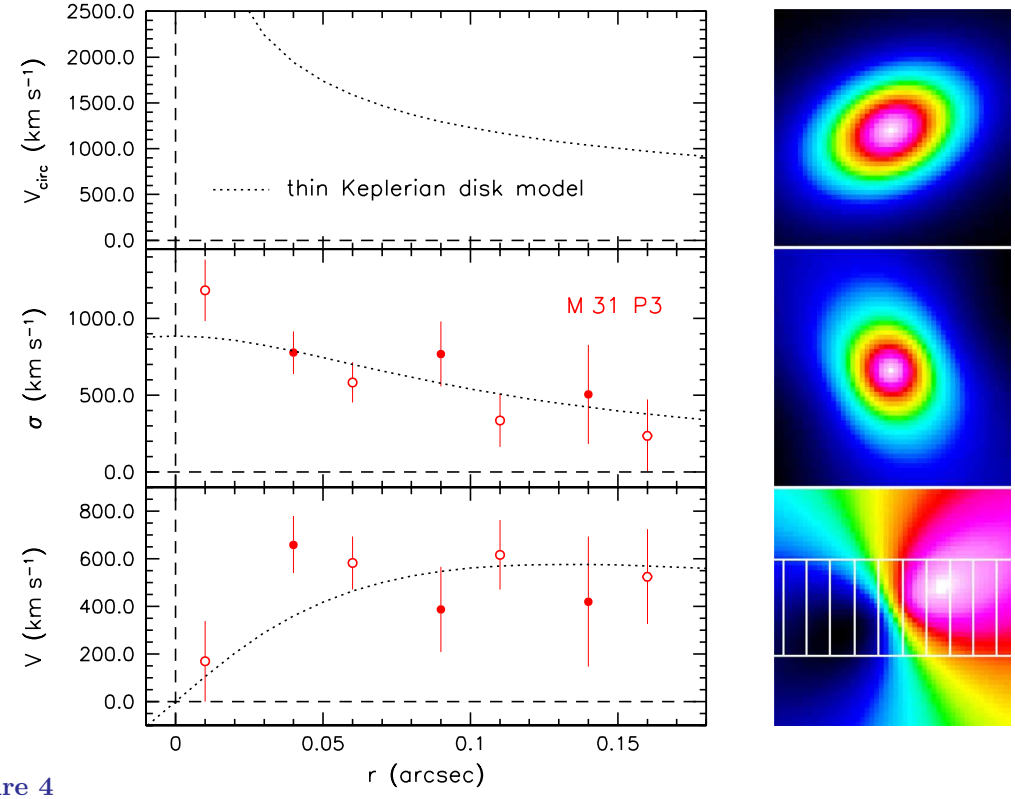

Figure 4

The bottom two plots show the measured rotation velocity V and velocity dispersion σ along the major axis of P3 with light from P1 and P2 subtracted. Spectral decomposition is easy, because P3 is dominated by Balmer absorption lines that are essentially absent in the P1 and P2. Open and filled circles are from opposite sides of the center. Dotted curves show the best-fit Keplerian rotation curve of an infinitely thin disk at the top and, after PSF convolution and pixel sampling, in the bottom panels. The $0\farcs5 \times 0\farcs5$ color images show the model surface brightness (*top*, linear scale from 0 = black to 1 = white), apparent velocity dispersion (*middle*, black to white corresponds to 150 to 1000 km s^{-1}), and rotation velocity (*bottom*, black to white corresponds to -700 to $+700$ km s^{-1}). All three panels show PSF-convolved values; the bottom panel in addition superposes the spectrograph pixels on the rotation velocity field. Note that the apparent velocity dispersion is all due to the velocity range seen by each pixel. Figure adapted from Bender et al. (2005).

HST has taken us on a remarkable journey in M 31. At the beginning, we knew only that the nucleus is asymmetric in surface brightness (Light, Danielson & Schwarzschild 1974) and kinematics (Dressler & Richstone 1988; Kormendy 1988a). The BH was found by the latter papers, but asymmetries were ignored. HST revealed the double nucleus; this was interesting as a signature of stellar dynamics near BHs, but it raised concerns about the $M_\bullet$ determination. Higher-resolution STIS spectroscopy now takes us far inside P1 and P2 into the blue cluster that surrounds the BH. The double nucleus has become irrelevant in the same way that the bulge and disk are irrelevant to $M_\bullet$ measurement. HST reveals a flat apparent rotation curve from $r = 0\farcs05 \pm 0\farcs01$ to $0\farcs15 \pm 0\farcs01$; all of this radius range is well inside ground-based PSFs. The corresponding, intrinsic rotation velocities are 1000 – 2000 km s^{-1}, i. e., 0.003c to 0.007c, still far from relativistic but among the largest velocities seen in any galaxy. The above is exactly the kind of journey through several generations of improved observations that HST has so importantly made possible.

c: speed of light

2.3 Our Galaxy is the strongest BH case

By far the most remarkable series of improvements in BH observations are the ones in our Galaxy. It is decisively our best case for a supermassive BH. All of this work is ground-based.

The Galactic center is so close ($D \simeq 8.28 \pm 0.33$ kpc; Genzel, Eisenhauer & Gillessen 2010: GEG10) that individual stars can be resolved and followed through their orbits (**Figure 5**). The shortest orbit periods observed so far are 15.8 yr (star S2) and 11.5 yr (star S102). Each star will eventually provide an independent measure of $M_\bullet$, but robust results are available so far only for star S2.

The early history of BH mass measurements in our Galaxy is reviewed in Genzel, Hollenbach & Townes (1994) and in KR95. This work was based on spectroscopy of gas or stellar subpopulations, like that discussed in Sections 3.1 and 3.2, with the advantage of better spatial resolution but the disadvantage of discreteness and systematic effects connected with the types of stars observed. The $M_\bullet$ values in **Table 1** start with the first ones based on dynamical models (Genzel & Townes 1987 review earlier observations). Early $M_\bullet$ measurements in **Table 1** were based on the kinematics of individual stars or on integrated, K-band spectra of CO absorption bands. Their best resolution was a few arcsec, but even so, they attained values of $r_{\rm infl}/\sigma_* \simeq 8$ to 12. Thus our Galaxy enters **Table 1** at $r_{\rm infl}/\sigma_*$ values that are comparable to those of the best HST BH discoveries (**Figure 1**).

At that time, our Galaxy was a solid BH case, but it was not yet one of the best. Since then, spectacular advances in instrumentation culminating in adaptive optics (AO) work with effective resolution $\sim 0\farcs0146 \simeq 0.00059$ pc (see below) has transformed our Galaxy into the poster child for supermassive BHs. This progress is reviewed in GEG10. Our discussion is therefore brief.

Tour-de-force, independent observing programs by Reinhard Genzel and Andrea Ghez and their groups have dramatically improved the effective resolution. The first improvements were achieved with speckle observations that shrunk effective PSF sizes enough to resolve the nuclear cluster of stars at $r \sim 1''$. Both groups then participated in the development of AO, and now dozens of stars are seen in the central arcsec of our Galaxy. At $D = 8.3$ kpc, $1''$ corresponds to 0.04 pc or 8280 AU. The Galactic BH has a mass of $4 \times 10^6\ M_\odot$; at 0.04 pc, the circular-orbit rotation velocity is ~ 700 km s^{-1}, similar to that of the P3 disk in M 31. But the Galactic center is much closer. At radii that are accessible to ground-based AO, we enter a new realm of galactic observations. Normally, we see only snapshots of stellar positions and galactic structures whose changes are too slow to be observed in human lifetimes. But a circular orbit at $r = 0.04$ pc around the Galactic center has an orbital time of ~ 400 years. Farther in, it is possible to measure proper motions and watch stars orbit around the center. More than one complete orbit of the star S2 has already been observed (**Figure 5**). It gives $M_\bullet = 4.30 \pm 0.20\,({\rm stat}) \pm 0.30\,({\rm sys}) \times 10^6\ M_\odot$ (GEG10), the gold standard of available BH masses. Note that the estimated error is dominated by uncertainties in the distance. The same is true of many extragalactic BHs, even though most authors (and our **Tables 2** and **3**) do not include distance errors in $M_\bullet$ uncertainties.

The observation that the orbit of star S2 is (within errors) closed means that essentially all of the attracting mass is located inside its pericenter radius (Ghez et al. 2008; GEG10; and **Figure 5** give the constraint on any extended mass $M_{\rm extended}$; see Ghez et al. 2009 for a review). S2's pericenter radius is $0\farcs0146 \simeq 0.00059$ pc $= 122$ AU $\simeq 1400 r_S$. This is the effective spatial resolution of the BH mass measurement in our Galaxy. No journey through a sequence of improving observations and astrophysical arguments for supermassive BHs is as persuasive as the one in our Galaxy. The pericenter velocity of S2 is > 6000 km s$^{-1} \simeq 0.02c$. Star S16 is even more extreme. Its pericenter radius is 45 ± 16 AU $= (529 \pm 193) r_S$ and its pericenter velocity is $\sim 12,000$ km s$^{-1} = 0.04c$; it has been observed through pericenter but not yet through a complete 36 ± 17 yr orbit (Ghez et al. 2005). These observations set the standard for how close to the Schwarzschild radius $r_S \equiv 2GM_\bullet/c^2$ we have come with observations that provide stellar-dynamical BH detections and masses.

Adaptive optics (AO): wavefront sensors measure blurring by the atmosphere, and controllable, flexible mirrors partly correct it. Control frequencies are $\sim 10^2$ to 10^3 Hz. Contrast:

Active optics: The largest telescopes have thin mirrors that flex. Active optics control flexure to maintain an optimal mirror figure. Control frequencies are ~ 1 Hz.

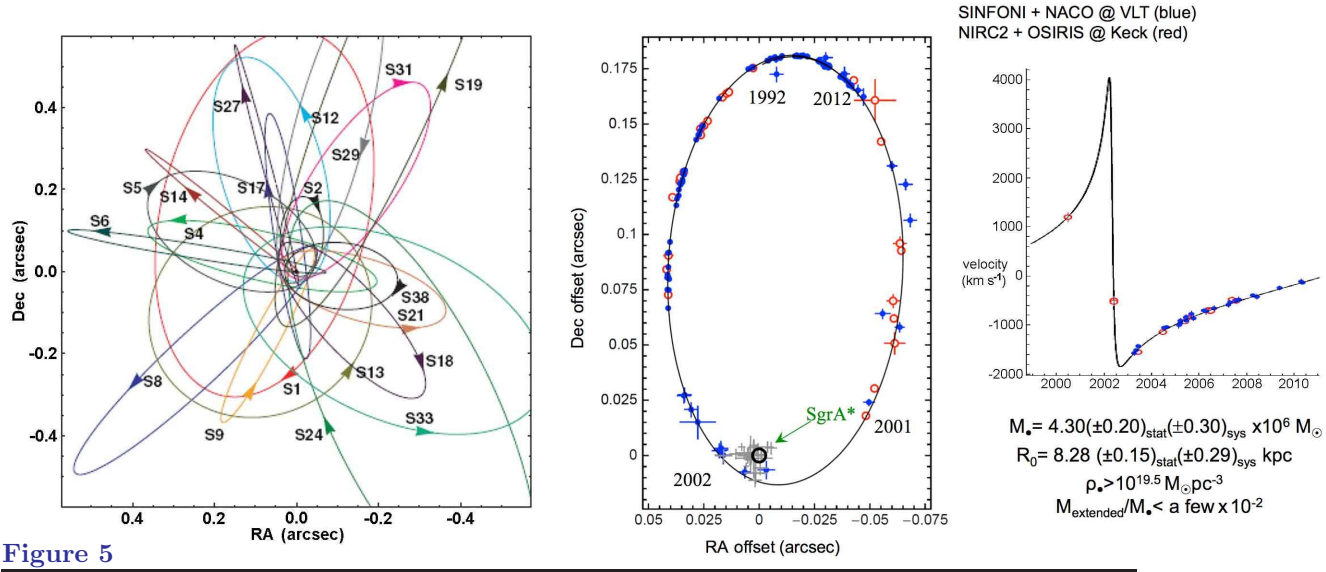

Figure 5

(*left*) Orbits of individual stars near the Galactic center. (*right*) Orbit of star S2 around the BH and associated radio source Sgr A* based on observations of its position from 1992 to 2012. Results from the Ghez group using the Keck telescope and from the Genzel group using the Europen Very Large Telescope (VLT) are combined. This figure is updated from Genzel, Eisenhauer & Gillessen (2010) and is kindly provided by Reinhard Genzel.

These results establish the existence and mass of the central dark object beyond any reasonable doubt. They also eliminate astrophysical plausible alternatives to a BH. These include brown dwarfs and stellar remnants (e. g., Maoz 1995, 1998; Genzel et al. 1997, 2000; Ghez et al. 1998, 2005) and even fermion balls (Ghez et al. 2005; GEG10). Boson balls (Torres et al. 2000; Schunck & Mielke 2003; Liebling & Palenzuela 2012) are harder to exclude; they are highly relativistic, they do not have hard surfaces, and they are consistent with dynamical mass and size constraints. But a boson ball is like the proverbial elephant in a tree: it is OK where it is, but how did it ever get there? GEG10 argue that boson balls are inconsistent with astrophysical constraints based on AGN radiation. Also, the Sołtan (1982) argument implies that at least most of the central dark mass observed in galaxies grew by accretion in AGN phases, and this quickly makes highly relativistic objects collapse into BHs. Finally (Fabian 2013), X-ray AGN observations imply that we see, in some objects, material interior to the innermost stable circular orbit of a non-rotating BH; this implies that these BHs are rotating rapidly and excludes boson balls as alternatives to all central dark objects. Arguments against the most plausible BH alternatives – failed stars and dead stars – are also made for other galaxies in Maoz (1995, 1998) and in Bender et al. (2005). Exotica such as sterile neutrinos or dark matter WIMPs could still have detectable (small) effects, but we conclude that they no longer threaten the conclusion that we are detecting supermassive black holes.

KR95 was titled "Inward Bound – The Search for Supermassive Black Holes in Galactic Nuclei." HST has taken us essentially one order of magnitude inward in radius. A few other telescopes take us closer. But mostly, we are still working at 10^4 to 10^5 Schwarzschild radii. In our Galaxy, we have observed individual stars in to $\sim$ 500 Schwarzschild radii. Only the velocity profiles of relativistically broadened Fe Kα lines (e. g., Tanaka et al. 1995; Fabian 2013) probe radii that are comparable to the Schwarzschild radius. So we are still inward bound. Joining up our measurements made at thousands of r_S with those probed by Fe Kα emission requires that we robustly integrate into our story the rich and complicated details of AGN physics; that is, the narrow– and broad–emission-line regions. That journey still has far to go.

2.4 HST Discovered Most BHs and Enabled Demographic Studies

This brings us to what is decisively the most important contribution that HST has made: Because it reliably delivers high spatial resolution, HST made it feasible to find BHs in many more galaxies. By opening the floodgates of discovery, it put work on BH demographics into high gear. As we write this paper, most dynamically detected BHs (**Tables 2, 3**) were discovered with HST.

The burst of BH discoveries centered in 2001 ± 2 is well illustrated in **Figure 1**. It fueled the first period of demographic work discussed in the Introduction, when all bulges and ellipticals – and, indeed, perhaps even objects as different as globular clusters – appeared to satisfy a single set of correlations between $M_\bullet$ and various properties of the host galaxies.

2.5 The Post-HST Era of Adaptive Optics and Maser BH Detections

Recently, this subject has emerged from the 15-year plateau of the above demographic picture. One reason is that AO enables new discoveries using ground-based telescopes (Beckers 1993; Davies & Kasper 2012). AO delivers an important advantage for late-type galaxies: it works best in the infrared, where problems with young stars and dust are minimized. Second, after a spectacular beginning with NGC 4258 (Miyoshi et al. 1995) and a dry period that followed, maser BH searches are starting to have substantial success again (e. g., Kuo et al. 2011). Both of these trends are visible in **Figure 1**. Third, $M_\bullet$ estimates via reverberation mapping of AGNs have become convincing. This adds new observations that are not included in **Figure 1**. All three techniques tend to work best for late-type galaxies, so the range of galaxy types with BH demographic information has grown broader. Fourth, dynamical modeling has made a quantum jump in sophistication (§ 3.1). Sections 6 and 7 review the resulting observations that are taking us beyond the demographic plateau of the past decade. We now find that $M_\bullet$ correlates (or fails to correlate) differently with different structural components in galaxies. This is rich and only partly explored territory.

3. PROGRESS IN BH DETECTION TECHNOLOGY. II. SPECTROSCOPY & DYNAMICAL MODELING

Early on in this subject, it was commonly believed that BHs could be detected photometrically. Based on experience with globular clusters, it was thought that brightness profiles of elliptical galaxies would flatten near the center into nearly-constant-density cores. This expectation may also have been influenced by analogy with stars, in which the density, temperature, and other properties are continuous, differentiable functions of radius near the center. If the luminosity density $j(r)$ is non-singular at the center of a spherical galaxy, then the surface brightness must vary with radius R as $I(R) = I_0 + aR^2 + \mathrm{O}(R^4)$ (Tremaine 1997). Adding a BH converts the volume brightness profile into a cusp with a singular central luminosity density. A power-law cusp, $j(r) \propto r^{1-\gamma}$, gives rise to a cusp in the surface density, $I(R) \propto R^{-\gamma}$, for $\gamma > 1$. The theory of such cusps was described in seminal papers by Peebles (1972), Bahcall & Wolf (1976), and Young (1980).

We now realize that brightness profiles by themselves provide no evidence for or against BHs. Kormendy (1993a) and KR95 showed that higher $M_\bullet$ is associated with shallower, not steeper, central brightness profiles. Also, it is straightforward to construct equilibrium stellar systems with power-law cusps that have no central point mass (e. g., Dehnen 1993; Tremaine et al. 1994). And N-body simulations of hierarchical clustering produce cuspy dark halos in the absence of any baryons (Navarro, Frenk & White 1997). Ironically, the cluster of old stars near the center of the Milky Way – the galaxy with the strongest evidence for a BH – appears to have a constant-density core with a core radius of $\sim$0.4 pc (Genzel, Eisenhauer, & Gillessen 2010). Some giant elliptical galaxies even contain partly hollow cores (Lauer et al. 2002). There is physics in this (Section 6.13).

Therefore detection of BHs in nearby galaxies requires both photometry to measure the density distribution of the stars and spectroscopy to measure their kinematics. For photometry, HST provides a PSF whose Gaussian core has a dispersion radius of $\sigma_{*\rm tel} \simeq 0\farcs036$ at visible wavelengths (van der Marel et al. 1997a; see **Table 1** here). For spectroscopy, taking pixel sizes and telescope PSF into account, HST provides a best resolution Gaussian dispersion radius $\sigma_* \simeq 0\farcs05$ (**Table 1**). Higher-resolution observations can be provided by AO, but the fraction of the light that is in the PSF core is much smaller for AO than it is for HST. Still higher resolution is available from radio interferomtery of water maser disks and for our Galaxy.

3.1 Stellar dynamics

Stellar-kinematic observations and dynamical models used to interpret them have improved dramatically during the $\sim$30 years of the BH search. This is important, because most BH detections in **Tables 2** and **3** are based on stellar dynamics. Also, the technique covers almost the whole range of observed BH masses. Therefore, improvements in modeling reliability have been central to our understanding of BH demographics and coevolution physics. Kormendy & Richstone (1995), Kormendy (2004), and Ferrarese & Ford (2005) review the history of modeling machinery from the first claimed BH detection (Sargent et al. 1978, who used spherical, isotropic models on observations of M87) to mass measurements based only on Equation 1, below, to spherical anisotropic models, and to oblate-spheroidal, two-integral models with distribution functions $f(E, L_z)$ based on energy and the axial component of angular momentum. Meanwhile, spectroscopy improved in two ways, (1) spatial resolution improved from $\sim 1''$ ground-based work to $\sim 0\farcs05$ for HST, and (2) the derived data improved from V and σ measurements using long-slit spectroscopy to measurement of full line-of-sight velocity distribtions (LOSVDs) to ground-based, two-dimensional spectroscopy. The history of these improvements is summarized here in Section 2, especially in **Table 1** and **Figure 2**. We concentrate here on the state of the art since $\sim$2000, i. e., three-integral models based on Schwarzschild's (1979, 1993) orbit superposition method.

The big difficulty in stellar dynamics is the unknown anisotropy in the velocity distribution. It is worth abstracting from Kormendy & Richstone (1995) the arguments about how and when this is important. A heuristic understanding is provided by the idealized case of spherical symmetry and a velocity ellipsoid that everywhere points at the center. Then the first velocity moment of the collisionless Boltzmann equation gives the mass $M(r)$ within radius r,

$$M(r) = \frac{V^2 r}{G} + \frac{\sigma_r^2 r}{G}\left[-\frac{d\ln\nu}{d\ln r} - \frac{d\ln\sigma_r^2}{d\ln r} - \left(1 - \frac{\sigma_\theta^2}{\sigma_r^2}\right) - \left(1 - \frac{\sigma_\phi^2}{\sigma_r^2}\right)\right], \qquad (1)$$

where V is the rotation velocity, σ_r, σ_θ, and σ_ϕ are the radial and azimuthal components of the velocity dispersion, and ν is the density of the tracer population whose kinematics we measure (not the total density). All quantities except M are unprojected. Thus V and σ contribute similarly to $M(r)$, but the $\sigma_r^2 r/G$ term is multiplied by the sum of four terms. The first two are almost always positive, but the anisotropy terms can be positive or negative. Anisotropy is most important when V is small and when the anisotropy terms threaten to cancel the first two terms in the bracket. Under what circumstances can this happen?

Sections 6.7, 6.13, and 8.4 discuss the distinction between elliptical galaxies that do or do not contain cores; i. e., breaks at $\sim 10^2$ pc in $\nu(r)$ from steep outer profiles to shallow inner power laws. This distinction matters here in two ways. First, core galaxies have shallow inner profiles with $0.5 \lesssim -d\ln\nu/d\ln r \lesssim 1$ (Kormendy et al. 1996c; Gebhardt et al. 1996). Coreless galaxies typically have $-d\ln\nu/d\ln r \simeq 1.9 \pm 0.3$. The $-d\ln\sigma_r^2/d\ln r$ term cannot easily be >1 and is larger in coreless galaxies. So the first two terms add up to 1 – 1.5 for core galaxies and almost 3 for coreless

galaxies. Secondly, coreless galaxies rotate more rapidly and are less anisotropic than galaxies with cores. So, for coreless galaxies (including classical bulges), the V^2r/G term is more important and the velocity anisotropy terms are both smaller and in competition with larger values of the first two terms. Velocity anisotropy is not negligible, but its effects tend to be small. In contrast, if a core elliptical has σ_θ and σ_ϕ as small as 60 – 70 % of σ_r, the anisotropy terms essentially cancel the first two terms. And $V^2r/G \sim 0$. Similarly, if σ_r is smaller than the other two components, the derived mass can easily double. So velocity anisotropy is a big issue for core ellipticals. And it is not safe to ignore it even for coreless ellipticals and bulges.

Dealing with anisotropy has controlled the history of stellar-dynamical BH work (e. g., **Figure 2**). Early BH detections did not involve dynamical models; they used Equation 1 to measure masses, much as H I rotation curves $V(r)$ give mass distributions $M(r) \simeq V^2r/G$ except that we also have to deal with σ, projection of the model light distribution and kinematics, and PSF convolution. These papers (Tonry 1984, 1987: M 32; Kormendy 1988a, b: M 31, NGC 4594; Kormendy & Richstone 1992: NGC 3115) succeeded because the galaxies were picked to have almost-edge-on bulges in which velocity anisotropy was known to be small (Kormendy & Illingworth 1982; Jarvis & Freeman 1985).

The first papers to incorporate anisotropy pointed out that, by suitably tuning $\sigma_r > \sigma_{\rm tangential}$ near the center, the Sargent et al. (1978) observations of M 87 can be fitted without a BH (Duncan & Wheeler 1980; Binney & Mamon 1982; Richstone & Tremaine 1985; Dressler & Richstone 1990). In the context of other work which showed that giant (but not lower-luminosity) ellipticals rotate slowly and are triaxial (e. g., Illingworth 1977; Binney 1978a, b; Davies et al. 1983), these papers firmly established that velocity anisotropy is the central problem in stellar-dynamical BH searches.

The broadest-impact advance in stellar-dynamical BH search technology – one whose descendants define the state of the art today – was application of Schwarzschild's (1979, 1993) orbit superposition method to model galaxies. The gravitational potential is defined as the sum of a central point mass $M_\bullet$ (to be determined) and stellar densities equal to the light distribution times the mass-to-light ratio M/L of the stellar population (to be determined) assumed to be constant with radius. Then "all possible orbits" in this mass distribution are calculated as functions of energy and angular momentum and integrated long enough to give three-dimensional distributions of time-averaged densities, velocities, and velocity dispersion components. Finally, an optimum linear combination of these orbital distributions is calculated to fit the observed light and velocity distributions after projection and PSF convolution. This method has the major advantage that an explicit distribution function f which is a solution to the collisionless Boltzmann equation need not be defined. Instead, all valid distribution functions can be calculated numerically, provided that all possible orbits are explored (see below). Uniqueness is a problem. But it is easy to minimize a "cost function" or maximize a "profit function" to accomplish specific goals that circumvent the uniqueness problem by finding extreme solutions that are of astrophysical interest. In particular, if the algorithm is required to minimize $M_\bullet$ at all cost to the other variables and if it fails, then a central dark mass has robustly been detected. A common profit function is maximization of an entropy $\simeq$ the integral of $-f \ln f$ over position and velocity space. Doing this makes the distribution function smoother but more specialized. Modern data are so detailed that smoothness is not an issue, so entropy maximization is given low weight. The earliest code made spherical models (Richstone & Tremaine 1984, 1985, 1988). Applications to the BH search were Dressler & Richstone (1988); Richstone, Bower, & Dressler (1990), and Kormendy & Richstone (1992). This code evolved into one of three extant modeling machines, i. e., the Nuker code (Gebhardt et al. 2000d, 2003; Richstone et al. 2004; Thomas et al. 2004; Siopis et al. 2009; Thomas 2010). The others are the Leiden code (van der Marel et al. 1998a; Cretton et al. 1999a; Cappellari et al. 2002, 2006; Verolme et al. 2002; Shapiro et al. 2006), and the Valluri code (Valluri, Merritt & Emsellem 2004; Valluri et al. 2005).

These codes are widely applied in BH searches and in other galaxy studies. Much science – including most of the results in this paper – depend on their success. Nevertheless, they involve nontrivial limitations and concerns that are not fully addressed in the literature. For example:

1. Until Gebhardt & Thomas (2009), BH modeling papers did not include halo dark matter. This problem is now essentially solved (see below).

2. Core ellipticals are known to be moderately triaxial, but the above codes make axisymmetric models. First explorations with triaxial models are discussed below. This remains an issue.

3. In many Nuker papers (e. g., Gebhardt et al. 2003; Gültekin et al. 2009b), galaxies are assumed to be edge-on. Limited tests show little systematic effect of varying the inclination i, but the main reason is that i couples with $M_\bullet$ and M/L strongly enough so that constraints on i are weak. This is a problem especially for round ellipticals, since studies of observed axial ratio distributions (Sandage, Freeman, & Stokes 1970; Binney & de Vaucouleurs 1981; Tremblay & Merritt 1996) show that intrinsically spherical ellipticals are rare. If galaxies are more face-on than we think, then we can underestimate $M_\bullet$. An example is NGC 3379, discussed below.

4. We highlight the need to sample "all possible orbits", because this has been a contentious issue. Valluri, Merritt, & Emsellem (2004) argue the danger that, given indeterminacies caused by unknown triaxiality, velocity anisotropy, inclination, and projection, many parameters (including $M_\bullet$ and M/L) are strongly coupled, so different distribution functions distributed along tilted valleys in multidimensional χ^2 space fit the data almost equally well. They warn us that, if too few orbits are used, any Schwarzschild code will fail to discover the freedom to explore this valley and will give a spuriously narrow valley in marginalized χ^2 around a minimum that may be biased. And they argue that, once the number of orbits is sufficiently increased, the problem will reveal itself as a flat bottom to the χ^2 valley that favors no particular minimum because the intrinsic, multidimensional χ^2 valley is also flat-bottomed.

   Richstone et al. (2004) test this problem for NGC 821, which has the second-most-poorly-resolved BH sphere of influence in Gebhardt et al. (2003): $r_{\rm infl}/\sigma_* \simeq 0.6$. They argue that the 7,000 orbits used in Gebhardt et al. (2003) were sufficient (althought the χ^2 minimum was rather jagged) by showing that 10,000, 15,000 and 30,000 orbits give the same BH mass. The χ^2 valley is moderately broad over a factor of slightly more than 2 in $M_\bullet$, but it is not flat-bottomed, and 1-σ error bars are well defined. Nevertheless, we now realize that sufficient sampling of "all possible orbits" is not easy. Shen & Gebhardt (2010) found that: "Our new $M_\bullet$ is about 2 times larger than the previous published value [for NGC 4649]; the earlier model did not adequately sample the orbits required to match the large tangential anisotropy in the galaxy center." Shen and Gebhardt used 30,000 orbits each for 16,000 models, compared with $\sim$7000 orbits used by Gebhardt et al. (2003). In recent work, it seems unlikely that orbit undersampling is still a problem, as authors have increased the sampling very substantially. For example, Gebhardt & Thomas (2009) use 25,000 orbits each for 25,000 orbit libraries calculated for M 87; Gebhardt et al. (2011) use 40,000 orbits per library; Rusli et al. (2013) use 24,000 orbits per library, and Cappellari et al. (2006) and Shapiro et al. (2006) use 444,528 orbits per library to fit 15,552 observables in NGC 3379.

Nevertheless, issues (1) and (2) remain. Two further developments are crucial to our confidence. First, we discuss intercomparisons, e. g., of $M_\bullet$ measurements made with the above codes on the same data or made with one of the above codes versus an entirely independent BH measurement. Second, we discuss two further astrophysical improvements, the addition of dark matter to the models and an initial exploration of the effects of triaxiality in NGC 3379 and in M 32.

Siopis et al. (2009) tested the Nuker code by comparing their stellar dynamical measurement of $M_\bullet = (3.3\pm0.2)\times10^7\,M_\odot$ in NGC 4258 with the known, accurate mass $M_\bullet = (3.81\pm0.04)\times10^7\,M_\odot$ obtained from the kinematics of a maser disk at $r = 0.1-0.3$ pc (Herrnstein et al. 2005; § 3.3.1 here). Their HST STIS and ground-based spectroscopy were similar to that used in other BH measures. The spatial resolution was good, $r_{\rm infl}/\sigma_* \simeq 5.8$. The HST-determined, stellar-dynamical mass is lower by $(13\pm5)\,\%$; i. e., by 3σ. But if the above were typical of RMS errors in stellar-dynamical mass measurements, then these would be negligibly small for most purposes. Moreover, NGC 4258 has complications that do not occur for most galaxies: (1) The light distribution used in the stellar-dynamical measurement is compromised at $r < 0\farcs2$ because AGN continuum radiation could not accurately be subtracted. (2) Dust in the bulge and especially near the center affects the light distribution. (3) The ellipticity varies from 0.26 at $r\sim0\farcs5$ to $0.4-0.45$ in much of the bulge to 0.6 in the inclined disk. However, the model ellipticity was fixed at 0.35. Assuming $\epsilon = 0.45$ increased the mass estimate to $M_\bullet = (3.5\pm0.4)\times10^7\,M_\odot$, closer to and formally consistent with the accepted value. (4) NGC 4258 is weakly barred and strongly oval; the kinematic signatures of both features (see Bosma 1981 for ovals) are clear in the H I velocity field (van Albada 1980). Van Albada derives an inclination of 72° based on the assumption that the outer H I is in circular motion. However, if the nested ovals in the light distribution are elongated normally, i. e., perpendicular to the bar at large r (Kormendy 1982, 2012), then the galaxy could be more face-on. For $i = 62°$, "a value close to the lowest inclination angles that we found in the literature", $M_\bullet = (3.6\pm0.4)\times10^7\,M_\odot$ (Siopis et al. 2009). So it is appears that the stellar-dynamical and maser masses are not formally inconsistent. In any case, underestimates of BH masses are less worrying than overestimates, because overestimates could cause us to believe that a BH has been detected when none is present.

A test of independent observations and model codes is available for the core elliptical NGC 3379. From HST Faint Object Spectrograph (FOS) and ground-based, long-slit spectroscopy, Gebhardt et al. (2000d, see Gültekin et al. 2009c) got $M_\bullet = 1.2^{+0.8}_{-0.6}\times10^8\,M_\odot$ (1-σ errors) for $D = 11.7$ Mpc. Based on two-dimensional spectroscopy from SAURON at large radii and CFHT OASIS at small radii, Shapiro et al. (2006) got $M_\bullet = 1.6^{+3.0}_{-1.1}\times10^8\,M_\odot$ (3-σ errors). Both groups assumed that the galaxy is edge-on, although Shapiro includes results at $i = 50°$ in the error bars. NGC 3379 is a difficult galaxy; the Gebhardt BH mass was based largely on the asymmetry in the central LOSVD. With HST, Gebhardt had $r_{\rm infl}/\sigma_* \sim 2.2$, whereas Shapiro had $r_{\rm infl}/\sigma_* \sim 0.7$ for the CFHT data. However, the Shapiro data are two-dimensional and of very high S/N. The resulting $M_\bullet$ is substantially more robust than the HST value. This emphasizes a problem that is usually unstated: given the difficulty of getting HST time, observers ask for approximately the minimum S/N that they believe will be adequate. This is unfortunate. Still, the above comparison is reassuring, because the measurements and dynamical models are entirely independent.

A less reassuring test of independent observations and analysis codes is available for the core elliptical NGC 1399, the brightest galaxy in the Fornax cluster. Houghton et al. (2006) measure $M_\bullet = 1.26(0.63-1.78)\times10^9\ M_\odot$ based on NAOS-CONICA AO spectroscopy with the European Southern Observatory's Very Large Telescope. The effective resolution is $\sigma_* = 0\farcs086$ as defined in the notes to **Table 1**. The models are a variant on the Leiden code. In contrst, Gebhardt et al. (2007) measure $M_\bullet = 0.50(0.43-0.57)\times10^9\ M_\odot$ based on HST STIS spectra with $\sigma_* = 0\farcs070$. The number of orbits used by the two studies is comparable ($\sim10^4$). Their 1-σ error bars almost overlap. Nevertheless, the comparison is sobering. We adopt the mean of the two results in Section 5.

Two additional modeling improvements have proven to be very important:

Since 2009, halo dark matter has been included in stellar-dynamical $M_\bullet$ measurements. Omitting it was dangerous, mostly for ellipticals with cores. Because these are more anisotropic than coreless ellipticals, stars visit larger ranges of radii. Even if dark matter densities near the center are small compared to stellar densities (and this is not guaranteed), the stars in the radius range in which we have kinematic data can visit large radii where dark matter dominates the potential. Then the brightness profile gives the wrong potential and hence the wrong orbit structure. Including dark matter almost inevitably increases $M_\bullet$ estimates. This is because we assume that stellar population M/L ratios are independent of radius. If we add dark matter to the models and therefore attribute some of the mass density at large radii to that dark matter, then M/L must be decreased there. Therefore we decrease M/L near the center, too. As a result, $M_\bullet$ must be increased to maintain a good fit to the kinematics. In their first study of M 87, Gebhardt and Thomas (2009) found that $M_\bullet = (6.1 \pm 0.5) \times 10^9\, M_\odot$ for $D = 17$ Mpc, essentially double the mass $M_\bullet = (3.6 \pm 1.0) \times 10^9\, M_\odot$ given by the emission-line rotation curve (Macchetto et al. 1997). This review was delayed for several years because the same problem existed for other core galaxies, too, but we had no revised BH masses. Now, this problem is moot. All core galaxies with stellar-dynamical BH masses except NGC 3607 and NGC 5576 have been (re)analyzed using models that include dark matter (see **Table 2**). This includes new BH mass measurements. We are grateful to S. Rusli and R. Saglia for communicating nine new BH masses before publication. Figure 9 in Rusli et al. (2013) shows how the correction factor for $M_\bullet$ derived without using dark matter depends on the spatial resolution of the spectroscopy. We also have an independent calibration of the corrections from Schulze & Gebhardt (2011). However, as noted in the notes to **Table 2** (see Supplemental Information), the two calibrations agree poorly at the low effective resolution for NGC 3607, so we cannot reliably correct $M_\bullet$. We therefore consider the BH detection to be valid, but we omit the galaxy from correlation fits (see **Figure 12**). NGC 5576 is the only other galaxy that required a significant correction to $M_\bullet$. That correction is robustly determined and has been applied in **Table 2**.

The second improvement is a first exploration of triaxial models. Developed by van den Bosch et al. (2008), these have been applied to the core galaxy NGC 3379 and the coreless galaxy M 32 by van den Bosch & de Zeeuw (2010). Triaxial models are expensive in complexity and in the computing resources needed for an exploration of the (much enlarged) parameter space. But the improvement in $M_\bullet$ is important for core galaxies. For NGC 3379, axisymmetric models produced a well-defined estimate of $M_\bullet = 1.6^{+0.3}_{-0.9} \times 10^8\ M_\odot$ (1-σ errors) (Shapiro et al. 2006). Van den Bosch & de Zeeuw (2010) confirm this result when they force their models to be axisymmetric. But their triaxial models give a three-times-higher mass, $M_\bullet = (4.6 \pm 1.1) \times 10^8\ M_\odot$. Triaxiality is more important than usual for NGC 3379, because it is a core elliptical that looks nearly round. We noted above that intrinsically spherical ellipticals are rare. So NGC 3379 is likely to be nearly face-on, and a wide range of near-face-on inclinations are allowed by triaxial models that are excluded by axisymmetric models. We use van den Bosch's BH mass in **Table 2**, but we note with concern that other core ellipticals have not been analyzed with triaxial models.

In contrast, for the coreless elliptical M 32, the triaxial models of van den Bosch & de Zeeuw (2010) give a BH mass $M_\bullet = (2.45 \pm 1.05) \times 10^6\, M_\odot$ that is consistent with results from axisymmetric models. It is less likely that triaxiality is a problem for $M_\bullet$ measurements in coreless galaxies.

For $\sim$25 years, there has been a disconnect between the good agreement of various authors' $M_\bullet$ measurements and worst-case scenarios motivated by the worries in our discussion of Equation 1, allowed formally by the collisionless Boltzmann equation, and exemplified by Valluri et al. (2004). Results almost always turn out more benign than the worst-case scenarios. Galaxies do not use their freedom to indulge in perverse orbit structures. In practice, velocity distributions are nearly

isotropic near galaxy centers; in core galaxies, $\sigma_\theta > \sigma_r$ inside the core radius, and $\sigma_r > \sigma_\theta$ and σ_ϕ at large radii. There is physics in this. Near-isotropy at small radii results from the destruction of box orbits that pass close enough to BHs to scatter off of them (Norman, May, & van Albada 1985; Gerhard & Binney 1985; Merritt & Quinlan 1998). A bias toward circular orbits can result (1) from embedded nuclear disks, (2) from slow BH accretion (Young 1980; Goodman & Binney 1984), and (3) from core scouring by binary BHs (Gebhardt 2004). Orbits at large radii tend to be radial because stars get flung there from small radii during violent relaxation. Thus, the physics of galaxy formation limits the distribution functions that galaxies can have. Despite this, and despite the reassuring tests discussed in this section, nagging doubts remain about stellar-dynamical BH masses. As data and models improve, statistical error bars shrink. Almost certainly, they are already smaller than systematic errors that we do not know how to evaluate. Systematics that cause concern include (1) triaxiality in core ellipticals, (2) radial mass-to-light ratio variations caused by radial gradients in stellar populations (a very solvable problem), and (3) whether we have the correct density profiles of dark matter after realistic merger histories and baryonic pulling. For these reasons, we do not concentrate on the scatter in BH–host-galaxy correlations. Rather, we focus on more qualitative results about the differences in such correlations for different kinds of galaxy components.

3.1.1 What Spatial Resolution Do We Need To Measure $M_\bullet$ With Stellar Dynamics?

Gebhardt et al. (2003) answer this question for the three-integral, orbit-superposition models constructed with the Nuker code. They derive $M_\bullet$ using HST and ground-based spectroscopy. They also measure how $M_\bullet$ estimates change when they use only the ground-based spectroscopy. The HST spectra are higher in resolution by a mean factor of 11.2 ± 1.2. We assume here that masses based on these spectra are accurate. Then results based only on the ground-based spectra can be used to map out how $M_\bullet$ estimates deteriorate at $r_{\rm cusp}/\sigma_* \lesssim 1$. Gebhardt et al. (2003) conclude that $M_\bullet$ error bars are larger when the HST data are omitted but that systematic errors in $M_\bullet$ are small. In particular, results from the three-integral models are reliable provided that $r_{\rm cusp}/\sigma_* \gtrsim 0.3$. All stellar-dynamical BH detections in **Tables 2** and **3** satisfy this criterion. At lower resolution, the error bars grow, but there is no sign that they are unrealistic or that $M_\bullet$ is systematically wrong.

All of the ground-based BH discoveries listed in KR95 had $r_{\rm cusp}/\sigma_* > 1$ except the earliest papers on M 32. **Figure 2** shows that they overestimated $M_\bullet$. But HST BH discoveries that are made with $r_{\rm cusp}/\sigma_* \simeq 0.3$ to 1 are more secure than these early results on M 32, because we now fit LOSVDs and because three-integral models are more reliable than simpler models.

3.2 Ionized gas dynamics

Gas-dynamical mass measurements in principle offer several major advantages compared to stellar-dynamical modeling. The central few hundred parsecs of practically all spiral galaxies and $>50\%$ of S0 and elliptical galaxies have detectable optical nebular line emission (Ho, Filippenko, & Sargent 1997a). The inferred amount of warm (10^4 K) ionized gas is quite modest, typically only $\sim 10^4 - 10^5\,M_\odot$ (Ho, Filippenko, & Sargent 2003), but it is readily detectable at ground-based and (Hughes et al. 2005; Shields et al. 2007) HST resolution. From a practical point of view, nebular emission lines are much easier to measure than stellar absorption lines. They not only have larger equivalent widths, but their relatively simple line profiles make measurement of velocities and velocity dispersions straightforward. By contrast, the stellar-based approach relies on measurement of higher-order moments of the LOSVDs of weaker spectral features, which is often tremendously challenging for more massive, lower surface brightness galaxies. For example, stellar-dynamical analysis of brightest cluster galaxies has only recently become feasible (e. g., McConnell et al. 2011a, 2012), but only with the use of 8 – 10-meter-class telescopes equipped with AO; the 2.4-meter HST is simply not up to this task.

Another appeal of using gas instead of stars lies in the conceptual simplicity of the dynamical modeling. If the gas is in Keplerian rotation in a dynamically cold disk, the analysis is vastly less intricate and computationally cheaper than the orbit-based machinery needed to treat the stars. Moreover, complexities such as orbital anisotropy, triaxiality, or the influence of the dark matter halo can be neglected. The basic steps involved in the modeling process were outlined in Macchetto et al. (1997) and further refined in van der Marel & van den Bosch (1998b), Barth et al. (2001), Maciejewski & Binney (2001), and Marconi et al. (2001, 2003). Starting with the assumption that the gas is in a thin disk that rotates in circular orbits in the principal plane of the galaxy potential, the goal is to compute a model velocity field that simultaneously matches the observed velocities, velocity dispersions, and surface brightness distribution of the line emission. The gravitational potential of the galaxy consists of the contribution from stars as measured by the projected stellar surface brightness and an assumed stellar M/L plus an additional dark mass (i. e., the BH). To compare the model with the data, one must take into consideration the instrumental PSF, the size of the spectroscopic aperture, and the intrinsic spatial distribution of the line emission. An additional problem that commonly accompanies emission-line gas is dust that complicates the analysis of the light distribution.

Early HST BH searches capitalized on the perceived advantages of gas measurements. The first iconic observation by Harms et al. (1994) targeted the 100-pc-scale circumnuclear disk in M 87 detected in Hα emission by Ford et al. (1994). Although the single-aperture FOS provided limited spatial sampling, the observations demonstrated that ionized gas in two positions at radii $0\farcs25$ on either side of the center has velocities ± 500 km s^{-1} relative to the systemic velocity of the galaxy. Assuming that the gas is in Keplerian rotation, the implied enclosed mass is $\sim (2.4 \pm 0.7) \times 10^9\,M_\odot$. The corresponding central mass-to-light ratio, $(M/L)_I = 170\,(M_\odot/L_\odot)$, implies that most of the mass is dark and presumably attributable to the much-sought-after supermassive BH. Similar cases quickly followed: NGC 4261 (Ferrarese, Ford, & Jaffe 1996), NGC 7052 (van der Marel & van den Bosch 1998b), NGC 6251 (Ferrarese & Ford 1999), and IC 1459 (Verdoes Kleijn et al. 2000). These studies adopted the same strategy, focusing on massive ellipticals known to host radio jets, which, as expected, often turn out to be accompanied by a nuclear disk of dust and gas aligned perpendicular to the jet axis. A supermassive BH was discovered in every case. The modeling analysis used in some of these early studies did not take into account all the effects described above. Moreover, the line widths, while clearly observed to be quite substantial, were either ignored or treated in a highly simplified manner. The disks were largely assumed to be dynamically cold.

Macchetto et al. (1997) reobserved the circumnuclear disk of M 87 with the long-slit mode of the Faint Object Camera (FOC), using a $0\farcs063\times13\farcs5$ slit positioned on the center and in two parallel, flanking positions. Apart from the higher spatial resolution of the FOC, the new data provided much improved spatial coverage to better map the distribution of the gas. This is essential to establish the detailed kinematics of the nuclear disk. Moreover, these authors demonstrated the importance of considering the instrumental effects of the telescope PSF and finite slit size, as well as folding into the analysis the spatial distribution of the line emission. As with the FOS observations, the line widths were broader than the instrumental resolution, but apparently they could be fit self-consistently with the radial velocities using a thin disk in Keplerian rotation about a central mass of $(3.2 \pm 0.9) \times 10^9\,M_\odot$.

However, gas dynamics have worse complications than we naively imagine. Requirements to apply it successfully are more stringent than we usually believe, and the probability that galaxies cooperate to meet these requirements turns out in hindsight to be disappointingly low. At a most basic level, gas must be distributed in radius to properly sample the BH sphere of influence. At the same time, the kinematics of the gas need to be ordered enough to be interpretable. Unlike stars, gas is a collisional fluid, and it responds to nongravitational perturbations such as turbulence, shocks, radiation pressure, and magnetic fields. Gas is easy to push around. Every galaxy must be scrutinized on a case-by-case basis to check *a posteriori* whether the gas has sufficiently settled into an equilibrium configuration whose kinematics are dominated by gravity. And there is a problem that is not often considered: dust absorption may make the gas distribution opaque enough so that we cannot assume that we see through it in projection.

Unfortunately, the majority of galaxies, especially disk systems, *do not* fulfill these requirements. Beginning with the seminal observation of M 84 = NGC 4374 by Bower et al. (1998), the long-slit capability of the Space Telescope Imaging Spectrograph (STIS) has been used to map the circumnuclear regions of relatively large numbers of nearby galaxies. Most efforts have focused on the bulges of early- to mid-type S0 and spiral galaxies (e. g., Hughes et al. 2005; Shields et al. 2007), but ellipticals have also been observed (Noel-Storr et al. 2003). While these efforts have yielded a number of BH discoveries and masses (Barth et al. 2001; Sarzi et al. 2001; Verdoes Kleijn et al. 2002; Devereux et al. 2003; Marconi et al. 2003; Atkinson et al. 2005; Coccato et al. 2006; De Francesco, Capetti, & Marconi 2006, 2008; Pastorini et al. 2007; Dalla Bontà et al. 2009; Walsh, Barth, & Sarzi 2010), the success rate of these programs has been much lower than was anticipated. Fewer than 20% of randomly selected nearby bulges have regular, symmetric velocity fields amenable to dynamical analysis. Preselection by narrow-band imaging or dust-lane morphology boosts the chances of finding promising candidates (Ho et al. 2002), but morphological regularity does not guarantee that velocities are well behaved. E. g., NGC 3379 has a regular-looking nuclear gas disk, but it shows strong non-circular motions that are difficult to interpret (Shapiro et al. 2006). Another challenge is the determination of disk orientations. The inclination angles of disks are often poorly constrained using just their kinematics. Then we resort to the morphological appearance of the gas or dust distribution on resolvable scales. The assumption that the gas is coplanar is unlikely always to hold, especially in cases where the disk appears warped. Patchy emission and dust obscuration complicate matters further. Because $M_\bullet \propto 1/\sin^2 i$, a significant fraction of the final error budget in the mass estimate comes from the uncertainty in the disk orientation.

As a consolation prize, the low success rate of gas-kinematic programs has yielded a collection of more than 100 $M_\bullet$ upper limits (Sarzi et al. 2002; Verdoes Kleijn, van der Marel, & Noel-Storr 2006; Beifiori et al. 2009). With a typical detection sensitivity of a few$\times10^6\,M_\odot$, these limits provide useful constraints on the BH–host-galaxy scaling relations, especially for galaxy types that are sparsely populated by current detections (Beifiori et al. 2012).

Even when emission-line gas clearly rotates about the center, it almost always shows line widths that are substantially larger than instrumental and thermal broadening. These velocity dispersions usually increase toward the center, and they can be comparable to the rotation velocities, ranging from $\sigma/v \lesssim 0.3$ to $\sigma/v \gg 1$ (e. g., Verdoes Kleijn et al. 2000; Barth et al. 2001; Dalla Bontà et al. 2009). In some galaxies, the observed line widths can be attributed to unresolved rotation (e. g., M 87: Macchetto et al. 1997; NGC 3998: De Francesco, Capetti & Marconi 2006), but excess dispersion is definitely present in others (e. g., NGC 3245: Barth et al. 2001; NGC 4374: Walsh, Barth, & Sarzi 2010). The nature of this intrinsic gas dispersion is not understood. It is the biggest systematic uncertainty that plagues gas-based BH mass estimates. There is no universal agreement about whether gas velocity dispersions are dynamically important or about how to deal with them. The problem lies in their physical interpretation. If the line widths arise from nongravitational processes such as local turbulence (e. g., van der Marel & van den Bosch 1998b), then they can be

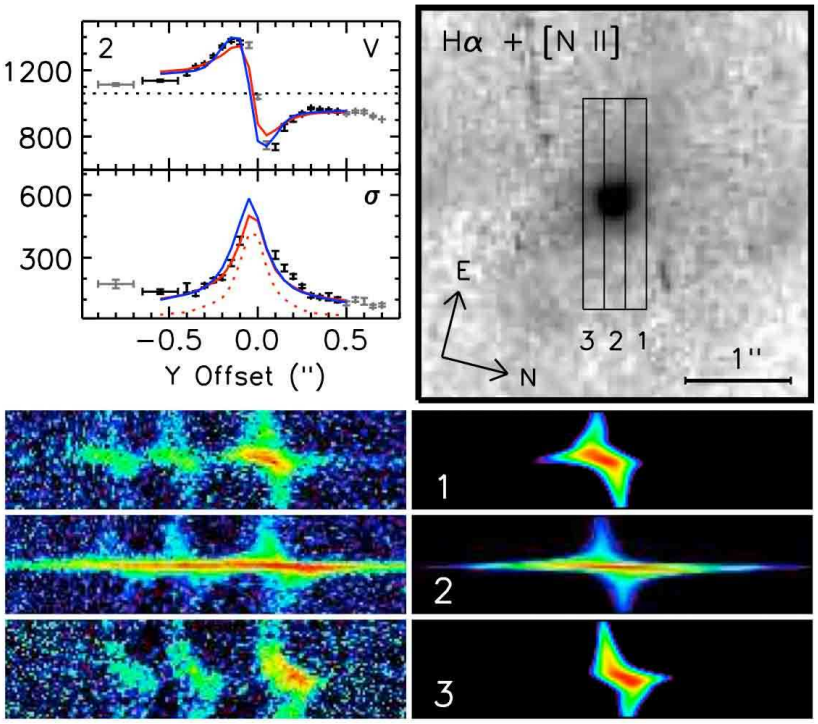

Figure 6

STIS observations of NGC 4374 (Bower et al. 1998) as analyzed by Walsh, Barth, & Sarzi (2010). The top-right panel is a WFPC2 continuum-subtracted Hα+[N II] image showing the nuclear disk of ionized gas. The footprints of the three slits are overlaid. The top-left panels show the radial profiles of [N II] λ6583 mean velocity and velocity dispersion (in km s^{-1}) along the central slit position. Superposed are predictions of the best BH model with (*blue curve*) and without (*red solid curve*) correction for asymmetric drift. The red dotted curve shows the contribution from rotational line broadening; because these velocity dispersions are smaller than the ones observed, the intrinsic velocity dispersion must be significant. The bottom panels show the continuum-subtracted, two-dimensional STIS spectra of the Hα+[N II] region (*left*) and the synthetic spectra of [N II] λ6583 (*right*). The vertical axis is the spatial direction, and the horizontal axis shows wavelength increasing toward the right. The three slit positions correspond to the locations labeled in the top grey-scale image.

neglected in the mass models. Alternatively, the line widths may measure the internal velocity structure of a dynamically hot distribution of clouds. Then the dispersion contributes to the hydrostatic support of the gas against gravity, and the observed mean rotation velocity is less than the circular velocity. Not accounting for this "asymmetric drift" then causes us to underestimate the central mass.

Walsh, Barth, & Sarzi (2010) reanalized the Bower et al. (1998) STIS observations of NGC 4374 following the techniques of Barth et al. (2001). Their model fully accounts for the propagation of line profiles through the HST and STIS optics. It reproduces the distinctive rise toward the center in the rotation curve and also the large and complicated line widths (**Figure 6**). Note that, among all galaxies whose gas kinematics have been studied with HST, NGC 4374 is the only object whose BH sphere of influence is well enough resolved to show Keplerian rotation, $V(r) \propto r^{-1/2}$. The best-fit model requires an intrinsic velocity dispersion, which the authors model as asymmetric drift, using analysis machinery that is familiar from stellar dynamics (Barth et al. 2001). The resulting BH mass, $M_\bullet = 9.3^{+1.0}_{-0.9} \times 10^8\,M_\odot$ (**Table 2**), is significantly smaller than Bower's original value of $1.6^{+1.2}_{-0.7} \times 10^9\,M_\odot$, but it is a factor of two larger than the result obtained when asymmetric drift is neglected.

Strictly speaking, the formalism for the asymmetric drift correction is only valid in the limit $\sigma/v \ll 1$ (Binney & Tremaine 2008). NGC 4374 has $\sigma/v \approx 0.4 - 0.6$ and so approximately fulfills this condition. So does NGC 3245, whose disk has $\sigma/v < 0.35$ (Barth et al. 2001). Its applicability, however, is more suspect in some giant ellipticals, which have $\sigma/v > 1$. Where do we go from here? Our options are quite limited under these circumstances. As a limiting – if unrealistic – case, we can ascribe all of the observed velocity dispersion to gravity and treat the gas as a spherical, isotropic distribution of collisionless cloudlets governed by the Jeans equation. This approach typically yields masses that are factors of $\sim 3 - 4$ larger than the opposite limiting case of a pure thin disk (e. g., Verdoes Kleijn et al. 2000; Cappellari et al. 2002). The truth lies in between. A physically better motivated but still tractable alternative is to consider a kinematically hot disk with an isotropic pressure. This is the model employed by Häring-Neumayer et al. (2006) and Neumayer et al. (2007) for NGC 5128.

Given the many problems that cloud the reliability of gas-dynamical models, it is crucial that BH masses derived using this technique be verified independently. Stellar-dynamical masses provide a cross-check. Eight galaxies (not counting the Milky Way) have been studied using both methods. We do not include NGC 3227 and NGC 4151 because their bright active nuclei make the dynamical modeling especially challenging for both gas (Hicks & Malkan 2008) and stars (Davies et al. 2006; Onken et al. 2007). **Figure 7** compares the BH mass measurements for the remaining objects. At first glance, the results do not look encouraging. The scatter is large and most of the gas-based masses are systematically smaller than the star-based masses. To be fair, three of the objects (plotted as open symbols) do not provide stringent tests because of difficulties involving one or both of the masses estimates (IC 1459: Cappellari et al. 2002; NGC 3379: Shapiro et al. 2006; NGC 4335: Verdoes Kleijn et al. 2002). Removing these three helps to bring the two sets of measurements into better agreement at the expense of decimating an already small sample to the point that we cannot conclude much that is statistically meaningful.

Still, three points deserve notice. The two spiral galaxies (M 81 and NGC 4258) lie reasonably close to the 1:1 line, although the relatively large uncertainty of the mass based on ionized gas kinematics for NGC 4258 (Pastorini et al. 2007) precludes a rigorous comparison with the stellar-dynamical mass from Siopis et al. (2009). The excellent agreement for M 81 comes as a bit of a surprise, considering the preliminary nature of the stellar-dynamical mass (Bower et al. 2000) and the highly simplified analysis applied to the gas data (Devereux et al. 2003). The gas kinematics of

NGC 5128 (Cen A) have been revisited many times using both ground-based and HST observations (Marconi et al. 2001, 2006; Häring-Neumayer et al. 2006; Krajnović, Sharp & Thatte 2007). The latest efforts by Neumayer et al. (2007) give a gas-dynamical mass that is a factor of 4 smaller than the stellar-dynamical mass from Silge et al. (2005). But it agrees well with the mass from Cappellari et al. (2009), which is based on the same set of AO data used for the gas analysis. These results are listed and discussed further in the notes to **Table 2**.

The two most worrisome points are those for M 87 and NGC 3998. As illustrated in **Figure 12**, their gas-based BH masses are almost factors of 2 and 4 smaller than their star-based masses, respectively (Gebhardt et al. 2011; Walsh et al. 2012). The ionized gas disks of both of these objects display very large line widths, up to FWHM $\gtrsim 1000$ km s^{-1} near the centers. Is asymmetric drift to blame for the systematically smaller gas-based masses? Upward $M_\bullet$ corrections by factors of 2 – 4 are certainly plausible for some galaxies (Verdoes Kleijn et al. 2000; Häring-Neumayer et al. 2006; Walsh, Barth & Sarzi 2010), although, according to Macchetto et al. (1997) and De Francesco, Capetti, & Marconi (2006), rotational broadening alone can reproduce the observed line widths in these two objects. Gas-dynamical analyses in general urgently need to be checked.

In view of all this, it is legitimate to question the accuracy of BH masses that are based on ionized gas kinematics when broad emission lines were not explicitly taken into account. **Tables 2** and **3** list 16 galaxies analyzed using ionized gas techniques. The most massive ellipticals are of special concern. Their nuclear spectra not only show large line widths, but their kinematics often suggest the presence of substantial random motions (Noel-Storr et al. 2003; Noel-Storr, Baum, & O'Dea 2007) presumably agitated by nongravitational forces associated with radio jets (Verdoes Kleijn, van der Marel, & Noel-Storr 2006). Section 6.3 compares the gas-based BH masses systematically against the BH mass correlations determined using other techniques. We conclude there that $M_\bullet$ values determined from ionized gas kinematics that do not include corrections for large line widths are systematically underestimated. We regard the BH discoveries in these objects as legitimate, and we list them in **Tables 2** and **3**, but we list them in turquoise color. We omit them from all correlation diagrams subsequent to **Figure 12**, and we omit them from all correlation fits.

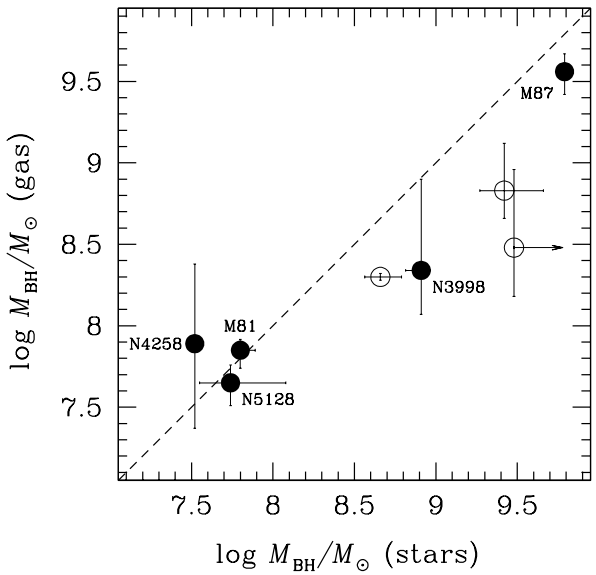

Figure 7

Comparison between BH masses derived from gas and stellar dynamics. Three objects (*open circles*) do not have sufficiently accurate masses from one or both of the methods.

3.3 Maser dynamics of molecular gas

The Miyoshi et al. (1995) study of the Keplerian central rotation curve of NGC 4258 established radio interferometry of water maser emission from circum-BH molecular gas disks as one of the most powerful techniques of measuring BH masses. In favorable cases, it is reliable; it reaches angular radii of a few milliarcsec (two dex better than almost all other techniques), and it is most useful in just the galaxies – gas-rich, optically obscured, star-forming, and often with AGN emission – that cannot be studied well by other techniques. Excellent angular resolution is particularly important because these galaxies tend to have small BHs. Maser dynamics greatly strengthen both the accuracy and the dynamic range of our $M_\bullet$ measurements.

The early success in NGC 4258 was reviewed in KR95 and updated in Moran (2008). We review this story as the prototypical example of two independent ways of using masers to measure $M_\bullet$, (§ 3.3.1) using the Keplerian rotation curve of the non-systemic-velocity components and (§ 3.3.2) using the drift and centripetal acceleration of the near-systemic components. Section 3.3.3 reviews the main complication: masing molecular disks often have masses that are comparable to $M_\bullet$.

NGC 4258 is a normal SABbc (**Figure 8**), one of the latest-type galaxies that has a classical bulge (Siopis et al. 2009). Kormendy & Bender (2013b) derive $B/T = 0.12 \pm 0.02$. NGC 4258 is a Seyfert 1.9 (Ho, Filippenko, & Sargent 1997a) with curved radio jets (Cecil et al. 2000; cf. van der Kruit, Oort, & Mathewson 1972) shown in the middle panel of **Figure 8**. They are believed to be responsible for the similarly-curved, "anomalous" Hα spiral arms (e. g., Cecil, Wilson, & De Pree 1995) and the nearly-coincident X-ray emission (Yang et al. 2007; right panel of **Figure 8**). How the jets heat the disk is complicated, because they curve out of the disk plane. The important point here is that, at $r \lesssim 0.1$ pc, the jets have PA $\simeq -3°$ and are perpendicular to the masing gas disk (Cecil et al. 2000). Its orientation, structure, and rotation curve are illustrated in **Figure 9**.

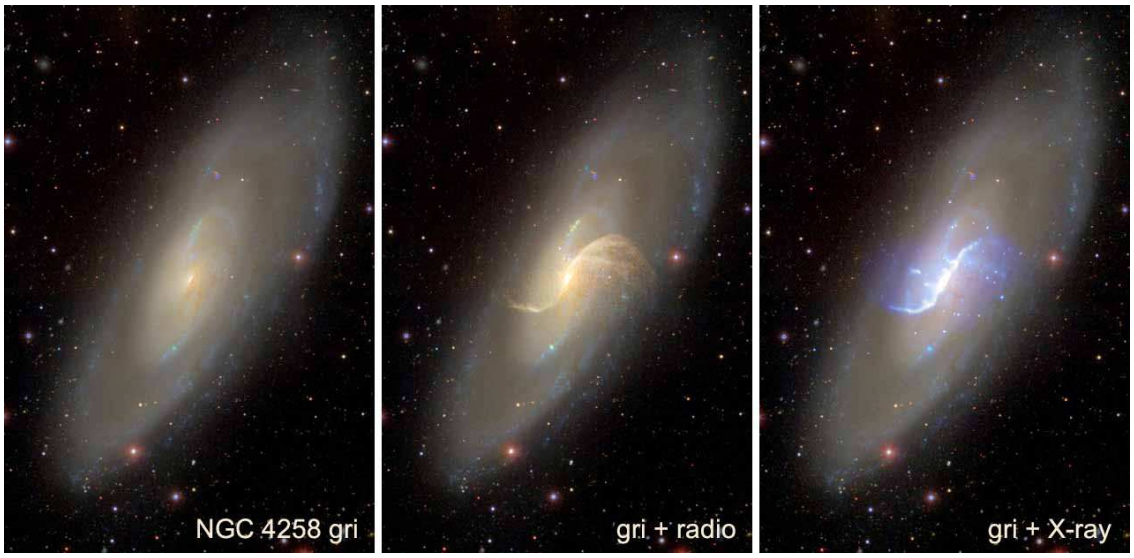

Figure 8

NGC 4258 (*left*) in an Sloan Digital Sky Survey (SDSS) *gri* color image from NED, (*center*) with the addition in orange of the image of the radio jet (Cecil et al. 2000), and (*right*) with the addition instead and in blue of the X-ray image from Yang et al. (2007). The radio and X-ray images are from **http://chandra.harvard.edu/photo/2007/ngc4258**. The right side of the galaxy is the near side; the north = top side is receding. The maser disk has PA $\simeq 84°$, and the east = left side is receding. The maser disk therefore counter-rotates with respect to the main galaxy disk.

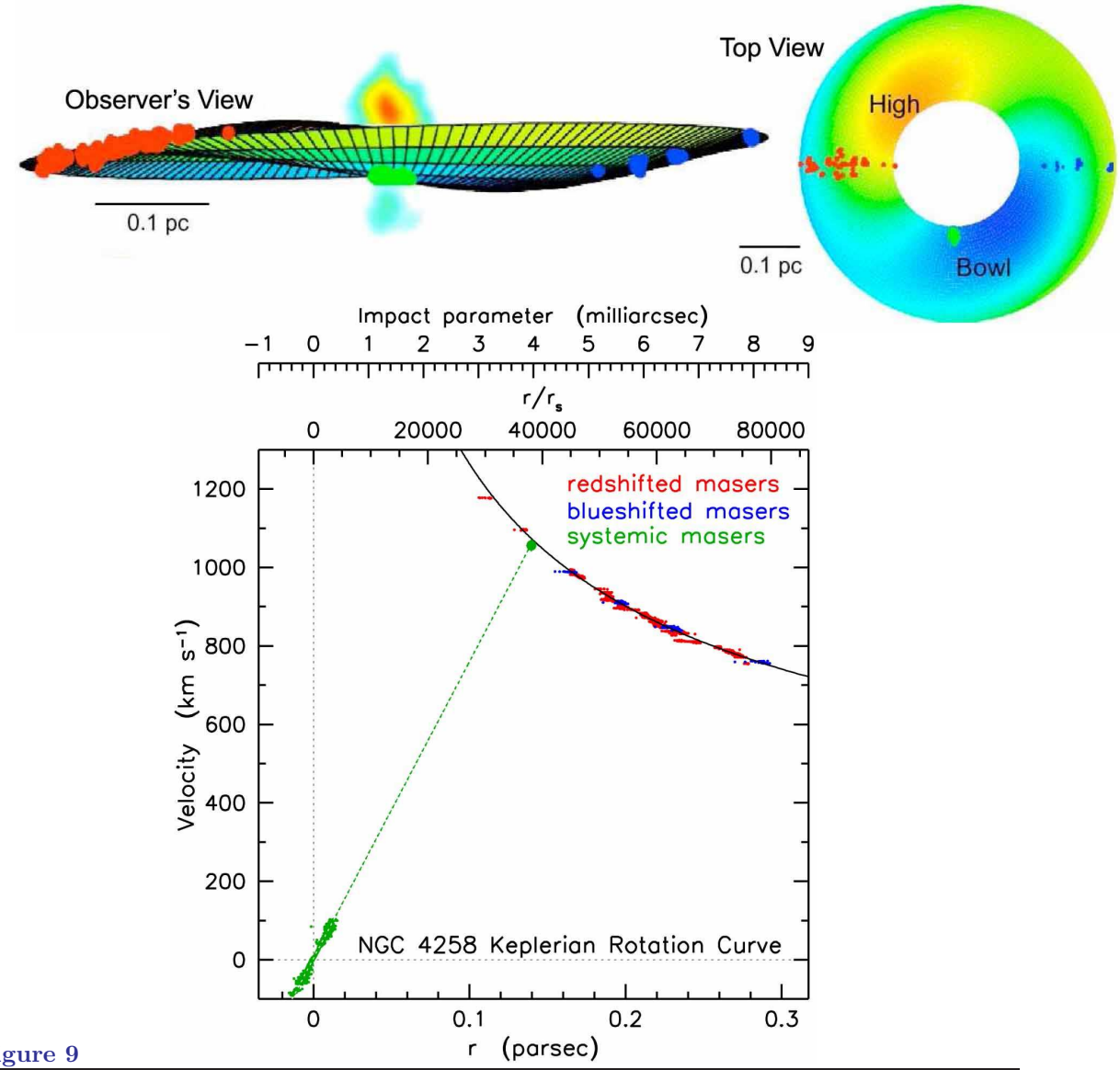

Figure 9

(*top*) Schematic views of the almost-edge-on, warped maser disk of NGC 4258 (from Moran 2008) with warp parameters from Herrnstein et al. (2005) and including the inner contours of the radio jet. The relative positions of the receding, near-systemic, and approaching masers are indicated by red, green, and blue spots, respectively. Differences in line-of-sight projection corrections to the slightly tilted maser velocities account for the departures in the high-$|V|$ masers from exact Keplerian rotation. The near-systemic masers are seen tangent to the bottom of the maser disk bowl along the line of sight. They drift from right to left in ~ 12 years across the green patch where amplification is sufficient for detection; this patch subtends $\pm 4°$ as seen from the center (Moran 2008).
(*bottom*) NGC 4258 rotation curve $V(r)$ versus radius in units of pc (*bottom axis*), Schwarzschild radii (*top axis*), and milliarcsec (*extra axis*). The black curve is a Keplerian fit to 4255 velocities of red- and blue-shifted masers (*red and blue dots*). The small green points and line show 10036 velocities of near-systemic masers and a linear fit to them. The green filled circle is the corresponding mean $V(r)$ point (§ 3.3.2). The maser data are taken from Argon et al. (2007).

3.3.1. Keplerian Rotation Curve of the Non-Systemic Masers. The high-velocity masers in NGC 4258 (*red and blue points* in **Figure 9**) almost exactly have $V \propto r^{-1/2}$, so it is likely (but not quite guaranteed: § 3.3.3) that the disk mass is negligible and that $M_\bullet = V^2 r/G$. Here, $V(r)$ was constructed by assuming that all masers move exactly toward or away from us. The illustrated fit is $V(r) = 2083/\sqrt{r} + 27$ km s^{-1}, where r is in milliarcsec. The fit is not quite Keplerian, and the innermost masers fall slightly below the curve. This simplest fit gives $M_\bullet = 3.65 \times 10^7\ M_\odot$.

Herrnstein et al. (2005) "*find* $\sim 2\sigma$ *evidence for deviation from Keplerian rotation in the NGC 4258 disk, with a preferred rotation law of* $r^{-0.48\pm0.01}$" (their emphasis). "This amounts to a total flattening in the high-velocity rotation curve of about 9.0 km s^{-1} across the high-velocity masers." This is the inward flattening in **Figure 9**. Herrnstein and collaborators investigate several possible explanations, including the effects of a central dark cluster with finite radius or alternatively a massive accretion disk. Their preferred explanation is that the true rotation curve is exactly Keplerian but that the 9 km s^{-1} total apparent departure from a Keplerian is accounted for by projection corrections applied to differently tilted velocities of masers in a thin disk that is differently almost edge-on at different radii. Herrnstein et al. (2005) fit a warped-disk geometry to the maser positions (**Figure 9,** *top*) and find that the disk inclination varies from 81.°4 at $r = 3.9$ milliarcsec to $\sim 91°$ at $r = 9.1$ milliarcsec. Then the true rotation curve is Keplerian and the central mass is $M_\bullet = (3.81 \pm 0.01) \times 10^7\ M_\odot$ for our adopted distance of 7.27 Mpc (**Table 3**). However, the error bars depend on the assumptions that the adopted geometry is correct and that the angles between the galactocentric radius vectors of the masers and our lines of sight are all 90°. In view of the uncertainties in the assumptions, we adopt the above BH mass but use as the error bar the RMS of the mass determinations from the pure Keplerian fit, the central cluster model, the massive disk model, and the preferred warp model. The result is $M_\bullet = (3.81 \pm 0.04) \times 10^7\ M_\odot$.

3.3.2. Rotation Curve of the Near-Systemic Masers. We can also derive $M_\bullet$ independently of the non-systemic-velocity components using only the near-systemic masers. To do this, we need measurements of the centripetal acceleration $V(r)^2/r$ and the linear velocity gradient along the line of central masers. The latter is measured in km s^{-1} milliarcsec^{-1} but is easily converted to km s^{-1} pc^{-1} using the assumed distance. It is then V/r. This can be done for every individual maser source that provides both an acceleration and a drift measurement, so it could be used to measure $V(r)$. Here, we derive $M_\bullet$ from the ensemble of 10036 systemic masers plotted in **Figure 9**. We derive their mean V = (acceleration)/(drift) and hence r and the single $V(r)$ point that is plotted as the filled green circle in the figure. Given that the masers are projected nearly in the direction to the center, the only assumption is that they are in circular motion around the center.

This method was used in early papers written before the high-$|V|$ masers in NGC 4258 were discovered (Haschick, Baan, & Peng 1994; Watson & Wallin 1994). However, it has been overpowered by the appeal of the Keplerian rotation curve of the high-$|V|$ components, and it does not seem to have been used since their discovery. For NGC 4258, this method provides important verification that the maser orbits are circular. In other galaxies in which high-velocity masers are not discovered, it nevertheless can provide $M_\bullet$ (caveat § 3.3.3), especially if $V(r)$ can be measured. Mass measurements using near-systemic maser components, although less accurate than ones based on well-defined high-$|V|$ rotation curves, are nevertheless often more accurate than ones based on (say) stellar dynamics. These measurements deserve a place in our BH sample.

For the systemic masers, we measure a mean drift of $V = (266.5 \pm 0.3)$ km s^{-1} milliarcsec^{-1} (*green dashed line* in **Figure 9**). We adopt the mean of 12 measurements of the centripetal accelerations listed in Table 4 of Humphreys et al. (2008), $V^2/r = (8.17 \pm 0.12)$ km s^{-1} yr^{-1}. Including a 1 % correction (to r) for the 8° tilt of the maser disk, $M_\bullet = (3.65 \pm 0.09) \times 10^7\ M_\odot$.

We adopt the weighted mean of the two independent results, $M_\bullet = (3.78 \pm 0.04) \times 10^7\ M_\odot$.

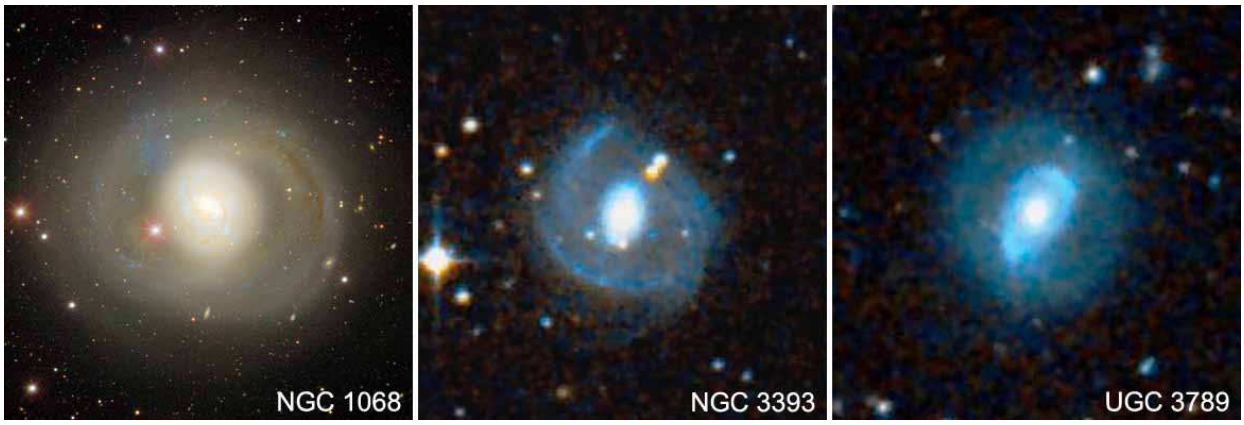

Figure 10

Three almost-face-on galaxies that contain edge-on maser disks. All three show the two nested ovals of different surface brightness, axial ratio, and position angle that identify oval disks (Kormendy 1982; Kormendy & Kennicutt 2004). Their axial ratios (face-on $b/a \sim 0.8$) and PAs (perpendicular to each other) imply that all three galaxies are not far from face-on. All three contain pseudobulges; $PB/T \simeq 0.30$, 0.27 ± 0.06, and 0.32 ± 0.03 in NGC 1068, NGC 3393, and UGC 3789, respectively. NGC 1068 and NGC 3393 are well-known Seyfert 2 galaxies, and the high-excitation narrow-line spectrum of UGC 3789 implies that it also contains a Seyfert 2 nucleus. NGC 1068 is from the SDSS. The others are from the Digital Sky Survey via **http://www.wikisky.org**; these have much bluer color balances than the SDSS. NGC 1068 is an Sb; the other galaxies are Sab in Hubble type.

Within errors, the rotation curve of NGC 4258 from the high-velocity masers agrees with the single point, $V(0.140 \pm 0.002 \text{ pc}) = (1055 \pm 15)$ km s^{-1} (*filled green circle* in **Figure 9**), derived from the systemic masers. This confirms that the masers are in circular orbits around the BH. The check is relevant, because eccentric disks are easily possible at $r \ll r_{\rm infl}$ (Tremaine 1995).

Published data allow a similar comparison of a Keplerian rotation curve from high-$|V|$ masers with a single $V(r)$ measurement from near-systemic masers for only one other galaxy. This is the face-on oval galaxy UGC 3789 shown in **Figure 10**. Reid et al. (2009), Braatz et al. (2010), and Kuo et al. (2011) show that the galaxy contains an edge-on masing disk with a rotation curve that is essentially as clean and Keplerian as that of NGC 4258. From these data, Braatz et al. (2010) derive a distance of 49.9 ± 7.0 Mpc. Then $V(r) = 440.4 \pm 3.0$ km s^{-1} mas$^{1/2}$ and the gravitating mass is $M = (1.09 \pm 0.15) \times 10^7\ M_\odot$ (Braatz et al. 2010). Kuo et al. (2011) reanalyze the same data with a different dynamical center and obtain $(1.12 \pm 0.05) \times 10^7\ M_\odot$.

Braatz et al. (2010) show that the near-systemic masers are divided into two groups with different velocities and accelerations. They therefore lie in rings at different galactocentric radii. For "ring 1", they find an acceleration of 1.50 ± 0.13 km s^{-1} yr^{-1} and a velocity drift of 695 ± 65 km s^{-1} mas^{-1}. Ring 2 shows acceleration of 4.96 ± 0.34 km s^{-1} yr^{-1} and velocity drift of 1654 ± 440 km s^{-1} mas^{-1}. From these, we derive two $V(r)$ and M values that are independent of each other and of the results from the high-$|V|$ masers. Ring 1 implies that $V(0.179 \pm 0.028 \text{ pc}) = 513 \pm 59$ km s^{-1}, compared with 513 ± 3 km s^{-1} expected from the high-$|V|$ masers. Ring 2 implies that $V(0.11 \pm 0.04 \text{ pc}) = 712 \pm 196$ km s^{-1}, compared with 671 ± 5 km s^{-1} from the high-$|V|$ masers. The ring 1 value confirms that these masers are accurately in circular motion around the center. Rings 1 and 2 imply that the gravitating mass is $M = (1.09 \pm 0.26) \times 10^7\ M_\odot$ and $M = (1.23 \pm 0.67) \times 10^7\ M_\odot$, respectively. Ring 1 accurately confirms the mass implied by the high-$|V|$ masers. For NGC 4258, which also has a Keplerian rotation curve, we identified this gravitating mass as $M_\bullet$. This turns out to be valid (Huré et al. 2011). Here, we consider a caveat—finite maser disk mass—before we decide on $M_\bullet$.

3.3.3. Molecular Disks With Masses $M_{disk} \sim M_\bullet$ prove to be the major complication of maser BH measurements. For example, NGC 1068 (**Figure 10**) has a sub-Keplerian rotation curve, $V(r) \propto r^{-0.31\pm0.02}$ (Greenhill et al. 1996). Possible explanations include massive molecular disks (Huré 2002; Lodato & Bertin 2003; Huré et al. 2011), nuclear star clusters with radii comparable to those of the gas disks (Kumar 1999), and disk warps. In many cases, warps are disfavored, because the masers are observed with VLBI to lie along a thin straight line. Nuclear clusters are more difficult to exclude. Masers are almost necessarily associated with high obscuration. Many of these galaxies also contain AGNs. So we do not generally have photometric constraints on nuclear star clusters. We only have indirect hints from observations of nearby, non-masing galaxies. But in large, late-type galaxies, nuclei with masses of 10^6 to $10^{7.5}$ $M_\odot$ and effective radii of 0.3 to 10 pc similar to the radii of maser disks are common (Walcher et al. 2005; Kormendy et al. 2010). Still, it is astrophysically plausible that maser disks have significant mass, and most attention has been give to this alternative. The differences in mass contributions by disks and by spherical clusters are several tens of percents. It would be prudent to keep in mind that quoted $M_\bullet$ values may be overestimated and that quoted errors based on analyses of massive disks may be underestimated. With this caveat, we review $M_\bullet$ measurements based on the approximation that departures from Keplerian rotation are due to massive molecular disks.

Huré et al. (2011) emphasize that the rotation curve $V^2 = GM_\bullet/r + rd\Phi_{disk}/dr$ of a BH plus accretion disk is in general not a power law in radius. Also, the disk potential Φ_{disk} is complicated (Binney & Tremaine 1987, 2008). For practical reasons, different authors make different simplifying assumptions. Lodato & Bertin (2003) assume that the disk is self-regulated at the threshold of axisymmetric Jeans instability in the presence of rotation, $Q \equiv c_s\kappa/\pi G\Sigma = 1$, where c_s is the sound speed, κ is the epicyclic frequency, and Σ is the disk surface density. This involves poorly known physics. In contrast, Huré et al. (2011) develop a formalism to deal with massive accretion disks that surround point masses on the basis of the mathematically tractable assumption that the disk surface density is $\Sigma \propto r^{-s}$, where $0 \lesssim s \lesssim 3$ is astrophysically plausible (see their discussion) and adequate to fit real data. NGC 1068 provides an example. For distance $D = 15.9$ Mpc, Lodato & Bertin (2003) find that $M_{disk} = (9.5 \pm 0.6) \times 10^6$ $M_\odot$ and that $M_\bullet = (8.9 \pm 0.3) \times 10^6$ $M_\odot$. Similarly, Huré et al. (2011) get $M_{disk} = 12.1 \times 10^6$ $M_\odot$ and $M_\bullet = (8.0 \pm 0.3) \times 10^6$ $M_\odot$. Huré (2002) also finds similar results with a more specialized disk model. We adopt the mean of the Lodato and Huré estimates, $M_\bullet = (8.39 \pm 0.44) \times 10^6$ $M_\odot$.

NGC 1068 and similar galaxies below raise a concern about $M_\bullet$ as measured with lower (e. g., HST) spatial resolution in late-type galaxies that could contain substantial nuclear gas. Even if the measurement of the contained mass is correct, any BH could have a significantly smaller mass. For example, we reject the $M_\bullet$ measurement in the Sc galaxy NGC 3079 because the maser rotation curve is flat (Kondratko, Greenhill & Moran 2005). Better constrained maser $M_\bullet$ measurements add important dynamic range to our demographic results, but we retain them with due caution.

Returning to UGC 3789: Despite the convincingly Keplerian rotation curve (Reid et al. 2009; Kuo et al. 2011), Huré et al. (2011) find a clean solution in which $M_{disk}/M_\bullet \simeq 0.77$. They therefore suggest that $M_\bullet = 0.81 \times 10^7$ $M_\odot$. The difference between this value and the total gravitating mass M derived in § 3.3.2 affects no conclusions in this paper. We will be conservative and adopt the mean, using the difference as an error estimate. Thus we adopt $M_\bullet = (9.65 \pm 1.55) \times 10^6$ $M_\odot$.

Two objects analyzed by Huré et al. (2011) have $M_{disk} > M_\bullet$. IC 1481 has $M_{disk} = 3.55 \times 10^7$ $M_\odot$ and $M_\bullet = 1.30 \times 10^7$ $M_\odot$. It proves to be a merger in progress, so the galaxy is listed in **Table 2** and discussed in the Table notes for elliptical galaxies. NGC 3393 (*middle panel* of **Figure 10**) has $M_{disk} \sim 6M_\bullet$ according to Huré et al. (2011). Particulars are discussed in the **Table 3** notes for galaxies with pseudobulges.

The galaxies illustrated in **Figure 10** are remarkably similar and serve to emphasize an important puzzle about BHs. Each BH is embedded in an edge-on accretion disk that is nearly perpendicular to the disk of the host galaxy. Each host galaxy is oval and contains a pseudobulge that is growing secularly. It is easy to identify a global mechanism that feeds gas toward the center. So why are the angular momentum vectors of this gas and the gas in the accretion disk almost perpendicular? Maser disks (Greenhill et al. 2009) and, more generally, AGN jets (Kinney et al. 2000) are oriented randomly with respect to their host galaxies. In NGC 4258, the maser disk even counter-rotates with respect to the host galaxy (**Figure 8**).

Note that, if the mass of the accretion disk is comparable to or larger than the mass of the BH, the answer is not that the spinning BH tips the accretion disk until it is in the BH's equatorial plane.

3.3.4. Other Maser BH Cases. Greenhill (2007) reviews the early history of maser detections in galaxies. Finding maser disks is difficult, not least because they must be edge-on, and the orientation of the host galaxy gives no clue about when this is the case. After the spectacular start with NGC 4258, further progress was slow. Other early detections not reviewed above include Circinus and NGC 4945. They are discussed in the notes to **Table 3**.

Now, progress on this subject is accelerating, in part because of the advent of the highly sensitive Robert C. Byrd Green Bank Telescope of the National Radio Astronomy Observatory (Greene et al. 2010). Kuo et al. (2011) report maser disk detections and BH mass measurements in seven galaxies: NGC 1194, an edge-on S0 with a prominent classical bulge; NGC 2273, an unusual (RR)SB(rs)a galaxy with a small pseudobulge; UGC 3789 (§ 3.3.3 and **Figure 10**); NGC 2960, a merger in progress, hence listed in **Table 2** with ellipticals; NGC 4388 (edge-on SBbc); NGC 6264 (SBb), and NGC 6323 (SBab). The host galaxies are discussed in Greene et al. (2010) and Kormendy & Bender (2013b); parameters adopted here are from the latter paper. When necessary, summaries are given in the notes to **Table 3**. In all cases, the masers are distributed along lines indicative of edge-on disks with little or no warp. The radius range is large enough in all cases to reveal outward-decreasing rotation curves, and mostly, the evidence for a Keplerian disk is strong. The most uncertain case is NGC 4388. These galaxies are very important to BH demographic results at low $M_\bullet$ and especially to our understanding of BHs in pseudobulges (Greene et al. 2010; § 6.8 here).

Several more galaxies arguably have maser-based BH discoveries but $M_\bullet$ measurements that are not accurate enough for our sample. Promising objects are discussed by Wilson, Braatz & Henkel (1995), Kondratko, Greenhill & Moran (2006), and Greenhill et al. (2009). It is reasonable to expect rapid progress in this subject.

3.4 BH mass measurements for active galactic nuclei (AGNs)

Reverberation mapping and single-epoch spectroscopy of AGN broad emission lines now provide large numbers of BH masses for objects in which we cannot resolve $r_{\rm infl}$. They greatly extend the range in Hubble types, distances, and AGN luminosities of galaxies with BH demographic data. However, these methods require a dedicated review. Also, we use them only in a limited way in Section 7. Therefore we include only a short summary in the Supplementary Information.

4. CLASSICAL BULGES VERSUS PSEUDOBULGES

The morphological similarity between elliptical galaxies and giant bulges in disk galaxies (e. g., the Sombrero galaxy: **http://heritage.stsci.edu/2003/28/big.html**) is a well-known part of the Hubble classification scheme (Hubble 1930; Sandage 1961; de Vaucouleurs et al. 1991; Buta, Corwin, & Odewahn 2007). That similarity is quantitative: it includes fundamental plane and other parameter correlations (e. g., Bender, Burstein, & Faber 1992; Kormendy & Bender 2012). One of the biggest success stories in galaxy formation is the demonstration that these bulges and elliptical galaxies formed in the same way, when the dynamical violence of major galaxy mergers scrambles disks into ellipsoids. Extensive evidence is based on theory (Toomre & Toomre 1972; Toomre 1977), observations (e. g., Schweizer 1990), and numerical modeling (e. g., Barnes 1989, 1992). "By the time of the reviews of Schweizer (1990, 1998), Barnes & Hernquist (1992), Kennicutt (1998b), and Barnes (1998), the merger revolution in our understanding of elliptical galaxies was a 'done deal' " (Kormendy 2012). Since then, our picture of the formation of ellipticals has grown still richer, both observationally and through detailed modeling (see KFCB and Kormendy 2012 for reviews). When ellipticals accrete cold gas and grow new disks around themselves (Steinmetz & Navarro 2002), we stop calling them "ellipticals" and instead call them "bulges" (Renzini 1999). Thus merger-built bulges are well understood within our picture of galaxy formation. And they can be identified purely observationally. We refer to them as "classical bulges."

Beginning in the 1980s (e. g., Kormendy 1982), it became apparent that elliptical-galaxy-like classical bulges are not the only kinds of dense stellar systems found at the centers of disk galaxies. Another kind of "bulge" is distinguished observationally as having diskier properties than do classical bulges. Concurrent work on the slow ("secular") internal evolution of isolated disks showed that outward angular momentum transport by bars and other nonaxisymmetries dumps large amounts of gas into galaxy centers. The Schmidt (1959) – Kennicutt (1989, 1998a) observation that star formation rates increase rapidly with gas density then leads us to expect that gas infall feeds starbursts. Meanwhile, intense nuclear starbursts were observed preferentially in barred and oval galaxies. And they have timescales that are reasonable to grow disky bulge-like components similar to those seen in barred and oval galaxies. That is, we see the growth of these high-density, disky centers of galaxies in action. Gradually, the observed disky bulges and the theoretical evolution scenario were connected into a now-robust picture of internal galaxy evolution that complements hierarchical clustering. These often-disky central components are now known as "pseudobulges" to take account of their superficial similarity to classical bulges (with which they were often confused) while recognizing that they formed mainly by slow processes that do not involve major mergers. This subject is reviewed in Kormendy & Kennicutt (2004) and in Kormendy (1993b, 2012).

The distinction between classical and pseudo bulges is important because (Section 6.8) we find that classical bulges and ellipticals correlate closely with $M_\bullet$, but pseudobulges hardly correlate with BHs at all. Observational criteria that have nothing to do with BHs divide central components into two kinds that correlate differently with BHs. This is a substantial success of the secular evolution picture.

In **Tables 2** and **3** in the next section, (pseudo)bulge classifications and (pseudo)bulge-to-total luminosity ratios, B/T and PB/T, are taken from Kormendy & Bender (2013b). The observational criteria used to distinguish classical bulges from pseudobulges are listed in Kormendy & Kennicutt (2004). They have since been refined slightly via new observations; the criteria as used in Kormendy & Bender (2013b) and in this paper are listed in the Supplementary Information.

Classifications are more robust if they are based on many criteria. All of our classifications are based on at least two and sometimes as many as five criteria.

5. BH DATABASE

This section is an inventory of galaxies that have BH detections and $M_\bullet$ measurements based on stellar dynamics, ionized gas dynamics, CO molecular gas disk dynamics, or maser disk dynamics. **Table 2** lists ellipticals, including mergers-in-progress that have not yet relaxed into equilibrium. **Table 3** lists disk galaxies with classical bulges (upper part of table) and pseudobulges (lower part of table). The demographic results discussed in the following sections are based on these tables. Both tables are provided in machine-readable form in the electronic edition of this paper.

We reviewed the $M_\bullet$ measurements in Sections 2 and 3. Notes on individual objects in **Tables 2** and **3** follow the tables and provide more detail. Derivation of host galaxy properties is relatively straightforward for ellipticals as discussed in the notes and in Supplementary Information. These derivations are more complicated for disk-galaxy hosts, because (pseudo)bulge classification is crucial and because (pseudo)bulge – disk photometric decomposition is necessary. This work is too long to fit here; it is published in a satellite paper written in parallel with this review (Kormendy & Bender 2013b). Some details are repeated here in the table notes for the convenience of readers.

Implicit in the tables are decisions about which published $M_\bullet$ measurements are reliable enough for inclusion. No clearcut, objective dividing line separates reliable and questionable measurements. Our decisions are personal judgments. Our criteria are similar to those in Gültekin et al. (2009c); when we made a different decision, this is explained in the notes on individual objects. We try to be conservative. With a few exceptions that are not included in correlation fits, stellar-dynamical masses are retained only if they are based on three-integral models. Nevertheless (Section 3), it is likely that systematic errors – e. g., due to the neglect of triaxiality in giant ellipticals – are still present in some data. For this reason, we do not discuss correlation scatter in much detail. We do, however, derive the most accurate correlations that we can with present data (Section 6.6).

The sources of the adopted $M_\bullet$ measurements are given in the last column of each table, and earlier measurements are discussed in the notes on individual objects. The $M_\bullet$ error bars present a problem, because different authors present error bars with different confidence intervals. For consistency, we use approximate one-sigma standard deviations, i. e., 68 % confidence intervals. When authors quote two-sigma or three-sigma errors, we follow Krajnović et al. (2009) and estimate that one-sigma errors are N times smaller than N-sigma errors. Flags in Column 12 of **Table 2** and Column 19 of **Table 3** encode the method used to determine $M_\bullet$, whether the galaxy has a core (ellipticals only), and whether $M_\bullet$ was derived with models that include triaxiality or dark matter and large orbit libraries. Only the models of M 32, NGC 1277, and NGC 3998 include all 3.

We use a distance scale (Column 3) based mainly on surface brightness fluctuation measurements at small distances and on the WMAP 5-year cosmology at large distances ($H_0 = 70.5\,\mathrm{km\,s^{-1}\,Mpc^{-1}}$; Komatsu et al. 2009). Details are in the notes that follow **Tables 2** and **3**. Velocity dispersions σ_e (Colums 11 and 17 of **Tables 2** and **3**) are problematic; they are discussed in the table notes.

We discuss luminosity correlations only in terms of K_s-band absolute magnitudes. However, we also provide V magnitudes for the convenience of readers and because we use them to check the K_s magnitudes. Readers should view $(B-V)_0$ as a galaxy color that contains physical information but $(V-K)_0$ mainly as a sanity check of the independent V and K_s magnitude systems. Our K_s magnitudes are on the photometric system of the Two Micron All Sky Survey (2MASS: Skrutskie et al. 2006); the effective wavelength is ~ 2.16 μm. To good approximation, $K_s = K - 0.044$ (Carpenter 2001; Bessell 2005), where K is Johnson's (1962) 2.2 μm bandpass. Except in this paragraph and in the tables, we abbreviate K_s as K for convenience. **Tables 2** and **3** list K_s apparent magnitudes of the galaxies from the 2MASS Large Galaxy Atlas (Jarrett et al. 2003) or from the online Extended Source Catalog. Corrections (usually a few tenths of a mag) have been made for some of the brightest or angularly largest galaxies as discussed in the table notes.

Table 2 Supermassive black holes detected dynamically in 45 elliptical galaxies (December 2012)

Galaxy	Type	Distance (Mpc)	K_s	M_{KsT}	M_{VT}	$(V-K_s)_0$	$(B-V)_0$	$\log M_{\rm bulge}$ ($M_\odot$)	$M_\bullet$(low $M_\bullet$ – high $M_\bullet$) ($M_\odot$)	σ_e (km s^{-1})	Flags M C $M_\bullet$	Source
(1)	(2)	(3)	(4)	(5)	(6)	(7)	(8)	(9)	(10)	(11)	(12)	(13)
M 32	E2	0.805 7	5.10	−19.45	−16.64	2.816	0.895	9.05 ± 0.10	$2.45(1.43 - 3.46) \times 10^6$	77 ± 3	1 0 1	van den Bosch + 2010
NGC 1316	E4	20.95 1	5.32	−26.29	−23.38	2.910	0.871	11.84 ± 0.09	$1.69(1.39 - 1.97) \times 10^8$	226 ± 9	1 0 0	Nowak + 2008
NGC 1332	E6	22.66 2	7.05	−24.73	−21.58	3.159	0.931	11.27 ± 0.09	$1.47(1.27 - 1.68) \times 10^9$	328 ± 9	1 0 0	Rusli + 2011
NGC 1374	E0	19.57 1	8.16	−23.30	−20.43	2.874	0.908	10.65 ± 0.09	$5.90(5.39 - 6.51) \times 10^8$	167 ± 03	1 0 1	Rusli+2013
NGC 1399	E1	20.85 1	6.31	−25.29	−22.43	2.863	0.948	11.50 ± 0.09	$8.81(4.35 - 17.81) \times 10^8$	315 ± 03	1 1 0	see notes
NGC 1407	E0	29.00 2	6.46	−25.87	−22.89	2.980	0.969	11.74 ± 0.09	$4.65(4.24 - 5.38) \times 10^9$	276 ± 2	1 1 1	Rusli+2013
NGC 1550	E1	52.50 9	8.77	−24.87	−21.89	2.974	0.963	11.33 ± 0.09	$3.87(3.16 - 4.48) \times 10^9$	270 ± 10	1 1 1	Rusli+2013
NGC 2778	E2	23.44 2	9.51	−22.34	−19.39	2.955	0.911	10.26 ± 0.09	$1.45(0.00 - 2.91) \times 10^7$	175 ± 8	1 0 1	Schulze + 2011
NGC 2960	E2	67.1 9	9.78	−24.36	−21.30	3.068	0.880	11.06 ± 0.09	$1.08(1.03 - 1.12) \times 10^7$	166 ± 16	3 0 0	Kuo + 2011
NGC 3091	E3	53.02 9	8.09	−25.54	−22.56	2.980	0.962	11.61 ± 0.09	$3.72(3.21 - 3.83) \times 10^9$	297 ± 12	1 1 1	Rusli+2013
NGC 3377	E5	10.99 2	7.16	−23.06	−20.08	2.980	0.830	10.50 ± 0.09	$1.78(0.85 - 2.72) \times 10^8$	145 ± 7	1 0 1	Schulze + 2011
NGC 3379	E1	10.70 2	6.27	−23.88	−21.01	2.867	0.939	10.91 ± 0.09	$4.16(3.12 - 5.20) \times 10^8$	206 ± 10	1 1 1	van den Bosch + 2010
NGC 3607	E1	22.65 2	6.99	−24.79	−21.92	2.872	0.911	11.26 ± 0.09	$1.37(0.90 - 1.82) \times 10^8$	229 ± 11	1 1 0	Gültekin + 2009b
NGC 3608	E1	22.75 2	7.62	−24.17	−21.19	2.980	0.921	11.01 ± 0.09	$4.65(3.66 - 5.64) \times 10^8$	182 ± 9	1 1 1	Schulze + 2011
NGC 3842	E1	92.2 9	8.84	−25.99	−23.01	2.980	0.941	11.77 ± 0.09	$9.09(6.28 - 11.43) \times 10^9$	270 ± 27	1 1 1	McConnell + 2012
NGC 4261	E2	32.36 2	6.94	−25.62	−22.64	2.980	0.974	11.65 ± 0.09	$5.29(4.21 - 6.36) \times 10^8$	315 ± 15	2 1 0	Ferrarese + 1996
NGC 4291	E2	26.58 2	8.42	−23.72	−20.76	2.954	0.927	10.85 ± 0.09	$9.78(6.70 - 12.86) \times 10^8$	242 ± 12	1 1 1	Schulze + 2011
NGC 4374	E1	18.51 1	5.75	−25.60	−22.62	2.980	0.945	11.62 ± 0.09	$9.25(8.38 - 10.23) \times 10^8$	296 ± 14	2 1 0	Walsh + 2010
NGC 4382	E2	17.88 1	5.76	−25.51	−22.53	2.980	0.863	11.51 ± 0.09	$1.30(0.00 - 22.4\ ) \times 10^7$	182 ± 5	1 1 0	Gültekin + 2011
NGC 4459	E2	16.01 1	7.15	−23.88	−20.91	2.975	0.909	10.88 ± 0.09	$6.96(5.62 - 8.29) \times 10^7$	167 ± 8	2 0 0	Sarzi + 2001
NGC 4472	E2	16.72 1	4.97	−26.16	−23.18	2.980	0.940	11.84 ± 0.09	$2.54(2.44 - 3.12) \times 10^9$	300 ± 7	1 1 1	Rusli + 2013
NGC 4473	E5	15.25 1	7.16	−23.77	−20.89	2.874	0.935	10.85 ± 0.09	$0.90(0.45 - 1.35) \times 10^8$	190 ± 9	1 0 1	Schulze + 2011
M 87	E1	16.68 1	5.27	−25.85	−22.87	2.980	0.940	11.72 ± 0.09	$6.15(5.78 - 6.53) \times 10^9$	324^{+28}_{-12}	1 1 1	Gebhardt + 2011
NGC 4486A	E2	18.36 1	9.49	−21.83	−18.85	2.980	...	10.04 ± 0.09	$1.44(0.92 - 1.97) \times 10^7$	111 ± 5	1 0 0	Nowak + 2007
NGC 4486B	E0	16.26 1	10.39	−20.67	−17.69	2.980	0.991	9.64 ± 0.10	$6.\ (4.\ - 9.\ ) \times 10^8$	185 ± 9	1 0 0	Kormendy + 1997
NGC 4649	E2	16.46 1	5.49	−25.61	−22.63	2.980	0.947	11.64 ± 0.09	$4.72(3.67 - 5.76) \times 10^9$	380 ± 19	1 1 1	Shen+Gebhardt 2010
NGC 4697	E5	12.54 1	6.37	−24.13	−21.33	2.799	0.883	10.97 ± 0.09	$2.02(1.52 - 2.53) \times 10^8$	177 ± 8	1 0 1	Schulze + 2011
NGC 4751	E6	32.81 2	8.24	−24.38	−21.22	3.158	0.983	11.16 ± 0.09	$2.44(2.07 - 2.56) \times 10^9$	355 ± 14	1 0 1	Rusli + 2013
NGC 4889	E4	102.0 9	8.41	−26.64	−23.63	3.007	1.031	12.09 ± 0.09	$2.08(0.49 - 3.66) \times 10^{10}$	347 ± 5	1 1 1	McConnell + 2012
NGC 5077	E3	38.7 9	8.22	−24.74	−21.66	2.949	0.987	11.28 ± 0.09	$8.55(4.07 - 12.93) \times 10^8$	222 ± 11	2 1 0	De Francesco + 2008
NGC 5128	E	3.62 6	3.49	−24.34	−21.36	2.980	0.898	11.05 ± 0.09	$5.69(4.65 - 6.73) \times 10^7$	150 ± 7	1 1 0	Cappellari + 2009
NGC 5516	E3	55.3 9	8.31	−25.47	−22.50	2.970	0.993	11.60 ± 0.09	$3.69(2.65 - 3.79) \times 10^9$	328 ± 11	1 1 1	Rusli + 2013
NGC 5576	E3	25.68 2	7.83	−24.23	−21.29	2.939	0.862	11.00 ± 0.09	$2.73(1.94 - 3.41) \times 10^8$	183 ± 9	1 1 0	Gültekin + 2009b
NGC 5845	E3	25.87 2	9.11	−22.97	−19.73	3.238	0.973	10.57 ± 0.09	$4.87(3.34 - 6.40) \times 10^8$	239 ± 11	1 0 1	Schulze + 2011
NGC 6086	E	138.0 9	9.97	−25.74	−22.84	2.884	0.965	11.69 ± 0.09	$3.74(2.59 - 5.50) \times 10^9$	318 ± 2	1 1 1	McConnell + 2011b
NGC 6251	E1	108.4 9	9.03	−26.18	−23.18	2.998	...	11.88 ± 0.09	$6.14(4.09 - 8.18) \times 10^8$	290 ± 14	2 1 0	Ferrarese + 1999
NGC 6861	E4	28.71 2	7.71	−24.60	−21.42	3.179	0.962	11.25 ± 0.09	$2.10(2.00 - 2.73) \times 10^9$	389 ± 3	1 0 1	Rusli + 2013
NGC 7052	E3	70.4 9	8.57	−25.70	−22.86	2.841	0.86	11.61 ± 0.10	$3.96(2.40 - 6.72) \times 10^8$	266 ± 13	2 1 0	van der Marel + 1998b
NGC 7619	E3	53.85 2	8.03	−25.65	−22.83	2.821	0.969	11.65 ± 0.09	$2.30(2.19 - 3.45) \times 10^9$	292 ± 5	1 1 1	Rusli + 2013
NGC 7768	E4	116.0 9	9.34	−26.00	−23.19	2.811	0.906	11.75 ± 0.09	$1.34(0.93 - 1.85) \times 10^9$	257 ± 26	1 1 1	McConnell + 2012
IC 1459	E4	28.92 2	6.81	−25.51	−22.42	3.081	0.966	11.60 ± 0.09	$2.48(2.29 - 2.96) \times 10^9$	331 ± 5	1 0 0	Cappellari + 2002
IC 1481	E1.5	89.9 9	10.62	−24.17	...	...	...	...	$1.49(1.04 - 1.93) \times 10^7$	...	3 0 0	Huré + 2011
A1836 BCG	E	152.4 9	9.99	−25.95	−22.64	3.310	1.043	11.81 ± 0.10	$3.74(3.22 - 4.16) \times 10^9$	288 ± 14	2 1 0	Dalla Bontá + 2009
A3565 BCG	E	49.2 9	7.50	−25.98	−23.03	2.948	0.956	11.78 ± 0.09	$1.30(1.11 - 1.50) \times 10^9$	322 ± 16	2 1 0	Dalla Bontá + 2009
Cygnus A	E	242.7 9	10.28	−26.77	−23.23	3.54	...	...	$2.66(1.91 - 3.40) \times 10^9$	270 ± 90	2 1 0	Tadhunter + 2003

Column 1 is the galaxy name; BCGs are brightest cluster galaxies in the Abell clusters named. Cyan listings are not included in the fits (Section 6.3).
Column 2 is Hubble type (mostly RC3). Green lines are for mergers in progress (Section 6.4). If only $M_\bullet$ is cyan, we accept it but do not include it in the correlation fits (see Section 6.6).
Column 3 is the assumed distance from the following sources, starting with the highest-priority sources:
(1) Blakeslee et al. (2009) surface-brightness fluctuation (SBF) distances for individual galaxies in the Virgo and Fornax clusters;
(2) Tonry et al. (2001) SBF corrected via Equation A1 in Blakeslee et al. (2010);
(3) Mei et al. (2007) SBF mean distance to the Virgo W′ cloud (de Vaucouleurs 1961);
(4) Mei et al. (2007) SBF mean distance to the Virgo cluster (no W′ cloud);
(5) Thomsen et al. (1997) SBF distance to NGC 4881 in the Coma cluster;
(6) mean of distance determinations adopted in Kormendy et al. (2010); sources are given there;
(7) Monachesi et al. (2011); agrees with (8);
(8) mean of many determinations listed on NED, using mainly Cepheids, SBF, TRGB, and RR Lyrae stars.
(9) As a last resort, we adopt D (Local Group) given by NED for the recession velocity of the galaxy (if isolated) or its group (if in a group or cluster) and for the WMAP 5-year cosmology parameters (Komatsu et al. 2009).
(10) van den Bosch et al. (2012).
Column 4 is the 2MASS K_s total magnitude. When $(V-K_s)_0 = 2.980$ in Column 7, K_s has been corrected as discussed in **Apparent Magnitude Corrections** in the Table notes in the Supplemental Information.
Columns 5 and 6 are the K_s- and V-band absolute magnitudes based on the adopted distances and Galactic absorption corrections from Schlegel et al. (1998) as recalibrated by Schlafly & Finkbeiner (2011). The V-band magnitudes are taken, in order of preference, from KFCB, from RC3, or from Hyperleda (usually "integrated photometry" but sometimes the main table if it implies a more realistic $(V-K_s)_0$ color).
Columns 7 and 8 are the $V-K_s$ and $B-V$ colors of the galaxy corrected for Galactic reddening.
Column 9 is the base-10 logarithm of the bulge mass (Section 6.6.1).
Column 10 is the measured BH mass with 1-sigma range in parentheses from sources in Column 13.
Column 11 is the stellar velocity dispersion σ_e. We adopt the usual convention that σ_e^2 is the intensity-weighted mean of $V^2+\sigma^2$ out to a fixed fraction of the effective radius r_e that contains half of the light of the galaxy. As discussed in **Corrections to effective velocity dispersions** in the table notes, we adopt $r_e/2$ when we calculate σ_e from photometry and published kinematics (see notes on individual objects). When no note is given, σ_e is from the $M_\bullet$ source paper or from Gültekin et al. (2009c).
Column 12 lists three flags: "M" encodes the method used to measure $M_\bullet$, using 1 for stellar dynamics, 2 for ionized gas dynamics, and 3 for maser dynamics. "C" = 1 implies that the galaxy has a core (e. g., Lauer et al. 1995). "$M_\bullet$" = 1 implies that the BH mass has been "corrected" by making dynamical models that include large orbit libraries and triaxiality (M 32 and NGC 3379) or dark matter halos.

Table 3 Supermassive black holes detected dynamically in spiral and S0 galaxies galaxies (21 with classical bulges; 22 with pseudobulges; December 2012)

Object	Type	Distance (Mpc)	K_s	M_{KsT}	$M_{Ks,\rm bulge}$	$M_{Ks,\rm disk}$	B/T	PB/T	M_{VT}	$M_{V,\rm bulge}$	$M_{V,\rm disk}$	$(V-K_s)_0$	$(B-V)_0$	$\log M_{\rm bulge}$ ($M_\odot$)	$M_\bullet$(low $M_\bullet$ – high $M_\bullet$) ($M_\odot$)	σ_e (km s^{-1})	$V_{\rm circ}$ (km s^{-1})	Flags M $M_\bullet$	Source
(1)	(2)	(3)	(4)	(5)	(6)	(7)	(8)	(9)	(10)	(11)	(12)	(13)	(14)	(15)	(16)	(17)	(18)	(19)	(20)
M 31	Sb	0.774 8	0.573	−23.89	−22.62	−23.85	0.31	0.0	−21.14	−19.64	−20.83	2.746	0.865	10.35 ± 0.09	$1.43(1.12 - 2.34) \times 10^8$	169 ± 8	250 ± 20	1 0	Bender + 2005
M 81	Sb	3.604 8	3.831	−23.98	−22.81	−23.53	0.34	0.0	−21.06	−19.89	−20.61	2.913	0.879	10.42 ± 0.09	$6.5\ (5. - 9.) \times 10^7$	143 ± 7	240 ± 10	1,2 0	see notes
NGC 524	S0	24.22 2	7.163	−24.78	−24.69	−22.04	0.92	0.0	−21.86	−21.77	−19.12	2.923	0.977	11.26 ± 0.09	$8.67(8.21 - 9.61) \times 10^8$	247 ± 12	...	1 0	Krajnović + 2009
NGC 821	S0	23.44 2	7.715	−24.17	−24.11	−20.92	0.95	0.0	−21.19	−21.13	−17.94	2.980	0.893	10.98 ± 0.09	$1.65(0.92 - 2.39) \times 10^8$	209 ± 10	...	1 1	Schulze + 2011
NGC 1023	SB0	10.81 2	6.238	−23.95	−22.93	−23.41	0.39	0.0	−20.99	−19.96	−20.45	2.964	0.946	10.53 ± 0.09	$4.13(3.71 - 4.56) \times 10^7$	205 ± 10	251 ± 15	1 0	Bower + 2001
NGC 1194	S0/	57.98 9	9.758	−24.08	−23.33	−23.33	0.5	0.0	−21.16	−20.40	−20.40	2.925	0.893	10.64 ± 0.09	$7.08(6.76 - 7.41) \times 10^7$	148 ± 24	203 ± 16	3 0	Kuo + 2011
NGC 1277	S0/	73. 10	9.813	−24.63	−23.98	−23.76	0.55	0.0	−21.31	−20.67	−20.45	3.313	0.985	11.00 ± 0.09	$1.7\ (1.4 - 2.0) \times 10^{10}$	333 ± 17	...	1 1	van den Bosch + 2012
NGC 2549	S0/	12.70 2	8.046	−22.49	−20.99	−22.18	0.25	0.0	−19.55	−18.05	−19.24	2.942	0.912	9.71 ± 0.09	$1.45(0.31 - 1.65) \times 10^7$	145 ± 7	...	1 0	Krajnović + 2009
NGC 3115	S0/	9.54 2	5.883	−24.03	−23.91	−21.53	0.90	0.0	−21.13	−21.01	−18.63	2.901	0.928	10.92 ± 0.09	$8.97(6.20 - 9.54) \times 10^8$	230 ± 11	315 ± 20	1 1	Emsellem + 1999
NGC 3245	S0	21.38 2	7.862	−23.80	−23.41	−22.49	0.70	0.0	−20.88	−20.50	−19.58	2.914	0.888	10.69 ± 0.09	$2.39(1.63 - 2.66) \times 10^8$	205 ± 10	...	2 0	Barth + 2001
NGC 3585	S0	20.51 2	6.703	−24.88	−24.80	−21.99	0.93	0.0	−21.93	−21.85	−19.04	2.951	0.913	11.26 ± 0.09	$3.29(2.71 - 4.74) \times 10^8$	213 ± 11	280 ± 20	1 0	Gultekin + 2009b
NGC 3998	S0	14.30 2	7.365	−23.42	−23.24	−21.36	0.85	0.0	−20.63	−20.46	−18.57	2.786	0.936	10.67 ± 0.09	$8.45(7.79 - 9.15) \times 10^8$	275 ± 7	...	1 1	Walsh + 2012
NGC 3998	S0	14.30 2	7.365	−23.42	−23.24	−21.36	0.85	0.0	−20.63	−20.46	−18.57	2.786	0.936	10.67 ± 0.09	$2.27(1.43 - 3.28) \times 10^8$	275 ± 7	...	2 0	DeFrancesco + 2006
NGC 4026	S0	13.35 2	7.584	−23.05	−22.51	−22.03	0.61	0.0	−20.01	−19.47	−18.99	3.043	0.900	10.33 ± 0.09	$1.80(1.45 - 2.40) \times 10^8$	180 ± 9	300 ± 20	1 0	Gultekin + 2009b
NGC 4258	SABbc	7.27 6	5.464	−23.85	−21.55	−23.71	0.12	0.0	−20.94	−18.64	−20.80	2.907	0.676	9.86 ± 0.09	$3.78(3.74 - 3.82) \times 10^7$	115 ± 10	208 ± 6	3 0	Section 3.3
NGC 4342	S0	22.91 3	9.023	−22.78	−22.40	−21.48	0.70	0.01	−19.50	−19.11	−18.19	3.287	0.932	10.31 ± 0.09	$4.53(3.05 - 7.18) \times 10^8$	225 ± 11	...	1 0	Cretton + 1999b
NGC 4526	S0/	16.44 2	6.473	−24.61	−24.15	−23.47	0.65	0.0	−21.44	−20.98	−20.30	3.170	0.941	11.02 ± 0.09	$4.51(3.48 - 5.91) \times 10^8$	222 ± 11	290 ± 20	4 0	Davis + 2013
NGC 4564	S0	15.94 2	7.937	−23.09	−22.65	−21.88	0.67	0.0	−20.06	−19.62	−18.85	3.028	0.899	10.38 ± 0.09	$8.81(6.38 - 11.26) \times 10^7$	162 ± 8	...	1 1	Schulze + 2011
NGC 4594	Sa	9.87 2	4.625	−25.36	−25.28	−22.55	0.925	0.01	−22.38	−22.30	−19.57	2.980	0.934	11.47 ± 0.09	$6.65(6.24 - 7.05) \times 10^8$	240 ± 12	360 ± 10	1 1	Jardel + 2011
NGC 4596	SB0	16.53 4	7.463	−23.64	−22.21	−23.29	0.27	0.0	−20.72	−19.30	−20.38	2.913	0.920	10.20 ± 0.09	$7.67(4.43 - 11.41) \times 10^7$	136 ± 6	230 ± 30	2 0	Sarzi + 2001
NGC 7457	S0	12.53 2	8.179	−22.33	−20.82	−22.02	0.25	0.0	−19.45	−17.94	−19.14	2.880	0.844	9.56 ± 0.09	$0.90(0.36 - 1.43) \times 10^7$	67 ± 3	145 ± 6	1 1	Schulze + 2011
Galaxy	Sbc	0.00828	...	−23.7	−21.9	−23.5	0.0	0.19	−20.8	−18.9	−20.5	2.980	...	10.09 ± 0.10	$4.30(3.94 - 4.66) \times 10^6$	105 ± 20	220 ± 20	1 0	Genzel + 2010
Circinus	SABb:	2.82	4.71	−22.85	−21.55	−22.47	0.0	0.30	−19.80	−18.49	−19.41	3.052	0.410	9.63 ± 0.14	$1.14(0.94 - 1.34) \times 10^6$	79 ± 3	155 ± 5	3 0	Greenhill + 2003
NGC 1068	Sb	15.9 9	5.788	−25.23	−24.25	−24.66	0.0	0.41	−22.23	−20.92	−21.84	3.000	0.710	10.92 ± 0.10	$8.39(7.95 - 8.83) \times 10^6$	151 ± 7	283 ± 9	3 0	Lodato+2003, Huré+2002
NGC 1300	SBbc	21.5 9	7.564	−24.11	−21.71	−23.98	0.0	0.11	−21.32	−18.92	−21.19	2.791	0.653	9.84 ± 0.10	$7.55(3.89 - 14.75) \times 10^7$	88 ± 3	220 ± 10	2 0	Atkinson + 2005
NGC 2273	SBa	29.5 9	8.480	−23.89	−22.07	−23.67	0.0	0.19	−20.88	−19.06	−20.66	3.007	0.827	10.08 ± 0.09	$8.61(8.15 - 9.07) \times 10^6$	125 ± 9	220 ± 6	3 0	Kuo + 2011
NGC 2748	Sc	23.4 9	8.723	−23.13	−20.56	−23.02	0.0	0.094	−20.27	−17.70	−20.16	2.862	0.707	9.41 ± 0.10	$4.44(2.62 - 6.20) \times 10^7$	115 ± 5	150 ± 10	2 0	Atkinson + 2005
NGC 2787	SB0/a	7.45 2	7.263	−22.14	−21.06	−21.64	0.11	0.26	−19.10	−18.02	−18.60	3.038	0.944	9.78 ± 0.09	$4.07(3.55 - 4.47) \times 10^7$	189 ± 9	226 ± 10	2 0	Sarzi + 2001
NGC 3227	SBa	23.75 2	7.639	−24.25	−21.83	−24.12	0.0	0.108	−21.55	−19.13	−21.43	2.696	0.800	9.99 ± 0.09	$2.10(0.98 - 2.79) \times 10^7$	133 ± 12	250 ± 10	1 0	Davies + 2006
NGC 3368	SABab	10.62 2	6.320	−23.99	−22.48	−23.68	0.0	0.25	−21.14	−19.63	−20.82	2.854	0.838	10.26 ± 0.09	$7.66(6.13 - 9.19) \times 10^6$	125 ± 6	204 ± 5	1 0	Nowak + 2010
NGC 3384	SB0	11.49 2	6.750	−23.65	−22.56	−23.15	0.0	0.37	−20.55	−19.46	−20.05	3.105	0.906	10.34 ± 0.09	$1.08(0.59 - 1.57) \times 10^7$	146 ± 7	160 ± 10	1 1	Schulze + 2011
NGC 3393	SABa	49.2 9	9.059	−24.45	−23.03	−24.11	0.0	0.27	−21.48	−20.05	−21.14	2.968	0.813	10.48 ± 0.09	$1.57(0.58 - 2.55) \times 10^7$	148 ± 10	...	3 0	Kondratko+2008, Huré+2011
NGC 3489	SABa	11.98 2	7.370	−23.29	−22.15	−22.82	0.11	0.24	−20.17	−19.03	−19.70	3.120	0.815	10.11 ± 0.09	$5.94(5.11 - 6.78) \times 10^6$	113 ± 4	...	1 0	Nowak + 2010
NGC 3945	SB0	19.5 9	7.526	−23.93	−22.88	−23.41	0.04	0.34	−20.95	−19.90	−20.43	2.980	0.925	10.50 ± 0.09	$8.8\ (0.00 - 25.5) \times 10^6$	192 ± 10	...	1 0	Gültekin + 2009b
NGC 4388	SBbc	16.53 4	8.004	−23.10	−20.55	−22.99	0.0	0.096	−20.14	−17.60	−20.03	2.955	0.711	9.41 ± 0.10	$7.31(7.13 - 7.48) \times 10^6$	99 ± 10	200 ± 10	3 0	Kuo + 2011
NGC 4736	Sab	5.00 2	5.106	−23.39	−22.29	−22.91	0.0	0.36	−20.68	−19.58	−20.20	2.710	0.735	10.13 ± 0.10	$6.77(5.21 - 8.33) \times 10^6$	120 ± 6	181 ± 10	1 0	Gebhardt + 2013
NGC 4826	Sab	7.27 2	5.330	−23.99	−22.24	−23.75	0.0	0.20	−20.98	−19.23	−20.74	3.009	0.803	10.14 ± 0.09	$1.56(1.17 - 1.95) \times 10^6$	104 ± 3	155 ± 5	1 0	Gebhardt + 2013
NGC 4945	Scd	3.58	4.438	−23.38	−20.50	−23.30	0.0	0.07	−20.58	−17.70	−20.50	2.801	1.20	9.35 ± 0.12	$1.35(0.87 - 2.03) \times 10^6$	134 ± 20	174 ± 10	3 0	Greenhill + 1997
NGC 6264	SBb	147.6 9	11.407	−24.5	−22.6	−24.3	0.0	0.17	...	...	...	...	...	10.36 ± 0.09	$3.08(3.04 - 3.12) \times 10^7$	158 ± 15	...	3 0	Kuo + 2011
NGC 6323	SBab	113.4 9	10.530	−24.80	−21.55	−24.75	0.0	0.050	...	...	...	...	...	9.94 ± 0.09	$1.01(1.00 - 1.03) \times 10^7$	158 ± 26	...	3 0	Kuo + 2011
NGC 7582	SBab	22.3 9	7.316	−24.43	−21.96	−24.31	0.0	0.103	−21.78	−19.31	−21.66	2.649	0.738	10.02 ± 0.10	$5.51(4.56 - 6.81) \times 10^7$	156 ± 19	226 ± 10	2 0	Wold + 2006
IC 2560	SBbc	37.2 9	8.694	−24.19	−22.05	−24.02	0.0	0.14	−21.65	−19.51	−21.48	2.541	0.886	10.12 ± 0.09	$5.01(0.00 - 5.72) \times 10^6$	141 ± 10	196 ± 3	3 0	Yamauchi + 2012
UGC 3789	SABab	49.9	9.510	−24.03	−22.79	−23.61	0.0	0.32	−21.13	−19.89	−20.71	2.9	0.86	10.39 ± 0.09	$9.65(8.10 - 11.20) \times 10^6$	107 ± 12	273 ± 20	3 0	Kuo+2011, Huré+2011

Column 1 is the galaxy name. Rows are printed in red for galaxies with classical bulges; these are plotted with red symbols in BH correlation diagrams. Blue text and plot symbols are used for pseudobulges. The cyan $M_\bullet$ for NGC 3998 is plotted only in **Figure 12**. Otherwise, if $M_\bullet$ is shown in cyan, we accept the BH mass but do not include it in correlation fits (Sections 6.5, 6.6).
Column 2 is the galaxy Hubble type, mostly from RC3 with a few corrections from Kormendy & Bender (2013b).
Column 3 is the assumed distance (see notes to **Table 2**). For our Galaxy, Circinus, NGC 4945, and UGC 3789, see supplemental notes on individual galaxies.
Column 4 is the 2MASS K_s total magnitude. For three galaxies, it has been corrected as discussed in **Apparent Magnitude Corrections** in the table notes in Supplementary Information. These corrections are generally negligible for disk galaxies, which usually have steep (nearly exponential) outer profiles, unless their images are both very large and very bulge-dominated. The adopted corrections are −0.363 mag for NGC 4594 (which has an outer brightness profile like that of a giant ellipticals) and −0.411 mag for M 31 (which has an exceptionally large image on the sky). Both corrections were determined in order to make $(V-K_s)_0 = 2.980$. M 31 is discussed in the notes.
Columns 5 – 7 are the corresponding total, (pseudo)bulge, and disk K_s-band absolute magnitudes based on the adopted distances and Galactic absorption corrections from the Schlafly & Finkbeiner (2011) recalibration of Schlegel et al. (1998) as tabulated in NED.
Columns 8 and 9 are the classical-bulge-to-total luminosity ratio B/T and the pseudobulge-to-total luminosity ratio PB/T from Kormendy & Bender (2013b). These values used in K_s band are determined as close to K_s band as feasible; for some galaxies (especially S0s), they are determined in the optical but can be used in the infrared with relatively small errors. Parameters for the Galaxy and for Circinus are summarized further in the notes on individual galaxies.
Columns 10 – 12 are the V-band total, (pseudo)bulge, and disk absolute magnitudes. Total magnitudes are taken from Kormendy & Bender (2013b) or from the RC3 and Hyperleda. We generally used the mean of the RC3, Hyperleda main table, and Hyperleda "integrated photometry" B_T values and subtracted $(B-V)_T$, usually from RC3. When the RC3 or Hyperleda magnitude gave a much more realistic $(V-K)_0$ color, we used these values. The V-band B/T and PB/T values are usually assumed to be the same as the K_s-band values. For two galaxies, optical and infrared measurements imply different (pseudo)bulge-to-total ratios. Then we used $(B/T)_V = 0.25$ for M 31 and $(PB/T)_V = 0.30$ for NGC 1068 to get the V-band (pseudo)bulge magnitudes.
Columns 13 and 14 are the $V-K_s$ and $B-V$ colors of the galaxy corrected for Galactic reddening.
Column 15 is the base-10 logarithm of the (pseudo)bulge stellar mass derived from $M_{Ks,\rm bulge}$ and from the average of the M/L_{Ks} values given by Equations 8 and 9 in Section 6.6.1.
Column 16 is the measured BH mass with 1-σ range in parentheses from sources in Column 20.
Column 17 is the stellar velocity dispersion σ_e, mostly from Gültekin et al. (2009c) or the source in Column 20. Checks or corrections are described in table notes. For the definition of σ_e, see **Corrections to effective velocity dispersions** in the table notes.
Column 18 is the asymptotic, circular-orbit rotation velocity $V_{\rm circ}$ at large radii, usually from H I observations, as documented in Kormendy & Bender (2013b).
Column 19 lists two flags: "M" encodes the method used to measure $M_\bullet$, using 1 for stellar dynamics, 2 for ionized gas dynamics, 3 for maser dynamics, and 4 for CO rotation curve dynamics. "$M_\bullet$" = 1 implies that the BH mass has been "corrected" by making dynamical models that include large orbit libraries and dark matter halos. Flag "C" which identifies galaxies with cores in **Table 2** is not necessary here: None of these galaxies have cores, although NGC 524 has often been classified as a core galaxy (see Kormendy & Bender 2013b).
Column 20 is the source of the BH mass in Column 16. When there is more than one $M_\bullet$ measurement, the other sources are given in the notes on individual galaxies. If a galaxy does not appear there, then the reference in Column 20 is also the BH discovery paper.

Quantities not otherwise credited are discussed in the notes on individual objects in the Supplementary Information or are from Gültekin et al. (2009c), Kormendy & Bender (2013b), or Kormendy et al. (2010).

Notes on Technical Problems with the Parameters in Tables 2 and 3:

Apparent Magnitude Corrections: Section S1 in the Supplemental Information discusses the reasons for and derives corrections to 2MASS K magnitudes for the biggest and brightest galaxies. A summary is provided here.

An important consistency check on V- and K-band apparent magnitudes is provided by the observation that galactic-absorption-corrected $(V-K)_0$ colors are exceedingly well behaved for almost all galaxies. Exceptions are the most internally absorbed or starbursting galaxies, but they are not relevant here. For other galaxies, we find a tight correlation between $(V-K)_0$ and $(B-V)_0$ for $0.6 \lesssim (B-V)_0 \lesssim 1.2$. Classical bulges and ellipticals have $(V-K)_0 \simeq 2.980$ with a total scatter (not a dispersion) of about ± 0.15. Both colors are tabulated in **Tables 2** and **3**. We use them to check the apparent magnitudes. For a few, usually faint galaxies, discrepant colors suggest that the V magnitudes in NED and Hyperleda are wrong, usually by a few tenths of a magnitude. For these, 2MASS is more accurate, and we correct the V magnitudes to make $(V-K)_0 = 2.980$. More often – usually for the largest galaxies on the sky – the 2MASS magnitudes are the problem. We correct them as follows.

The 2MASS photometric system is very accurate; Jarrett et al. (2003) state that the photometric zero-point calibration is accurate to 2 % – 3 % across the sky. To the extent that we have been able to check them (Kormendy & Bender 2013b), their integrated magnitudes are correspondingly accurate at least within the radii out to which they have data. The survey is somewhat shallow; the 1-sigma sky noise is 20.0 mag arcsec^{-2} in K, although profiles can be derived somewhat fainter than this by averaging over many pixels. When there is a problem, it is with the extrapolation to total magnitudes, called $K_{\rm tot}$ in Jarrett et al. (2003) and `k_m_ext` in the online catalog. The extrapolation is made by fitting a Sérsic function to the parts of the profile that are relatively safe from noise and from the PSF and then integrating the extrapolated function out to "about four disk scale lengths." This procedure works best for disk galaxies, i. e., ones that have nearly exponential outer profiles. For ellipticals, the radial range is too small to yield an accurate Sérsic index (Section A2 in KFCB), and their tabulated Sérsic indices are too small. The result is to underestimate the total brightnesses of ellipticals, particularly giant ellipticals that have $n > 4$. The derivation of this conclusion and how we correct for it are the subjects of Section S1. In brief, the $(V-K)_0$ colors of our BH hosts are well enough behaved so that we can use them and the V magnitudes to correct the K magnitudes in problem cases. We are conservative in making this correction – we make it only when we observe a color $(V-K)_0 < 2.75$ that is much too blue. That is, if the correction is less than 0.230 mag, we do not use it. Also, in some marginal cases, it is not clear whether the V or the K magnitude is the problem. In all these cases, we use the total magnitude from 2MASS, even for ellipticals. In fact, so little is known about some of the more distant BH hosts that the 2MASS magnitudes are much more accurate than any available V-band measurements. Finally, in a few cases, our own photometry yields a composite, K-band profile with 2MASS zeropoint whose integral is more accurate than the 2MASS result because our measurements reach out to much larger radii. We adopt these total magnitudes also.

The largest correction, $\Delta K = -0.411$, is derived for M 31. Jarrett et al. (2003) warn us that "The Andromeda result should be viewed with caution, as we are not fully confident that the total flux of M 31 has been captured, because of the extreme angular extent of the galaxy and the associated difficulty with removing the infrared background." This problem happens in V band, too. We adopt $V_T = 3.47 \pm 0.03$ from Walterbos & Kennicutt (1987; the error estimate is optimistic). Then the 2MASS magnitude $K = 0.984$ implies that $(V-K)_0 = 2.335$. This is much too blue for an Sb galaxy with $(B-V)_0 = 0.87$ (**Figure S1**). As in other such cases, we correct $K \to K - 0.411$ to make $(V-K)_0 = 2.980$ for the bulge only. The V-band bulge magnitude is determined from the V-band $B/T = 0.25 \pm 0.01$. The correction gives us a K-band magnitude for the bulge only. The infrared $B/T = 0.31 \pm 0.01$ then gives us the total observed magnitude of the galaxy, $K_T = 0.573$. Including both the red bulge and the bluer disk, the total colors of the galaxy are $(B-V)_0 = 0.87$ and $(V-K)_0 = 2.75$ (cf. **Figure S1**).

In summary, 2MASS quoted errors on K-band magnitudes, usually 0.02 – 0.04 mag, are most reliable for disk galaxies but can be too optimistic for giant Es. We believe that our corrected magnitudes are generally accurate to ~ 0.1 mag, although the values for M 31 and for galaxies with $(V-K)_0$ very different from 2.980 are more uncertain. We quote K_s to higher precision because we do not wish to lose precision in arithmetic.

Corrections to stellar-dynamical $M_\bullet$ for core galaxies: Gebhardt & Thomas (2009), Shen & Gebhardt (2010), Schulze & Gebhardt (2011), and Rusli et al. (2013) demonstrate convincingly that stellar dynamical mass models that do not include dark matter halos underestimate $M_\bullet$ by factors of 2 or more when the BH sphere of influence is not extremely well resolved. The effect is small for coreless galaxies; we neglect it when models that include dark matter are not available. Fortunately, almost all stellar-dynamical $M_\bullet$ estimates for core galaxies are now based on models that include dark matter. For one exception, NGC 5576, we correct $M_\bullet$ as discussed in the notes on individual objects. For NGC 3607, the correction is too uncertain and we omit the object (see table notes and orange point in **Figure 12**).

Corrections to effective velocity dispersions: The velocity dispersion σ_e that we correlate with $M_\bullet$ is more heterogeneously defined in different papers and less consistently measured within these definitions than we suppose. This stealth "can of worms" could be a bigger problem than the more obvious uncertainties in measuring $M_\bullet$ that preoccupy authors. We check values when we can and fix a few problems. But the necessary data are not available for all objects. Fortunately, we can show that this problem is not severe.

The worries are these: (1) *A priori*, we do not know how best to define σ_e so that we learn important physics from the $M_\bullet - \sigma_e$ correlation. Clearly we should not include data at $r \lesssim r_{\rm infl}$ in the average. But inside what fraction of r_e should we average $\sigma(r)$? We usually claim that we average inside r_e and call the result σ_e. However: (2) Accurate values of r_e are known for few galaxies. KFCB demonstrate via high-dynamic-range photometry that brightness profiles of giant ellipticals extend farther out than we have thought. The r_e values derived in KFCB are more accurate than previous results, and they are larger than previous values for almost all giant ellipticals. We use them here. But we do not have such data for most BH hosts. It is safe to assume that the r_e values in common use are too small. For bulges, the situation is worse. Accurate decompositions are available for a few galaxies, but they are being derived for most galaxies in parallel with the writing of this paper (Kormendy & Bender 2013b). (3) Different fractions of r_e are used by different authors. For example, Ferrarese & Merritt (2000) use $r_e/8$, whereas the Nuker team uses r_e. (4) Different authors perform the radial averaging differently. We follow the Nuker team practice (e. g., Pinkney et al. 2003; Gültekin et al. 2009c) and use σ_e^2 = average of $V(r)^2 + \sigma(r)^2$, weighting by $I(r)dr$. In most cases, we adopt σ_e from the $M_\bullet$ source paper or from Gültekin et al. (2009c). When we calculate it, we perform the average inside $r_e/2$ and include a comment in the notes on individual objects. However, the above practice can be contrasted with σ_e values from the SAURON team: They add spectra that sample the galaxy in two dimensions inside r_e or inside the SAURON field, whichever is smaller (Emsellem et al. 2007). Because σ and V rather than $\sigma^2 + V^2$ are averaged and because the weighting of different radii is essentially by $2\pi r I(r) dr$ rather than by $I(r)dr$, the resulting σ_e values are smaller than the ones that we use. No study has proved that the Nuker definition produces a tighter $M_\bullet - \sigma_e$ correlation or that a tighter correlation is more physically meaningful. However, because it is most commonly used and therefore most widely available, we use the Nuker definition here.

In view of these concerns, it is prudent to check how much our results might depend on the definition of σ_e or on how well its measurement follows that definition. **Figure 11** compares our σ_e values, adopted after much private wailing and gnashing of teeth, with central velocity dispersions tabulated in HyperLeda and with σ_e values calculated as described above by the SAURON/ATLAS3D team. Clearly, adopting either alternative would have minimal effect on the scatter in the $M_\bullet - \sigma_e$ correlation and essentially no effect on qualitative conclusions.

HyperLeda includes a few bad measurements; these are particularly expected for pseudobulges, which can have small dispersions that are undersampled by poor wavelength resultion and serious problems with dust and star formation. But it is relatively easy to find and discard these problems and get an improved central σ that would agree with our σ_e as well as classical bulges and ellipticals do.

SAURON/ATLAS3D σ_e values mostly agree very well with ours. Some SAURON values are smaller, as expected. But conclusions would not be changed if we had SAURON σ_e values for all galaxies. The average shift $\Delta \log \sigma_e = \log(\text{Nuker } \sigma_e) - \log(\text{SAURON } \sigma_e) = 0.0299$ or a factor of 1.07 will be relevant in Section 8 when we compare the $z \simeq 0$ $M_\bullet - \sigma_e$ relation with ones derived for galaxies at large redshifts. High-z observations necessarily add spectra (not σ^2) inside apertures that are large in kpc. SAURON σ_e values are the closest match at $z \simeq 0$. We therefore use the above factor to correct our least-squares fit to the local $M_\bullet - \sigma_e$ correlation for comparison with high-z objects.

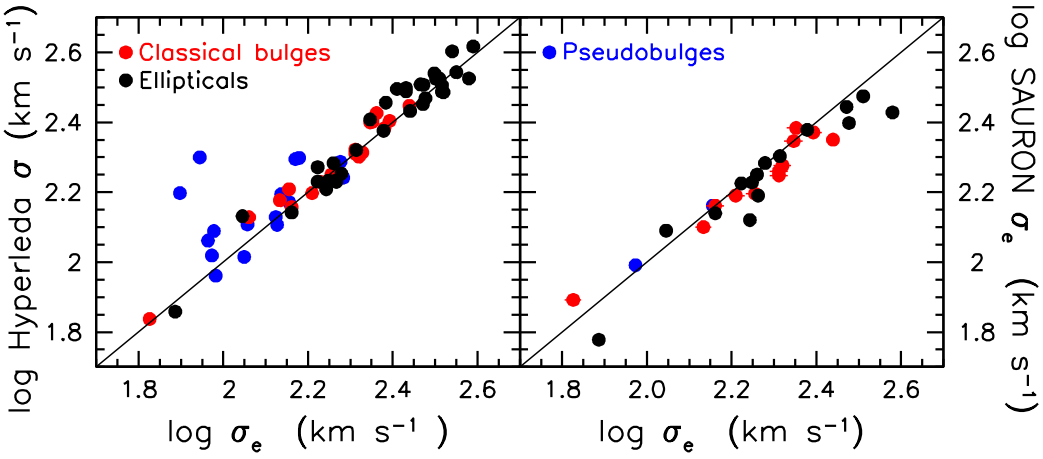

Figure 11

Comparison of our adopted σ_e (**Tables 2** and **3**) to (*left*) the central velocity dispersion as tabulated in HyperLeda and (*right*) the σ_e value tabulated by the SAURON/ATLAS3D teams (Emsellem et al. 2007; Cappellari et al. 2013). The straight lines are not fits; they indicate equality. Given our definition, it is reassuring that our σ_e is approximately the geometric mean of HyperLeda central and SAURON/ATLAS3D σ_e.

Notes on Individual Elliptical Galaxies:

M 32: The BH discovery papers and history of $M_\bullet$ measurements are discussed in § 2.2.1. We adopt $M_\bullet$ from the triaxial models of van den Bosch & de Zeeuw (2010). We calculate $\sigma_e = 77 \pm 3$ km s^{-1} from our photometry ($r_e/2 = 38''/2$) and kinematics in Simien & Prugniel (2002). The value averaged inside r_e is 1 km s^{-1} smaller. This is in good agreement with $\sigma_e = 75 \pm 3$ km s^{-1} in Tremaine et al. (2002), Gültekin et al. (2009c), and McConnell & Ma (2013). In contrast, Graham & Scott (2013) adopt $\sigma_e = 55$ km s^{-1}, presumably by not including $V(r)$.

NGC 2778, NGC 3608, NGC 4291, NGC 4473, NGC 4649, NGC 4697, and NGC 5845: The BH discovery is by Gebhardt et al. (2003).

NGC 1316: This galaxy is bluer than the typical giant E, with $(B-V)_0 = 0.87$ (NED). Based on our experience with published total magnitudes of bright galaxies (e. g., KFCB), we adopt $B_T = 9.17$ from the Hyperleda integrated photometry table. This yields $M_{VT} = -23.38$. The 2MASS $K = 5.587$ magnitude then implies that $(V-K)_0 = 2.64$. This is implausible for the $(B-V)_0$ color, indicating that the K luminosity is underestimated. We use the $(V-K)_0$ versus $(B-V)_0$ correlation to derive $(V-K)_0 = 2.91$ and hence to correct the K magnitude by -0.268 magnitudes to $K = 5.319$. This is a typical correction for a nearby giant elliptical.

NGC 1332 and NGC 4751: These galaxies initially presented us with an interpretation dilemma. We believe that it is solved and that both galaxies are best interpreted as (rather extreme) ellipticals. However, realizing this required us to learn somthing new about elliptical galaxies. This note explains our conclusions and summarizes the consequeunces of the more canonical alternative that these are S0 galaxies.

Both galaxies are highly flattened (E6) and contain prominent, almost-edge-on nuclear dust disks. It is remarkable how many BH host ellipticals contain nuclear dust disks: NGC 1332, NGC 3379 (faintly), NGC 3607, NGC 4261, NGC 4374, NGC 4459, NGC 4486A and NGC 5845 (in which much of the nuclear gas disk has formed stars), NGC 4697, NGC 4751, NGC 6251, NGC 6861, NGC 7052, NGC 7768, A1836 BCG, A3565 BCG, and probably IC 1459. Several more contain nuclear disks of stars that plausibly formed out of gas-and-dust disks in the manner illustrated by NGC 4486A (Kormendy et al. 2005) and NGC 5845 (Lauer et al. 1995). Of course, this does not prove that all these objects – especially NGC 1332 and NGC 4751 – are ellipticals; bona fide S0$_3$ galaxies contain nuclear dust disks, too (e. g., NGC 5866 in the *Hubble Atlas*, Sandage 1961). One reason why dust-lane E and S0 galaxies are preferentially found among BH hosts is that seeing a dust lane motivates authors to measure an emission-line rotation curve. The prevalence of central gas disks in BH hosts is interesting from a BH feeding point of view, but their importance in this note is that they tell us that NGC 1332 and NGC 4751 are almost edge-on.

Images of NGC 1332 and NGC 4751 suggest that both galaxies contain two components, a central one that is relatively round and that has a steep brightness gradient and an outer one that looks flatter and that has a shallower brightness gradient. These are defining features of S0 galaxies. If the central component is interpreted as a bulge and the outer one as a disk, then plausible decompositions are possible and give $B/T = 0.43$ for NGC 1332 (Rusli et al. 2011) and $B/T = 0.55 \pm 0.05$ for NGC 4751 (Kormendy & Bender 2013b). We emphasize: *If these interpretations are correct, then NGC 1332 closely resembles the S0 galaxies NGC 1277 and MGC 4342 in having a bulge that contains an abnormally high-mass BH (see* **Figure 14** *for illustration). NGC 4751 is similar but less extreme. Like NGC 1277 and NGC 4486B, both galaxies then also have high velocity dispersions that are well outside the scatter in the Faber-Jackson (1976) correlation between E or bulge luminosity and velocity dispersion. That is, if NGC 1332 and NGC 4751 are S0s, then they are further examples of the high-$M_\bullet$ deviant galaxies discussed in Section 6.5.*

However, a compelling argument suggests that these galaxies are extremely flattened extra-light ellipticals:

KFCB present and review evidence that Virgo cluster ellipticals are naturally divided into two kinds, $M_{VT} < -21.6$ galaxies that have cores and $M_{VT} \geq -21.5$ galaxies that have central extra light above the inward extrapolation of the outer $n \simeq 3 \pm 1$ Sérsic-function main body (see Sections 6.X and 6.9 here). They suggest that and (e. g.) Hopkins et al. (2009b) model how extra-light ellipticals form in wet mergers, such that the main body of the galaxy is the scrambled-up remnant of the pre-merger disk and bulge stars and the extra-light component was manufactured by a starburst during the merger. In Virgo ellipticals, the fraction of the stellar mass that is in the extra-light component is $\sim 5\,\%$ (if just the extra light is counted: KFCB) or as much as a few 10s of percents (if a standard Sérsic-Sérsic decomposition is applied: Hopkins et al. 2009b). Both kinds of ellipticals are represented among our BH hosts; NGC 3377 and NGC 4459 are typical extra light ellipticals.

Huang et al. (2013a) make a similar study of ellipticals in field environments. They show that field ellipticals are different from cluster ellipticals in three ways that are relevant here: (1) extra light (their "two inner components") makes up a larger fraction $\sim 20\,\%$ to $40\,\%$ of the galaxies, (2) extra-light ellipticals extend to higher luminosity in the field than in the Virgo cluster, and (3) field ellipticals can be as flat as E6 (their Figure 1). In the context of these results, NGC 1332 and NGC 4751 are more plausible interpreted as extra-light ellipticals, not S0s. In fact, even though NGC 1332 is exceedingly close to edge-on, its isophotes are more rectangular than those of an edge-on thin disk; this motivated Sandage & Bedke (1994) to emphasize (their italics) that the galaxy contains a "*thick disk*".

We now believe that there may be almost a continuum in the properties (although not a seamless overlap in numbers) of outer bodies of these galaxies from E5 ellipticals with a modest amount of extra light (NGC 3377) to E6 ellipticals that are roughly half extra light (NGC 4751 and NGC 6861) to E6 galaxies whose outer parts resemble thickened disks (NGC 1332) to true S0s with thin disks (NGC 5866). Objects like NGC 4751 and NGC 1332 may be rare, and it appears that they are confined to the field, perhaps because this environment favors formation by a small number of gentle mergers that involve progenitors with large gas fractions. This is the interpretation of NGC 1332 and NGC 4751 that we adopt when we construct BH correlation diagrams and least-squares fits. **Figure 15** illustrates both interpretations for NGC 1332.

NGC 1399: As discussed in Section 3.1, we adopt the mean $M_\bullet$ measured by Houghton et al. (2006) and by Gebhardt et al. (2007). Conservatively, we adopt 1-σ errors that span the complete range obtained in both measurements. Also, $\sigma_e = 315$ km s^{-1} is calculated using kinematic data from Graham et al. (1998), intensity-weighting $V^2 + \sigma^2$ out to $0.5r_e = 56''$ using our photometry.

NGC 2778 had a BH detection in Gebhardt et al. (2003) but only a $M_\bullet$ upper limit in Schulze & Gebhardt (2011). However, $M/L_K = 3.3$ is too big for an old stellar population minus dark matter, implying that the $M_\bullet$ limit is too small. We illustrate it in **Figure 12** and then omit it.

NGC 2960: The BH discovery paper is Henkel et al. (2002); a reliable BH mass was determined by Kuo et al. (2011). NGC 2960 has frequently been classified as Sa? (RC3, UGC, NED), but Kormendy & Bender (2013b) show that it is a merger in progress. The galaxy is therefore listed here, with the ellipticals. The dispersion is from Greene et al. 2010.

NGC 3377: The BH was found by Kormendy et al. (1998), whose measurements $M_\bullet = (2.1 \pm 0.9) \times 10^8\ M_\odot$ and $M/L_V = 2.0 \pm 0.2$ agree well with $M_\bullet = (1.9 \pm 1.0) \times 10^8\ M_\odot$ and $M/L_V = 2.3 \pm 0.4$ in Schultze & Gebhardt (2011). The reasons are (1) that the resolution of the CFHT spectroscopy was very good, (2) that the assumption by Kormendy of an isotropic velocity distribution in this low-luminosity, extra-light (Kormendy 1999), and rapidly rotating (Emsellem et al. 2004) elliptical was close enough to the truth, and (3) that this E5 galaxy is essentially guaranteed to be edge-on. The BH mass in NGC 3377 was also measured in Gebhardt et al. (2003). The 2MASS K-band magnitude gives an implausible color of $(V-K)_0 = 2.69$. We have corrected K_s in **Table 2** to give the mean color for giant ellipticals, $(V-K)_0 = 2.980$.

NGC 3379 is a core elliptical with dynamical models that include triaxiality (the only core galaxy that has such models) but not dark matter (van den Bosch & de Zeeuw 2010). However, the HST FOS spectra (Gebhardt et al. 2000d) resolve the BH sphere of influence with $r_{\rm infl}/\sigma_* \simeq 7.1$. Schulze & Gebhardt (2011) and Rusli et al. (2013) show that $M_\bullet$ does not require a significant correction for dark matter under these circumstances.

NGC 4374 (M 84) is the fifth-brightest elliptical in the Virgo cluster, but it is only 0.61 mag fainter than NGC 4472 (KFCB). Like many radio galaxies, it (3C 272.1) has a nuclear gas and dust disk (Bower et al. 1997), which makes it feasible to search for a BH relatively independently of the stellar mass distribution (Walsh, Barth & Sarzi 2010) by measuring the emission-line gas rotation curve. NGC 4374 is the first galaxy in which a BH discovery was made using HST STIS (Bower et al. 1998). STIS's long-slit capability made it possible to see the prominent zig-zag in the emission lines that is the signature of the BH.

However, as discussed in Section 3.2, the line profile is complicated by a two-component structure, and this has led to some uncertainty in $M_\bullet$. Bower et al. (1998) decompose the line profiles into slowly- and rapidly-rotating components and use the latter to get $M_\bullet = 1.63(0.99-2.83)\times10^9\ M_\odot$. Maciejewski & Binney (2001) suggest that the complicated line profile is caused by integrating the light of the nuclear disk inside a spectrograph slit that is broader (0.″2 wide) than the telescope PSF. They estimate $M_\bullet = 4.4 \times 10^8\ M_\odot$. The large difference between these two determinations has been a cause of concern, not only for NGC 4374 but also for other $M_\bullet$ determinations based on emission lines. Recently, Walsh, Barth & Sarzi (2010) model the observations in much greater detail and – importantly – include the effects of the velocity dispersion in the gas. After application of this "asymmetric drift" correction, they get $M_\bullet = 9.25(8.38\ -\ 10.23) \times 10^8\ M_\odot$. We adopt their value but note (§ 3.2) that there are still significant uncertainties in emission-line $M_\bullet$ measurements. Certainly the folklore that gas rotation curves give $M_\bullet$ easily and without the complications and uncertainties in stellar-dynamical modeling is too optimistic.

NGC 4382: The Gültekin et al. (2011) $M_\bullet$ limit is based on stellar-dynamical models that do not include dark matter. For $M_\bullet \le 1.3^{+5.2}_{-1.2} \times 10^8\ M_\odot$, $r_{\rm infl}/\sigma_* \simeq 0.3$ is not well resolved. Since this is a core galaxy, we need to ask whether an upward correction to the $M_\bullet$ limit is required. Examination of Gültekin's analysis persuades us that no correction is needed: (1) The core is unusually small (break radius $r_b = 81$ pc, Lauer et al. 2005) for the high luminosity of the galaxy. Our only BH host E that has a smaller $r_b = 54$ pc in Lauer et al. (2005) is NGC 3608, for which Schulze & Gebhardt (2011) find the same $M_\bullet$ with and without dark matter. (2) The kinematic measurements analyzed by Gültekin only reach $0.28\,r_e$, i. e., the inner part of the galaxy that is most dominated by visible matter. Large $M_\bullet$ corrections in Schulze et al. (2011) happen when the ground-based observations reach larger fractions of r_e. In confirmation, (3) Gültekin et al. (2011) remark: "Within ~ 2 kpc, about the outer extent of our data, [Nagino & Matsushita 2009, who] study the gravitational potential as revealed by X-ray emission from the interstellar medium, ... find a constant B-band mass-to-light ratio consistent with a potential dominated by stellar mass." We therefore use Gültekin's BH mass limit as published.

NGC 4459 is the second-brightest extra-light elliptical in the Virgo cluster and the brightest one that has Sérsic $n < 4$ ($n = 3.2 \pm 0.3$: KFCB). Therefore – as indicated by the normal color, $(V-K)_0 = 2.975$ – the 2MASS K_T magnitude is accurate. The galaxy has a prominent nuclear dust disk; in this sense, it closely resembles NGC 1332, NGC 4751, and many other BH host ellipticals discussed in the notes to those objects.

M 87: The early history of BH searches is reviewed in KR95. We consider the BH discovery paper to be the HST gas-dynamical study by Harms et al. (1994). They derived $M_\bullet = (2.7 \pm 0.8) \times 10^9\ M_\odot$ (all masses are corrected to the SBF distance of 16.68 Mpc: Blakeslee et al. 2009). For many years, the definitive mass measurement – also based on HST gas kinematics – was $M_\bullet = (3.6 \pm 1.0) \times 10^9\ M_\odot$ (Macchetto et al. (1997). Stellar-dynamical measurement of $M_\bullet$ is difficult, because the central brightness profile is shallow inside the break radius $r_b = 5.''66$ that defines the "core" (Lauer et al. 1992, 2007b). The result (Kormendy 1992a, b) is unfavorably small luminosity weighting inside the BH sphere of influence, $r_{\rm infl} \simeq 3.''1$. Even a steep central increase in $\sigma(r)$ is strongly diluted by projection. Measuring LOSVDs helps if one can detect the resulting high-velocity wings (van der Marel 1994b). M 87 remains too expensive for HST absorption-line spectroscopy, but high-S/N ground-based spectroscopy is successful. Gebhardt & Thomas (2009) fit a variety of kinematic measurements, including two-dimensional spectroscopy from SAURON (Emsellem et al. 2004) and higher-resolution, long-slit spectroscopy from van der Marel et al. (1994a: seeing FWHM = 0.″6; slit width = 1″). They for the first time include dark matter in the dynamical models; this is important because the tradeoff in mass between dark and visible matter inevitably decreases the measured stellar mass-to-light ratio at large radii. Analysis machinery is still based on the assumption that M/L is independent of radius, so the consequence is to reduce M/L near the center, too. To maintain a good fit to the kinematics, $M_\bullet$ must be increased. Gebhardt & Thomas (2009) derive $M/L_V = 10.9 \pm 0.4$ and $M_\bullet = (2.1 \pm 0.6) \times 10^9\ M_\odot$ without including dark matter and $M/L_V = 6.8 \pm 0.9$ and $M_\bullet = (6.0 \pm 0.5) \times 10^9\ M_\odot$ including dark matter. The change is in the expected sense. Recently, Gebhardt et al. (2011) add Gemini telescope integral-field spectroscopy aided by laser-guided AO; the resulting PSF has a narrow core (FWHM = 0.″06) that contributes 14 – 45 % of the PSF light. Such good resolution allows a substantial improvement in the reliability of the BH mass measurement. They get and we adopt $M_\bullet = 6.15(5.78\ -\ 6.53) \times 10^9\ M_\odot$.

As in many other galaxies in which stellar- and gas-dynamical $M_\bullet$ measurements can be compared, the stellar-dynamical mass is substantially larger. In M 87, it is a factor of 1.74 ± 0.50 larger than the Macchetto et al. (1997) value. Such comparisons are discussed further in Section 3.2.

NGC 4486A: This galaxy has a bright star 2.″5 from its center that affects most published magnitude measurements. KFCB measure the total $V_T = 12.53$ magnitude without this star, and this provides $M_{VT} = -18.85$. The 2MASS magnitude appears to include the star, so we do not use it. Instead, we adopt the well determined $(V-K)_0 = 2.980$ color for old elliptical galaxies and derive $M_{KT} = -21.83$ from M_{VT}. For $M_\bullet$, we read 1-σ error bars from the χ^2 contour diagram in Figure 6 of Nowak et al. (2007).

NGC 4486B is one of the lowest-luminosity, normal ellipticals known. The most accurate photometry (KFCB) gives $V_T = 13.42$ and, with the present distance, $M_{VT} = -17.69$. M 32 is about 1 mag fainter. Again, we adopt $(V-K)_0 = 2.980$ in preference to the 2MASS K magnitude to get $M_{KT} = -20.67$. The BH mass $M_\bullet \simeq 6.1^{+3.0}_{-2.0} \times 10^8\ M_\odot$ is the only one based on spherical, isotropic stellar-dynamical models that we use in this paper. We use it (1) because the central velocity dispersion $\sigma = 291 \pm 25$ km s^{-1} is much larger than the upper envelope $\sigma \sim 160$ km s^{-1} (for the galaxy's luminosity) of the scatter in the Faber-Jackson (1976) correlation. As in the case of NGC 1277 (q. v.), this is a strong indicator of unusually high masses, even though anisotropic models can formally fit the data without a BH. However, we have already noted that low-luminosity, coreless ellipticals (e. g., M 32) are not generally very anisotropic. NGC 4486B is a rapid rotator. (2) We do not use $M_\bullet$ in any correlation fits. Instead, we include NGC 4486B as the earliest discovery of a compact, early-type galaxy which deviates from the $M_\bullet$–host-galaxy correlations in the direction of abnormally high $M_\bullet$. The most extreme such galaxy is NGC 1277 (**Table 3** and **Figure 15**).

NGC 5077: We use the BH mass that was calculated including emission-line widths in the analysis (De Francesco et al. 2008, see p. 361) and adopt the same high-$M_\bullet$ error bar. The low-$M_\bullet$ error bar is from the analysis that does not include line widths.

NGC 5128: At a distance of 3.62 Mpc, NGC 5128 = Centaurus A is the second-nearest giant elliptical (after Maffei 1 at 2.85 Mpc) and the nearest radio galaxy. It is therefore very important for the BH search. It is also a merger-in-progress, although that merger may be relatively minor. It will prove to be important to our conclusion in Section 6 that mergers-in-progress often have BH masses that are small compared to expectations from the $M_\bullet$–host-galaxy correlations.

The problem is that the many published $M_\bullet$ measurements show disquieting disagreements (Section 3.2). Five measurements based on the rotation of a nuclear gas disk are available. In recent years, as measurements and modeling have improved, the mass measurements have converged reasonably well: We have

$M_\bullet = 2.07(0.62 - 5.18) \times 10^8\ M_\odot$ (Marconi et al. 2001) based on ESO VLT observations without AO;

$M_\bullet = 1.14(0.60 - 1.24) \times 10^8\ M_\odot$ (Marconi et al. 2006) based on HST STIS spectroscopy and including uncertainties from the poorly constrained inclination of the gas disk in the error bars;

$M_\bullet = 0.63(0.55 - 0.69) \times 10^8\ M_\odot$ (Häring-Neumayer et al. 2006) based on VLT with AO and including the gas velocity dispersion in the estimate;

$M_\bullet = 0.85(0.71 - 0.93) \times 10^8\ M_\odot$ (Krajnović, Sharp, & Thatte 2007) based on Gemini telescope spectroscopy without AO; the Paβ rotation curve is consistent with zero velocity dispersion; and

$M_\bullet = 0.47(0.43 - 0.52) \times 10^8\ M_\odot$ (Neumayer et al. 2007) based on VLT SINFONI spectroscopy with AO; the gas dispersion is taken into account.

The convergence of $M_\bullet$ measurements based on gas dynamics is reassuring. However, two stellar-dynamical measurements agree poorly:

$M_\bullet = 2.49(2.28 - 2.80) \times 10^8\ M_\odot$ (Silge et al. 2005) based on Gemini observations without AO, and

$M_\bullet = 0.57(0.47 - 0.67) \times 10^8\ M_\odot$ (Cappellari et al. 2009) based on VLT SINFONI spectroscopy with AO.

The last set of measurements has the highest resolution and S/N, and it agrees with the latest gas-dynamical results. We adopt this $M_\bullet$.

NGC 5576: This is a core elliptical (Lauer et al. 2007b) with a BH detection and $M_\bullet$ measurement in Gültekin et al. (2009b). Halo dark matter was not included in the dynamical models, but the resolution $r_{\rm infl}/\sigma_* = 3.3$ is good enough so that we can apply a correction calibrated by Schulze & Gebhardt (2011) and by Rusli et al. (2013). The mean of the two corrections is a factor of 1.6 ± 0.3. We applied this correction and added the uncertainty in the correction to the uncertainty in Gültekin's $M_\bullet$ measurement in quadrature to give the estimated 1-σ error quoted in the table.

NGC 6861 is classified as an $S0_3$ galaxy in Sandage & Tammann (1981) because of its prominent nuclear dust disk. Méndez-Abreu et al. (2008) estimate that $B/T \simeq 0.64$. However, our preliminary photometry (Kormendy & Bender 2013b) shows little or no significant departure from an $n \simeq 2$ Sérsic-function main body with central extra light. That is, the galaxy is similar to NGC 4459, another extra-light elliptical (KFCB) with a central dust disk that motivated an $S0_3$ classification in Sandage & Tammann (1981). There could be a faint disk component in NGC 6861 such as the one in NGC 3115; if so, it will make no difference to any conclusions in this paper. We therefore classify the galaxy as an extra-light elliptical.

IC 1459: The BH discovery by Verdoes Kleijn et al. (2000) is based on HST WFPC2 photometry, HST FOS spectroscopy through six apertures to measure the emission-line rotation curve, and ground-based (CTIO 4 m telescope) spectroscopy with FWHM $\sim 1\farcs9$ seeing to measure the stellar kinematics. They get $M_\bullet \sim$ (4 to 6) $\times\ 10^9\ M_\odot$ from stellar dynamical modeling but $M_\bullet \sim$ (0.2 to 0.6) $\times\ 10^9\ M_\odot$ from the HST gas dynamics. In contrast, Cappellari et al. (2002) combine HST STIS spectroscopy with high-S/N ground-based spectroscopy (CTIO 4 m telescope; seeing FWHM $\approx 1\farcs5$; slit width = $1\farcs5$; CCD scale = $0\farcs73$ pixel^{-1}) that provide both emission-line and absorption-line kinematics. Again, the agreement between gas and star measurements is not superb: stellar dynamics give $M_\bullet = 2.65(2.28 - 3.03) \times 10^9\ M_\odot$ (which we adopt), whereas gas dynamics give $M_\bullet \approx 3.6 \times 10^9\ M_\odot$. As noted in § 3.2, the comparison between gas and stellar dynamics is not reassuring.

At $r \le 43''/2 = r_e/2$, we measure $\sigma_e = 329$ km s^{-1} from the kinematic data in Cappellari et al. (2002) and $\sigma_e = 332$ km s^{-1} from the kinematic data in Samurović & Danziger (2005). We adopt $\sigma_e = 331 \pm 5$ km s^{-1}. The data reach far enough out to measure a value inside r_e; this would be only 2.6 km s^{-1} smaller than the value that we adopt. Our photometry shows that this is an extra-light elliptical with $n \simeq 3.1^{+0.4}_{-0.3}$.

IC 1481: The BH discovery paper is Mamyoda et al. (2009). They detect maser sources distributed along a line indicative of an edge-on molecular disk, and they see a symmetrical rotation curve. But $V(r) \propto r^{-0.19 \pm 0.04}$ is substantially sub-Keplerian. They conclude that the maser disk is more massive than the BH. Huré et al. (2011) present an analysis method that is suitable for a wide range of disk-to-BH mass ratios. They measure $M_\bullet = (1.59 \pm 0.45) \times 10^7\ M_\odot$ and a maser disk mass of about $4.1 \times 10^7\ M_\odot$ (see § 3.3.3). We adopt these values.

The host galaxy is discussed in Kormendy & Bender (2013b). SDSS images show loops, shells, and dust lanes characteristic of a major merger in progress. The overall light distribution is that of a normal extra-light elliptical with Sérsic $n = 2.5^{+0.25}_{-0.2}$ (KFCB). Consistent with this, the central $2'' \times 2''$ of the galaxy has an A – F, post-starburst spectrum (Bennert, Schulz & Henkel 2004). The ellipticity profile shows that this object is turning into an E1.5 elliptical, so we list it in **Table 2**. In discussions in the next section, we include it among mergers in progress.

Notes on Disk Galaxies With Classical Bulges:

M 31: The BH mass measurements are discussed in § 2. We adopt $M_\bullet$ determined from P3, the blue cluster part of the triple nucleus (Bender et al. 2005). We recomputed $\sigma_e = 169 \pm 8$ km s^{-1} from our photometry and kinematic data in Saglia et al. (2010). Integrating to r_e or $r_e/2$ gives the same result. Agreement with $\sigma_e = 160 \pm 8$ km s^{-1} in Gültekin et al. (2009c) is good. Chemin, Cargnan & Foster (2009) provide $V_{\rm circ}$.

Photometry is difficult, because the galaxy is large. The V- and K-band magnitudes are discussed in the table notes on **Apparent Magnitude Corrections** as an example of the correction of 2MASS magnitudes. Since our BH correlations are derived in K band, we use an infrared measurement of the bulge-to-disk ratio. This is the mean $B/T = 0.31 \pm 0.01$ of four, L-band measurenets by Seigar, Barth & Bullock (2008), Tempel, Tamm & Tenjes (2010), Kormendy et al. (2010), and Courteau et al. (2011). We list this value in **Table 3**. However, $B/T = 0.25 \pm 0.01$ is smaller in V band, and we use this smaller value in deriving the V-band bulge and disk magnitudes.

M 81: The BH discovery and $M_\bullet = 6\,(\pm 20\,\%) \times 10^7\ M_\odot$ measurement are reported in Bower et al. (2000). There are two concerns: this result is based on axisymmetric, two-integral stellar-dynamical models, and it has never been published in a refereed journal. Also, Devereux et al. (2003) measure $M_\bullet$ using HST STIS spectroscopy to get the ionized gas rotation curve; the problems here are that the [N II] emission lines are blended with and had to be extracted from broad Hα emission and that the width of the [N II] emission lines is not discussed. But, whereas the danger is that the emission-line rotation curve will lead us to underestimate $M_\bullet$, Devereux et al. (2003) get $M_\bullet = 7.0(6.0 - 8.9) \times 10^7\ M_\odot$, larger than Bower's value. Both measurements are problematic, but they agree. Also, Bower's measurement of $M_\bullet$ in NGC 3998 in the same abstract agrees with a reliable stellar-dynamical measurement in Walsh et al. (2012). So we adopt the average of the Bower and Devereux $M_\bullet$ measurements.

Available B/T measurements in the visible and infrared agree within errors. We adopt the mean $B/T = 0.34 \pm 0.02$ (Kormendy & Bender 2013b).

NGC 524: Krajnović et al. (2009) use $\sigma_e = 235$ km s^{-1} from Emsellem et al. (2007), but this is from a luminosity-weighted sum of spectra inside r_e. It is therefore not consistent with the Gültekin et al. (2009c) definition. For consistency, we computed $\sigma_e = 247$ km s^{-1} from kinematic data in Simien & Prugniel (2000) and our photometry.

NGC 821, NGC 3384, NGC 4564, and NGC 7457: The BH discovery is by Gebhardt et al. (2003).

NGC 821 is usually considered to be an elliptical galaxy, but the shapes of the isophotes in the image in the Carnegie Atlas of Galaxies (Sandage & Bedke 1994) suggests that it is an almost-edge-on S0. In fact, Scorza & Bender (1995) did a bulge-disk decomposition and got $B/T = 0.943$. Kormendy & Bender (2013b) collect V-band photometry; they get $V_T = 10.96$ and $B/T = 0.969$. We adopt $B/T = 0.95$ here. We emphasize that no conclusions depend on B/T or on our reclassification of the galaxy as an S0. The bulge Sérsic index is ~ 4.9; under these circumstances, it is commonly necessary to correct the 2MASS K_T magnitude slightly. We determine a correction of $\Delta K_T = -0.185$ and apply it to derive the photometric parameters listed in **Table 3**.

NGC 1023: The asymptotic outer rotation velocity $V_{\rm circ} = 251 \pm 15$ km s^{-1} is from Column (12) of Table 1 in Dressler & Sandage (1983).

NGC 1277: We adopt the Perseus cluster distance and NGC 1277 BH mass from van den Bosch et al. (2012). However, our analysis of the host galaxy (Kormendy & Bender 2013b) is different from that of van den Bosch, who decompose the light distribution into four radially overlapping components. This is operationally analogous to a multi-Gaussian expansion in the sense that it forces the Sérsic indices of all components to be small. Partly for this reason, they concluded that the bulge is not classical. We find that the ellipticity at large radii is similar to the ellipticity near the center; this is a sign also seen in many edge-on S0s in the Virgo cluster (Kormendy & Bender 2012) and indicates that the bulge dominates at both small and large radii. We decomposed the galaxy into two components such that the bulge dominates at both small and large radii. The decomposition is robust, the bulge has a Sérsic index of 3.5 ± 0.7, and $B/T = 0.55 \pm 0.07$. Both results imply that the bulge is classical.

NGC 2549: Krajnović et al. (2009) find that $M_\bullet = (1.4^{+0.2}_{-1.3}) \times 10^7\ M_\odot$ for $D = 12.3$ Mpc, quoting 3-σ errors. In this case, dividing the 3-σ error bars by 3 would obscure the fact that this is an unusually weak BH detection. We therefore read the 1-σ errors directly from the χ^2 contours shown in their paper. The result is approximate, $M_\bullet = 1.45(0.31 - 1.65) \times 10^7\ M_\odot$ for our adopted $D = 12.70$ Mpc, but more realistic.

NGC 3115: Kormendy & Richstone (1992) discovered the BH and got $M_\bullet = 1.0(0.3{-}3.3){\times}10^9\ M_\odot$ from isotropic models and a smallest possible $M_\bullet = 1{\times}10^8\ M_\odot$ from the most extreme anisotropic model that fit their CFHT kinematic data. These are consistent with $M_\bullet{=}0.90(0.62{-}0.95){\times}10^9\ M_\odot$ adopted from Emsellem, Dejonghe & Bacon (1999). Additional measurements have ranged from $5{\times}10^8\ M_\odot$ to $2{\times}10^9\ M_\odot$ (Kormendy et al. 1996b; Magorrian et al. 1998).

NGC 3585: The outer rotation velocity $V_{\rm circ}$ for the embedded disk is from Scorza & Bender (1995).

NGC 3998 is listed twice in **Table 3**, once with the BH mass that we adopt from stellar-dynamical models (Walsh et al. 2012) and once with the smaller BH mass based on the emission-line rotation curve (De Francesco et al. 2006). We illustrate this in **Figure 12** as an example of why we do not use $M_\bullet$ values determined from ionized gas rotation curves when line widths are not taken into account.

We use $B/T = 0.85 \pm 0.02$ from bulge-disk decompositions in Kormendy & Bender (2013b) and in Sánchez-Portal et al. (2004). With this B/T, NGC 3998 is the most significant bulge outlier to the $M_\bullet - M_{K,\rm bulge}$ correlation, as Walsh et al. (2012) concluded. There is a possibility that a three-component, bulge-lens-disk decomposition is justified; if so, B/T would be smaller, ~ 0.66. Then NGC 3998 would be a more significant outlier, in the manner of NGC 4342 and the galaxies discussed in Section 6.5. For σ_e, we adopt the mean of $\sigma_e = 270$ km s^{-1} found by Walsh for $r_e \simeq 18''$ from our photometry and $\sigma_e = 280$ km s^{-1} which we find using Gültekin's definition, our photometry, and kinematic data from Fisher (1997).

NGC 4526: This is the brightest S0 galaxy in the Virgo cluster and the first galaxy to have a BH discovered using the central CO rotation curve (Davis et al. 2013). We use $B/T = 0.65 \pm 0.05$ from Kormendy & Bender (2013b) and $\sigma_e = 222 \pm 11$ km s^{-1} from Davis et al. (2013), but we checked that σ_e is consistent with our definition of how to average $V^2(r) + \sigma^2(r)$. The asymptotic circular velocity is from Pellegrini, Held, & Ciotti (1997), but it is uncertain whether the measured rotation curve reaches far enough out in this and almost any bulge-dominated S0.

NGC 4258: The spectacular H_2O maser disk and consequent accurate BH mass measurement were discovered by Miyoshi et al. (1995). Herrnstein et al. (1999) uses the masers to measure a direct geometric distance $D = 7.2 \pm 0.3$ Mpc to NGC 4258. Herrnstein et al. (1999) interprets small departures from precise Keplerian rotation in terms of a warped gas disk and derives an improved BH mass. Our adopted mass is based in large part on this result. Section 3.3 provides the details. Sources for $V_{\rm circ}$ are listed in Kormendy et al. (2010).

Given a "bomb-proof" accurate BH mass in a conveniently inclined galaxy, NGC 4258 has been used to test both stellar-dynamical and ionized-gas-dynamical $M_\bullet$ measurement machinery (Sections 3.1 and 3.2, respectively).

NGC 4594 = M 104 = the Sombrero Galaxy: The BH discovery paper was Kormendy (1988b), who obtained $M_\bullet = 5.5(1.7\ -\ 17) \times 10^8\ M_\odot$. The quoted error bar was conservative, but the best-fitting mass was within 17 % of the present adopted value, $M_\bullet = 6.65(6.24\ -\ 7.05) \times 10^8\ M_\odot$ (Jardel et al. 2011). The BH detection was confirmed at HST resolution by Kormendy et al. (1996a), but the mass was estimated only by reobserving at HST resolution a set of models that were designed for ground-based data. As a result, $M_\bullet \sim 1.1 \times 10^9\ M_\odot$ was not very accurate. Emsellem et al. (1994) measured $M_\bullet \sim 5.3 \times 10^8\ M_\odot$ and Magorrian et al. (1998) got $M_\bullet = 6.9(6.7\ -\ 7.0) \times 10^8\ M_\odot$ based on two-integral models. The presently adopted BH mass is based on three-integral models.

We adopt the total magnitude measurement $B_T = 8.71$ in Burkhead (1986) and correct the 2MASS K magnitude to give $(V - K)_0 = 2.980$. Also, $V_{\rm circ}$ is from Faber et al. (1977) and Bajaja et al. (1984).

NGC 4596: We adopt the $M_{\rm BH,fix}$ mass in Table 2 of Sarzi et al. (2001). Also, $B/T = 0.27 \pm 0.04$ comes from comparing Benedict's (1976) decomposition at surface brightnesses $\lesssim 23.5$ B mag arcsec^{-2} with the adopted total magnitude $B_T = 11.37$, i. e., the mean of values in RC3, the Hyperleda main table, and the Hyperleda integrated photometry table. The rotaton velocity corrected for asymmetric drift is from Kent (1990).

NGC 7457: We confirm Gültekin's value of $\sigma_e = 67 \pm 3$ km s^{-1} with our photometry and kinematic measurements. The outer disk circular velocity is from our kinematic data and those of Cherepashchuk et al. 2010, corrected for asymmetric drift by them but for our assumed inclination of the galaxy, $i = 59^\circ \pm 2^\circ$.

Notes on Disk Galaxies With Pseudobulges:

Our Galaxy: Photometric parameters are discussed in Kormendy & Bender (2013b). Our Galaxy requires special procedures because we live inside it. For the convenience of readers, we summarize the provenance of the photometric parameters here. The Galaxy has a "boxy bulge" (Weiland et al. 1994; Dwek et al. 1995) that is generally understood as an almost-end-on bar (Combes & Sanders 1981; Blitz & Spergel 1991). It is therefore a pseudobulge – a component built out of the disk. There is no photometric or kinematic sign of a classical bulge (see Freeman 2008, Howard et al. 2009, Shen et al. 2010, and Kormendy et al. 2010 for reviews and for some of the evidence). We average pseudobulge-to-total luminosity ratios from Kent, Dame & Fazio (1991) and Dwek et al. (1995) to get $PB/T = 0.19 \pm 0.02$. To get $M_{KsT} = -23.7$, we adopt the total K-band luminosity $L_K = 6.7 \times 10^{10}\ L_{K\odot}$ from Kent, Dame & Fazio (1991) and convert it from their assumed distance of 8 kpc to our assumed distance of 8.28 kpc from Genzel et al. (2010). The disk and pseudobulge absolute magnitudes follow from PB/T. Finally, V-band magnitudes are derived from K-band magnitudes by assuming that $(V - K)_0 = 2.980$. The bulge absolute magnitude is reasonably accurate, because the bulge is old; the main effect of estimating $M_{V,\rm bulge}$ from $M_{K,\rm bulge}$ is to implicitly correct for internal extinction. The disk magnitude is much more uncertain, because the assumed color does not take young stars into account. However, this has only minimal effects on our conclusions.

The adopted BH mass is now securely derived from the orbits of individual stars. The history of the remarkable improvement in $M_\bullet$ measurements is reviewed in Genzel, Eisenhauer & Gillessen (2010); early stages were covered in KR95. The velocity dispersion σ_e is from Tremaine et al. (2002).

Circinus is like M 31 in structure and inclination, but it is a smaller galaxy with a gas-rich pseudobulge, and it has a smaller BH than M 31. It is a difficult case, because it is close to the Galactic plane. The Galactic absorption is large, and our estimates of it are uncertain. Kormendy & Bender (2013b) measure the galaxy's photometric parameters; the total apparent magnitude is $K_T = 4.71$. The pseudobulge classification and $PB/T = 0.30 \pm 0.03$ are from the same paper and from Fisher & Drory (2010). We adopt $V_T = 10.60 \pm 0.04$ as the average of values tabulated in the RC3 (de Vaucouleurs et al. 1991) and Hyperleda (Paturel et al. 2003). Comparing K_T and V_T in the context of various published estimates of the Galactic absorption, we adopt $A_V = 3.15$ from Karachentsev et al. (2004), because it gives the most reasonable total color for the galaxy, $(V - K)_0 = 3.05$. This then determines the other photometric parameters, including the distance $D = 2.82$ Mpc (Karachentsev et al. 2004).

Greenhill et al. (2003) measure masers both in outflowing gas and in a well-defined, essentially edge-on accretion disk. The latter masers show a well-defined Keplerian rotation curve which implies that $M_\bullet = (1.14 \pm 0.20) \times 10^6\ M_\odot$. We adopt this value, although Huré et al. (2011) find hints

that $M_\bullet$ may be smaller. We are uncomfortable about the conflicting published velocity dispersion measurements: Oliva et al. (1995) measure 168 km s^{-1} consistently (RMS = 10 km s^{-1}) from four infrared CO bands; their instrumental resolutions ($\sigma_{\rm instr} \simeq 80$ and 51 km s^{-1} should be sufficient. But Maiolino et al. (1998) measure $\sigma \simeq 79 \pm 3$ km s^{-1} at $\sigma_{\rm instr} \simeq 64$ km s^{-1} in the 2.3 – 2.4 μm CO bands using an integral-field spectrograph and AO; there is little gradient in the central $1\farcs2$ except that the nucleus has a bulge-subtracted velocity dispersion of $\sigma = 55 \pm 15$ km s^{-1}. More recently, Müller-Sánchez et al. (2006) use SINFONI AO integral-field specrtoscopy on the VLT to measure $\sigma \simeq 80$ km s^{-1} in the central $0\farcs4 \times 0\farcs4$. We adopt $\sigma_e = 79 \pm 3$ km s^{-1}.

NGC 1068 is a prototypical oval galaxy (Kormendy & Kennicutt 2004) with an unusually massive pseudobulge that is more than a magnitude more luminous and a factor of ~ 4 more massive than the classical bulge of M 31. Kormendy & Bender (2013b) find that the pseudobulge-to-total luminosity ratio is quite different in the optical and infrared; $PB/T \simeq 0.41$ at H but $\simeq 0.3$ at r and i. We use these values at K and V, respectively. We adopt $\sigma_e = 151 \pm 7$ km s^{-1} from Gültekin et al. (2009c) and $V_{\rm circ} = 283 \pm 9$ km s^{-1} from Hyperleda but note that the latter value is uncertain. We know of no two-dimensional analysis of the outer velocity field that takes the two differently oriented nested ovals into account; for a galaxy that is close to edge-on, this is very important.

The BH discovery papers are Gallimore et al. (1996) and Greenhill et al. (1996) who found and measured positionally resolved H_2O maser emission with the VLA and with VLBA, respectively. The case is not as clean as that in NGC 4258, because the rotation velocity in the non-systemic-velocity sources decreases with increasing radius more slowly than a Keplerian, $V(r) \propto r^{-0.31 \pm 0.02}$ (Greenhill et al. 1996). The simplest and most plausible explanation is that the mass of the masing disk is not negligible with respect to the BH. Ignoring this, the above papers derive a first approximation to $M_\bullet$ of 1×10^7 $M_\odot$. Greenhill & Gwinn (1997) report additional VLBI observations and refine the total mass to 1.54×10^7 $M_\odot$. Lodato & Bertin (2003) confirm this: they get $M_\bullet = (1.60 \pm 0.02) \times 10^7$ $M_\odot$ using the approximation of a Keplerian rotation curve. However, both Lodato & Bertin (2003) and Huré (2002; see also Huré et al. 2011) derive models that account for the disk mass, and we adopt the average of their results, $M_\bullet = (8.39 \pm 0.44) \times 10^6$ $M_\odot$ (Section 3.3.3).

Note again the extreme misalignment of the maser disk, which is essentially edge-on, and the rest of the galaxy, which is $\sim 21^\circ$ from face-on.

NGC 1300: We adopt D (Local Group) = 21.5 Mpc, consistent with the distances to neighbors NGC 1297 and NGC 1232, all members of grouping 51 −7 +4 (Tully 1988). However, Tonry et al. (2001) find $D = 28.5$ Mpc for NGC 1297. We cannot tell whether there is a problem with one of the distances or whether NGC 1297 is fortuitously close to NGC 1300 in the sky but half of the distance from us to the Virgo cluster behind it. This is one example of a general problem: Distances remain uncertain, and we do not fold these uncertainties into our error estimates.

The effective radius of the pseudobulge is $r_e \simeq 4\farcs5 \pm 0\farcs1$ (Fisher & Drory 2008; Weinzirl et al. 2009). For σ_e, we use the mean dispersion 88 ± 3 km s^{-1} interior to $3\farcs5$ as shown in Figure 6 of Batcheldor et al. (2005).

NGC 2273: We calculated $\sigma_e = 125 \pm 9$ km s^{-1} from our photometry and from kinematic data in Barbosa et al. (2006). Also, $V_{\rm max} = 196 \pm 5$ km s^{-1} is from H I data in Noordermeer et al. (2007).

NGC 2787 is our only explicit example of a phenomenon that must be moderately common – a galaxy that contains both a classical and a pseudo bulge. Erwin et al. (2003) make a decomposition with $B/T = 0.11$ and $PB/T = 0.26$. We adopt this decomposition to make the above point. However, at our present level of understanding, trying to separate bulges from pseudobulges is risky. In other galaxies, we identify the dominant component and assign all of the (pseudo)bulge light to it. Here, too, Columns 6 and 11 list the magnitudes of the bulge and pseudobulge together, and we treat this as a pseudobulge galaxy. The outer rotation velocity $V_{\rm circ}$ is from Shostak (1987) and from van Driel & van Woerden (1991).

NGC 3227: We use the corrected SBF $D = 23.75$ Mpc for companion galaxy NGC 3226 (Tonry et al. 2001). Mundell et al. (1995) provide $V_{\rm circ}$.

NGC 3368 is a pseudobulge-dominated S(oval)ab spiral galaxy with a central decrease in σ at $r < 1''$ (Nowak et al. 2010). As emphasized by these authors, different definitions give different values of σ_e and this affects whether or not the BH falls within the scatter of the $M_\bullet - \sigma_e$ relation. Luminosity-weighted within the VLT SINFONI field of view of $3'' \times 3''$, $\sigma = 98.5$ km s^{-1} and the BH is consistent with $M_\bullet - \sigma_e$. However, we use the definition that σ_e is the luminosity-weighted mean of $V^2 + \sigma^2$ within approximately r_e (the exact radius makes little difference). Because rotation contributes and because $r_e \simeq 11\farcs2 \pm 2\farcs7$ for the pseudobulge, we get a substantially larger value of $\sigma_e \simeq 125 \pm 6$ km s^{-1}. This is based on our photometry and on kinematic data in Héraudeau et al. (1999) corrected inside $r_e/2$ to agree with Nowak et al. (2010). Sarzi et al. (2002) derived $\sigma_e = 114 \pm 8$ km s^{-1} using dispersions only; this shows approximately how much difference rotation makes to the definition. Many pseudobulge galaxies are similar in that central velocity dispersions are much smaller than the σ_e that is obtained from the $V^2 + \sigma^2$ definition.

Nowak et al. (2010) suggest that NGC 3368 contains a small classical bulge in addition to the dominant pseudobulge. We add them together.

NGC 3384: Gültekin et al. (2009c) used $\sigma_e = 143 \pm 7$ km s^{-1}. We essentially confirm this: With our photometry and kinematic measurements, we get $\sigma_e = 150 \pm 8$ km s^{-1}. We adopt the mean.

NGC 3393 is another prototypical oval galaxy with a large pseudobulge. **Figure 10** is included to emphasize its similarity to NGC 1068: It is only $\sim 13^\circ$ from face-on (Cooke et al. 2000), but it contains an edge-on, masing accretion disk.

All measurements of this galaxy are somewhat uncertain. Kormendy & Bender (2013b) find a preliminary $PB/T = 0.27 \pm 0.06$. The BH mass measurement is based on the rotation curve of a masing molecular disk (Kondratko, Greenhill & Moran 2008). The maser sources are well distributed along a line indicative of an edge-on disk, but they cover only a small radius range, so they do not securely measure the rotation curve shape. They are consistent with Keplerian; this gives an enclosed mass of $M_\bullet = (3.55 \pm 0.23) \times 10^7$ $M_\odot$ at $r \leq 0.41 \pm 0.02$ pc. But there are signs that the rotation curve is slightly flatter than Keplerian. For their best-fitting sub-Keplerian rotation curve, Kondratko et al. (2008) get $M_\bullet \simeq 2.97 \times 10^7$ $M_\odot$. In contrast, Huré et al. (2011) find a good solution with a maser disk that is 6 times as massive as the BH. Then $M_\bullet \simeq 0.67 \times 10^7$ $M_\odot$. This is the only galaxy in our sample in which two such analyses give substantially different results. We adopt the mean of the two masses and half of the difference as our error estimate.

The velocity dispersion σ_e is securely measured by Greene et al. (2010), but $V_{\rm circ}$ is too uncertain, because the galaxy is too close to face-on.

NGC 3489 is a weakly barred S0 with a dominant (pseudo)bulge that contributes $\sim 35\,\%$ of the light of the galaxy (Nowak et al. 2010). These authors argue plausibly that about one-third of this component is a classical bulge. We conservatively add them together. Also, we derive $\sigma_e = 113 \pm 4$ km s^{-1} from our photometry and kinematic data in McDermid et al. (2006).

NGC 4388: We have only central velocity dispersion data for this galaxy. Greene et al. (2010) measure $\sigma = 107 \pm 7$ km s^{-1}; Ho et al. (2009) get 91.7 ± 9.5 km s^{-1}, and we adopt the average, $\sigma_e = 99 \pm 10$ km s^{-1}. This is likely to be an underestimate of σ_e as we define it, because it neglects rotation inside the half-light radius $r_e \simeq 3\farcs0$ of the pseuodbulge.

NGC 4736 and NGC 4826: We are most grateful to Karl Gebhardt for making $M_\bullet$ available before publication (Gebhardt et al. 2013). For NGC 4736, we calculated σ_e from our photometry (Kormendy & Bender 2013b) and kinematic data in Möllenhoff et al. (1995). For NGC 4826, σ_e is from our photometry and kinematic data in Rix et al. (1995). For both galaxies, the result is not significantly different if we integrate inside the pseudobulge $r_e \simeq 9\farcs7$ and $16\farcs7$, respectively (Fisher & Drory 2008) or inside $r_e/2$. Sources for $V_{\rm max}$ are given in Kormendy et al. (2010).

NGC 4945 is an edge-on, dusty Scd with a small pseudobulge ($PB/T = 0.07$) that is heavily absorbed at optical wavelengths. We use $D = 3.58$ Mpc, i. e., the mean of two "TRGB" distances determined from the magnitude of the tip of the red giant branch in the stellar color-magnitude diagram (3.36 Mpc: Mouhcine et al. 2005 and 3.80 Mpc: Mould & Sakai 2008). We adopt $K_T = 4.438$, i. e., the integral of the surface brightness and ellipticity profiles measured in Kormendy & Bender (2013b). For comparison, 2MASS lists $K_s = 4.483$. Our total magnitude implies a slightly more plausible color $(V - K)_0 = 2.712$.

The BH detection in Greenhill, Moran & Herrnstein (1997) was rejected by Gültekin et al. (2009c) because the maser rotation curve is asymmetric and because the maser disk inclination is only approximately constrained to be edge-on by its linear distribution at PA $\approx 45^\circ$. Still, the assumption that the disk is edge-on is at least as secure as many other assumptions that we routinely make. And the rotation curve decreases cleanly with radius on one side of the center. Thus $M_\bullet$ is not more uncertain than the most problematic cases based on stellar and ionized gas dynamics.

The maser disk and the galaxy disk have similar PA, are similarly edge-on, and rotate in the same direction (Greenhill et al. 1997).

NGC 6264 and NGC 6323 are the most distant disk galaxies with maser BH detections. Kormendy & Bender (2013b) measure r- and K-band brightness profiles, respectively. No HST imaging is available for either galaxy, although CFHT images with PSF dispersion radii of $\sigma_* = 0\farcs23$ are available for NGC 6323. Both galaxies have small pseudobulges; NGC 6264 has $PB/T \simeq 0.17 \pm 0.03$ and NGC 6323 has $PB/T \simeq 0.05 \pm 0.01$. For both galaxies, we adopt σ_e equal to the central velocity dispersion measured by Greene et al. (2010).

IC 2560: Evidence for a BH based on the dynamics of a H_2O maser disk was reported in Ishihara et al. (2001) and refined with further observations in Yamauchi et al. (2012). We adopt $M_\bullet$ and its upper error bar from the latter paper. However, only one point in the rotation curve is observed from high-$|V|$ masers, so we cannot tell whether the rotation curve is Keplerian. Centripetal acceleration of the systemic masers is accurately measured, but their velocity gradient with position along the major axis of the disk is not accurately enough known to give a second meaningful (V, r) point as discussed in Section 3.3.2. Since some maser disks have gas masses that are a significant fraction of the BH mass, we must regard the BH mass determination for IC 2560 as an upper limit. Nevertheless, $M_\bullet$ is clearly small enough to support our conclusion that BHs do not correlate with pseudobulges in the same way as they do with classical bulges.

We have only a central velocity dispersion measurement (Greene et al. 2010). The outer rotation velocity $V_{\rm circ}$ is from Hyperleda.

UGC 3789: We adopt the geometric distance $D = 49.9 \pm 7.0$ Mpc from Braatz et al. (2010). It provides a check of our D (Local Group) distances (**Table 2**, Column 3, source 9), which would have been 47.8 Mpc. The K magnitude is from 2MASS, but the V magnitude is estimated from K using a photoelectric measurement of $B - V = 0.92$ in a $50''$ diameter aperture by Arkhipova & Saveleva (1984). The correlation of $(V - K)_0$ with $(B - V)_0$ then gives $(V - K)_0 \simeq 2.90$.

UGC 3789 is an another example of a surprisingly common phenomenon for which we know no explanation: It is a prototpical, almost-face-on oval galaxy with an edge-on molecular disk surrounding the BH (**Figure 10**). The velocity dispersion is from Greene et al. (2010) and $V_{\rm circ}$ is from Hyperleda.

Notes on Discarded Galaxies (Cyan Lines in Tables 2 and 3):

NGC 2778 is discarded (1) because it provides only an upper limit on $M_\bullet$ (Schulze & Gebhardt 2011) and (2) because the implied mass-to-light ratio $M/L_K = 3.3$ is too large for an old stellar population from which the dark matter has been subtracted and modeled separately (Section 6.6). We conclude that dark matter is still included and therefore that the $M_\bullet$ upper limit is substantially too small. This galaxy is a good illustration of the importance of adding M/L constraints to our mass measurements, something that has not heretofore been done

NGC 3607 is a core elliptical with a BH detection and $M_\bullet$ measurement in Gültekin et al. (2009b). The modeling did not include dark matter. Schulze & Gebhardt (2011) and Rusli et al. (2013) show that this is not a large problem if $r_{\rm infl}$ is very well resolved, but they show that $M_\bullet$ is systematically underestimated if $r_{\rm infl}/\sigma_* \lesssim 5$. Both papers provide calibrations of how the $M_\bullet$ correction factor depends on $r_{\rm infl}/\sigma_*$, but the two calibrations disagree even though they both use variants of the Nuker code. The disagreement may result from technical details such as the number of orbits used in the modeling. But the problem is severe for NGC 3607, for which the apparent value of $r_{\rm infl}/\sigma_* \simeq 1.5$. Based on the Schulze calibration, we should multiply the Gültekin $M_\bullet = 1.4 \times 10^8\ M_\odot$ (**Figure 12**) by a factor of $\sim$2. The Rusli calibration gives a factor of $\sim$4.7. We conclude that the BH detection is reliable but that we do not know the BH mass well enough to retain NGC 3607 in our sample.

NGC 4261, NGC 6251, NGC 7052, A1836 BCG, and A3565 BCG: All of these galaxies have valid BH detections based on optical emission-line kinematic observations in the papers listed in Column 12. However, the widths of the emission lines are comparable to the rotation velocities near the center, and these widths were not taken into account in estimating $M_\bullet$. As discussed in the BH discovery papers and in Section 3.2 here, it is not guaranteed that line widths imply a "contribution" to $M_\bullet$ as they would for absorption-line velocity dispersions. But it is likely that they are not ignorable. In Section 6.2, we compare these BH masses to the BH–host-galaxy correlations that we derive for the most reliable BH masses. We find that the above galaxies do indeed have anomalously small BH masses. The conservative conclusion therefore is that neglecting emission-line widths can result in underestimated BH masses. We therefore omit all such masses, even those for lower-luminosity bulges in which the measured $M_\bullet$ does not obviously deviate from the correlations.

Cygnus A: The BH discovery (Tadhunter et al. 2003) is based on the optical emission-line rotation curve measured with HST STIS. The authors note that the emission lines are very broad, but they do not include line widths in their $M_\bullet$ determination. Therefore the BH mass is probably underestimated. The velocity dispersion is from Thornton et al. (1999) and is very uncertain; it is based on the observed width of the Ca infrared triplet absorption lines but not on any of the standard methods of comparing the spectrum to a standard star. Finally, although we used the brightest V-band magnitude in the literature (from Paturel et al. 2000 as listed by Hyperleda), the $(V - K)_0 = 3.54$ color is implausibly large. It may be affected by large internal absorption. If so, the K-band magnitude may be usable. Nevertheless, for all of the above reasons, this galaxy is plotted in Section 6.2 and thereafter is omitted from all correlations and fits.

Photometric decomposition of brightness distributions into (pseudo)bulge and disk components is carried out in the same way for classical and pseudo bulges. The procedure (Kormendy 1977) begins by assuming a functional form for bulge brightness profiles that is motivated by pure-bulge galaxies (ellipticals) and a functional form for disk brightness profiles that is motivated by pure-disk galaxies. Here, we fit bulges with Sérsic (1968) functions, $\log I(r) \propto r^{1/n}$. Many studies have shown that the Sérsic index n is generally > 4 for giant ellipticals, ~ 2 to 3 for smaller ellipticals, $\gtrsim 2$ for classical bulges, and $\lesssim 2$ for pseudobulges (see KFCB; Kormendy 2012 for reviews). Disks are usually exponential, $I(r) \propto e^{-r/r_0}$, where r_0 is the scale length (e. g., Freeman 1970; see van der Kruit & Freeman 2010 for a review). We then decompose the observed, bulge + disk profile into two components with these analytic forms that add up to the observed profile. Sometimes a third component (usually a bar or a lens) is needed; such components are included in disk light.

Fifteen of the galaxies in **Table 3** have $(P)B/T$ measurements from 2 – 7 independent sources. The rest have only one reliable source; most of them are measured in Kormendy & Bender (2013b). Composite brightness profiles are derived there from our own images and from images available through online archives. The HST archive is particularly important, because we need as much spatial resolution as possible to provide leverage on bulges that dominate over disks within only a small radius range near the center. However, no $(P)B/T$ ratio is seriously compromised by the lack of HST data. Various decomposition algorithms are used in published papers; many are carried out on two-dimensional images. Kormendy & Bender (2013b) construct Sérsic-exponential decompositions of major-axis profiles but take ellipticity profiles fully into account in calculating $(P)B/T$. This is more reliable than two-dimensional decomposition when, in constructing the latter, it is assumed that the flattening of each component is constant with radius. This assumption is often wrong, especially for bulges. Then two-dimensional algorithms must resort to decompositions into many components that are not physically meaningful in order to fit the isophote ellipticities. When we can, we average $(P)B/T$ from multiple sources; this helps to estimate uncertainties. A galaxy can contain both a classical bulge and a pseudobulge (Section 4), so both B/T and PB/T can be > 0. The resulting B/T and PB/T values are listed in **Table 3**.

5.1 Comparison of Our Sample With Recent BH Studies

Our sample has 45 ellipticals, 20 classical bulges, and 22 pseudobulges. Of these, we omit seven ellipticals and one classical bulge from correlation fits, because $M_\bullet$ was determined using ionized gas kinematics without taking broad emission-line widths into account. We regard these as valid BH discoveries, but $M_\bullet$ may be underestimated, at least for the bigger galaxies (Section 6.3). These galaxies are identified with cyan lines in tables and with cyan symbols in plots. NGC 4382 and NGC 3945 have only $M_\bullet$ upper limits, but these will be important to the conclusions. Almost all core ellipticals with $M_\bullet$ measurements based on stellar dynamics have halo dark matter included in the models; when not, and when a correction to $M_\bullet$ is required, this is discussed in the Supplementary Information table notes on **Corrections to stellar-dynamical BH masses for core galaxies** and in notes to individual objects.

It is useful to compare this study with three recent studies of BH–host-galaxy correlations:

Gültekin et al. (2009c) had 25 ellipticals, 14 classical bulges, and 10 pseudobulges. However, they did not have $(P)B/T$ ratios for 17 galaxies, so the $M_\bullet - M_{B,\rm bulge}$ sample is smaller than the $M_\bullet - \sigma$ sample. Gültekin did not have enough information to conclude that $M_\bullet$ values based on emission lines that did not model line widths should be omitted; at that time, these galaxies still included M 87. The stellar-dynamical models used did not include dark matter.

McConnell & Ma (2013) have 36 elliptical galaxies and 34 bulges. Classical and pseudo bulges are not distinguished, although early- and late-type galaxies are distinguished. This is almost but not quite the same thing. Here, we argue that the bulge-pseudobulge distinction is crucial, because

classical bulges show $M_\bullet$–host-galaxy correlations whereas pseudobulges largely do not. Almost all of the $M_\bullet$ determinations based on stellar dynamics do include dark matter in the models. Galaxies with $M_\bullet$ based on emission-line rotation curves for which line widths were ignored are not discarded from fits. This paper is an extension of Gültekin et al. (2009c) mostly in the classical tradition of exploring a single set of $M_\bullet$–host-parameter correlations but with clear signs of some of the present results (especially the "saturation" of $M_\bullet - \sigma$ at high $M_\bullet$).

Graham & Scott (2013) have 30 ellipticals and ostensibly 48 disk galaxies, but 7 "disk galaxies" (M 32, NGC 1316, NGC 2960, NGC 3607, NGC 4459, NGC 5128, and Cygnus A) are ellipticals. Graham and Scott do not distinguish between classical bulges and pseudobulges; instead, they compare barred and unbarred galaxies. But many unbarred galaxies contain pseudobulges, and many barred galaxies contain classical bulges. Some stellar-dynamical BH masses include dark matter in the models (the McConnell et al. 2011a, b, 2012 galaxies), but many do not (the Gebhardt et al. 2003 galaxies) even though masses that include dark matter in the models are published (Schulze & Gebhardt 2011). The sample also contains a number of questionable $M_\bullet$ values. For example, NGC 2778 now has just an upper limit on $M_\bullet$ (Schulze & Gebhardt 2011) not a BH detection (Gebhardt et al. 2003). Also, Graham and Scott include seven BH masses read off of an unlabeled plot in Cappellari et al. (2008). Michele Cappellari (private communication) recommends that we not use these preliminary values. We follow his suggestion. Graham also retains $M_\bullet$ values that were derived from emission-line rotation curves for which line widths were ignored.

Comparisons with results in the above papers are included in Section 6.

6. BH CORRELATIONS – OBSERVATIONS

Based on **Tables 2** and **3**, this section rederives and brings up to date the correlations between BH masses and host galaxy components. In doing so, we review the two phases of BH demographic studies that we differentiated in Section 1.2.

Sections 6.1 and 6.2 review the first phase, i. e., the pre-HST and HST-era derivations of the correlations between $M_\bullet$ and bulge luminosity or mass and velocity dispersion, respectively. These derivations mostly did not differentiate between ellipticals and the bulges of disk galaxies or between bulges of different types. A single set of correlations ($M_\bullet - L_{\rm bulge}$, $M_\bullet - M_{\rm bulge}$, and $M_\bullet - \sigma$) was found for all hot stellar parts of galaxies. This period was a decade-long plateau in our demographic picture in which the focus was on debates about correlation slopes, zeropoints, and scatter, based on different choices of analysis machinery, on different selection of objects (e. g., inactive galaxies versus AGNs), and on different views of what constitutes a reliable BH sample. Theoretical work on BH–host-galaxy coevolution focused on using a single parameter – the gravitational potential well depth as measured by bulge velocity dispersion – to control the effects of AGN feedback.

Now, we have moved beyond this plateau in our understanding as it has become possible to distinguish different correlations for different kinds of host-galaxy components. The rest of Section 6 updates the BH correlations using our Section 5 sample, and in doing so, it reviews and further develops this new phase in BH demographic studies. Section 6 is long, so a road map is useful:

Section 6.3 is a "lemma" which discusses why we omit from correlation studies those BH masses that were derived from optical, emission-line rotation curves without taking (usually large) emission line widths into account. In much the same way that stellar dynamics would cause us to underestimate $M_\bullet$ if we ignored large velocity dispersions, we now have clear signs that these emission-line-based measurements underestimate $M_\bullet$. Section 6.3 also identifies two other galaxies for which we believe that $M_\bullet$ has been underestimated.

Section 6.4 presents a new result. We and Bender et al. (2013) find (essentially independently) that major mergers in progress deviate from the $M_\bullet$–host-galaxy correlations in having unusually small BHs for their galaxy luminosities, stellar masses, and velocity dispersions.

Section 6.5 discusses a small number of galaxies that are known to deviate in the opposite sense: They have unusually large BH masses, outside the scatter shown by BHs in other galaxies. We discuss what these galaxies may be telling us. Both kinds of deviators – large-$M_\bullet$ monsters and small-$M_\bullet$ BHs in mergers – are omitted from derivations of BH parameter correlations.

Section 6.6 derives, for ellipticals and for classical (elliptical-galaxy-like) bulges only, updated correlations between $M_\bullet$ and host luminosity, stellar mass, and velocity dispersion. We revise the derivation of the ratio of BH mass to bulge mass. The new ratios are substantially larger than ones in past papers, and the ratio increases slightly with increasing bulge mass.

Section 6.7 introduces the observed distinction between two kinds of elliptical galaxies that, we suggest, are remnants of major, dissipational ("wet") and dissipationless ("dry") mergers. With our new and larger sample, we confirm the strong hints seen by applying the Faber-Jackson (1976) $M_{\rm bulge} \propto \sigma^{(\sim 4)}$ relation (Lauer et al. 2007a) and more directly by recent papers on the biggest BHs (McConnell et al. 2011a, b; 2012) that the $M_\bullet - \sigma$ correlation saturates at high $M_\bullet$ and that this happens only for core galaxies. For these, $M_\bullet$ becomes essentially independent of σ (but not $M_{\rm bulge}$) at the highest BH masses. This in turn is evidence that the most recent evolution of core ellipticals was via dry mergers, because then BH and galaxy masses grow but σ is essentially preserved.

After this update of the tight BH correlations with classical bulges and ellipticals, we broaden the discussion by examining correlations with other kinds of galaxy components:

Section 6.8 shows that BHs do not correlate tightly enough with pseudobulges to imply close coevolution. Pseudobulge BHs generally deviate by having smaller masses than the scatter of points in the correlations for classical bulges and ellipticals. This motivates the suggestion in Sections 8.1 and 8.3 that there are two different modes of BH feeding for classical and pseudo bulges.

Section 6.9 confirms that $M_\bullet$ does not correlate with the properties of galaxy disks.

Section 6.10 reviews in more detail the arguments of Kormendy, & Bender (2011) that BHs do not correlate tightly enough with the properties of dark matter halos to imply that there is any special coevolution physics beyond what is already implied by the BH – bulge correlations. Of course, dark matter gravity ultimately controls hierarchical clustering and therefore much of galaxy formation. But the data require no conceptual leap beyond the physics of wet major mergers to the idea that additional coevolution physics is controlled by dark matter in the absence of bulges.

Section 6.11 reviews the close but puzzling connection between BHs and nuclear star clusters in their relations with host galaxies.

Section 6.12 discusses the even more remarkable correlation between BHs and globular cluster systems that surround elliptical galaxies.

Section 6.13 reviews correlations of $M_\bullet$ with the stellar light and mass whose "absence" defines the shallow-density-gradient cores of the biggest elliptical galaxies. The now-canonical explanation is that cores are scoured by black hole binaries that are made in galaxy mergers. The BHs in a binary then decay toward an eventual BH–BH merger by flinging stars away from the center. The tightness of the observed correlations between $M_\bullet$ and core properties provides a "smoking gun" connection between BHs and cores that does much to support the above picture.

Sections 6.14 and 6.15 mention other BH correlations, e. g., bivariate, "fundamental plane" correlations between $M_\bullet$ and any two of σ, effective radius, and effective brightness. Finally:

Section 6.16 is our summary: BH masses correlate tightly enough to imply strong coevolution (Section 1.4) only with classical bulges and ellipticals and with no other galaxy component.

Section 7 then continues by discussing BHs in pure-disk galaxies; that is, ones that contain no classical bulges and essentially no pseudobulges. With all of our observational results in place, Section 8 then updates our understanding of what we learn about the coevolution (or not) of BHs and their host galaxies.

6.1 The $M_\bullet$ – L_{bulge} and $M_\bullet$ – M_{bulge} correlations

The earliest BH demographic result was the correlation between $M_\bullet$ and the luminosity of the bulge component of the host galaxy. Based on two objects, Dressler & Richstone (1988) already noted that "the [central dark] object in M 31 is 5 – 10 times more massive than the one in M 32, closer to the ratio of spheroid luminosities (~ 15) than it is to the ratio of total luminosities (~ 70)." This foreshadowed the correlation of $M_\bullet$ with bulge but not disk luminosity. Dressler (1989) was the first to propose such a correlation, based on five objects. Independently, Kormendy (1993a) was the first to illustrate the correlation, based on seven objects. In 1993, it was still possible that we were discovering only the easiest cases, so the correlation could have been the upper envelope of a distribution that extended to lower $M_\bullet$. Remarkably, the mean ratio of BH mass to bulge mass = (bulge luminosity) $*$ (mass-to-light ratio) was $\langle M_\bullet/M_{\rm bulge}\rangle = 0.0022^{+0.0017}_{-0.0009}$, consistent with more recently published values, $\sim 0.13\,\%$, and smaller than the ratio that we find here in Section 6.6.1. So the BH sample was not severely biased. An update of the $M_\bullet - L_{\rm bulge}$ correlation that includes the maser BH discovery in NGC 4258 is in KR95.

Magorrian et al. (1998) made the first study of a large sample of galaxies that were not chosen to favor easy BH detection. Virtues were the large and unbiased sample of 32 galaxies and the uniform analysis machinery of axisymmetric, two-integral dynamical models. The "down side" was that the data were very heterogeneous, ranging from high-spatial-resolution kinematic observations from Mauna Kea and Palomar (**Table 1**; notes to **Tables 2** and **3**) to ground-based spectroscopy with several arcsec resolution. BH masses proved to be accurate when based on high-resolution data but were overestimated for poorly resolved galaxies (e. g., Merritt & Ferrarese 2001; Kormendy 2004). Nevertheless, this paper provided an important "sanity check" on the generality of published BH discoveries. Also, BH detections in all but six of the 32 galaxies led to the belief that essentially all bulges contain BHs that satisfy the $M_\bullet - L_{\rm bulge}$ correlation.

Further elaboration of the $M_\bullet - L_{\rm bulge}$ correlation followed for larger and different kinds of galaxy samples and for different $M_\bullet$ quality cuts (e. g., Ho 1999a; Merritt & Ferrarese 2001; Laor 2001; Kormendy & Gebhardt 2001; McLure & Dunlop 2002; Marconi & Hunt 2003; Ferrarese & Ford 2005; Graham 2007; Gültekin et al. 2009c; Sani et al. 2011; Kormendy et al. 2011; Vika et al. 2012; Graham & Scott 2013; McConnell & Ma 2013). Particularly important was the change from visible-light (B- to R-band) absolute magnitudes to K band in order to minimize effects of internal absorption and young stars; this resulted in significantly reduced scatter (Marconi & Hunt 2003).

The $M_\bullet$–$L_{\rm bulge}$ correlation was always implicitly about bulge mass, but it was important to derive masses directly and to express the correlation explicitly in terms of $M_{\rm bulge}$. Bulge masses were derived using the virial theorem, $M_{\rm bulge} \propto r_e\sigma^2$, where r_e is the effective radius and σ is the velocity dispersion (Marconi & Hunt 2003) or from dynamical modeling (Magorrian et al. 1998; Häring & Rix 2004) or from scaling relations implied by Fundamental Plane parameter correlations (McLure & Dunlop 2002). The results were generally consistent in finding a good correlation with a few outliers (e. g., NGC 4342). Most studies are consistent with a linear relation, $M_\bullet \propto M_{\rm bulge}$, but a few studies have found hints (Häring & Rix 2004) or more of a steeper-than-linear relationship, $M_\bullet \propto M_{\rm bulge}^{1.54\pm0.15}$ (Laor 2001 complete sample). It is difficult to compare these studies fairly, because some include BH masses from AGN emission-line widths (Laor 2001) and others do not. Section 6.6 updates these results with the present sample.

There has been good agreement on the mean ratio of BH mass to bulge mass and its scatter. Merritt & Ferrarese (2001) got $\langle M_\bullet/M_{\rm bulge}\rangle = 0.0013$ with a standard deviation of a factor of 2.8; Kormendy & Gebhardt (2001) got $\langle M_\bullet/M_{\rm bulge}\rangle = 0.0013$; McLure & Dunlop (2002) got $\langle M_\bullet/M_{\rm bulge}\rangle = 0.0012$; Marconi & Hunt (2003) got $\langle M_\bullet/M_{\rm bulge}\rangle = 0.00234$ with an intrinsic dispersion of 0.27 dex, and Häring & Rix (2004) got $\langle M_\bullet/M_{\rm bulge}\rangle = 0.0014\pm0.0004$. Even the more

indirect indications via the mutual correlations between BH mass, the "mass deficit" that defines the cores of elliptical galaxies and BH mass fraction all point to a typical ratio $\langle M_\bullet/M_{\rm bulge}\rangle \simeq 0.001$ with hints of a scatter to values 10 times smaller (Kormendy & Bender 2009). However, with recent upward corrections to BH masses in giant ellipticals, with the omission of emission-line-based BH masses that we argue are underestimated, and with separate consideration for pseudobulges, we will find a larger ratio of $M_\bullet/M_{\rm bulge}$ for classical bulges and ellipticals listed in **Tables 2** and **3**.

The correlation between $M_\bullet$ and bulge mass or luminosity remains a well established, useful result that, in coming sections, will open the door to new conclusions about which parts of galaxies coevolve with AGNs. Certainly it kindled suspicions that galaxy and BH growth affect each other. However, the event that electrified the community and that – to paraphrase Christopher Marlowe – "launched a thousand [papers]" on BH–galaxy coevolution was the discovery of the tighter correlation between $M_\bullet$ and host galaxy velocity dispersion.

6.2 The $M_\bullet - \sigma$ correlation

Avi Loeb suggested independently to Karl Gebhardt and to Laura Ferrarese that they should look for a correlation between BH mass and galaxy velocity dispersion. It is remarkable in retrospect and a testament to the unpredictable way that research lurches forward that the correlation was not found much earlier. In any case, a tight $M_\bullet - \sigma$ correlation was discovered, announced at the Spring 2000 meeting of the American Astronomical Society by Gebhardt (see Kormendy et al. 2000) and by Ferrarese and published in Ferrarese & Merritt (2000) and in Gebhardt et al. (2000a).

The immediate reaction was that the fundamental relationship between BHs and host galaxies had been found. The reason was that the scatter was "only 0.30 dex ... over almost 3 orders of magnitude in $[M_\bullet]$" and "most of this is due to observational errors" (Gebhardt et al. 2000a). Ferrarese & Merritt (2000) similarly concluded that the "scatter [is] no larger than expected on the basis of measurement error alone." Both papers emphasized that the correlation is important at a practical level because it allows accurate prediction of $M_\bullet$ from an easy-to-make measurement and because it implies that BH growth and bulge formation are closely linked.

Many papers have expanded on this result with bigger samples and have explored its applicability to AGNs, to other kinds of objects (e. g., globular clusters, § 7.4 here), and to the distant Universe. Papers that elaborate on the $M_\bullet - \sigma$ relation as revealed by the growing sample of BH detections include Merritt & Ferrarese (2001); Kormendy & Gebhardt (2001); Tremaine et al. (2002); Marconi & Hunt (2003); Ferrarese & Ford (2005); Wyithe (2006a, b); Graham (2007, 2008a, b); Hu (2008); Gültekin et al. (2009c); Greene et al. (2010); Graham et al. (2011); Sani et al. (2011); Kormendy et al. (2011); McConnell et al. (2011a); Beifiori et al. (2012); Graham & Scott (2013); and McConnell & Ma (2013).

We update the $M_\bullet - \sigma$ correlation in Sections 6.6 and 6.7. One conclusion will be that the $M_\bullet - M_{\rm bulge}$ and $M_\bullet - \sigma$ correlations have the same intrinsic scatter. This is important because we calculate $M_\bullet$ in part from σ. Therefore, when we plot $M_\bullet$ against σ, we are to some degree plotting a function of σ against σ (See Section 6.5). Seeing the same small scatter in the $M_\bullet - M_{\rm bulge}$ correlation is therefore compelling.

6.3 We omit BH masses based on kinematics of ionized gas when broad emission line widths are not taken into account.

Section 3.2 showed why we believe that BH masses based on ionized gas rotation curves are often underestimated when large emission-line widths are not taken into account. It is not *a priori* certain that large line widths imply that some dynamical support of the gas comes from random motions, so that an "asymmetric drift correction" (Mihalas & Routly 1968; Binney & Tremaine 1987) is required, as it would be for a stellar system in which $\sigma \sim V$. However, when the same galaxy is analyzed using emission- and absorption-line kinematics and both show large line widths, we almost always get larger $M_\bullet$ estimates from absorption lines than from emission lines. The examples of M 87 and NGC 3998 are shown in **Figure 12** with pairs of points, a cyan point for the low-$M_\bullet$, emission-line result connected with a cyan line to a black point for the high-$M_\bullet$ result from stellar dynamics. The correction is particularly big for NGC 3998. Thus, it is reasonable to suspect, even when we cannot check them, that $M_\bullet$ values are underestimated by ionized gas rotation curves when large line widths are not taken into account. These cases are listed in cyan in the tables and are shown by cyan points in **Figure 12**. Also shown in black with cyan centers are three BH masses that are based on emission-line measurements in which line widths were taken into account.

These latter points agree with the $M_\bullet$ correlations determined from stellar and maser dynamics. So do cyan points for galaxies with $\sigma_e \sim 160 \pm 20\,\mathrm{km\,s^{-1}}$. But when $\sigma_e > 250\,\mathrm{km\,s^{-1}}$, many cyan points fall near the bottom of or below the scatter for black points. For M 87, both points fall within the scatter, but using the emission-line $M_\bullet$ would – and, historically, did – contribute to our missing a scientific result, i. e., that σ_e "saturates" at high $M_\bullet$ (Section 6.7). Other conclusions are at stake, too. Because Graham & Scott (2013) retain the cyan points but do not have the high-$M_\bullet$ BHs from Rusli et al. (2013), they incorrectly conclude that the $M_\bullet - M_{K,\mathrm{bulge}}$ correlation has a kink to lower slope at high $M_\bullet$ whereas we conclude that it has no kink, and they see little or no kink in $M_\bullet - \sigma_e$ whereas we conclude that σ_e saturates at high $M_\bullet$. From here on, we omit the all-cyan points from plots and fits. We also omit NGC 2778 (M/L_K is too big) and NGC 3607 (we cannot correct $M_\bullet$ for the omission of dark matter from the dynamical models – see table supplementary notes on individual objects).

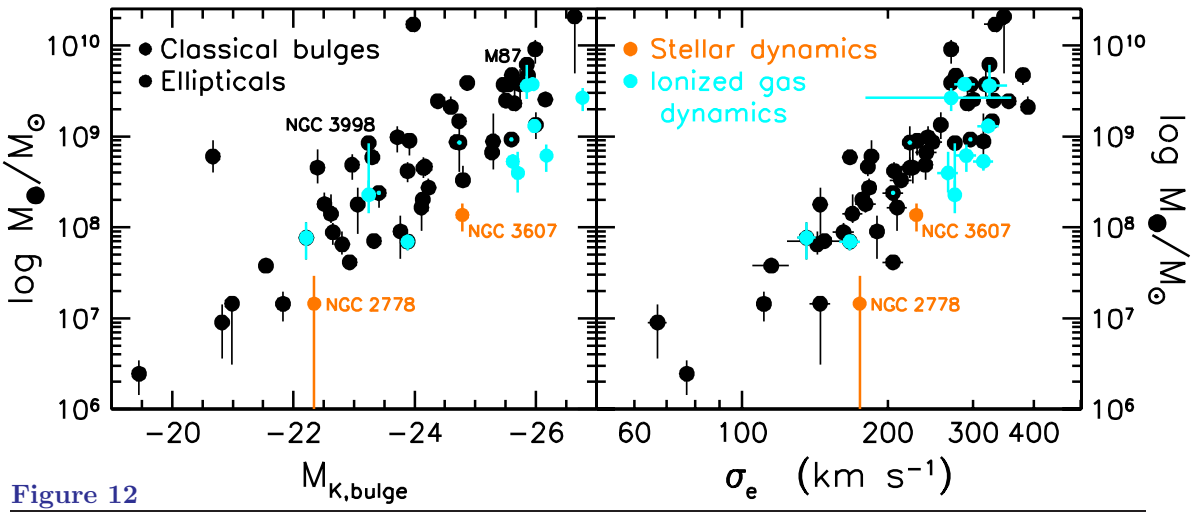

Figure 12

Correlations between BH mass $M_\bullet$ and (*left*) the K-band absolute magnitude of the classical bulge or elliptical and (*right*) its effective velocity dispersion for the sample in **Tables 2** and **3**. Galaxies or $M_\bullet$ measurements that we omit from further illustrations and fits are shown in orange and cyan.

6.4 Mergers in progress have abnormally small BH masses.

BHs are detected dynamically in 5 galaxies that are mergers in progress (green lines in **Table 2**). The two that are least well known are illustrated in **Figure 13**. When we add these mergers to the BH correlations (**Figure 14**), we find that at least these five BHs have abnormally small masses for their (giant!) galaxies' luminosities. They have more marginally low BH masses for their σ_e.

Hints of this result were noticed in some of the BH discovery papers, but a comprehensive picture has never emerged. Misses are easy to understand. NGC 2960 was misclassified as Sa? in the RC3, and IC 1481 was misclassified as Sb: pec in van den Bergh, Li & Filippenko (2002). So authors have considered NGC 2960 to be one example among many of a pseudobulge (Greene et al. 2010) or a late-type galaxy (McConnell & Ma 2013) with a relatively small BH. Neither McConnell & Ma (2013) nor Graham & Scott (2013) have IC 1481 in their sample. However, both galaxies clearly show tidal tails, loops, and shells that are characteristic of mergers in progress (**Figure 13**). Also, Cappellari et al. (2009) correctly noted that NGC 5128 satisfies the $M_\bullet - \sigma_e$ correlation.

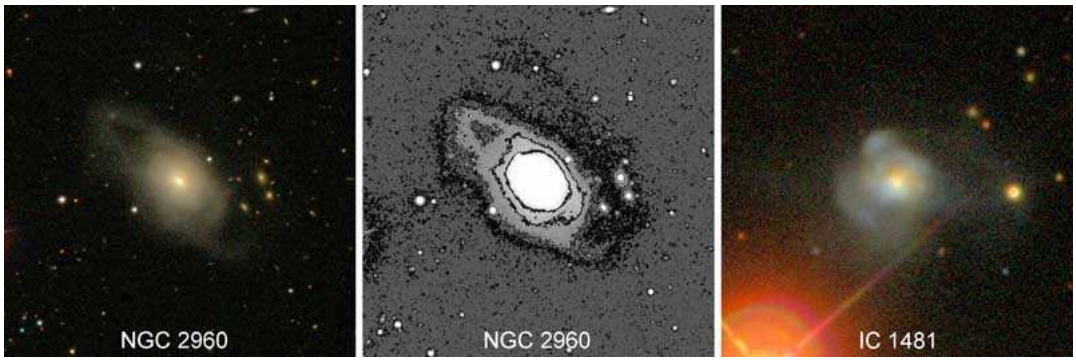

Figure 13

(*left*) SDSS `WIKISKY` image and (*center*) isophotes of NGC 2960 (Kormendy & Bender 2013b). (*right*) SDSS `WIKISKY` image of IC 1481. The merger nature of NGC 4382 is illustrated in KFCB (their Figure 9). Additional mergers with abnormally small $M_\bullet$ are added by Bender et al. (2013).

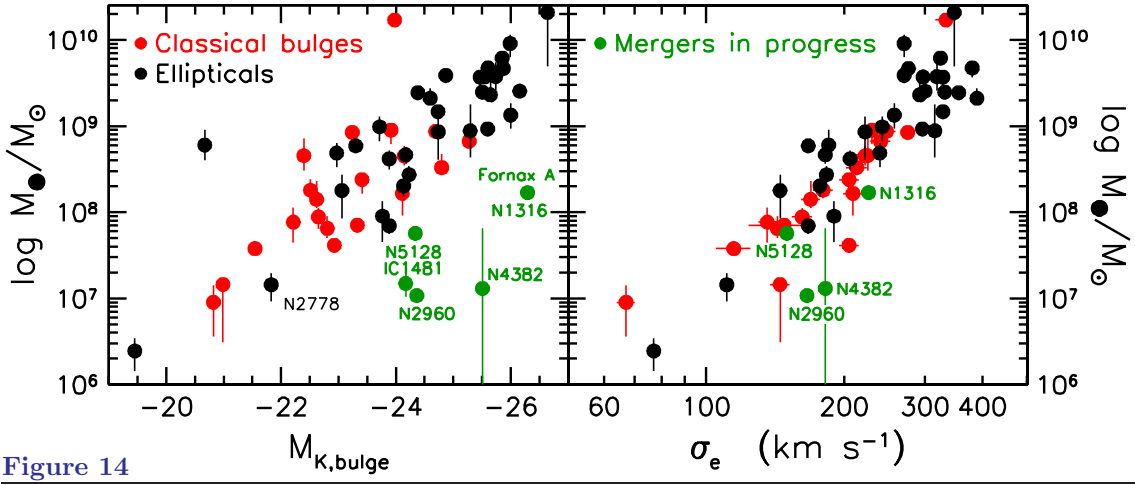

Figure 14

Correlations between $M_\bullet$ and (*left*) the K-band absolute magnitude of the bulge or elliptical and (*right*) its effective velocity dispersion for classical bulges, ellipticals, and mergers in progress.

However, Nowak et al. (2008) certainly realized that, while NGC 1316 = Fornax A satisfies the $M_\bullet - \sigma_e$ correlation, its BH mass is "a factor of ~ 4 smaller than expected from its bulge mass and the Marconi & Hunt [2003] relation". The deviation is even larger with the corrected BH masses in **Figure 14**. And Gültekin et al. (2009c) discussed whether $M_\bullet$ is anomalously low in NGC 4382. They concluded that the 1σ upper bound on $M_\bullet$ is consistent with the 1σ lower envelope of the scatter in the $M_\bullet - \sigma_e$ relation. On the other hand, the 1σ lower envelope of the $M_\bullet - L_V$ correlation implies a BH mass that "is more than a factor of 2 larger than our 3σ upper limit for the black hole mass [in NGC 4382]. In this sense, the black hole mass is anomalously low".

We now see that this is generally true for the five mergers in progress that are in our sample. It is not plausible that their stellar populations are so young that K-band luminosities are brightened over those of old stellar populations by enough to account for the horizontal deviations of the green points in **Figure 14** (*left*). Gültekin et al. (2009c) get $M/L_V = 3.74 \pm 0.10\, M/L_{V\odot}$ for NGC 4382, a normal value (Schulze & Gebhardt 2011). Nowak et al. (2008) get $M/L_K = 0.58^{+0.07}_{-0.04}$ (3σ) $M/L_{K\odot}$ for NGC 1316, and Cappellari et al. (2009) get $M/L_K = 0.63 \pm 0.14$ (3σ) $M/L_{K\odot}$ for NGC 5128. These are only slightly smaller than the normal values for old stellar populations that are given, e. g., by Equations 8 and 9 in Section 6.6.1. We use K-band magnitudes in **Figure 14** precisely so that stellar population effects are minimized.

Bender et al. (2013) discuss the galaxies in **Figure 13** in more detail and find a new example of an anomalously low-$M_\bullet$ BH in a merger in progress.

Why does this happen? We suggest several possibilities. Some involve merger physics and others involve limitations in our search techniques. It is not clear that they add up to the whole story.

The merger physics possibility is this: In a major merger of two disk-dominated galaxies at $z \sim 0$, all pre-merger disk mass gets scrambled up into a new elliptical but – unlike the situation at high z – little gas is available to feed up the BH mass in proportion to how much the bulge mass has grown. This can easily account for a factor of ~ 2 or more deviation in the $M_\bullet - M_{K,\mathrm{bulge}}$ relation. It can account for much larger deviations if one or both progenitors had pseudo or no bulges with (consequently) low-mass BHs (see Section 6.8). However, NGC 1316 and NGC 4382 have such large stellar masses that they cannot be products of one major merger of two pure-disk galaxies.

In terms of BH detection technology, we could imagine the "dark horse" possibility that one of the progenitor BHs has not yet arrived at the center. We suffer the problem of the drunkard looking for his keys under a lamppost: the center is usually the only place where we look and perhaps the only place where we can succeed. Thus, it is reassuring that two of our five merger-in-progress BHs were discovered by their maser emission and could have been discovered elsewhere in the galaxy provided that they were accreting water. Moreover, the $M_\bullet$ measurement in NGC 2960 is relatively secure (the rotation curve is nicely Keplerian, Kuo et al. 2011), though the measurement of IC 1481 is more uncertain (the molecular disk mass is larger than the BH mass, Section 3.3.3). The measurements of NGC 1316 and NGC 5128 are also very robust. And M/L_V is not particularly small in NGC 4382. In fact, our biggest qualm in terms of BH detection is that all five BHs are so close to the centers of their galaxies. Has there really been time for the BHs to settle to the center after all the recent merger violence? Also, to the extent that we can tell (maser disks and nonthermal AGNs help) none of these five BHs are doubles. Galaxies like those discussed in this section should be the most obvious place to look for the BH binaries that are expected to result from mergers.

It is possible that the deviations in **Figure 14** are the sum of several small effects; e. g., mergers of low-$M_\bullet$ disks, or systematic errors in $M_\bullet$ measures, or errant, non-central BHs. But the apparently low BH masses in mergers are general enough to be compelling, and it is possible that some new and interesting physics awaits discovery. Or an unrecognized problem with our BH searches.

For reasons of clarity, we omit the mergers in progress from further correlation diagrams.

6.5 BH monsters in relatively small bulges and ellipticals

Prominent in the late-2012 news was the discovery of a spectacularly overmassive BH in the normal-looking, almost-edge-on S0 NGC 1277 in the Perseus cluster (van den Bosch et al. 2012). At $M_\bullet = (1.7 \pm 0.3) \times 10^{10}\, M_\odot$, it is essentially as massive as the biggest BH known. But that BH lives in NGC 4889, one of the two giant, central galaxies in the Coma cluster, whereas NGC 1277 is an obscure S0 galaxy that is two magnitudes fainter. **Figure 15** shows it in the $M_\bullet$ correlations. At left, the high-luminosity end of the $M_{K,\rm bulge}$ error bar is at the total luminosity of the galaxy. But BHs correlate with classical bulges, not (it will turn out) with disks, and the bulge constitutes $\lesssim 1/2$ of the galaxy. Van den Bosch et al. (2012) make a photometric decomposition into four components; the sum of the inner two gives $B/T = 0.27$, and this provides the faint end of the $M_{K,\rm bulge}$ error bar in **Figure 15** (*left*). Our photometry (Kormendy & Bender 2013b) shows only two components, a normal, Sérsic $n = 3.5 \pm 0.7$ classical bulge that dominates the light at both large and small radii and an exponential disk. We get $B/T = 0.55 \pm 0.07$. This gives the absolute magnitude of the point plotted in **Figure 15**. For any of these magnitudes, the BH is more massive than the upper envelope of the scatter in the $M_\bullet$–$M_{K,\rm bulge}$ correlation by at least an order of magnitude.

A similarly overmassive BH was found in NGC 4486B by Kormendy et al. (1997). This is a tiny ($M_{VT} = -17.7$) but otherwise normal elliptical (KFCB), a companion of M 87. Spectroscopy with the CFHT in FWHM $= 0\farcs52$ seeing reveals an extraordinarily steep velocity dispersion gradient to $\sigma = 291 \pm 25$ km s^{-1} at the center. This value is characteristic of giant ellipticals that are $\gtrsim 4$ mag brighter than NGC 4486B. Not surprisingly, isotropic dynamical models imply a large MH mass of $M_\bullet = 6^{+3}_{-2} \times 10^8\, M_\odot$. Extreme anisotropic models can explain the kinematics without a BH, so the BH detection has been regarded as weak. But NGC 4486B and NGC 1277 are equally remarkable in having steep inward velocity dispersion gradients up to central σ values that are far outside the scatter in the Faber-Jackson (1976) relation. Both $M_\bullet$ determinations have some uncertainties (we have trouble understanding how NGC 1277 can have a completely normal-looking bulge when all of it lives inside the sphere-of-influence radius of its BH). But it seems unlikely that we are wrong in concluding that both galaxies have unprecedentedly large BH-to-bulge mass ratios. For NGC 4486B, our estimate of M/L_K gives $M_\bullet/M_{\rm bulge} = 0.14^{+0.05}_{-0.04}$. For NGC 1277, our measurement of B/T and M/L_K gives $M_\bullet/M_{\rm bulge} \simeq 0.18^{+0.06}_{-0.04}$ (**Figure 18**). Who ordered this?

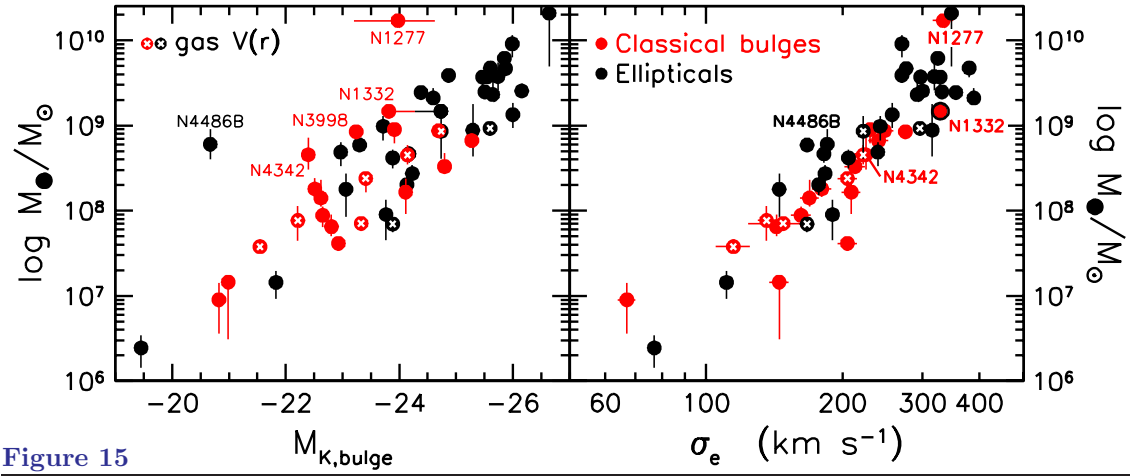

Figure 15

The $M_\bullet - M_{K,\rm bulge}$ and $M_\bullet - \sigma_e$ correlations with abnormally high-mass BHs identified. NGC 1332 is plotted twice; the points are joined by a line. If it is an S0, then it contains a marginal example of a BH monster. If, as we suggest in the Table notes, it is an elliptical, then its BH is normal.

These objects are rare in the $z \sim 0$ universe, but they are not unique. Van den Bosch et al. (2012) are working on additional compact galaxies with extraordinarily high central σ (their Table 1). And we have had hints of more subtle examples. The best known is NGC 4342, another edge-on S0, this time in the Virgo W′ cloud. The BH mass determined by Cretton & van den Bosch (1999b), together with our measurement of $B/T = 0.70$, makes it the biggest outlier among more normal classical bulges in the $M_\bullet - M_{K,\rm bulge}$ correlation. It has $M_\bullet/M_{\rm bulge} \simeq 0.023^{+0.007}_{-0.006}$ (**Figure 18**). Another possible example is NGC 4350, a Virgo cluster, edge-on S0 with a bulge magnitude of $M_{K,\rm bulge} = -22.2$ and $M_\bullet \sim (7 \pm 2) \times 10^8\, M_\odot$ (Pignatelli, Salucci & Danese 2001). We do not include it in **Table 3** and **Figure 15** partly because the BH mass is based only on isotropic dynamical models but mostly because the velocity dispersion is normal for the bulge luminosity. However, if the mass is correct, it is a bigger outlier in $M_\bullet - M_{K,\rm bulge}$ than NGC 4342. Finally, in case we are wrong in the **Table 2** notes and NGC 1332 should be classified as an S0 rather than an elliptical, we note that it would be at the high-$M_\bullet$ extreme of the scatter in **Figure 15** (*left*). However, as explained in the notes, we henceforth regard it as an elliptical (black point connected to the red point in the figure). Note: NGC 3998, the next most extreme outlier, is quite a different sort of galaxy; with $B/T = 0.85$, it is almost an elliptical.

In summary, we have two BH monsters, hints of more to come, and signs that these are extremes of a distribution of overmassive BHs that connects up with the scatter in the $M_\bullet$ correlations.

It is worth emphasizing that none of these galaxies are major outliers in the $M_\bullet - \sigma_e$ correlation. In Section 6.4, too, merger BHs were extreme outliers in $M_\bullet - M_{K,\rm bulge}$ but only marginal outliers in $M_\bullet - \sigma_e$. It is common to think of the small scatter in $M_\bullet - \sigma_e$ as astrophysically magic. But we see in these two sections that we learn rather more from the luminosity correlation. The sobering lesson may be this: $M_\bullet$ is measured by interpreting central changes (for example, a slight increase $\delta\sigma$) in σ (and, of course, rotation) from values $\simeq \sigma_e$ that vary only slowly at large radii. But the same $\delta\sigma$ gives a bigger BH mass for a bigger σ_e. We may get a small scatter in $M_\bullet - \sigma_e$ for galaxies in general and for $M_{K,\rm bulge}$ outliers in particular in part because we are plotting a function of σ_e against σ_e. Note the astonishingly small scatter for classical bulges in **Figure 15**. When we resolve $r_{\rm infl}$ exceedingly well, this concern should vanish. But many $M_\bullet$ values are based on subtle features in the LOSVDs near galaxy centers. This caution applies throughout this review.

At the same time, **Figure 15** includes an important check. If $M_\bullet$ was measured using an emission-line rotation curve of gas, then the point is marked with a white cross. This includes galaxies in which optical emission-line widths were taken into account and even two low-σ_e galaxies (NGC 4459 and NGC 4596) for which line widths were not taken into account. The other points are for maser measurements and for one molecular gas measurement (NGC 4526: Davis et al. 2013). These points are immune from the above worry. But they are fully consistent with the small scatter in $M_\bullet - \sigma_e$, including that for bulges. The weakest stellar-dynamical BH measurements – including those of the monsters – should be checked. But we are reassured by the gas points in **Figure 15**.

What do we learn from BH monsters? We do not have a definitive answer; we only float a speculation for further study. It is interesting to note that the bulge of NGC 1277 has an effective radius of $r_e \simeq 0.97$ kpc. NGC 4486B is tinier, $r_e = 0.20 \pm 0.01$ kpc (KFCB). But even the bulge of NGC 1277 is similar to the compact "red nuggets" that constitute most early-type galaxies at high redshifts (e. g., Szomoru, Franx & van Dokkum 2012). We know from spectral energy distributions that these were already old then. We also struggle to understand how at least some BHs grew supermassive very quickly in the early universe. It will be interesting to investigate whether objects like NGC 1277 are remnants – this one now cloaked in a disk – of early red nuggets that already had overmassive BHs at high z. Is NGC 1277 left over from a bygone era before the present BH correlations were engineered?

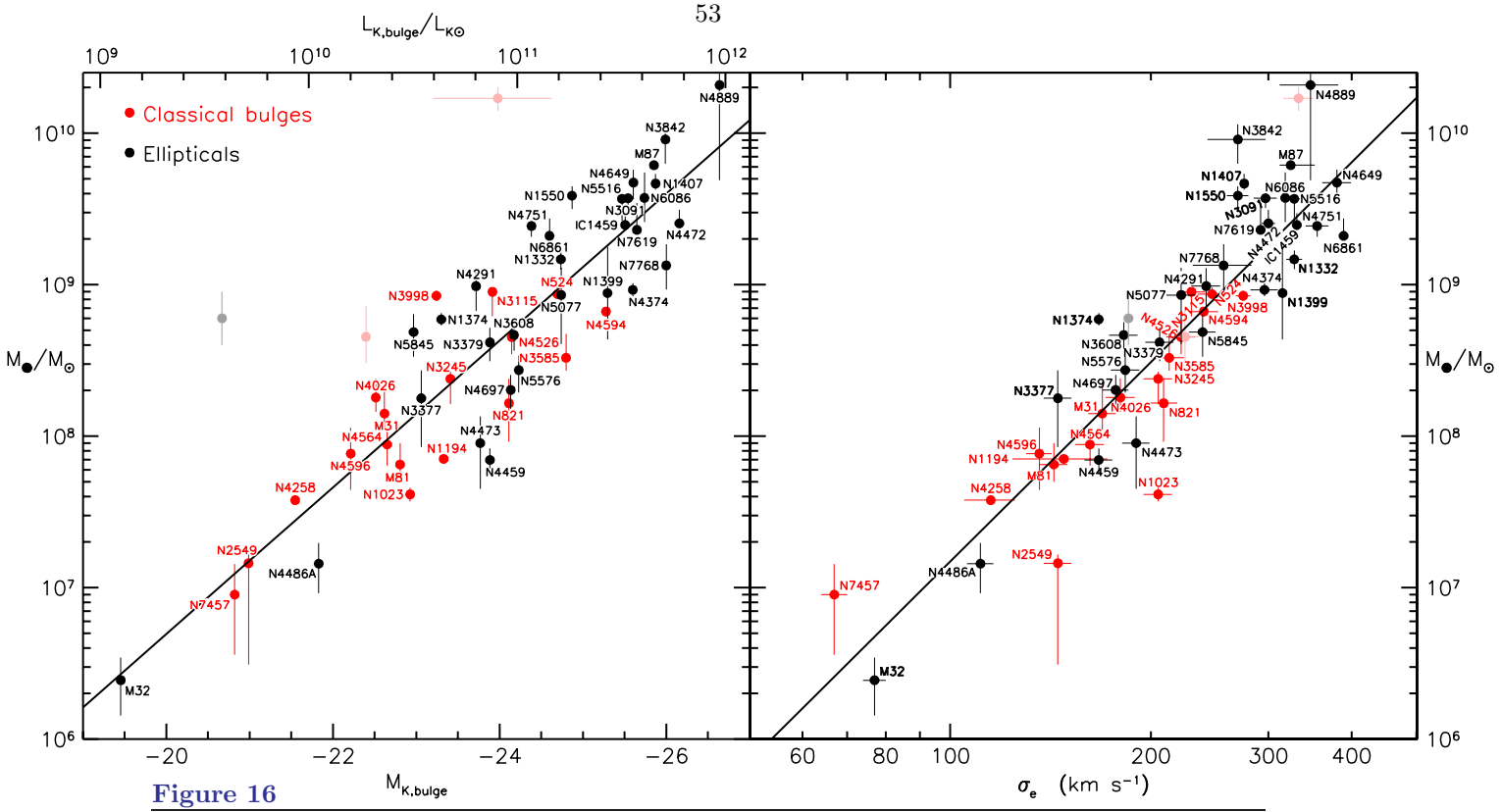

Figure 16

Correlation of dynamically measured BH mass $M_\bullet$ with (*left*) K-band absolute magnitude $M_{\rm K,bulge}$ and luminosity $L_{K,\rm bulge}$ and (*right*) velocity dispersion σ_e for (*red*) classical bulges and (*black*) elliptical galaxies. The lines are symmetric least-squares fits to all the points except the monsters (*points in light colors*), NGC 3842, and NGC 4889. **Figure 17** shows this fit with 1-σ error bars.

6.6 The $M_\bullet - L_{\rm bulge}$, $M_\bullet - M_{\rm bulge}$, and $M_\bullet - \sigma_e$ correlations for classical bulges and elliptical galaxies

Figure 16 shows the updated correlations of $M_\bullet$ with bulge luminosity and velocity dispersion. Recent advances allow us to derive more robust correlations and to better understand the systematic effects in their scatter. First, we distinguish classical bulges that are structurally like ellipticals from pseudobulges that are structurally more disk-like than classical bulges. There is now a strong case that classical bulges are made in major mergers, like ellipticals, whereas pseudobulges are grown secularly by the internal evolution of galaxy disks. We show in Section 6.8 that pseudobulges do not satisfy the same tight $M_\bullet$–host-galaxy correlations as classical bulges and ellipticals. Therefore we omit them here. Second, we now have bulge and pseudobulge data for all BH galaxies (Kormendy & Bender 2013b). Third (Section 3), we have more accurate BH masses, partly because of improvements in data (ground-based AO and integral-field spectroscopy), partly because of improvements in modeling (e. g., three-integral models that include dark matter), and partly because we are now confident that emission-line rotation curves underestimate $M_\bullet$ unless broad line widths are taken into account (Section 6.3). We omit these masses. Fourth, we have reasons to omit BH monsters, mergers in progress, and (Section 6.7) the two largest BHs known in ellipticals. Finally, the sample of galaxies with dynamical BH detections is larger and broader in Hubble types. These developments lead to a significant recalibration of the ratio of BH mass to the mass of the host bulge and, as we have already begun to see, to qualitatively new conclusions.

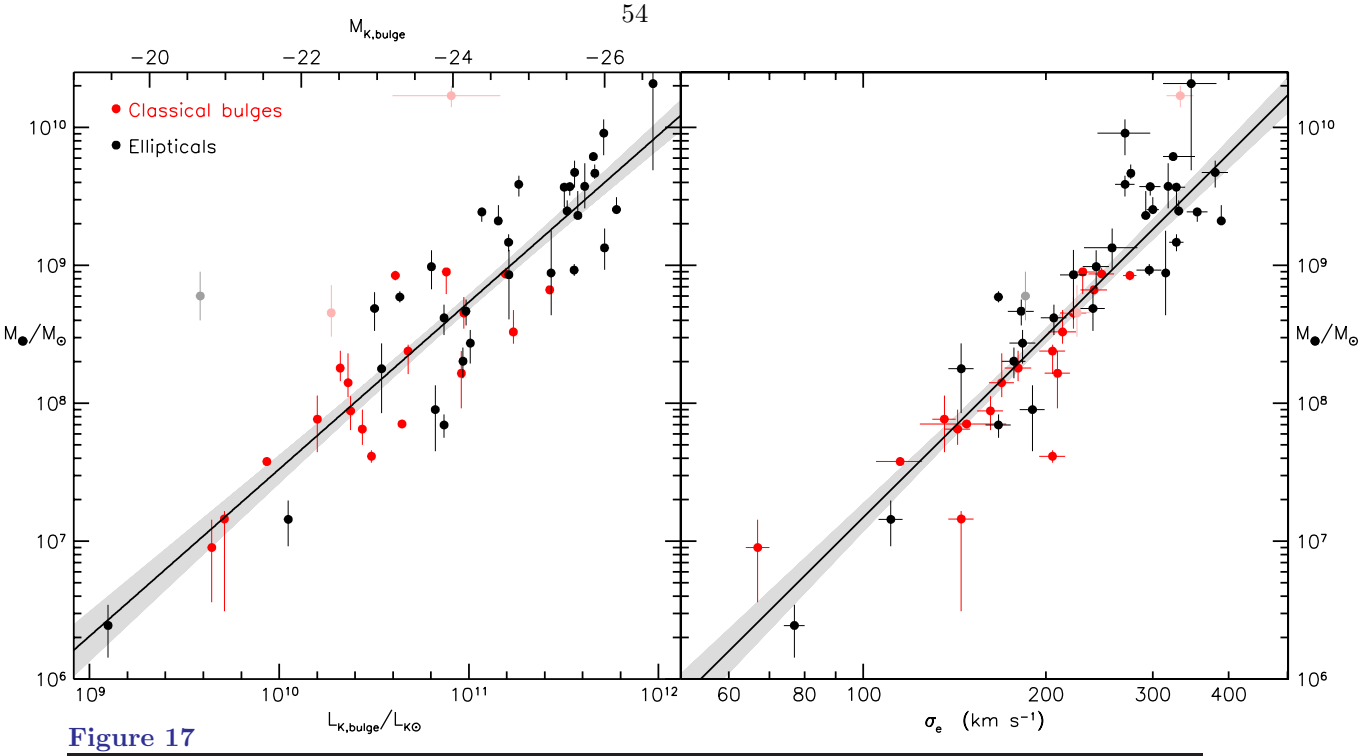

Figure 17

The $M_\bullet$–$M_{\rm K,bulge}$ and $M_\bullet$–σ_e correlations with symmetric (Tremaine et al. 2002) least-squares fits (Equations 2 and 3) and the 1σ range of the fits (*gray shading*). Here we give equal weight to all the points. Fits that use the individual $M_\bullet$ measurement errors (Equations 4 and 5) are almost identical. Among the plotted points, all fits omit the BH monsters (*points in light colors*), $M_\bullet$ values determined from ionized gas rotation curves without taking line widths into account (NGC 4459 and NGC 4596), and the two highest-$M_\bullet$ ellipticals (NGC 3842 and NGC 4889, see text). The bottom axis at left shows K-band luminosity. Uncertainties in $M_{K,\rm bulge}$ are typically ±0.2, smaller for some ellipticals and significantly larger for a few bulges with uncertain B/T ratios.

Figure 17 shows our adopted symmetric, least-squares fits calculated as in Tremaine et al. (2002). Symmetrizing around $L_{K,\rm bulge} = 10^{11}\,L_{K\odot}$ and $\sigma_e = 200$ km s^{-1}, these are

$$\log\left(\frac{M_\bullet}{10^9\,M_\odot}\right) = -(0.266\pm0.052) - (0.484\pm0.034)(M_{K,\rm bulge}+24.21);\ \text{intrinsic scatter} = 0.31; \quad (2)$$

$$\log\left(\frac{M_\bullet}{10^9\,M_\odot}\right) = -(0.510\pm0.049) + (4.377\pm0.290)\log\left(\frac{\sigma}{200\ \text{km s}^{-1}}\right);\ \text{intrinsic scatter} = 0.29. \quad (3)$$

For the above version, we adopt equal errors of $\Delta M_{K,\rm bulge} = 0.2$ and $\Delta \log M_\bullet = 0.117$ = the mean for all fitted galaxies. If, instead, we use individual errors in $M_{K,\rm bulge}$ ($\pm\,0.2$) and $\log\sigma_e$ and add individual errors in $\log M_\bullet$ to the intrinsic scatter in quadrature and iterate the intrinsic scatter until the reduced $\chi^2 = 1$, then

$$\log\left(\frac{M_\bullet}{10^9\,M_\odot}\right) = -(0.253\pm0.052) - (0.484\pm0.036)(M_{K,\rm bulge}+24.21);\ \text{intrinsic scatter} = 0.31; \quad (4)$$

$$\log\left(\frac{M_\bullet}{10^9\,M_\odot}\right) = -(0.501\pm0.049) + (4.414\pm0.295)\log\left(\frac{\sigma}{200\ \text{km s}^{-1}}\right);\ \text{intrinsic scatter} = 0.28. \quad (5)$$

The difference between the two sets of fits is small. Taking account of a variety of fits, we conclude

that the intrinsic $\log M_\bullet$ scatter in $M_\bullet$–$M_{K,\rm bulge}$ is 0.31 ± 0.02, almost the same as the intrinsic scatter 0.29 ± 0.03 in $M_\bullet$–σ_e. This conclusion has also been reached by other authors who use infrared luminosities (e. g., Marconi & Hunt 2003; Sani et al. 2011).

We adopt the Equations 2 and 3 fits, because they do not give undue weight to a few points that fortuitously have tiny error bars but that could be anywhere in the intrinsic scatter. When the intrinsic scatter is much larger than the measurement errors for a few but not all points, it is preferable to give all points equal weight (see Tremaine et al. 2002 for further discussion). Note that all of the intrinsic scatter is assumed to be in $\log M_\bullet$.

Rewriting Equations 2 and 3 in physically more transparent forms,

$$\frac{M_\bullet}{10^9\ M_\odot} = \left(0.542^{+0.069}_{-0.061}\right) \left(\frac{L_{K,\rm bulge}}{10^{11}\ L_{K\odot}}\right)^{1.21\pm0.09} \tag{6}$$

$$\frac{M_\bullet}{10^9\ M_\odot} = \left(0.309^{+0.037}_{-0.033}\right) \left(\frac{\sigma}{200\ \rm km\ s^{-1}}\right)^{4.38\pm0.29} \tag{7}$$

6.6.1. The $M_\bullet - M_{\rm bulge}$ correlation and the ratio of BH mass to bulge mass

Galaxy formation work requires the mass equivalent of Equation 6, the $M_\bullet - M_{\rm bulge}$ correlation. This is trickier to derive than it sounds. It is not just a matter of multiplying the bulge luminosity by a mass-to-light ratio that is provided automatically by the stellar dynamical models that give us $M_\bullet$. Bulge mass is inherently less well defined than bulge luminosity. Mass-to-light ratios of old stellar populations are uncertain; (1) the initial mass function (IMF) of star formation is poorly known; it may vary with radius in an individual galaxy or from galaxy to galaxy; (2) stellar population age and metallicity distributions affect M/L and are famously difficult to disentangle; one consequence is that late stages of stellar evolution – especially asymptotic giant branch (AGB) stars – affect M/L but but are poorly constrained observationally (Portinari & Into 2011). Most important, (4) dark matter contributes differently at different radii and probably differently in different galaxies.

Graves & Faber (2010) discuss these problems. They conclude that all of the above are important, that stellar population age and metallicity account for $\sim 1/4$ of the variations in optical mass-to-light ratios, and that some combination of IMF and dark matter variations account for the rest. However, this field is unsettled; extreme points of view are that even K-band mass-to-light ratios vary by factors of ~ 4 from galaxy to galaxy and that all of this range is due to IMF variations (Conroy & van Dokkum 2012) or contrariwise that IMFs vary little from one place to another (Bastian, Covey, & Meyer 2010).

These problems are background worries that may yet hold unpleasant surprises, but mostly, they are beyond the scope of this paper. The extensive work of the SAURON and ATLAS3D teams (Cappellari et al. 2006, 2013) shows that dynamically determined I- and r-band mass-to-light ratios are very well behaved. For 260 ATLAS3D galaxies, $M/L_r \propto \sigma_e^{0.69\pm0.04}$ with an intrinsic scatter of only 22 %. Since M/L_K is likely to vary less from galaxy to galaxy than M/L_r, this suggests that we proceed by finding a way to estimate M/L_K. In particular, we want an algorithm that does not involve the use of uncertain effective radii r_e. Here's why:

Published studies often derive $M_{\rm bulge}$ dynamically from r_e, σ_e, and a virial-theorem-like relation $M_{\rm bulge} = k\sigma_e^2 r_e/G$, where k is, e. g., 3 (Marconi & Hunt 2003) or 5 (Cappellari et al. 2006, 2010) or 8 (Wolf et al. 2010). This situation is unsatisfactory; different assumptions about the density profile are one reason why k is uncertain. Also, r_e values are less well measured than we think. An example of the problem can be found in Marconi & Hunt (2003): they derive mass-to-light ratios that range from $M/L_K = 0.31$ for NGC 3384 to $M/L_K = 1.94$ for NGC 4649. The machinery that we adopt below gives a much smaller difference in M/L_K for these two galaxies that are both made of old stars. They may contain different fractional contributions of dark matter within $r \sim r_e$.

But the difference could also signal a problem with the r_e data (see KFCB for a review). Given heterogeneous r_e measurements, we prefer to avoid using any relation of the form $M_{\rm bulge} \propto \sigma_e^2 r_e$.

Cappellari et al. (2006, 2013) and other papers on early-type galaxies (see Gerhard 2013 for a review) find that dark matter contributes $\sim 10-40\,\%$ of the mass within r_e, differently in different galaxies. This is one reason why we choose not to use M/L ratios from the papers that derive $M_\bullet$. Observations reach differently far out into the dark-matter-dominated parts of different galaxies, and different papers take dark matter into account (or not) in different ways. We hoped that accounting separately for dark matter would provide mass-to-light ratios that are representative of pure, old stellar populations, but (for example) the M/L_K ratios derived from the 12 galaxies in Schulze & Gebhardt (2011) range over a factor of more than 10. This is a bigger variation than we get below even from purely dynamical, total mass-to-light ratios that include dark matter.

We also have no guidance about whether we should include halo dark matter in $M_{\rm bulge}$ or not. It seems silly even to try; bulge stars and dark matter are distributed differently in radius, so how we combine them would depend (e. g.) on an arbitrary choice of radius. Anyway, most dark matter is at large radii, and it distribution is unknown. Moreover, we conclude in Section 6.10 that BH masses do not correlate with halo dark matter in any way that goes beyond the correlation with bulge properties. On the other hand, dark matter certainly contributes most of the gravity that makes hierarchical clustering happen. So it must affect BH accretion indirectly. It seems prudent neither to ignore halo gravity completely nor to attempt to add all halo mass to the stellar mass. We adopt an intermediate approach that essentially averages stellar population mass-to-light ratios and ones that are determined from dynamics. But we use a zeropoint based on stellar dynamics.

As a matter of principle, we prefer to derive mass-to-light ratios in a way that is as independent as possible of the $M_\bullet$ measurements. We also need an algorithm that can be applied to galaxies without dynamical M/L measurements; e. g., the maser BH galaxies. And we need an algorithm that can be applied to pseudobulges with poorly observed but young stellar populations. This is one reason why we base our results in part on mass-to-light ratios from stellar population models. We use M/L_K because it is relatively insensitive to dust absorption and to stellar population age. But the contribution of AGB stars to K-band light is of paramount importance and had not until recently been sufficiently taken into account. Fortunately, Into & Portinari (2013) provide a revised calibration of mass-to-light ratios against galaxy colors, both over a wide range of bandpasses. In particular, they find a much steeper dependence of M/L_K on $(B-V)_0$ color than did (e. g.) Bell & de Jong (2001). With their calibration, *the dependence of stellar population mass-to-light ratio M/L_K on σ_e is completely consistent with that given by the dynamical models used below.*

We therefore use two independent methods to estimate M/L_K, one from the galaxy's $(B-V)_0$ color and Into & Portinari's (2013) Table 3 and the other using a dynamically measured correlation between M/L_K and σ_e. The normalization of the stellar population M/L values is uncertain for reasons given above. In particular, the population mass is dominated by low-mass stars that we do not observe. So an IMF must be assumed. Into & Portinari (2013) assume a Kroupa (2001) IMF. However, we adopt a dynamically measured zeropoint, as follows.

We begin with Williams, Bureau & Cappellari (2009), who determine masses and K-band luminosities for 14 S0 galaxies using axisymmetric dynamical models that have contant anisotropies in the meridional plane. Cappellari et al. (2006) provide mass-to-light ratios M/L_I determined from detailed dynamical models for 12 additional galaxies that either are known BH hosts or that have photometry available in KFCB. We use our V_T, $(V-I)_e$ from Hyperleda, and Cappellari's M/L_I values to calculate bulge masses and then M_{KT} to determine M/L_K values. These are very consistent with the Williams et al. (2009) results. All 26 galaxies together show a shallow correlation of M/L_K with σ_e. The four largest values, $M/L_K \geq 1.6$, are outliers and are omitted.

Presumably these galaxies contain larger contributions of dark matter that we choose not to include. The remaining 22 galaxies satisfy $\log(M/L_K) = 0.287\log\sigma_e - 0.637$ with an RMS scatter of 0.088. As expected, the relation is shallower than the one in r band (above). It has essentially the same scatter of $\sim 23\,\%$. Dynamically, $M/L_K = 1$ at $\sigma_e = 166$ km s^{-1}, where the Into & Portinari (2013) calibration gives $M/L_K \simeq 0.76$. Cappellari et al. (2006) argue that the difference may be due to the inclusion of some dark matter in the dynamical models. We use the dynamical zeropoint.

To shift the Into & Portinari $\log M/L_K$ values to the above, dynamical zeropoint, we first use their Table 3 relation $\log M/L_K = 1.055(B-V)_0 - 1.066$ to predict an initial, uncorrected M/L_K. This correlates tightly with σ_e: $\log M/L_K = 0.239\log\sigma_e - 0.649$ with an RMS scatter of only 0.030. We then apply the shift $\Delta\log M/L_K = 0.1258$ or a factor of 1.34 that makes the corrected Into & Portinari mass-to-light ratio agree with the dynamic one, $M/L_K = 1.124$, at $\sigma_e = 250$ km s^{-1}.

We then have two ways to predict M/L_K that are independent except for the above shift,

$$\log M/L_K = 0.2871\log\sigma_e - 0.6375; \qquad \text{RMS} = 0.088; \tag{8}$$

$$\log M/L_K = 1.055(B-V)_0 - 0.9402; \qquad \text{RMS} = 0.030, \tag{9}$$

where we use the RMS scatter of the correlation with σ_e to estimate errors for the latter equation. We adopt the mean of the mass-to-light ratios given by Equations 8 and 9. For the error estimate, we use $0.5\sqrt{0.088^2 + 0.030^2 + (\text{half of the difference between the two } \log M/L_K \text{ values})^2}$. We use the resulting M/L_K together with $M_{K,\text{bulge}}$ to determine bulge masses. For the $\log M_{\text{bulge}}$ error estimate, we add the above in quadrature to $(0.2/2.5)^2$. The results are listed in **Tables 2** and **3**.

Figure 18 shows the correlation of $M_\bullet$ with bulge mass M_{bulge}. A symmetric, least-squares fit to the classical bulges and ellipticals omitting the monsters and (for consistency with $M_\bullet - \sigma_e$), the emission-lime $M_\bullet$ values for NGC 4459 and NGC 4596 plus NGC 3842 and NGC 4889 gives the mass equivalent of Equation 6,

$$\frac{M_\bullet}{10^9\ M_\odot} = \left(0.49^{+0.06}_{-0.05}\right)\left(\frac{M_{\text{bulge}}}{10^{11}\,M_\odot}\right)^{1.16\pm0.08}; \text{ intrinsic scatter} = 0.29 \text{ dex}. \tag{10}$$

Thus the canonical BH-to-bulge mass ratio is $M_\bullet/M_{\text{bulge}} = 0.49^{+0.06}_{-0.05}\,\%$ at $M_{\text{bulge}} = 10^{11}\,M_\odot$.

This BH mass ratio at $M_{\text{bulge}} = 10^{11}\,M_\odot$ is 2–4 times larger than previous values, which range from $\sim 0.1\,\%$ (Sani et al. 2011), $0.12\,\%$ (McLure & Dunlop 2002), and $0.13^{+0.23}_{-0.08}\,\%$ (Merritt & Ferrarese 2001; Kormendy & Gebhardt 2001) to $0.23^{+0.20}_{-0.11}\,\%$ (Marconi & Hunt 2003). The reasons are clear: (1) we omit pseudobulges; these do not satisfy the tight correlations in Equations 2 – 7; (2) we omit galaxies with $M_\bullet$ measurements based on ionized gas dynamics that do not take broad emission-line widths into account; (3) we omit mergers in progress. All three of these tend to have smaller BH masses than the objects that define the above correlations. Also, the highest BH masses occur in core ellipticals (more on these below), and these have been revised upward, sometimes by factors of ~ 2, by the addition of dark matter to dynamical models. Moreover, thanks to papers like Schulze & Gebhardt (2011) and Rusli et al. (2013), we have many such objects.

The exponent in Equation 10 is slightly larger than 1, in reasonable agreement with Häring & Rix (2004), who got $M_\bullet \propto M_{\text{bulge}}^{1.12\pm0.06}$ and again a lower normalization, BH mass fraction $\simeq 15\,\%$ at $M_{\text{bulge}} = 10^{11}\,M_\odot$. McConnell & Ma (2013) get a similar range of exponents from 1.05 ± 0.11 to 1.23 ± 0.16 depending on how the bulge mass is calculated (dynamics versus stellar populations).

To better emphasize the slight variation in $M_\bullet/M_{\rm bulge}$, we plot this ratio expressed as a percent against bulge mass in **Figure 18**. A direct fit to these points gives

$$100\left(\frac{M_\bullet}{M_{\rm bulge}}\right) = \left(0.49^{+0.06}_{-0.05}\right)\left(\frac{M_{\rm bulge}}{10^{11}\,M_\odot}\right)^{0.14\pm0.08}, \quad \text{intrinsic scatter} = 0.29 \text{ dex.} \qquad (11)$$

BH mass ratios range from 0.1 % to ∼1.8 %, with NGC 4486B and NGC 1277 standing out at 14 % and 17 %, respectively. The systematic variation in $M_\bullet/M_{\rm bulge}$ with $M_{\rm bulge}$ is one reason why AGN feedback has little effect on galaxy structure at low BH masses and instead becomes important at the largest BH masses (Section 8). Note: the RMS scatter $\Delta \log M_\bullet = 0.327$ in **Figure 18** (*top*) is only marginally smaller than $\Delta \log M_\bullet = 0.341$ in the luminosity correlation (**Figures 16** and **17**). Conversion from $L_{K,\rm bulge}$ to $M_{\rm bulge}$ does not make much difference for old stellar populations.

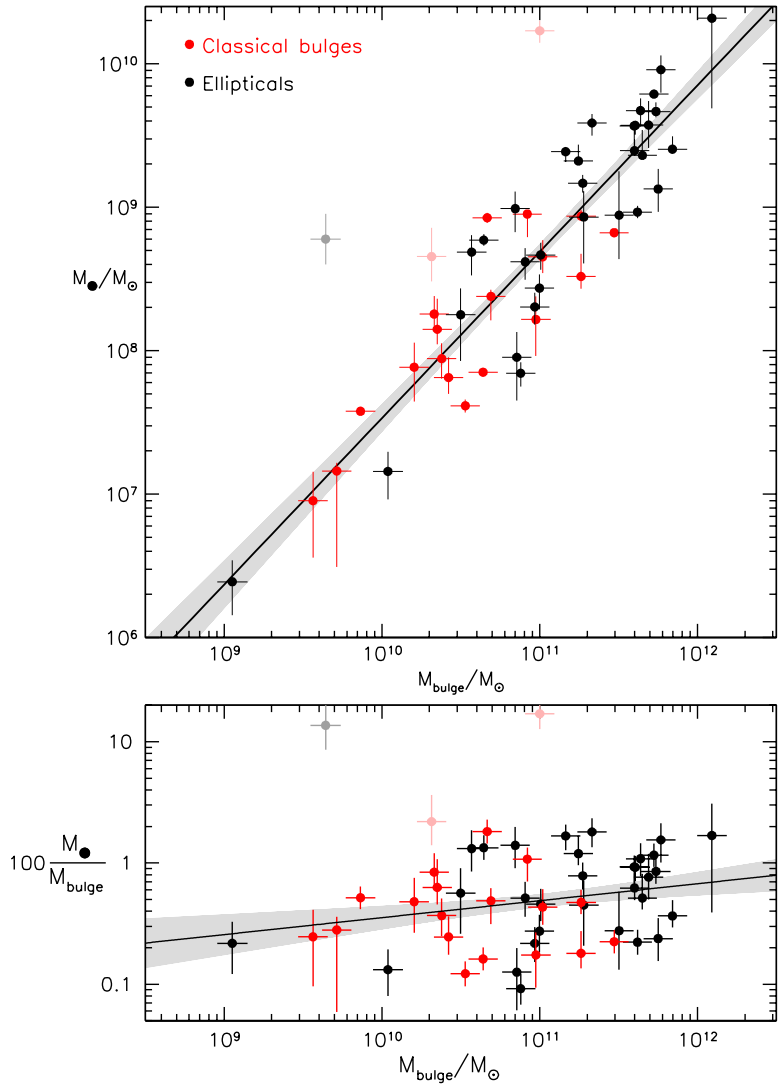

Figure 18

(*top*) BH mass and (*bottom*) percent ratio of BH mass to bulge mass as functions of bulge mass. The lines are Equations 10 and 11. The scatter in $M_\bullet/M_{\rm bulge}$ is larger than the systematic variation.

The history of our developing understanding of the upward revision in $M_\bullet/M_{\rm bulge}$ is an interesting sanity check. Early in the writing of this paper, when we first separated out pseudobulges and considered them separately from the BH–host correlations, we were uncomfortable to find that classical bulges were offset toward high $M_\bullet$ with respect to ellipticals. We were, of course, not entitled to assume that this was a problem – whether bulges and ellipticals have the same correlations is a scientific question that we need to ask. But the hint made us uncomfortable, especially since Gebhardt & Thomas (2009) had recently revised $M_\bullet$ upward in M 87, and soon afterward, van den Bosch & de Zeeuw (2010) revised $M_\bullet$ upward in NGC 3379. It was likely that $M_\bullet$ values in core galaxies would generally get revised upward, so we delayed the completion of this paper for several years until this was done. With the $M_\bullet$ revisions in Schulze & Gebhardt (2011) and the many new and large $M_\bullet$ values published by McConnell and Rusli and collaborators, the offset between classical bulges and ellipticals vanished. But then stellar-dynamical BH masses in classical bulges and ellipticals started convincingly to disagree with BH masses based on ionized gas kinematics, only, however, when the $M_\bullet$ derivation did not take broad emission-line widths into account (**Figure 12**). Our suspicions about those masses therefore crystallized and we began to omit them. Concurrently, the mergers in progress (**Figure 14**) began to disagree convincingly with the revised correlations, too. In this way, we converged on the correlations in **Figures 16** and **17** and the new, larger mean ratios of BH mass to bulge mass in **Figure 18**.

We emphasize that Equations 10 and 11 apply only to the classical bulges and ellipticals that participate in the tight BH–host-galaxy correlations. These dominate the BH mass budget. But small BHs in pseudobulges and in bulgeless galaxies have systematically smaller BH masses and BH-to-pseudobulge mass ratios, and these may be the most common BHs in the universe.

6.6.2. Comparison with Other Studies of BH–Host-Galaxy Correlations Explorations of the $M_\bullet - L_{\rm bulge}$, $M_\bullet - M_{\rm bulge}$, and $M_\bullet - \sigma_e$ correlations have become a major industry as BH samples have increased in size, as $M_\bullet$ estimates have become available for AGNs through methods such as reverberation mapping and single-epoch spectroscopy of broad emission lines, and as opportunities have become available to do photometry in the infrared. A partial list since Kormendy & Gebhardt (2001) includes Tremaine et al. (2002); McLure & Dunlop (2002); Marconi & Hunt (2003); Häring & Rix (2004); Ferrarese & Ford (2005); Greene & Ho (2006b, 2007c); Aller & Richstone (2007); Greene, Ho, & Barth (2008); Gültekin et al. (2009c); Kormendy, Bender, & Cornell (2011); Graham et al. (2011); Sani et al. (2011); Vika et al. (2012); Graham & Scott (2013); and McConnell & Ma (2013). Comparison of these papers with each other and with our results would take more space than we can afford and would be less illuminating than a few general comments.

With one main exception, published studies get shallower slopes than we do for all 3 correlations. Reasons: (1) they include giant Es for which we believe that $M_\bullet$ has been underestimated from emission-line rotation curves; (2) they include NGC 1316 or NGC 5128, which have low BH masses for their high bulge masses; (3) studies before 2011 have few or no BH masses that have been corrected upward as a result of the inclusion of dark matter in dynamical models; (4) even later studies do not generally have all the extraordinarily high-$M_\bullet$ objects published recently by McConnell, Gebhardt, Rusli, and collaborators. McConnell & Ma (2013) is closest to our study; they include the Rusli galaxies. Their fits to early-type galaxies give slopes of 1.11 ± 0.13 (we get 1.21 ± 0.09) for $M_\bullet - L_{\rm bulge}$ and 5.08 ± 0.38 (we get 4.38 ± 0.29) for $M_\bullet - \sigma_e$. For the above reasons and because we omit pseudobulges, published studies also generally get lower $M_\bullet$ zeropoints.

Published studies get steeper slopes than we do when they include pseudobulges or the high-$M_\bullet$ BHs in NGC 3842 and NGC 4889 or both. Pseudobulge BHs deviate from the correlations primarily to low $M_\bullet$, and they do so at small pseudobulge masses. Including them steepens the correlations. Also, we will see in the next section what is already apparent in **Figures 16** amd **17**: The $M_\bullet - \sigma_e$

correlation "saturates" at the high end such that $M_\bullet$ becomes essentially independent of σ_e. We found it sufficient to account for this by excluding only NGC 3842 and NGC 4889 from the fits. Including them steepens $M_\bullet - \sigma_e$ for the complete sample of galaxies. McConnell & Ma (2013) find this when they get an $M_\bullet - \sigma_e$ slope of 5.57 ± 0.33 and Graham and Scott (2013) find it when they get 6.08 ± 0.31 both for their complete galaxy samples. Even when Graham & Scott (2013) exclude barred galaxies, they get a slope of 5.14 ± 0.31. As we have noted, some SB galaxies contain classical bulges and many unbarred galaxies contain pseudobulges, so excluding barred galaxies does not more cleanly isolate unique physics than does not excluding them.

In this paper, we do not include fits that mix classical and pseudo bulges. We strongly believe that we learn the most physics when we make fits only to collections of objects that are sufficiently similar in formation and structure. The fits themselves tell us when this happens. E. g., when two samples that are distinguished on physical grounds have different correlations (classical bulges here and pseduobulges in Section 6.8), then finding this out supports the physical distinction. Similarly, when a correlation that is essentially linear over most of its dynamic range suddenly shows a kink at one end, this is plausibly a sign that new physics is involved. This happens in the next section, and it proves to be easy to diagnose the new physics.

6.7 The Distinction Between Core and Coreless Ellipticals: Dry Mergers and the Saturation of the $M_\bullet - \sigma_e$ Correlation

Ellipticals are divided into two kinds that differ in physical properties (see Kormendy 2009 for a summary and KFCB for a detailed review). This difference is important here because its origin explains – we suggest – an important feature in the $M_\bullet - \sigma_e$ correlation. Also, it will turn out in Section 8 that the two kinds of ellipticals have different forms of AGN feedback.

6.7.1 Two kinds of elliptical galaxies As illustrated in Section 6.13, giant ellipticals have cores: their brightness profiles show a break toward small radii from steep outer Sérsic functions to shallow inner cusps. In contrast, Virgo ellipticals that lack cores have extra light at small radii above the inward extrapolation of the outer Sérsic profile. The extra light is interpreted as the remnant of the central starbursts that happen in wet mergers (Mihos & Hernquist 1994; Kormendy 1999; Côté et al. 2007; KFCB; Hopkins et al. 2009a). Faber et al. (1997) show that core galaxies generally have boxy isophotes and rotate slowly, whereas coreless galaxies generally have disky isophotes and rotate rapidly. Lauer (2012) confirms that the distinction between core and coreless galaxies is essentially the same as the distinction between nonrotating and rotating ellipticals made by the SAURON and ATLAS^{3D} teams (Emsellem et al. 2007, 2011; Cappellari et al. 2007, 2011). Classical bulges are essentially equivalent to coreless ellipticals.

Coreless-disky-rotating ellipticals in the Virgo cluster have V-band absolute magnitudes $M_V \gtrsim -21.5$ and stellar masses $M_* \lesssim 2 \times 10^{11}\, M_\odot$. KFCB summarize the evidence that they formed by dissipative mergers that included central starbursts. Local prototypes are ULIRGs like Arp 220.

Core-boxy-nonrotating ellipticals have $M_V \lesssim -21.5$. Their most recent (one or more) major mergers were dissipationless. The relative importance of major and minor mergers is much debated in recent literature, so we present one piece of evidence below for the importance of major mergers.

The transition between coreless and core galaxies happens at a stellar mass that corresponds to a dark matter mass that is somewhat greater than $M_{\rm DM} \simeq 10^{12}\, M_\odot \equiv M_{\rm crit}$ that is invoked to control "$M_{\rm crit}$ quenching" of star formation by hot, X-ray-emitting gas (Dekel & Birnboim 2006; Cattaneo et al. 2006, 2009; Faber et al. 2007). Core ellipticals contain large amounts of X-ray gas and coreless galaxies do not; KFCB suggest that this is the reason for the difference between the two kinds. Section 8.4 reviews the evidence for this and discusses implications for AGN feedback. Here, we are interested in the implications of the two kinds of ellipticals for BH–host-galaxy correlations.

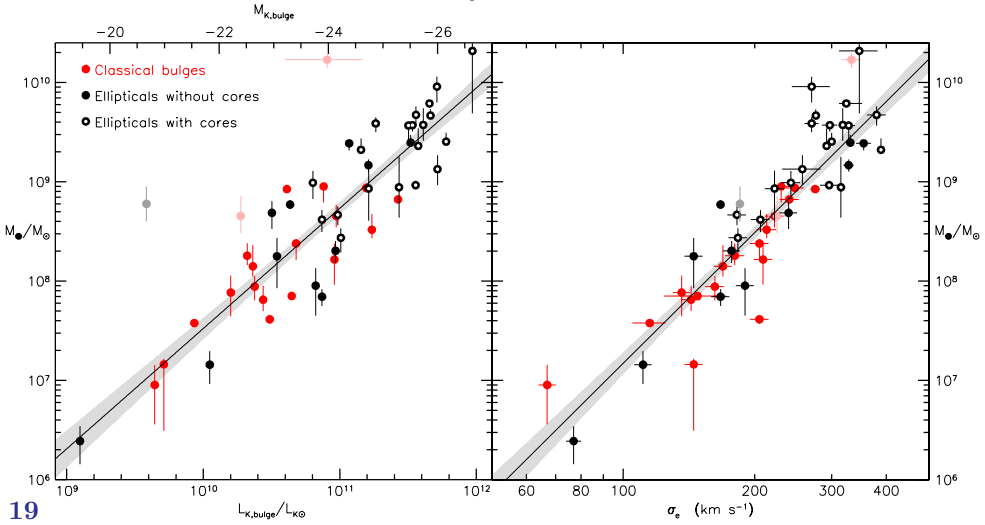

Figure 19

BH correlations and fits from **Figure 17** with core Es identified. The $M_\bullet - L_{K,\rm bulge}$ relation remains log-linear at high $M_\bullet$, but the biggest BHs have masses that become essentially independent of σ_e.

6.7.2 The $M_\bullet - \sigma_e$ relation saturates at high σ_e **Figure 19** suggests that the $M_\bullet - \sigma_e$ relation becomes vertical at $\sigma \gtrsim 270$ km s^{-1}. The sample is small, but indications are that core ellipticals are responsible. That is, for core ellipticals, $M_\bullet$ becomes almost independent of σ_e even while the correlation with bulge luminosity remains unchanged to the highest luminosities.

Hints of this effect were already seen as a result of the upward revision of the BH mass for M 87 (Gebhardt et al. 2011). It has the third-highest $M_\bullet$ in **Figure 19**. At that time, M 87 stood out more than it does now, because the similar-$M_\bullet$ Rusli et al. (2013) BH points were not available and because BH masses based on ionized gas rotation curves were still being included. The σ_e saturation was more convincingly found for the two highest-$M_\bullet$ BHs in NGC 3842 and NGC 4889 by their discoverers (McConnell et al. 2011a, 2012). Then, Kormendy (2013) and McConnell & Ma (2013) note that the upward kink in $M_\bullet - \sigma_e$ at high σ_e involves core galaxies. Kormendy (2013) and **Figure 19** further show that the three coreless galaxies at $\sigma_e > 300$ km s^{-1} – a tiny sample, to be sure – do not participate in this effect.

Most high-σ_e core galaxies scatter to the high-$M_\bullet$ side of the fit in **Figure 19** and in this sense contribute to the impression that σ_e saturates. However, in fact, only NGC 3842 and NGC 4889 are significantly outside the upper envelope of the scatter, and only they were omitted from our fits. We checked that the other high-$M_\bullet$ BHs do not significantly bias our correlation slope by also fitting only the galaxies that have $\sigma_e < 270$ km s^{-1}. These remaining 29 galaxies give

$$\log\left(\frac{M_\bullet}{10^9\,M_\odot}\right) = -(0.54\pm0.07) + (4.26\pm0.44)\log\left(\frac{\sigma}{200\ \rm km\ s^{-1}}\right);\ \text{intrinsic scatter} = 0.30. \quad (12)$$

The zeropoint and slope are closely similar to those, -0.51 ± 0.05 amd 4.38 ± 0.29, in Equation 3.

The saturation of $M_\bullet - \sigma_e$ is only now becoming apparent directly via the detection of higher-$M_\bullet$ BHs than fits predict, but this effect has been known indirectly for a long time. The "contradiction between the $M_\bullet$–σ and $M_\bullet$–L relationships" is illustrated for a large sample of galaxies in Figure 2 of Lauer et al. (2007a). It plots $M_\bullet$ predictions from the two relations against each other and shows that $M_\bullet$–L predicts $M_\bullet$ up to $\sim 10^{10}\,M_\odot$, whereas $M_\bullet$–σ predicts almost no $M_\bullet > 2\times10^9\,M_\odot$. The reason is well known: the Faber-Jackson (1976) $L \propto \sigma^m$ correlation, $m \sim 4$, "level[s] off for large L; indeed, there appears to be little relationship between σ and L for galaxies with $M_V < -22$" (Lauer et al. 2007a). Not coincidentally, this is where ellipticals switch from coreless galaxies to ones with cores. The saturation of the Faber-Jackson relation in the biggest galaxies has been noted before

(Davies et al. 1983; Oegerle & Hoessel 1991; Matković & Guzmán 2005). It is directly responsible for the saturation in $M_\bullet - \sigma_e$ that is now seen in **Figure 19**, as Lauer et al. (2007a) predicted.

High-L saturation in the Faber-Jackson relation is seen in merger simulations by Boylan-Kolchin, Ma, & Quataert (2006). They found that merger orbits become more radial for the most massive galaxies. Then, dry mergers feed more orbital energy into internal energy and help to puff up the remnant and thereby keep σ from growing. They, too, predicted that $M_\bullet - \sigma_e$ saturates at high L.

Figure 20 updates the Faber-Jackson relation for core and coreless ellipticals (from Kormendy & Bender 2013a). It is similar to Figure 3 in Lauer et al. (2007a) with a few core classifications and Hubble types corrected (KFCB) and a few low-luminosity ellipticals added. The coreless galaxies show the familiar relation $\sigma \propto L^{1/4}$. But the relation is very shallow for core Es, $\sigma \propto L^{0.12\pm0.02}$. Also, Kormendy & Bender (2013a) show that coreless galaxies have the above, steep slope and core galaxies have the above, shallow slope even in the absolute magnitude range where they overlap. The difference in slope in **Figure 20** and hence the $M_\bullet$–σ_e saturation in **Figure 19** result from different formation physics for core and coreless ellipticals.

A shallow slope for core ellipticals arises naturally if they form by dry major (not minor) mergers. Hilz et al. (2012) numerically simulate equal-mass mergers and remergers of bulges embedded in dark matter halos. They show that successive mergers lead to a slow increase in the stellar velocity dispersion, because violent relaxation broadens the energy distribution, so some bound particles become more tightly bound while some weakly bound particles escape. They find that the effective line-of-sight velocity dispersion increases as mergers increase the galaxy mass as $\sigma \propto M^{0.15}$. They also present results for growth by minor mergers. Such growth happens mostly by adding a low-σ halo at large radii, so it leads to a decrease in the total projected velocity dispersion, $\sigma \propto M^{-0.05}$.

If we convert $\sigma \propto L^{0.12\pm0.02}$ to a relation in mass M via $M/L \propto L_I^{0.32\pm0.06}$ (Cappellari et al. 2006), we get $\sigma \propto M^{+0.09(+0.03,-0.02)}$, similar to the Hilz and Boylan-Kolchin results. Kormendy & Bender (2013a) conclude that the shallow $\sigma - L$ correlation observed for core galaxies is consistent with their formation in major (not minor) mergers. This is consistent with KFCB.

We noted previously that core ellipticals are so massive that plausible immediate progenitors must have been bulge-dominated. Then we expect that each progenitor brings a BH to the merger and the galaxy and BH both grow together during the merger. But those mergers have relatively little effect on σ_e (see also Volonteri & Ciotti 2013). Thus we suggest that σ_e saturation becomes noticeable once a significant number of dry mergers have happened in a galaxy's formation history. Thus it seems reasonable that the faintest core ellipticals do not show the effect.

Another argument for dry major mergers is made in Section 6.13, where we note that BH binary mass ratios must be ~ 1 in order to lift a sufficient mass in stars to account for cores. And the mergers must be dry in order not to be swamped by a ULIRG-like starburst.

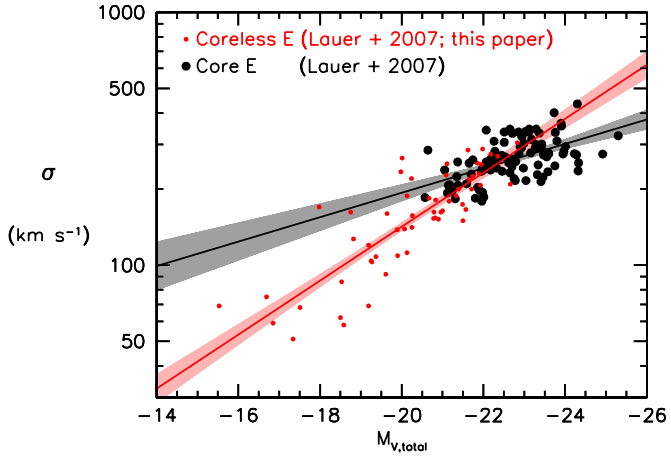

Figure 20

Faber-Jackson (1976) relations for core and coreless ellipticals (Kormendy & Bender 2013a). Total V-band absolute magnitudes $M_{V,\rm total}$, velocity dispersions σ, and profile types are mostly from Lauer et al. (2007b). The lines are symmetric least-squares fits to core (*black line*) and coreless galaxies (*red line*). One-sigma fit uncertainties are shaded. The coreless galaxies show the familiar relation, $\sigma \propto L_V^{0.27\pm0.02}$. But velocity dispersions in core ellipticals increase very slowly with luminosity, $\sigma \propto L_V^{0.12\pm0.02}$.

6.8 BHs do not correlate with pseudobulges of disk galaxies

Section 4 discusses the observational distinction between classical bulges, which are essentially indistinguishable from ellipticals, and pseudobulges, which usually have properties that are more disk-like than those of classical bulges. We believe that we understand why: Classical bulges are made by major galaxy mergers, whereas pseudobulges are grown secularly out of disks. But for this section, an explanation is not essential. The Supplementary Information expands on Kormendy & Kennicutt (2004) by listing observational criteria that can be used to distinguish between classical and pseudo bulges, independent of interpretation. Do they correlate similarly with BHs?

Papers on this issue are divided. Kormendy & Gebhardt (2001) were the first to ask the question. They concluded that classical and pseudo bulges correlate in the same way with BHs. They were wrong, because, with data available then, the classical bulges in NGC 4258 and NGC 7457 were mistakenly called pseudobulges and because their sample included only six (after correction: four) pseudobulges. Gültekin et al. (2009c) also did not see a significant difference, but their sample also was small, and 14 of their 23 disk galaxies had no available (pseudo)bulge parameters.

Other papers find different BH correlations for bulges and pseudobulges. This was first suggested by Hu (2008). He examined only the $M_\bullet - \sigma$ correlation, which is relatively safe, because it does not require bulge-disk decomposition. He used the pseudobulge classification criteria from Kormendy & Kennicutt (2004). His sample Tables 1 and 2 do not completely overlap with our **Tables 2** and **3**, because a few different judgments were made about reliable BH detections. But the sample was large enough and accurate enough to suggest that pseudobulges have smaller $M_\bullet$ at a given σ than do classical bulges and ellipticals. This proves to be a robust result.

A possible indirect detection of a difference is by Graham (2008a, 2008b) and Graham & Li (2009). They argued that the correlations are different for barred galaxies than they are for unbarred disk galaxies and ellipticals. The sense of the difference is similar to that found by Hu (2008): $M_\bullet$ is anomalously small or σ is anomalously large in barred galaxies. Graham adopted the latter explanation and suggested that velocity dispersions are enhanced in barred galaxies. This could be a detection of the effect that was seen by Hu, because barred galaxies preferably have pseudobulges (Kormendy & Kennicutt 2004). However, of Graham's (2008a) seven barred galaxies, three have classical bulges, and of his unbarred disk galaxies, at least one (NGC 1068) contains a prominent pseudobulge. Similar comments apply to the 2008b paper and to Graham & Scott (2013). Graham & Li (2009) derived BH masses from emission-line widths in AGNs; less is known about these more distant objects, but they are also offset from $M_\bullet - \sigma$ in the direction of low $M_\bullet$ or high σ.

Seven BH discoveries based on H_2O maser dynamics were recently published by Kuo et al. (2011). The host galaxy velocity dispersions were measured and their brightness distributions analyzed by Greene et al. (2010). They decisively concluded that the pseudobulges in their sample have smaller BH masses than predicted by the $M_\bullet - \sigma$ correlation for classical bulges and ellipticals. Our bulge-disk decompositions do not completely agree with theirs, but their sample is well suited to the problem, because maser galaxies tend to be late in type and therefore to contain pseudobulges.

Meanwhile, Kormendy, Bender, & Cornell (2011) measured (pseudo)bulge parameters for the full Gültekin et al. (2009c) sample and used them to conclude that BHs do not correlate significantly with either the luminosities or the velocity dispersions of their host pseudobulges. "Pseuodbulges at best show a much larger scatter [than do classical bulges and ellipticals]." "Whether pseudobulges correlate with $M_\bullet$ with large scatter or not at all, the weakness of any correlation ... makes no compelling case that pseudobulges and BHs coevolve, beyond the obvious expectation that it is easier to grow bigger BHs and bigger pseudobulges in bigger galaxies that contain more fuel."

Figure 21 confirms these results with the new sample from **Table 3**. The total amount of BH growth is not extremely different in classical and pseudo bulges. But the scatter in all panels is large.

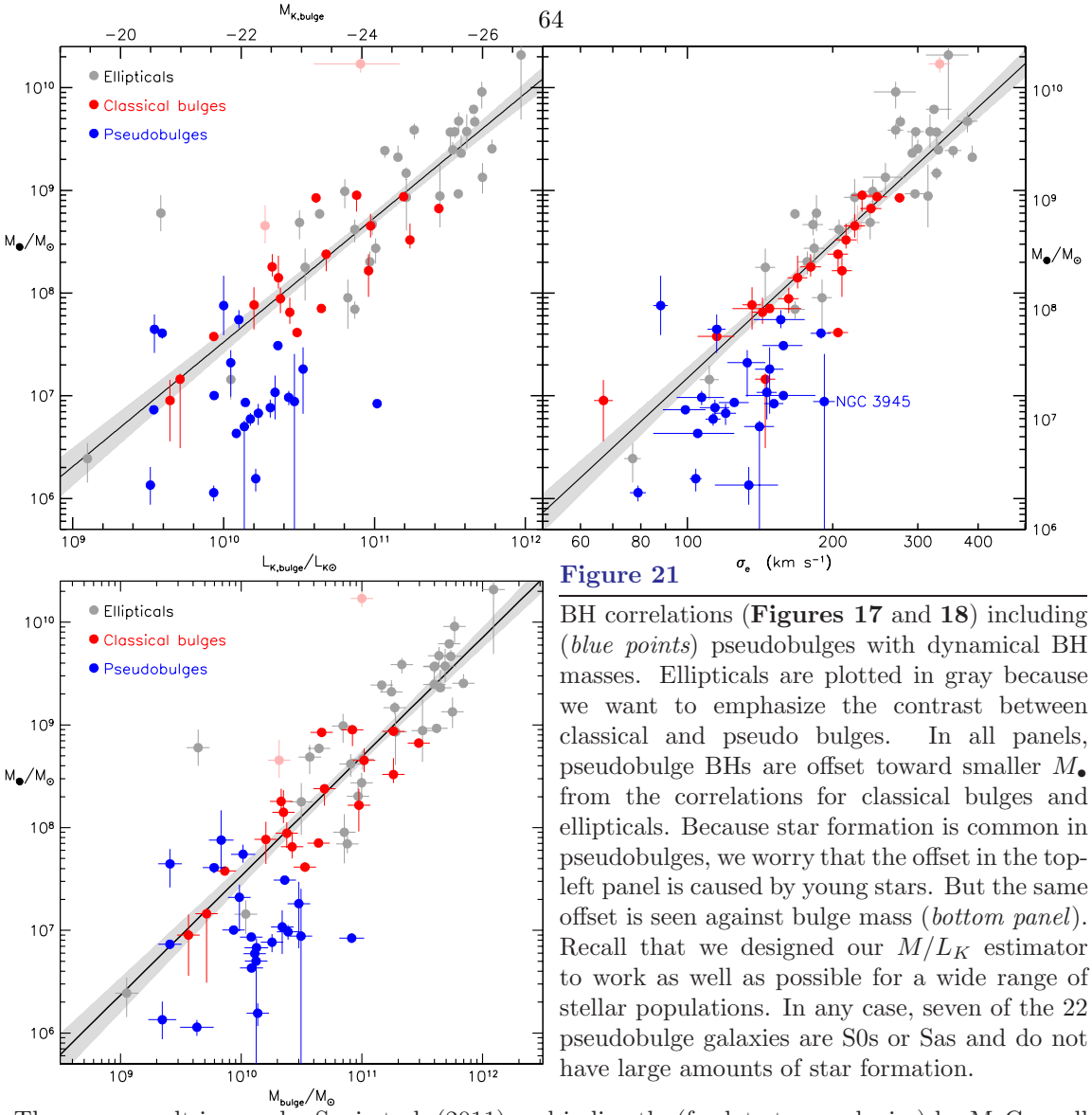

Figure 21

BH correlations (**Figures 17** and **18**) including (*blue points*) pseudobulges with dynamical BH masses. Ellipticals are plotted in gray because we want to emphasize the contrast between classical and pseudo bulges. In all panels, pseudobulge BHs are offset toward smaller $M_\bullet$ from the correlations for classical bulges and ellipticals. Because star formation is common in pseudobulges, we worry that the offset in the top-left panel is caused by young stars. But the same offset is seen against bulge mass (*bottom panel*). Recall that we designed our M/L_K estimator to work as well as possible for a wide range of stellar populations. In any case, seven of the 22 pseudobulge galaxies are S0s or Sas and do not have large amounts of star formation.

The same result is seen by Sani et al. (2011) and indirectly (for late-type galaxies) by McConnell & Ma (2013). Also, BH searches in pseudobulges appear to fail more often than those in classical bulges and ellipticals (e. g., NGC 3945: Gültekin et al. 2009b). For these galaxies, it is still possible that we detect only the largest-mass BHs and therefore see the upper envelopes of $M_\bullet$ distributions that extend down to smaller BHs than we can currently find (Barth, Greene, & Ho 2005).

Section 7.2 extends the $M_\bullet$ dynamic range by considering BH masses determined for AGNs. Taken together, AGN BHs of all masses do show some correlation with host properties even down to $M_\bullet \sim 10^5\ M_\odot$. But the scatter at low $M_\bullet$ is very large. No coevolution is implied. Nevertheless, we emphasize: We do not know whether the decrease in BH correlation scatter as we move from pseudobulges to classical bulges to ellipticals and as we look at larger $M_\bullet$ and $M_{\rm bulge}$ is due only to merger averaging (Section 8.5) or whether additional coevolution physics – presumably in wet mergers (Section 8.6) – is required. What we need most is more BH detections in small classical bulges and ellipticals to see whether and how much the scatter in their $M_\bullet$ –host correlations is smaller than that for pseudobulges in the BH mass range where they overlap.

6.9 BHs do not correlate with galaxy disks

Figure 22 confirms the results of Kormendy & Gebhardt (2001) and Kormendy et al. (2011) that BHs do not correlate with galaxy disks. The Kormendy & Gebhardt (2001) conclusion was based on showing that the good $M_\bullet - M_{B,\rm bulge}$ correlation essentially disappears when the total absolute magnitude is used instead of the bulge absolute magnitude. The Kormendy et al. (2011) result is more direct: it is based on a version of **Figure 22** for the Gültekin et al. (2009c) sample. The full sample of **Table 3** strengthens this result. Many pseudobulges are in late-type, star-forming disks; if $M_{K,\rm disk}$ were converted to disk mass, the corresponding blue points would move leftward with respect to the red points and the weak anticorrelation of $M_\bullet$ with disk luminosity would get weaker. Thus BHs do not "know about" disks at all. This extends previous results: BHs somehow coevolve with bulges but not with disks or with the total baryonic content of their host galaxies.

And yet, we now know that BHs can exist even in pure-disk galaxies. Some pure disks show AGN activity, although it is rare in bulgeless galaxies (Ho, Filippenko & Sargent 1997b; Ho 2004b, 2008). And BHs with $M_\bullet = 10^4 - 10^6\,M_\odot$ have confidently been discovered in (pseudo)bulge-less galaxies. The most extreme case is NGC 4395, an Sm galaxy with a tiny, globular-cluster-like nucleus that has an AGN powered by a BH (Filippenko & Ho 2003) with $M_\bullet = (3.6 \pm 1.1) \times 10^5\,M_\odot$ measured by reverberation mapping (Peterson et al. 2005). It is shown in **Figure 22**. Similar objects include NGC 1042 (Scd; Shields et al. 2008), NGC 3621 (Sd; Barth et al. 2009), NGC 4178 (Sdm; Secrest et al. 2012). Also, the Sph galaxy POX 52 contains an AGN powered by a BH of mass $M_\bullet \simeq 10^5\,M_\odot$ (Barth et al. 2004; Thornton et al. 2008). See Section 7.1 for details.

The lack of correlation of BHs with disks and pseudobulges plus the discovery of BHs in (pseudo)bulgeless galaxies are critical clues to BH evolution. They motivate the hypothesis in Section 8 that there are two feeding mechanisms for BHs, (1) a global feeding mechanism that is connected with bulge formation and therefore presumably with galaxy mergers and that engineers BH – bulge coevolution and (2) one or more local feeding mechanisms that operate even in pure-disk galaxies but that result in no BH coevolution with any part of the host galaxy.

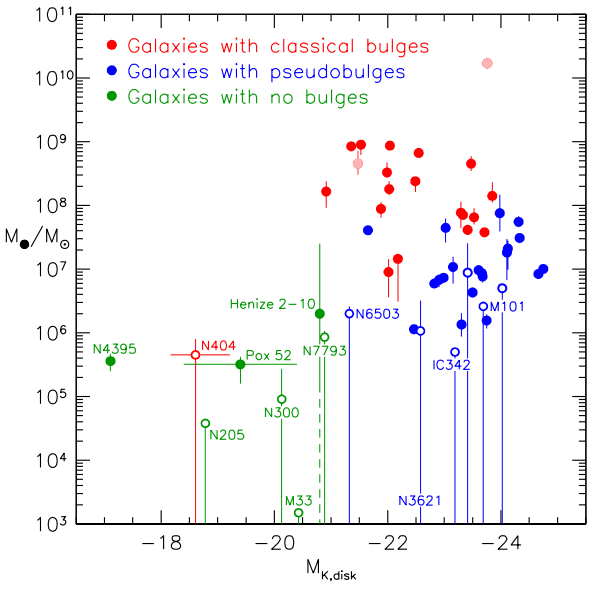

Figure 22

BH mass versus K-band absolute magnitude of the disk of the host galaxy. Red and blue filled circles are from **Table 3**. Open circles show $M_\bullet$ upper limits; the strongest is $M_\bullet \lesssim 1500\,M_\odot$ for M 33 (Gebhardt et al. 2001). M 101 and NGC 6503 are from Kormendy et al. (2010). IC 342 is from Böker et al. (1999). NGC 3621 is from Barth et al. (2009). Green points are for galaxies with no classical bulge and almost no or certainly no pseudobulge but only a nuclear star cluster. NGC 4395 (Peterson et al. 2005) and Pox 52 (Barth et al. 2004; Thornton et al. 2008) are discussed in Section 7.1. Henize 2-10 (Reines et al. 2011) is discussed in Section 7.3. Limits: NGC 205 is from Valluri et al. (2005); NGC 300 and NGC 7793 are from Neumayer & Walcher (2012; several other limits in that paper are broadly similar, but the galaxies are much farther away). NGC 404 is from Seth et al. (2010).

6.10 BHs do not correlate with dark matter halos in a way that is more fundamental than the $M_\bullet - M_{bulge}$ and $M_\bullet - \sigma_e$ correlations for classical bulges and ellipticals

Ferrarese (2002) suggested that $M_\bullet$ correlates as closely with DM halos of galaxies as it does with bulges and ellipticals. In fact, she suggested that the DM correlation is the more fundamental one. This was not based on galaxies with BH detections. Rather, she used proxy parameters: σ for $M_\bullet$ and the asymptotic outer rotation velocity $V_{\rm circ}$ of galaxy disks for DM. Ferrarese's conclusion was based on observing a tight correlation between σ and $V_{\rm circ}$. Baes et al. (2003) lent further support, and the idea quickly became popular in galaxy formation theory, because it provided a natural way for AGN feedback to control BH growth (Booth & Schaye 2010), and because it led to a simple prescription for including feedback in semianalytic models of galaxy formation. But the implications were more profound than this. The conclusion – if correct – implied that the unknown, exotic physics of nonbaryonic DM might be necessary to engineer BH–galaxy coevolution.

Ferrarese's conclusion was surprising and counterintuitive. It was known that BHs do not correlate with galaxy disks (Kormendy & Gebhardt 2001), whereas disks correlate closely with DM (van Albada & Sancisi 1986; Sancisi & van Albada 1987). How could BHs and disks separately correlate with DM without also correlating with each other?

Kormendy & Bender (2011) re-examined the $V_{\rm circ}$–σ correlation and concluded that BHs do not correlate with DM in a way that goes beyond the known correlations with bulges and ellipticals. Section 6.10.1 updates their arguments. Section 6.10.2 then presents a new, more direct argument that is based not on $V_{\rm circ}$ but rather on new results about global halo parameters.

6.10.1 The $V_{\rm circ} - \sigma$ correlation is shown in **Figure 23**. The left panel shows the correlation as Ferrarese derived it except that incorrect σ measurements are omitted or corrected (see below) and that new measurements of bulgeless galaxies are added. The right panel includes more galaxies.

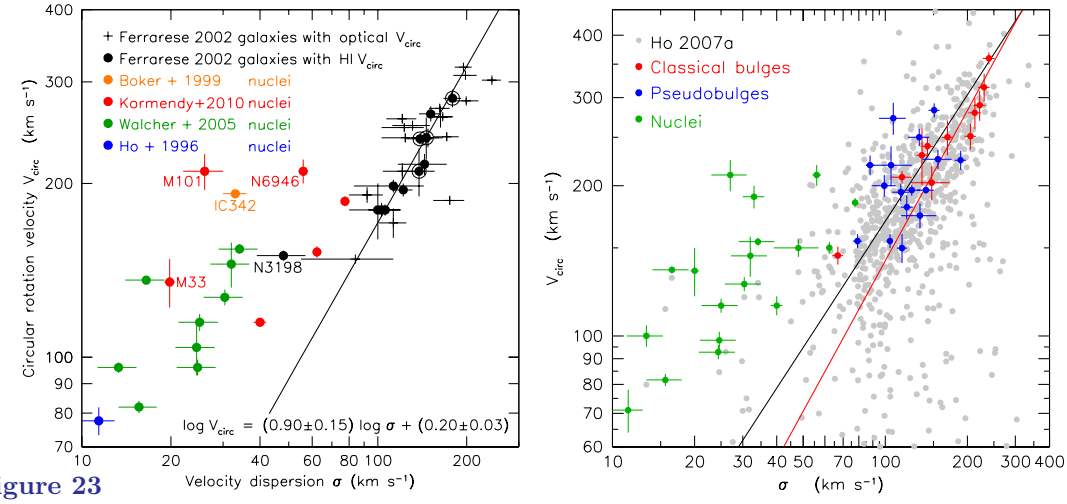

Figure 23

Outer rotation velocities $V_{\rm circ}$ of spiral galaxy disks vs. central velocity dispersions σ (Fig. 1 and S3 in Kormendy & Bender 2011). Left: Ferrarese (2002) correlation (black points, circled if the galaxy has a classical bulge). Ferrarese points are omitted if the σ measurement had insufficient velocity resolution or corrected if higher-resolution data are available. Added in color are points for galaxies that have no classical bulge and essentially no pseudobulge but that are measured with instrumental resolution (expressed as a dispersion) $\sigma_{\rm instr} < 10$ km s^{-1} high enough to resolve the smallest σ in galactic nuclei. The line (equation at bottom, velocities in units of 200 km s^{-1}) is a least-squares fit to the black circles omitting NGC 3198. Right: $V_{\rm circ}$–σ relation for the large sample in Ho (2007). It includes nuclei (*left panel*) and classical bulges and pseudobulges with BH detections (**Table 2**). The black line is Ferrarese's fit to her correlation. The red line is not a fit; it shows $V_{\rm circ} = \sqrt{2}\,\sigma$.

The Kormendy & Bender (2011) arguments were based on the left panel of **Figure 23** and on the right panel using the Gültekin et al. (2009c) subsample of the present, **Table 3** disk galaxies with dynamical BH detections. Ellipticals are not included; we cannot directly measure $V_{\rm circ}$ and do not have a sufficiently accurate way to measure DM that is not intimately connected with the stellar mass distribution. We already know that BHs correlate tightly with that stellar mass distribution.

Before we proceed, we need to be clear about what we are testing.

First, how do we measure DM? Here in Section 6.10.1, we assume that $V_{\rm circ}$ measures the inner parts of DM halos. Provided that the measurements reach out beyond most of the visible galaxy, rotation curve decompositions suggest that this is a good approximation. Ferrarese argues and we agree that H I rotation curves reach farther out into DM halos than optical ones and provide more reliable asymptotic $V_{\rm circ} \simeq$ constant measurements of halos. This is why the filled circles in **Figure 23** (*left*) show smaller scatter than the error bars withough central points. A variety of recent studies further support our assumption that $V_{\rm circ}$ is a good measure of the inner parts of DM halos; i. e., approximately the maximum rotation velocity of the halo if it has a Navarro, Frenk, & White (1997) density distribution (e. g., Dutton et al. 2010, 2011). Thus, in the rest of this section, we follow Ferrarese (2002) and use $V_{\rm circ}$ to measure DM. Then, in Section 6.10.2, we broaden the discussion to include estimates of the total dark matter content of galaxies. This will provide an additional point that is independent of the arguments in this section.

Second, what are we testing? The issue is not just whether a plot of $V_{\rm circ}$ versus σ shows a tight correlation. At stake are implications for BH growth and galaxy formation. We test two competing ideas. The known $M_\bullet - \sigma$ relation for bulges suggests that BHs and bulges coevolve. An equally tight $M_\bullet - V_{\rm circ}$ correlation would raise the possibility that baryons are irrelevant and that the physics of nonbaryonic DM controls BH growth. But we emphasize: Intermediate interpretations are part of the first alternative, because we know that DM gravity (but not its exotic physics) drives hierarchical clustering. So the issue is: *Do BHs correlate with DM in a way that goes beyond the BH – bulge relation? Does this BH – DM correlation demand the conceptual leap that it is not bulge growth but rather DM properties that engineer BH – galaxy coevolution?*

We begin using Ferrarese's (2002) correlation (**Figure 23**, *left*) and the assumption that σ serves as a surrogate for $M_\bullet$. The Kormendy & Bender (2011) arguments are:

1. Some σ values used by Ferrarese (2002) were measured with insufficient velocity resolution and are known to be incorrect. The bulgeless Scd galaxy IC 342 (orange point in **Figure 23** *left*) was shown at $\sigma = 77 \pm 12$ km s^{-1}, consistent with the black points. But the measurement (Terlevich, Díaz, & Terlevich 1990) had low resolution: the instrumental velocity dispersion $\sigma_{\rm instr} \equiv$ (resolution FWHM)/2.35 was 77 km s^{-1}, similar to σ measured in IC 342. Low resolution often results in overestimated σ. Terlevich et al. (1990) also got $\sigma = 77$ km s^{-1} for the nucleus of M 33, which has $\sigma = 20 \pm 1$ km s^{-1} as measured at high resolution (Kormendy & McClure 1993; Gebhardt et al. 2001; Kormendy et al. 2010). In fact, a high-resolution measurement of IC 342 was available: at $\sigma_{\rm instr} = 5.5$ km s^{-1}, Böker, van der Marel & Vacca (1999) got $\sigma = 33 \pm 3$ km s^{-1} (orange point). So **Figure 23** omits black points if $\sigma_{\rm instr} \gtrsim \sigma$. The range over which the remaining black points show a correlation is much reduced.
2. *If DM halos and not bulges control $M_\bullet$, then the galaxies that should demonstrate this are the biggest ones that do not contain bulges.* Thus motivated, Kormendy et al. (2010) measured σ in six Sc – Scd galaxies that contain nuclear star clusters ("nuclei") but no classical bulges. Even pseudobulges make up only a few percent of these galaxies. The observations were made with the 9.2 m Hobby-Eberly Telescope High Resolution Spectrograph at $\sigma_{\rm instr} = 8$ km s^{-1}. Results are shown by the red points in **Figure 23** together with other high-dispersion measurements of (pseudo)bulgeless galaxies (color points). Kormendy and Bender concluded that (pseudo)bulgeless galaxies show only a weak correlation between $V_{\rm circ}$ and σ. A weak correlation is expected, because bigger galaxies tend to have bigger nuclei (Böker et al. 2004;

Rossa et al. 2006). But the scatter is much larger than the measurement errors: $\chi^2 = 15.7$. No tight correlation is suggestive of any more compelling formation physics than the expectation that galaxies grow bigger nuclei when they contain more cold gas. The black and color points overlap for 180 km s^{-1} $\lesssim V_{\rm circ} \lesssim$ 220 km s^{-1}. In this DM range, galaxies participate in a tight $V_{\rm circ}$ – σ correlation only if they have bulges. That is, baryons and BH growth are closely connected only if they are in a bulge. Baryons in a disk are not enough. DM by itself is not enough. M 101 (*top-left red point*) has a halo that is similar to those of half of the galaxies in the remaining tight correlation, but that halo did not manufacture a canonical BH in the absence of a bulge. This suggests that bulges, not halos, coevolve with BHs.

3. The large, unbiased sample of galaxies studied by Ho (2007a) leads to the same conclusions. In **Figure 23** (*left*), the galaxy sample shown by the color points is intentionally biased against galaxies that contain bulges. There, we want to know whether DM correlates with BHs in the absence of the component that we know correlates with BHs. However, Ho (2007a) made a similar study of a large galaxy sample that is not biased against bulges. His results are shown by the gray points in **Figure 23** (*right*). He concluded that $V_{\rm circ}$ correlates weakly with σ, especially in galaxies that contain bulges, but the scatter is large and "these results render questionable any attempt to supplant the bulge with the halo as the fundamental determinant of the central black hole mass in galaxies."

4. Kormendy & Bender (2011) argued that the tight correlation of black points in **Figure 23** is a result of the conspiracy between baryons and DM to make featureless, nearly flat rotation curves with no distinction between radii that are dominated by baryonic and nonbaryonic matter (van Albada & Sancisi 1986; Sancisi & van Albada 1987). This is a natural consequence of the observation that baryons make up 16 % of the matter in the universe (Hinshaw et al. 2013) and that, to make stars, they need to dissipate inside their halos until they self-gravitate. This is enough to engineer that $V_{\rm circ}$ is approximately the same for DM halos and for the disks that are embedded in them (Gunn 1987; Ryden & Gunn 1987). That bulges participate in the conspiracy is less well known and not implied by the above arguments. However, in their Figures S1 and S2, Kormendy & Bender (2011) demonstrate that, when $V_{\rm circ} \simeq 200$ km s^{-1}, the bulge, disk, and halo all have approximately the same velocity scales. All galaxies that participate in the tight correlation in **Figure 23** have bulges or pseudobulges. The suggestion then is that that correlation is nothing more nor less than a restatement of the rotation curve conspiracy for bulges and DM. This means that the correlation of black points in **Figure 23** is a consequence of DM-mediated baryonic galaxy formation.

5. So far, we have discussed BH correlations indirectly using the assumption that σ is a surrogate for BH mass $M_\bullet$. However, Section 6.8 establishes that σ is not a valid surrogate for $M_\bullet$ in pseudobulges. Only 4 galaxies plotted with black points in **Figure 23** (*left*) contain classical bulges, M 31, NGC 2841, NGC 4258, and NGC 7331. Their points are circled. The other black filled circles represent pseudobulges. *For pseudobulges, the demonstration of a tight $V_{\rm circ}$ –σ correlation is not a demonstration that DM and BHs correlate. Moreover, the circled points for classical bulges agree with the correlation for pseudobulges. It is implausible to suggest that the correlation for the four circled points is caused by BH – DM coevolution whereas the identical correlation for the other points has nothing to do with BHs. Ferrarese's observation that classical and pseudo bulges show the same $V_{\rm circ}$ –σ correlation in* **Figure 23** *is by itself a strong argument against the hypothesis that either correlation reflects BH – DM coevolution.* Our BH galaxies show a tighter $V_{\rm circ}$ –σ correlation when they contain classical bulges than when they contain pseudobulges (**Figure 23**, *right*). This is consistent with our picture that pseudobulges grow by local processes that are not closely connected with the depth of the gravitational potential well, whereas (point 4, above) classical bulges form in a way that engineers the DM –visible-matter conspiracy revealed by rotation curve decomposition.

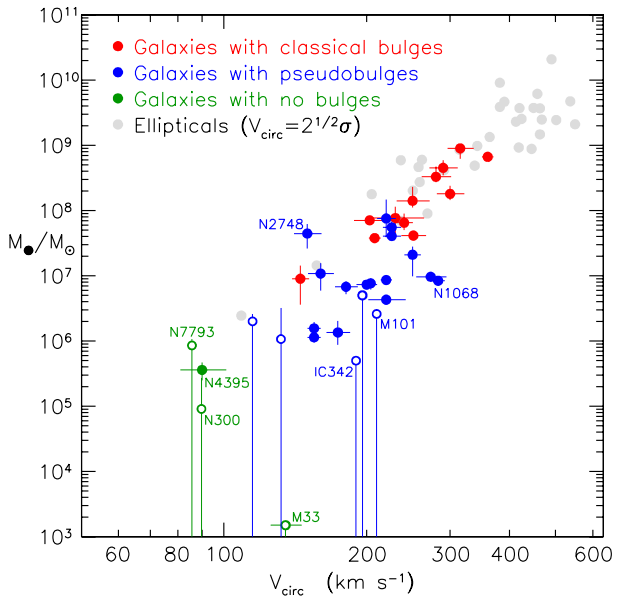

Figure 24

Dynamically detected BH mass versus asymptotic, outer circular rotation velocity of the disk of the host galaxy. Kormendy & Bender (2011) show this plot for the Gültekin et al. (2009c) sample in their Figure 2(d). The present version is for the **Table 3** sample. Open circles show $M_\bullet$ upper limits. Red points are for galaxies with classical bulges; blue points are for galaxies with pseudobulges, and green points are for galaxies with neither a classical nor a pseudo bulge but only a nuclear star cluster. Gray points for elliptical galaxies are plotted assuming that $V_{\rm circ} = \sqrt{2}\sigma$ (cf. **Figure 23**, *right*); they remind us that classical bulges and ellipticals have similar parameter correlations. Unlike arguments 1–5, this is a direct test for a BH–DM correlation. But it is a difficult one, because $V_{\rm circ}$ is not known for most bulge-dominated galaxies (hence our assumption for ellipticals).

6. **Figure 24** shows that dynamically measured BH masses do not correlate with $V_{\rm circ}$ and hence with DM for pseudobulges. For classical bulges and possibly for ellipticals, there is a good correlation, but it remains likely that this is a consequence of the rotation curve conspiracy. This confirms directly what we deduced indirectly above. No conceptual leap to a BH–DM correlation is compelled by the data.

7. A final point from Kormendy & Bender (2011) is reproduced here from their Supplementary Information. The DM halos of galaxy clusters predict giant BHs that are not observed. This is important in the context of Ferrarese's (2002) conclusion that more massive halos are more efficient in growing BHs. Her $V_{\rm circ} - \sigma$ correlation, reproduced to within errors in **Figure 23**, is

$$\log V_{\rm circ} = (0.84 \pm 0.49)\ \log\sigma + (0.55 \pm 0.19)\ , \qquad (13)$$

Substituting for σ in her $M_\bullet - \sigma$ relation,

$$M_\bullet = (1.66 \pm 0.32) \times 10^8\ M_\odot \left(\frac{\sigma}{200\ {\rm km\ s^{-1}}}\right)^{4.58\pm0.52}\ , \qquad (14)$$

yields

$$\frac{M_\bullet}{10^8\ M_\odot} = 0.168 \left(\frac{V_{\rm circ}}{200\ {\rm km\ s^{-1}}}\right)^{5.45}\ . \qquad (15)$$

As a check on previous arguments, $V_{\rm circ} = 210$ km s^{-1} for M 101 predicts $M_\bullet \simeq 2.2 \times 10^7\ M_\odot$. This conflicts with the observed upper limit, $M_\bullet \lesssim (2.6 \pm 0.5) \times 10^6\ M_\odot$ (Kormendy et al. 2010). At the high end of the range of $V_{\rm circ}$ values for DM halos, rich galaxy clusters typically have velocity dispersions $\sigma \sim 1000$ km s^{-1} and can have dispersions as high as ~ 2000 km s^{-1}. Whether we can use these cluster halos in our argument depends on whether the DM is already distributed in the cluster or whether it is still attached only to the galaxies, with the result that the total mass is large but that individual halos are not. Large-scale simulations of hierarchical clustering show

that, while substructure certainly exists, much of the DM in rich, relaxed clusters is distributed "at large" in the cluster (Springel et al. 2005b). In fact, DM hierarchical clustering is so nearly scale-free that "it is virtually impossible to distinguish [the halo of an individual galaxy from that of a cluster of galaxies] even though the cluster halo is nearly a thousand times more massive" (Moore et al. 1999). Therefore we can treat cluster halos like galaxy halos in predicting $M_\bullet$. They provide an especially important test of "baryon-free" BH – DM coevolution, because Ferrarese (2002) concluded that higher-mass DM halos are more efficient at growing large BHs.

DM halos of 10^{15} $M_\odot$ are not rare (Faltenbacher, Finoguenov & Drory 2010). A cluster like Coma has $\sigma \sim 1000$ km s^{-1} and therefore presumably has $V_{\rm circ} \sim \sqrt{2}\,\sigma \sim 1400$ km s^{-1} (Kent & Gunn 1982). Equation (15) then predicts that

$$M_\bullet \sim 1 \times 10^{11}\ M_\odot\ . \tag{16}$$

Sunk to the center of NGC 4874 or NGC 4889, such a BH would be hard to hide. Both galaxies have $\sigma \simeq 300$ km s^{-1} and normal, shallow $\sigma(r)$ profiles (Fisher, IIllingworth & Franx 1995). But an 10^{11}-$M_\odot$ BH would have a sphere-of-influence radius of $2\farcs2$. We would have found such a BH. In fact, we now have a measurement of $M_\bullet = 2.1(0.5-3.7) \times 10^{10}\ M_\odot$ in NGC 4889 (McConnell et al. 2012). But this mass is more appropriate for the host galaxy than it is for the cluster halo.

Therefore, if baryons do not matter—if the hypothesis is that DM makes BHs independent of how baryons are involved (as a galaxy, as a group of galaxies, or not at all)—then Equation (15) predicts unrealistically large BH masses for rich clusters of galaxies, *especially when there is not a giant elliptical at the cluster center.*

Combining 1 – 7: Over the whole range of $V_{\rm circ}$ values associated with DM halos, i. e., at least

$$50\ {\rm km\ s^{-1}} \lesssim V_{\rm circ} \lesssim 2000\ {\rm km\ s^{-1}}\ , \tag{17}$$

the only part of the range in which **Figure 23** shows a tight correlation between σ and $V_{\rm circ}$ is 150 – 300 km s^{-1} and only if the galaxy contains a classical bulge. At most $V_{\rm circ}$ values even in this range, there are DM halos that do not contain classical bulges, and then $V_{\rm circ}$ does not correlate with $M_\bullet$. Outside this $V_{\rm circ}$ range, Equation (15) gets into trouble with observations. This situation argues against the hypothesis that baryons are irrelevant and that DM controls BH growth. We conclude that BHs do not correlate causally with DM halos.

The consequences for galaxy formation are simple and profound. There is no reason to expect that the unknown, exotic physics of nonbaryonic DM directly influences BH growth. Even the presence of the halo's gravitational potential well appears not to be solely and directly responsible for BH – galaxy coevolution. Rather, coevolution physics appears to be as simple as it could be: it happens only in the context of the major galaxy mergers that make classical bulges and ellipticals.

6.10.2 The relationship between DM and stellar masses of galaxies and consequences for our understanding of BH – galaxy coevolution

Our discussion so far has been confined to the inner parts of DM halos, where rotation curve decomposition and other observations support the assumption that $V_{\rm circ}$ is a relatively secure measure of DM properties. However, rotation curves sample small fractions of galaxy DM halos. What new things do we learn if we can measure total halo mass $M_{\rm DM}$? Behroozi et al. (2010, 2012) review and extend recent work that provides a statistical connection between baryonic and DM masses of galaxies. A variety of techniques are involved, ranging from relatively direct observations of satellite dynamics, clustering properties, and weak lensing, to indirect but powerful methods such as abundance matching of DM halo masses in cosmological simulations with galaxy mass distributions observed in large volumes in the universe. References are given in the above papers and in **Figure 25**. From this work, we cannot correlate $M_\bullet$ with $M_{\rm DM}$ for individual galaxies, but we can – at least statistically – combine the $M_\bullet - M_{\rm bulge}$ correlation with the $M_*/M_{\rm DM} - M_{\rm DM}$ correlation to infer how $M_\bullet$ is related to $M_{\rm DM}$. For the purposes of this section, the difference between $M_{\rm bulge}$ and the total stellar mass M_* is unimportant; we assume that they are equal. The results provide a further argument that BHs coevolve with bulges and not with DM halos.

Figure 25 shows the relationship between visible matter (mainly stellar) mass and DM mass. The left panel shows the mass function of cold dark matter halos (*upper dashed curve*) and the expected baryonic mass function if all galaxies contained the cosmological baryon fraction of $\sim 1/6$. It is well known that the baryon content of galaxies falls short of the cosmological value at all masses. This is shown more directly at right, where Behroozi, Conroy, & Wechsler (2012) summarize results from many techniques on the stellar-to-DM mass ratios in galaxies, this time as a function of DM halo mass. At a "sweet-spot" DM mass of $\sim 1 \times 10^{12}\, M_\odot$, $M_*/M_{\rm DM}$ reaches a maximum of 1/5 of the cosmological value. But the stellar mass fraction is smaller at both lower and higher DM masses. The sweet-spot DM mass corresponds to $M_* \approx M_{\rm bulge} \simeq 3 \times 10^{10}\, M_\odot$. This is in the middle of the $M_\bullet - M_{\rm bulge}$ correlation in **Figure 18**. So $M_\bullet$ shows a simple, log-linear correlation with $M_{\rm bulge}$ but a complicated relation with $M_{\rm DM}$ that has a kink at the center of the $M_\bullet$ range. This argues that the more fundamental relation is the one between $M_\bullet$ and $M_{\rm bulge}$.

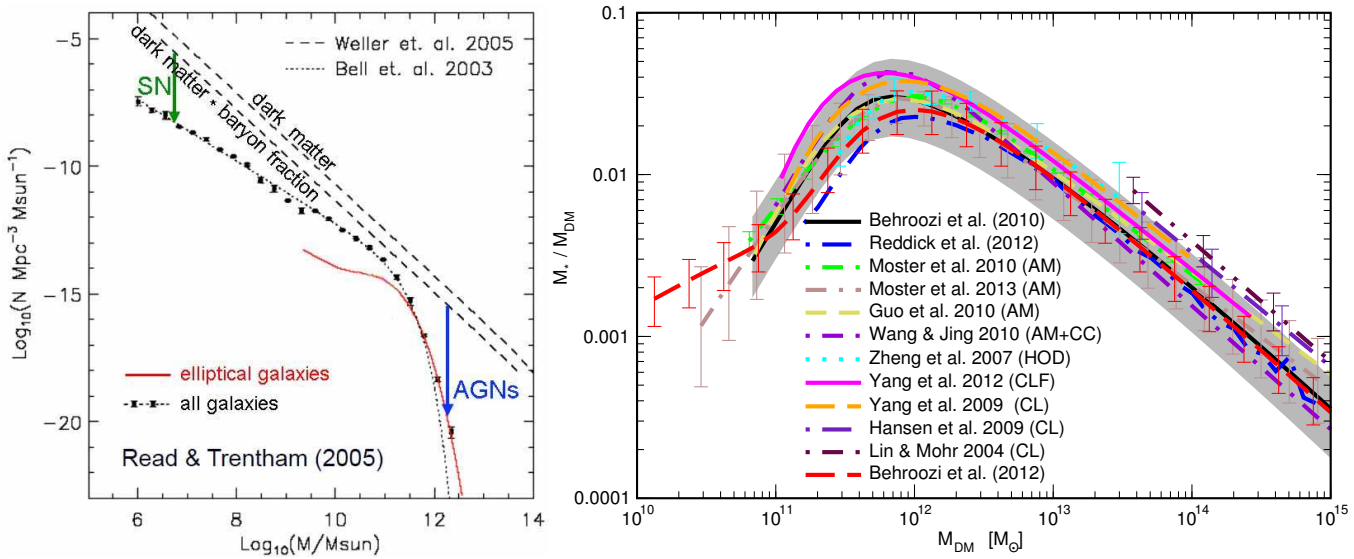

Figure 25

(*left*) From Read & Trentham & (2005), the total field galaxy baryonic mass function (*black points*) and Schechter (1976) function fit (Bell et al. 2003: *dotted curve)* compared to the mass spectrum of cold DM halos from numerical simulations by Weller et al. (2005) and to that DM mass function multiplied by the universal baryon fraction of 0.163 (Hinshaw et al. 2013) (*lower dashed curve*). (*right*) From Behroozi, Wechsler, & Conroy (2012), comparison of their abundance matching of DM halos and visible galaxies with published results. Abbreviations: AM = abundance matching; CC = clustering constraints; HOD = modeling of halo occupation distributions; CLF = conditional luminosity function; CL = various (e. g., X-ray) results on galaxy clusters; see Behroozi et al. (2012) for details. Gray shading shows 68 % confidence limits from a similar analysis in Behroozi et al. (2010). Both panels show that galaxies have baryon-to-DM mass fractions that are less than the cosmic value. The largest baryon mass fractions are seen in halos of mass $M_{\rm DM} \sim 10^{12}\, M_\odot$; the remaining shortfall there is believed to be in a Warm-Hot Intergalactic Medium (WHIM: Davé et al. 2001) and in cooler gas that has not yet accreted onto galaxies. Smaller galaxies are thought to miss progressively more baryons because they were ejected by (e. g., supernova-driven) winds (Dekel & Silk 1986). Halos that are much more massive than $M_{\rm crit} \equiv M_{\rm DM} \sim 10^{12}\, M_\odot$ are missing progressively more stars because baryons are kept suspended in hot gas by a combination of AGN feedback and cosmological gas infall (see Section 8.4). The important point here is this: Because $M_\bullet \propto M_*^{(1.16\pm0.08)}$ and because the ratio of stellar mass M_* to dark mass $M_{\rm DM}$ is not monotonic, therefore the relationship between BH mass and DM mass is complicated and not monotonic. This suggests that BH growth is controlled by stellar mass, not DM mass.

More specifically, Behroozi et al. (2010) find that $M_* \propto M_{\rm DM}^{2.3}$ when $M_{\rm DM} \ll 10^{12}\,M_\odot$ and that $M_* \propto M_{\rm DM}^{0.29}$ when $M_{\rm DM} \gg 10^{12}\,M_\odot$. Broadly similar results are obtained in many papers, some included in the above summary (e. g., Yang et al. 2009, 2012; Moster et al. 2010; Guo et al. 2010; Leauthaud et al. 2012). The lowest DM mass in **Figure 25** at which the above correlation is well defined (the low-mass end of the 68-%-probability gray confidence band) corresponds to a baryonic mass of $M_* \approx 2 \times 10^8\ M_\odot$ and the highest DM mass corresponds to a baryonic mass of $M_* \approx 4 \times 10^{11}\ M_\odot$. That is, the multivalued correlation of $M_*/M_{\rm DM}$ with $M_{\rm DM}$ in **Figure 25** holds over almost the same mass range as the $M_\bullet - M_{\rm bulge}$ correlation in **Figure 18**. Substituting $M_{\rm bulge} \approx M_*$ and $M_\bullet \propto M_{\rm bulge}^{1.16}$ (Equation 10) in the above, we conclude that

$$M_\bullet \propto M_{\rm DM}^{2.7} \quad \text{at} \quad M_{\rm DM} \ll 10^{12}\,M_\odot \tag{18}$$

and that

$$M_\bullet \propto M_{\rm DM}^{0.34} \quad \text{at} \quad M_{\rm DM} \gg 10^{12}\,M_\odot\ , \tag{19}$$

with a kink in the correlation at $M_{\rm DM} \simeq 10^{11.8\pm0.5}\,M_\odot$.

Moreover, we think we understand why the $M_*/M_{\rm DM} - M_{\rm DM}$ correlation in **Figure 25** changes slope in the middle; the explanation (figure caption) involves BHs only very indirectly. Meanwhile, the $M_\bullet - M_{\rm bulge}$ correlation is log linear with small scatter from the lowest to the highest bulge masses in **Figure 18**. That correlation shows no kink at $M_{\rm DM} \sim 10^{12}\ M_\odot$. The simplicity of the $M_\bullet - M_{\rm bulge}$ correlation versus the complexity of the $M_\bullet - M_{\rm DM}$ correlation is another argument in favor of the hypothesis that BHs coevolve with bulges and ellipticals and not with DM halos.

6.10.3 Revised strategies for including BHs in semianalytic models of galaxy formation

are suggested by the above results. For studies that focus on the mass inventory of BHs and stars, it is reasonable to ignore or simplify the distinction between classical and pseudo bulges. A way to do the latter would be to decrease the $M_\bullet/M_{\rm bulge}$ ratio by factors of several at (say) $M_\bullet < 10^8\,M_\odot$. Small BHs and small (pseudo)bulges do not dominate either mass budget. At high BH masses, one simple strategy continues to be to use the $M_\bullet - \sigma$ correlation but with our revised slope and especially with the larger $M_\bullet$ zeropoint in Equation 7. The shortcoming of this approach is the observation that σ saturates at high BH masses, and these are not negligible to the mass budget. So a more attractive approach is to start with $M_{\rm DM}$ from a cosmological simulation, then use the Behroozi et al. (2010, 2012) or similar results (**Figure 25** here) to estimate the associate $M_{\rm bulge}$, and then use our $M_\bullet - M_{\rm bulge}$ relation (Equation 10, including cosmic scatter) to get the BH mass.

6.11 Do galaxies contain either BHs or nuclear star clusters and do these correlate in the same way with host galaxies?

Wehner & Harris (2006), Ferrarese et al. (2006), and Rossa et al. (2006) were the first to find that the masses $M_\bullet$ of BHs and the masses $M_{\rm nuc}$ of nuclei show similar-slope correlations with the masses of the bulge (in the case of BHs) or whole galaxy (in the case of Virgo spheroidals). Côté et al. (2006) showed explicitly that BHs and nuclei (collectively "central massive objects" or "CMOs'") have the same distributions of the ratio of their mass to the mass of the host galaxy, in agreement with the Wehner and Ferrarese papers. In contrast, Rossa et al. (2006) found a zeropoint offset betweeen nuclei and BHs corresponding to a typical mass ratio $M_\bullet/M_{\rm nuc} \simeq 0.30$. Ferrarese et al. (2006) further found that $M_\bullet$ and $M_{\rm nuc}$ both correlate with galaxy velocity dispersion; the slopes of the correlations are the same, but nuclei are 10 times more massive than BHs at a given σ. However, they found that CMO masses have a single, continuous correlation with the virial mass $M_{\rm gal} = 5 r_e \sigma^2/G$ (Cappellari et al. 2006) of the host. Finally, Graham & Driver (2007) found a continuous correlation between CMO mass and host Sérsic index. These papers propose that BHs and nuclei form by similar processes that favor BHs in large galaxies and nuclei in small ones.

Some papers suggest further that galaxies contain either a BH or a nucleus but generally not both. The change from high-mass BHs to lower-mass nuclei happens at a CMO mass of $\sim 10^{7.5}\ M_\odot$.

We partly agree and we partly disagree. AGNs in late-type, bulgeless galaxies show that BHs exist even at the absolute magnitudes of dwarf galaxies that usually have nuclei (Ho 2008; Section 7 here). Also, we observe nuclei in bulgeless galaxies at high luminosities at which BHs predominate when galaxies have bulges (e. g., M 101 and NGC 6946). Most importantly, many galaxies contain both nuclei and BHs. So BHs and nuclei are not almost mutually exclusive. In contrast, they routinely coexist. However, the more important point of the above papers is well supported by the data: BHs and nuclei do show some remarkable similarities in masses, as discussed in this section.

We begin by expanding on the coexistence of BHs and nuclei in similar (often the same) galaxies. AGN-based $M_\bullet$ measurements discussed in Section 7 and illustrated in **Figure 32** show that many late-type, bulgeless galaxies contain BHs with $M_\bullet \simeq 10^5\ M_\odot$ to at least $10^{6.5}\ M_\odot$. Their central velocity dispersions range from $\sigma \sim 30$ km s^{-1} to at least 100 km s^{-1}. These $M_\bullet$ and σ values overlap with galaxy nuclei, but they show little correlation between $M_\bullet$ and σ, consistent with the result that BHs do not correlate with pseudobulges or disks (Sections 6.8 and 6.9). Also, **Figure 24** includes nuclei in some of the most massive pure-disk galaxies (blue open circles from Kormendy et al. 2010); these objects overlap about half of the $V_{\rm circ}$ range of BH galaxies. Lauer et al. (2005) show that nuclei also exist in brighter ellipticals. Therefore there is no segregation of galaxies into giants that only contain BHs and dwarfs that only contain nuclei.

Our second point is that BHs and nuclei coexist in many galaxies, and the ratio of BH mass to nuclear mass varies widely from $\gg 1$ to $\ll 1$ (Seth et al. 2008; Graham & Spitler 2009; KFCB). The most robustly determined comparisons of BH and nuclear masses are summarized in **Table 4**, ordered by $M_\bullet/M_{\rm nuc}$. We include upper limits on $M_\bullet$ when they constrain our discussion.

Table 4 Masses of coexisting nuclear star clusters and supermassive black holes

Galaxy	D (Mpc)	$M_\bullet$ ($M_{\rm low}$, $M_{\rm high}$) ($M_\odot$)	$M_{\rm nuc}$ ($M_\odot$)	$M_\bullet/M_{\rm nuc}$	Ref.
(1)	(2)	(3)	(4)	(5)	(6)
NGC 4026	13.35	$1.80\ (1.45\text{-}2.40) \times 10^8$	1.44×10^7	12.4	1
NGC 3115	9.54	$8.97\ (6.20\text{-}9.54) \times 10^8$	$(1.04 \pm 0.29) \times 10^8$	$8.6^{+5.0}_{-2.9}$	2,3
M 31	0.774	$1.43\ (1.12\text{-}2.34) \times 10^8$	$(3.5 \pm 0.8) \times 10^7$	$4.1^{+2.6}_{-1.2}$	4,5,6
NGC 1023	10.81	$4.13\ (3.71\text{-}4.56) \times 10^7$	0.99×10^7	4.1	1
NGC 3384	11.49	$1.08\ (0.59\text{-}1.57) \times 10^7$	2.3×10^7	0.48	7
NGC 7457	12.53	$8.95\ (3.60\text{-}14.3) \times 10^6$	2.7×10^7	0.33	7
Galaxy	0.0083	$4.30\ (3.94\text{-}4.66) \times 10^6$	$(2.9 \pm 1.5) \times 10^7$	$0.15^{+0.075}_{-0.075}$	8
NGC 4395	4.3	$3.6\ (2.5\text{–}4.7) \times 10^5$	$(3.5 \pm 2.4) \times 10^6$	$0.10^{+0.077}_{-0.077}$	7,9
ω Cen	0.0048	$4.7\ (3.7\text{–}5.7) \times 10^4$	$(2.6 \pm 0.1) \times 10^6$	0.018 ± 0.004	10,11
NGC 205	0.82	$\lesssim 2.4 \times 10^4$	$(1.4 \pm 0.1) \times 10^6$	$\lesssim 0.017$	12,13
G1	0.77	$1.8\ (1.3\text{–}2.3) \times 10^4$	$(8 \pm 1) \times 10^6$	0.0023 ± 0.0007	14
M 33	0.82	$\lesssim 1540$	$(1.0 \pm 0.2) \times 10^6$	$\lesssim 0.0015$	15

Column 2 is the assumed distance (e. g., **Table 3**). Column 3 is the BH mass from **Tables 2** and **3** or from sources given in the text. Column 4 is the nuclear mass. Column 5 is the ratio of BH mass to nuclear mass. Column 6 lists the references for the nuclear mass: 1 = Lauer et al. (2005); 2 = Kormendy et al. (1996b); 3 = Emsellem, Dejonghe & Bacon (1999); 4 = Kormendy & Bender (1999); 5 = Kormendy (1988a); 6 = Bacon et al. (1994); 7 = Seth et al. (2008); 8 = Launhardt, Zylka & Mezger (2002); 9 = Filippenko & Ho (2003); 10 = van de Ven et al. (2006); 11 = Jalali et al. (2011); 12 = Jones et al. (1996); 13 = De Rijcke et al. (2006); 14 = Baumgardt et al. (2003); 15 = Kormendy & McClure (1993); Kormendy et al. (2010).

Curiously absent from most discussions of this subject are the nuclei of M 31 and NGC 3115. They are examples of galaxies in which the BH is substantially more massive than the nucleus.

In contrast, our Galaxy is a typical example of galaxies in which $M_\bullet < M_{\rm nuc}$. It contains a normal nucleus composed of a mixture of old and young stars. The mass determined by Launhardt, Zylka, & Mezger (2002) is $M_{\rm nuc} = (2.9 \pm 1.5) \times 10^7\ M_\odot$ (see also Schödel, Merritt & Eckart 2009, who emphasize uncertainties). This gives $M_\bullet/M_{\rm nuc} = 0.15 \pm 0.075$.

NGC 4395 has the smallest $M_\bullet$ determined from reverberation mapping (Peterson et al. 2005). The nuclear mass is uncertain; the value in **Table 4** is the mean of one obtained from the effective radius and velocity dispersion of the nuclear cluster (Filippenko & Ho 2003 corrected for $M_\bullet$) and a value obtained using a typical I-band mass-to-light ratio of 0.5 (Seth et al. 2008).

We treat the Galactic globular cluster ω Cen and the M 31 globular cluster G1 as defunct galactic nuclei (see Section 7.4). Then, for ω Cen, the BH mass is from Noyola et al. (2010; see also Noyola, Gebhardt & Bergmann 2008) and the cluster mass is from Jalali et al. (2011, see also van de Ven et al. 2006 and D'Souza & Rix 2013). For G1, the BH mass is from Gebhardt, Rich & Ho (2002, 2005) and the cluster mass is from Baumgardt et al. (2003). The BH-to-nuclear mass ratios of ω Cen and G1 are the smallest that have so far been measured: $M_\bullet/M_{\rm nuc} = 0.018 \pm 0.004$ and 0.0023 ± 0.0007, respectively.

Finally, two upper limits on BHs in bulgeless galaxies have a strong impact on our argument. They are $M_\bullet \lesssim 1500\ M_\odot$ in M 33 (Gebhardt et al. 2001; see also Merritt, Ferrarese & Joseph 2001) and $M_\bullet \lesssim 2.4 \times 10^4\ M_\odot$ in NGC 205. For M 33, $M_\bullet/M_{\rm nuc} \lesssim 0.00015$.

Therefore $M_\bullet/M_{\rm nuc}$ ranges over factors of > 5000. If ellipticals were included (Lauer et al. 2005), the biggest $M_\bullet/M_{\rm nuc}$ ratios would be even bigger. So BHs and nuclei are not always similar in mass.

On the other hand, the more important point raised by the Côté, Ferrarese, Wehner, and Graham papers is the hint that $M_\bullet$ and $M_{\rm nuc}$ are similarly related to properties of their host galaxies. We confirm this result. In fact, the relationship is even more intriguing than the above papers suggest:

Figure 26 (*top*) plots the ratio of the CMO mass to the mass of the host (pseudo)bulge against (pseudo)bulge mass. The BH mass fraction $M_\bullet/M_{\rm bulge}$ for classical bulges and ellipticals shows the small scatter and near-independence from $M_{\rm bulge}$ that we noted in Section 6.6.1. The Equation 11 relation, $M_\bullet/M_{\rm bulge} \propto M_{\rm bulge}^{0.14\pm0.08}$, is shown. In contrast, BHs in pseudobulges show the larger scatter that we found in Section 6.8. The remarkable new result in **Figure 26** (*top*) emerges when we include the nuclei that coexist with BHs in seven galaxies. Consistent with published work, they have $M_{\rm nuc}/M_{\rm bulge}$ in the same range as the BHs. The intriguing new result is that, with one exception (NGC 1023), when the BH mass is slightly high with respect to the scatter in **Figure 26** (*top*), the nuclear mass is slightly low, and vice versa. To put it another way, $(M_\bullet + M_{\rm nuc})/M_{\rm bulge}$ shows less scatter than do either BHs or nuclei by themselves. **Figure 26** (*top*) therefore hints that the building of nuclei and the growth of BHs are somehow related. We do not understand either growth well enough to speculate about what the relation might be.

Figure 26 (*bottom*) compares CMOs to the total mass of the host galaxy. We can therefore include nuclei in bulgeless galaxies (e. g., NGC 4395). The points for ellipticals do not change. The points for classical bulges move to slightly smaller BH-to-host-galaxy mass ratios. The pseudobulge BHs move the most from the top panel, because PB/T is generally small. The differences between BHs in bulges and BHs in pseudobulges are accentuated.

From Seth et al. (2008), **Figure 26** (*bottom*) shows $M_{\rm nuc}/M_{\rm gal}$ for nuclei in early-type galaxies (red crosses), late-type galaxies (blue plus signs), and spheroidal galaxies (light green triangles). Nuclei from Table 1 and from Kormendy et al. (2010: large blue plus signs) are included. Relative masses of nuclei are slightly larger in Sphs than in late-type galaxies, consistent with the idea that Sphs are defunct late-type galaxies that lost some of their baryons (Kormendy 1985, 1987;

KFCB; Kormendy & Bender 2012). Minus spheroidals, **Figure 26** (*bottom*) strengthens previous results (e. g., Rossa et al. 2006; Seth et al. 2008) that nuclei in early-type galaxies have larger mass fractions than nuclei in late-tpe galaxies. It further confirms that BHs and nuclei in early-type galaxies have similar, somewhat large mass fractions, with nuclei showing more scatter than BHs. Nuclei in high-mass, late-type galaxies havesmaller mass fractions, like BHs in pseudobulges, which also occur predominately in late-type galaxies. There is a hint that nuclear mass fractions for late-type galaxies decrease toward the right approximately as $M_{\rm gal}$ increases. That is, much of the decrease in $M_{\rm nuc}/M_{\rm gal}$ is due to the increase in $M_{\rm gal}$.

These again are hints that BHs and nuclei are related. In fact, nuclei in early-type galaxies look more closely related to BHs in early-tpe galaxies than they are to nuclei in late-type galaxies. Similarly, late-type galaxy BHs and nuclei look more closely related to each other than either are to their counterparts in early-type galaxies.

These results appear at least superficially consistent with the suggestion in Sections 8 that different feeding mechanisms grow large BHs in bulges + ellipticals and small BHs in galaxies with pseudobulges or no bulges. Evidently, this is also true of nuclei. Nuclei in early-type galaxies are older than nuclei in late-type galaxies. It is possible (K. C. Freeman, private communication) that their higher masses are a consequence of the general downsizing with decreasing formation redshifts of the masses of the galaxy components that are produced by nearly all processes of galaxy formation. This clearly includes BHs. It also seems inevitable, if the largest BHs grow as much as is inherent in the Sołtan (1982) argument, that they will swallow any nuclei that are present. That is, the largest BHs may include any relevant nuclear mass. Beyond this, we do not speculate about the physics that underlies the BH – nucleus relationship.

The rest of this section compares our conclusions with recent published results. Graham (2012) and Scott & Graham (2013) find, as did Ferrarese et al. (2006), that, at a given CMO mass, nuclei are associated with smaller central velocity dispersions than are BHs. They also find that nuclei have shallower correlations with host luminosity, σ, and stellar mass. And they find that $M_{\rm nuc}/M_{\rm gal}$ decreases with increasing $M_{\rm gal}$; we do, too, but the decrease that they see (Figure 3 in Scott & Graham 2013) is steeper than the one that we find. They conclude that "nuclear stellar clusters and [BHs] do not form a single family of CMOs". Leigh, Böker, & Knigge (2012) agree. Their fit $M_{\rm nuc} \propto M_{\rm bulge}^{1.18\pm0.16}$ gives a mean $M_{\rm nuc}/M_{\rm bulge} \simeq 0.0023$ at $M_{\rm bulge} \simeq 10^{9.7}\ M_\odot$, roughly similar to the results in Scott & Graham (2013) and also to those in **Figure 26**. Like Graham and Scott, they conclude that nuclei and BHs "do not share a common origin". We do not necessarily disagree. However, we cannot easily interpret the above and many other papers on galactic nuclear star clusters in the context of the picture of galaxy structure and evolution that we advocate in this paper for the following reasons. (1) Most papers treat Sph galaxies as faint ellipticals (e. g., Ferrarese et al. 2006; Côté et al. 2006; Turner et al. 2012). We argue that elliptical and Sph galaxies are unrelated, so the relevant comparison in **Figure 26** is not between green triangles and red crosses. Rather, Sphs are transformed dwarf spiral and irregular galaxies, so the relevant comparison (discussed above) is between green triangles and blue crosses. (2) The above papers treat all central extra light above the inward extrapolation of an outer Sérsic function fit as nuclei. In contrast, Hopkins et al. (2009b, see Figure 45) show that extra light in low-luminosity ellipticals and nuclei in Sph and disk galaxies are physically different. We agree with Turner et al. (2012) that (faint) nuclei and (brighter) extra light components form differently. But they have different parameter correlations, and confusing them creates mixed correlations that are difficult to interpret. Finally, (3) the above papers do not differentiate between classical bulges and pseudobulges, both of which can contain nuclei. So they do not find the ▲+● or the ×●● continuities, nor do they see the difference between the ▲+● correlation and the much flatter ×●● correlation in **Figure 26**.

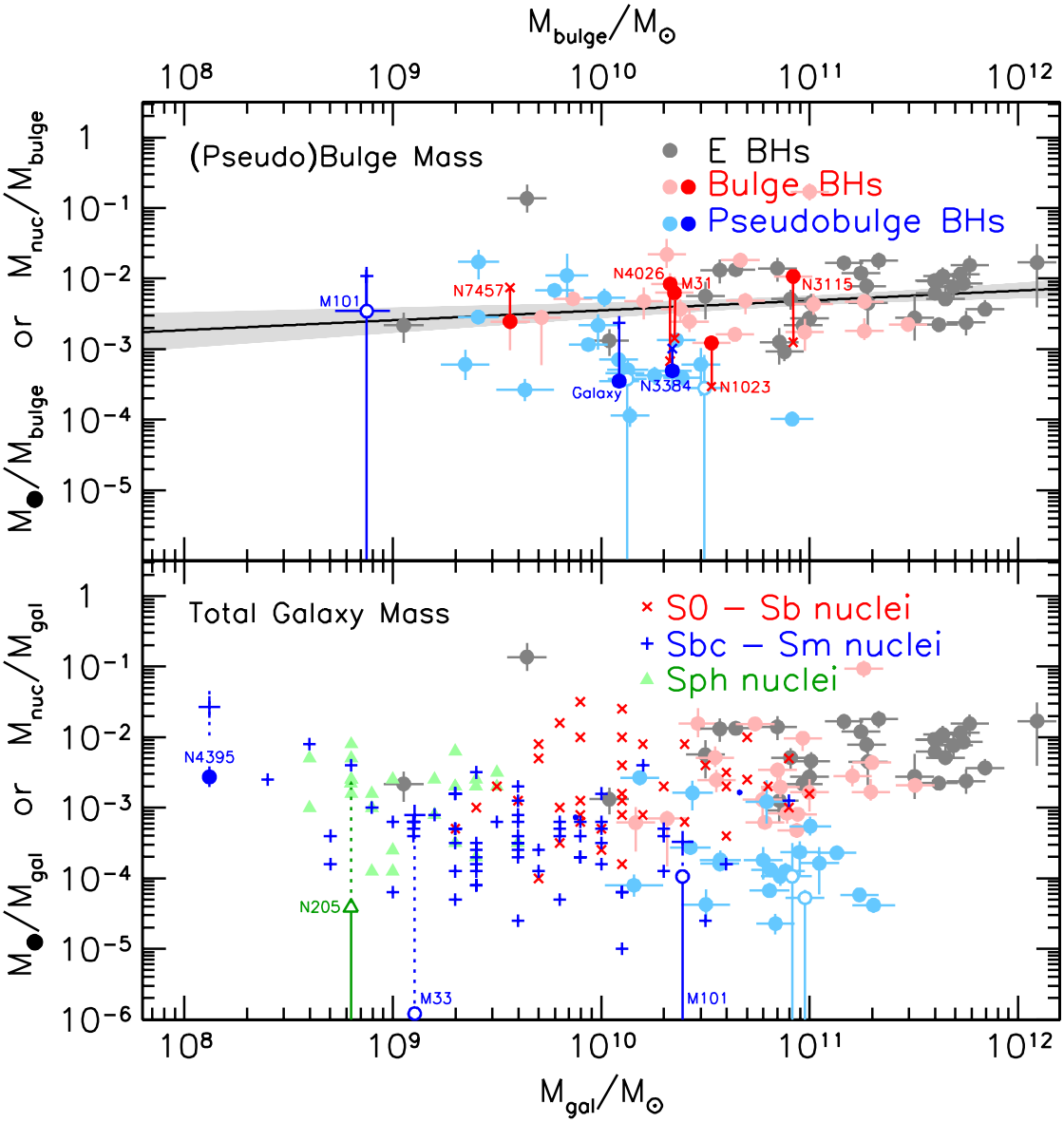

Figure 26

(*top*) Ratio of CMO mass ($M_\bullet$ or the mass $M_{\rm nuc}$ of the nuclear star cluster) to the mass $M_{\rm bulge}$ of the host (pseudo)bulge or elliptical galaxy plotted against $M_{\rm bulge}$. The black line with gray-shaded 1-sigma error is the least-squares fit to the classical bulges and ellipticals (Section 6.6.1, **Figure 18** and Equation 11). (*bottom*) Ratio of CMO mass to total host galaxy mass $M_{\rm gal}$ plotted against $M_{\rm gal}$. In both panels, filled circles denote galaxies with BH mass measurements (see the key). Open symbols denote galaxies with $M_\bullet$ upper limits. When BHs and nuclei coexist, the points for $M_\bullet$ and $M_{\rm nuc}$ are joined by a vertical line and the name of the galaxy is given. In the upper panel, NGC 3384 is an S0 with a pseudobulge, so $M_\bullet$ is plotted in blue; $M_{\rm nuc}/M_{\rm bulge}$ is also plotted blue for clarity. In the lower panel, crosses, plus signs, and filled light-green triangles denote nuclei in early- and late-type spirals and Sphs, respectively, all from Seth et al. (2008).

6.12 BHs correlate with globular cluster systems in bulges and ellipticals

Burkert & Tremaine (2010) discovered that BH masses correlate with the total numbers $N_{\rm GC}$ of globular clusters in galaxies. This was startling, because it connects the most compact objects at galaxy centers with one of the outermost galaxy components. The sample contained only 13 galaxies. But the rms scatter in $M_\bullet$ was remarkably small, only 0.2 dex. That is, the $M_\bullet - N_{\rm GC}$ correlation looks tighter than the $M_\bullet - \sigma$ correlation. To a good approximation, the total mass in globular clusters is the same as the mass in the central BH.

Harris & Harris (2011) confirmed these results for 33 galaxies. They, too, found that $N_{\rm GC} \propto M_\bullet$, with a cosmic scatter (in addition to measurement uncertainties) of 0.2 dex in either parameter. They got this result for ellipticals. Three spirals agree with it; one (our Galaxy) deviates, and S0s by themselves show no correlation. Our Galaxy, NGC 4382, NGC 5128, and NGC 7457 all deviate from the main trend in having BHs that are at least a factor of 10 undermassive. For the galaxies that satisfy the $M_{\rm GC} - M_\bullet$ correlation, $M_\bullet \simeq 1.5$ times the total mass of globulars.

Figure 27 (*left*) updates the Harris & Harris (2011) sample with $M_\bullet$ from **Tables 2** and **3**. **Figure 27** (*right*) shows $N_{\rm GC}$ versus galaxy velocity dispersion for BH hosts in **Tables 2** and **3** and for other galaxies with published globular cluster counts. Correcting several host-galaxy morphological types allows us to understand the puzzling results in the Harris & Harris paper in the context of other results presented in this paper.

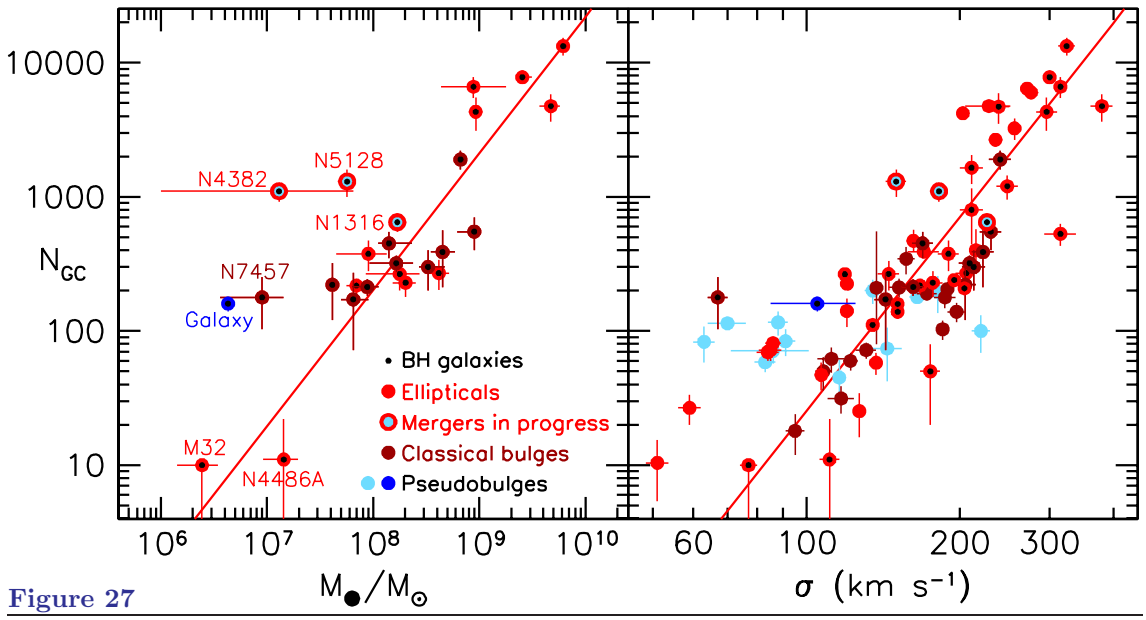

Figure 27

Correlation of the total number of globular clusters with (*left*) dynamically measured BH mass and (*right*) the velocity dispersion of the (pseudo)bulge or elliptical host. Galaxy types are given in the key. The left panel omits galaxies with reliable BH detections but uncertain BH masses (turquoise lines in **Tables 2** and **3**); these are included in the right panel. The right panel also shows additional galaxies with $N_{\rm GC}$ values from Peng et al. (2008), Spitler et al. (2008), Harris & Harris (2011), and Cho et al. (2012) that have velocity dispersions tabulated in Ho et al. (2009) or in Hyperleda. The lines are symmetrical least-squares fits to the classical bulges and ellipticals omitting mergers in progress, points that involve limits, and NGC 7457. We confirm that classical bulges and ellipticals show the same correlation between $N_{\rm GC}$ and BH mass or its proxy σ, whereas pseudobulges show little correlation. Pseudobulges and mergers in progress frequently contain undermassive BHs.

Elliptical galaxies and classical bulges satisfy the same linear correlations in both panels. The left panel is similar to the $M_\bullet - N_{\rm GC}$ correlations shown by Burkert & Tremaine (2010) and by Harris & Harris (2011), and the right panel is similar the $N_{\rm GC} - \sigma$ correlation shown by Snyder, Hopkins & Hernquist (2011). However, outliers are easier to interpret here.

In the left panel of **Figure 27**, a symmetric least-squares fit to the classical bulges and ellipticals omitting mergers in progress, points that involve limits, and NGC 7457 gives

$$\log\left(\frac{N_{\rm GC}}{500}\right) = (1.017 \pm 0.132)\ \log\left(\frac{M_\bullet}{10^8\ M_\odot}\right) - (0.393 \pm 0.106), \tag{20}$$

similar to the results in the Burkert and Harris papers. Harris finds that there are ~ 250 globulars per $10^8\ M_\odot$ of BH mass; we find 202^{+56}_{-44}.

The total rms scatter of all points with respect to the fit is 0.32 in both $\log N_{\rm GC}$ and $\log M_\bullet$. Ellipticals alone have an rms scatter of 0.34 dex in $\log N_{\rm GC}$. Ellipticals and spirals together have a scatter of 0.30 dex, whereas S0s have a scatter of 0.36 dex. These differences are not significant.

In constructing the above fit, we do not use the individual parameter errors but rather assume that all galaxies have the mean estimated error of ± 0.12 in $\log M_\bullet$ and ± 0.11 in $\log N_{\rm GC}$. If we assume that the intrinsic scatter is the same in both parameters, then that intrinsic scatter is $\epsilon(\log M_\bullet) = \epsilon(\log N_{\rm GC}) = 0.20$.

In the right panel of **Figure 27**, a symmetric least-squares fit, again omitting pseudobulges, mergers in progress, points that involve limits, and NGC 7457 gives

$$\log\left(\frac{N_{\rm GC}}{500}\right) = (4.80 \pm 0.39)\ \log\left(\frac{\sigma}{200\ {\rm km\ s^{-1}}}\right) + (0.150 \pm 0.064), \tag{21}$$

similar to the results in Snyder et al. (2011). The rms scatter for all points with respect to the above fit is 0.45 in $\log N_{\rm GC}$ and 0.095 in $\log \sigma$. The ellipticals alone have an rms scatter of 0.49 dex in $\log N_{\rm GC}$, and the classical bulges have a scatter of 0.29 dex. S0s do not have larger scatter than other galaxy types. In the above, we again do not use the individual parameter errors but rather assume that all galaxies have the mean estimated error of ± 0.019 in $\log \sigma$ and ± 0.10 in $\log N_{\rm GC}$. If we assume that the intrinsic scatter is the same in both parameters, then that intrinsic scatter is $\epsilon(\log \sigma) = \epsilon(\log N_{\rm GC}) = 0.089$.

Pseudobulges and mergers in progress deviate from the above correlations:

In Harris & Harris (2011), the deviant elliptical is NGC 5128 (Cen A). However, this is a merger in progress; i. e., an elliptical in formation. One deviant "S0" in the Harris paper is NGC 4382. KFCB show that this is also a merger in progress. An additional "S0", NGC 1316, is reclassified in **Figure 27** as a merger. The three mergers in progress behave the same way in **Figure 27** as they do in the $M_\bullet - M_{\rm K,bulge}$ and $M_\bullet - M_\sigma$ correlations in **Figure 14** (Section 6.4). They deviate from the correlations for ellipticals and classical bulges in the sense that $M_\bullet$ is unusually low for the galaxy K-band luminosity and for the number of globular clusters. The latter deviation confirms what we concluded in Section 6.4: the deviation there is not due to any temporary enhancement of the luminosity due to merger-induced star formation. The K-band luminosity is insensitive to modest amounts of star formation, and the main stellar populations of the mergers in progress are in any case old. The globular cluster systems are also old, and NGC 4382 and NGC 5128 have $\gtrsim 10$ times more globular clusters than "normal" for their BH masses. Even NGC 1316 lies near the top of the scatter in **Figure 27**. As in Section 6.4, we conclude that the BH masses are unusually low in these mergers in progress. The correlation with σ is more normal, as it was in **Figure 14**. All in all, **Figure 27** provides compelling independent corroboration for the BH results found in Section 6.4 for mergers in progress. Of course, the sample is very small. The importance of further BH and globular cluster measurements in ongoing mergers is correspondingly high.

In Harris & Harris (2011), NGC 7457 is the other S0 and our Galaxy is the spiral that deviates from the $N_{\rm GC}-M_\bullet$ correlation by having very small $M_\bullet$. But our Galaxy contains a boxy pseudobulge (Weiland et al. 1994; Dwek et al. 1995), now understood to be an almost-end-on bar (Combes & Sanders 1981; Blitz & Spergel 1991; see Kormendy & Kennicutt 2004 for a review). There is no photometric or kinematic sign of a merger-built classical bulge (Freeman 2008; Howard et al. 2009; Shen et al. 2010). It is therefore plotted in blue in **Figure 27**. For NGC 7457, bulge classification criteria provide "mixed signals" – the relatively round shape, high Sérsic index, and moderate rotation ($V/\sigma^* \simeq 1$, Kormendy et al. 2011) led us to classify the bulge as classical in **Table 3**, but its remarkably low velocity dispersion of $\sigma = 67 \pm 3$ km s^{-1} has long suggested that it is pseudo (Kormendy 1993b). We know that classical and pseudo bulges coexist in some galaxies. This may be one of them, and NGC 7457 may deviate from the **Figure 27** correlations for this reason. We know that pseudobulge properties correlate little with $M_\bullet$ and particularly that some pseudobulges contain smaller BHs than do classical bulges. This is how our Galaxy and NGC 7457 deviate in **Figure 27**. Burkert & Tremaine (2010) already note this result for our Galaxy. For NGC 7457, the unusually small σ in the right panel suggests that our classification in **Table 3** may be wrong and that the pseudobulge may be dominant. Classifying mixed cases is difficult.

In the right panel of **Figure 27**, pseudobulges are plotted in light blue. Bulges from Peng et al. (2008) and Spitler et al. (2008) are classified in Kormendy & Bender (2011) or here. The classical bulges form part of the correlation discussed above. Overall, the pseudobulges here are consistent with results from previous sections: they do not show the same correlations as classical bulges. However, it is still possible that the scatter in **Figure 27** (*right*) just increases toward lower $N_{\rm GC}$ and σ. More measurements would be welcome.

For completeness, we note that six Harris & Harris (2011) galaxies are omitted in **Figure 27**. NGC 4552, NGC 4621, NGC 5813, and NGC 5846 had BH masses from Graham (2008b) that were read from an unlabeled plot in Cappellari et al. (2008); see our discussion in Section 5.1. They agree with the **Figure 27** correlations. The NGC 4350 BH mass is based on observations with low spatial resolution (Section 6.5). And NGC 4486B is one of the "monsters" that deviate toward high $M_\bullet$ (Section 6.5). By and large, BHs that deviate from the correlations described in earlier sections also deviate in the same way here.

Returning to the main result of this section, what does the tight $M_\bullet - N_{\rm GC}$ correlation for bulges and ellipticals tell us about galaxy formation? The formation of globular cluster systems is an large subject with a long history (see Harris 1991 and Brodie & Strader 2006 for reviews). We confine ourselves to a few remarks:

Based on their conclusion that the $M_\bullet$ correlates more tightly with globular clusters than with σ, Burkert & Tremaine (2010) suggest that major mergers may provide the connection between the smallest and largest scales in galaxies. They suggest that the most rapid BH growth may happen in the most dissipative mergers that manufacture the most globular clusters (Ashman & Zepf 1992; Zepf & Ashman 1993). That suggestion is not invalidated by our results on mergers in progress, because mergers at low redshifts are almost certainly poorer in gas than mergers at high redshifts. We suggested in Section 6.4 that these mergers convert disk mass that does not correlate with $M_\bullet$ into bulge mass with relatively little new star formation; the resulting $M_\bullet$ is smaller than normal. Our mergers are not ultraluminous infrared galaxies; they are among the gas-poorest ones at low z. We do not expect much late formation of globular clusters. Even at $z \sim 1$, our understanding of cores requires that the most recent mergers that made the biggest elliptical galaxies were dry (Section 6.13). Any correlations between $M_\bullet$, σ, and $N_{\rm GC}$ likely were put in place very early. Late BH growth by "maintenance-mode accretion" from hot gas in clusters (Section 8.4) is unlikely to increase $M_\bullet$ by much, and it is unlikely to form globular clusters (Côté et al. 2001).

Harris & Harris (2011) note that most globulars have ages of ~ 10 to 13 Gyr, corresponding to redshifts $z \simeq 2$ to 7. They suggest that "$N_{\rm GC}$ and $M_\bullet$ should be closely correlated simply because they are both byproducts of similarly extreme conditions in high-density locations during the main period of galaxy formation" (cf. the Burkert & Tremaine 2010 picture). Both they and Burkert & Tremaine (2010) point out that the present similarity in the masses of BHs and globular cluster systems is a coincidence, because BHs have been growing and globular cluster systems have been suffering attrition for many billions of years.

Snyder et al. (2011) also argue that the tight $M_\bullet - N_{\rm GC}$ correlation does not imply any direct connection between globular clusters and BHs. Rather, they argue that $M_\bullet$ and $N_{\rm GC}$ both correlate primarily with galaxy binding energy $\propto M_* \sigma^2$, where M_* is the stellar mass of the galaxy. The $M_\bullet - M_* \sigma^2$ correlation is called the "black hole fundamental plane" (Hopkins et al. 2007a, b; Aller & Richstone 2007; Section 6.14 here). Rhode (2012) is another study of correlations between $M_\bullet$, $N_{\rm GC}$, and other host galaxy properties based on a sample that mostly overlaps with the above studies and with ours. She, too, concludes that BH masses and numbers of globular clusters are not directly linked but are correlated because both depend on the depths of galaxy potential wells.

It is well known that globular cluster systems are bimodal in color and metallicity. A metal-rich, red population is relatively concentrated to galaxy centers, whereas a metal-poor, blue population forms a radially more extended cloud; the red globulars are more nearly coeval with the main galaxy, whereas the blue globulars likely predate the main galaxy (e. g, Forbes, Brodie & Grillmair 1997; Larsen et al. 2001; Peng et al. 2006c; Harris et al. 2006; Strader et al. 2006; see Brodie & Strader 2006 for a review). It is important to emphasize: We do not yet know whether $M_\bullet$ correlates best with the red globulars, the blue globulars, or their sum. It will be important to make this test. But as Burkert & Tremaine (2010) note, this will be difficult, because the relative numbers of red and blue clusters do not vary by much from galaxy to galaxy.

Sadoun & Colin (2012) take a first step in this direction by showing that the correlation between $M_\bullet$ and the velocity dispersions of globular cluster systems (not the numbers of globular clusters) is tighter for red than for blue globular clusters. This is perhaps not surprising, because red globular cluster systems are more closely associated with the main bodies of their hosts and we already know that $M_\bullet$ correlates tightly with the velocity dispersions of those hosts. Nevertheless, it seems reasonable to suggest that, if larger samples that include cluster counts and perhaps other parameters confirm that BHs correlate best with red globulars, then this points to coevolution processes such as mergers and the origin of the BH fundamental plane. In contrast, if BHs correlate best with blue globular clusters, then this points to unknown initial conditions in the environments that later turn into giant ellipticals. E. g., M 87 now has one of the highest numbers of globular clusters and one of the highest BH masses. But we know almost nothing about the (probably many) progenitor pieces in which its stars were formed, and we know still less about the (probably earlier) times when its blue globular clusters formed. For further discussion, see, e. g., Ashman & Zepf (1992), Forbes, Brodie & Grillmair (1997), Kundu et al. (1999), Brodie & Strader (2006), Hopkins et al. (2007a, b), and Yoon et al. (2011).

6.13 BHs correlate with the "missing light" that defines galaxy cores

BHs modify the structures of their host galaxies out to several times the sphere-of-influence radius $r_{\rm infl} = GM_\bullet/\sigma^2$ inside which they dominate the gravitational potential. E. g., many stars which visit $r < r_{\rm infl}$ live on orbits that take them out to radii $r > r_{\rm infl}$ where they spend most of their time. Scattering off of the BH results in gradual changes to the orbital structure, a slow evolution that we do not have space to discuss (see Merritt 1999 for a review). More relevant here is this: We expect that galaxy mergers generally result in BH binaries, and their interactions with host galaxies have observable consequences. This *local* BH – galaxy coevolution driven by gravity is different from the *global* coevolution driven by AGN energy feedback that is the subject of Section 8. Local evolution driven by BH binaries provides a natural explanation – albeit one that is difficult to prove – of an almost ubiquitous feature of giant elliptical galaxies, namely galaxy cores.

The term "core" has a specific meaning, different from its colloquial use to refer to a galaxy center. It is illustrated in **Figure 28**. Observations over many years have shown that surface brightness profiles $I(r)$ of elliptical galaxies are well described by Sérsic (1968) functions $\log I(r) \propto r^{1/n}$, where $n \simeq 2$ to 12 is the "Sérsic index" (see KFCB for a review). For historical reasons (early data suggested that $n = 4$; de Vaucouleurs 1948), it is convenient to plot profiles against $r^{1/4}$; then profiles that are concave-up have $n > 4$ and profiles that are concave-down have $n < 4$. **Figure 28** shows that an $n = 6$ Sérsic function fits NGC 4472, the brightest elliptical in the Virgo cluster and one of our BH galaxies, over a range of a factor of more than 200 in radius and 6000 in surface brightness. Then, at small radii, $I(r)$ breaks downward from the inward extrapolation of the outer Sérsic profile. This region of lower surface brightness where $I(r)$ is a shallow power-law cusp is called the core. In contrast, the smaller BH elliptical NGC 4459 shows an inner break in the opposite direction; instead of a core, it has extra light at small radii with respect to the outer $n = 3.2$ Sérsic profile.

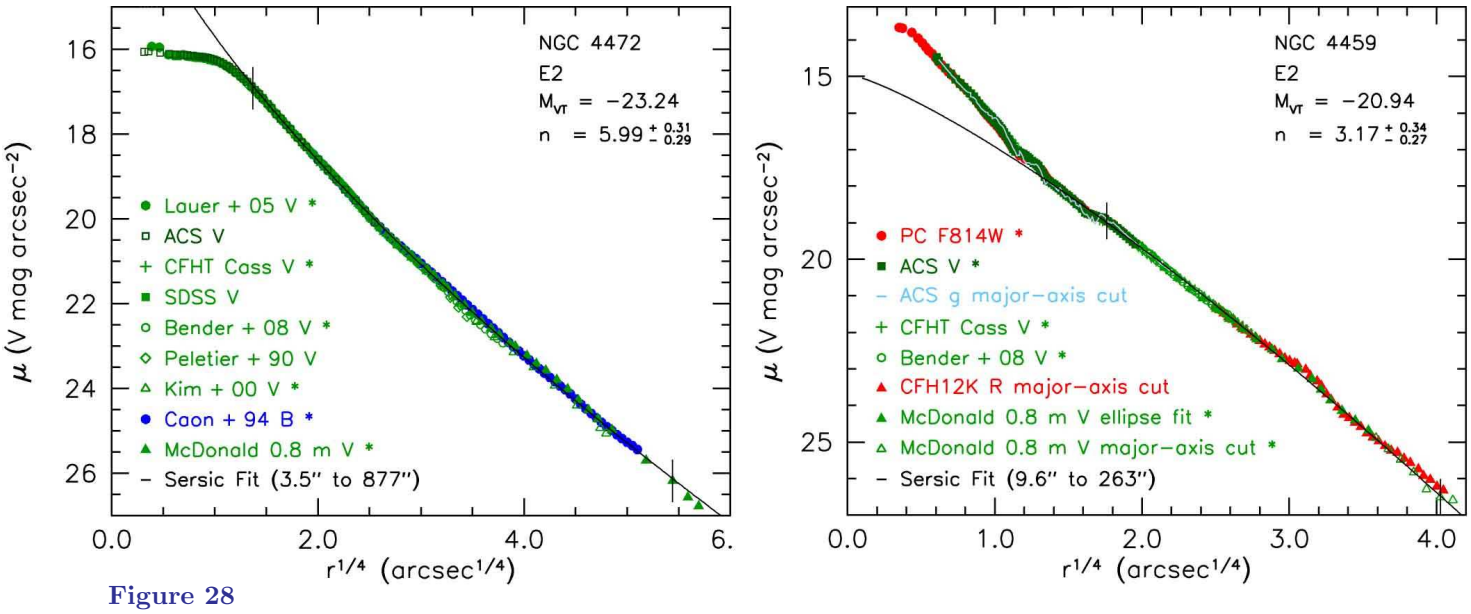

Figure 28

Observed V-band ($\sim$5500 Å) surface brightness profiles of (*left*) NGC 4472, a prototypical giant elliptical with a core, and (*right*) NGC 4459, a lower-luminosity elliptical with no core but instead with extra light at small radii above the inward extrapolation of the outer brightness profile. The photometry is from KFCB. References to data sources are in the key.

Section 6.7 introduced the difference between ellipticals with cores and ones with extra light as part of an "E – E dichotomy" that also involves dynamical properties (slow versus fast rotation), the presence or absence of X-ray-emitting gas, and the presence or absence of AGNs. The change from extra light to core happens in the Virgo cluster at an absolute magnitude of $M_V \simeq -21.5$, a luminosity of $\sim 3 \times 10^{10}\, L_{V\odot}$, a stellar mass of $\sim 2 \times 10^{11}\, M_\odot$, and a dark matter mass of $\sim 5 \times 10^{12}\, M_\odot$ (**Figure 25**). KFCB review these observations and suggest that the most recent mergers that formed core ellipticals were "dry" (no cold gas and no significant star formation), whereas the most recent mergers that formed extra-light ellipticals were "wet" (cold gas dissipation fed a starburst that built the extra-light component). The idea is not new; e. g., Faber et al. (1997) already suggested it as the explanation for the difference between core and coreless ellipticals. Sections 8.4 and 8.6 discuss the E – E dichotomy in the context of BH–host-galaxy coevolution.

Core formation is hard to understand in our standard picture in which ellipticals form by major galaxy mergers, i. e., ones in which the progenitors were equal in mass to within a factor of a few. **Figure 29** shows why. The surface brightness of the extra-light elliptical NGC 4459 is fainter than that of NGC 4472 at most radii, but it is brighter than NGC 4472 inside the latter's core. Absent BHs, dry mergers preserve the highest densities in the progenitor galaxies (Kormendy 1984; Barnes 1992; Barnes & Hernquist 1992; Holley-Bockelmann & Richstone 1999, 2000; Merritt & Cruz 2001; Boylan-Kolchin, Ma & Quataert 2004, 2005; Hopkins et al. 2009a, b). NGC 4472 is so bright that the only plausible progenitors are smaller ellipticals like NGC 4459. How do progenitors with dense centers merge to form remnant ellipticals with fluffy centers (Faber et al. 1997)?

The suggested solution is this: Cores may be scoured by the orbital decay of BH binaries that form in galaxy mergers (Begelman, Blandford & Rees 1980; Ebisuzaki, Makino & Okamura 1991; Makino & Ebisuzaki 1996; Quinlan & Hernquist 1997; Faber et al. 1997; Milosavljević & Merritt 2001; Milosavljević et al. 2002; Merritt 2006). When the BHs are far apart, they decay separately by dynamical friction. When they get close together, they form a binary, and then the tendency toward energy equipartition between light and heavy particles drives the very generic result that the BH binary decays by flinging stars away (Szebehely & Peters 1967 show a beautiful example).

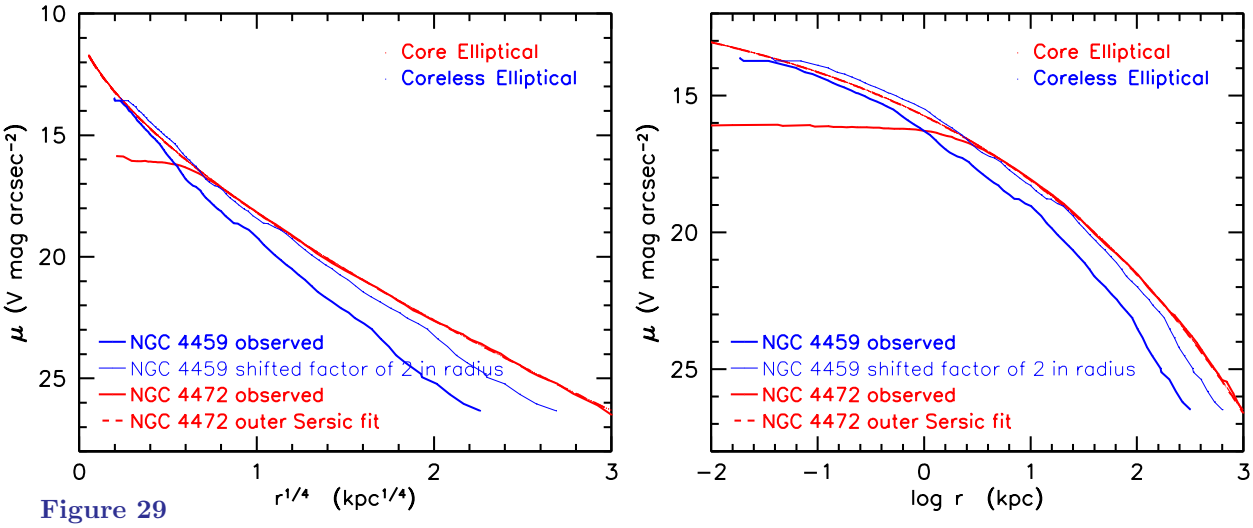

Figure 29

Major-axis brightness profiles of NGC 4472 and NGC 4459 corrected for Galactic absorption and plotted against $r^{1/4}$ (*left*) and $\log r$ (*right*). In each panel, the thin blue line is the observed profile of NGC 4459 shifted to larger radii by a factor of 2. Near the center, this shifted profile is similar to the inward extrapolation of the outer Sérsic fit to the core elliptical NGC 4472 (*red dashed line*).

This decreases the surface brightness and excavates a core. The effect of a series of mergers should be cumulative; if the mass deficit after one merger is $fM_\bullet$, then the mass deficit after N mergers should be $\sim NfM_\bullet$. The above papers predict that $f \sim 0.5$ to 2. Observations of mass deficits $M_{\rm def}$ are consistent with this picture; $M_{\rm def} \propto M_\bullet$ and $Nf \sim 1-5$, consistent with formation by several dry mergers (e. g., Milosavljević & Merritt 2001; Milosavljević et al. 2002; Ravindranath, Ho & Filippenko 2002; Graham 2004; Ferrarese et al. 2006; Merritt 2006; Hopkins & Hernquist 2010).

As an explanation of cores, scouring by binary BHs is "the only game in town". Still, how can we be sure that any mass is missing? How can we know what the density profile would be in the absence of any proposed mechanism such as core scouring? Differences between different authors' estimates of mass deficits result mainly from different assumptions about this unmodified profile.

Following Kormendy & Bender (2009), we argue here that the best way to calculate $M_{\rm def}$ is by comparing the observed core profile with the inward extrapolation of a Sérsic function fitted to the profile at larger radii (Graham 2004; Ferrarese et al. 2006; KFCB; Kormendy & Bender 2009). The arguments for calculating $M_{\rm def}$ in this way are:

1. Some authors assume that the central profile before scouring was an inward extrappolation of a power law fitted just outside the core. **Figure 29** (*right*) shows why this is not ideal. Plotted against $\log r$, the outer profile is curved at all radii. Over large radius ranges, elliptical galaxy profiles are not power laws. Picking a small radius range near the center in which to fit a power law requires a choice that is essentially arbitrary. The figure also shows that a power-law extrapolation lies above the Sérsic extrapolation at all r. It is therefore a less conservative choice than a Sérsic extrapolation.
2. We can, in fact, know something about merger progenitors. Core ellipticals are more luminous than any other galaxies in the nearby universe. NGC 4472 is ~ 8 times more luminous than NGC 4459. Faber et al. (2007) and KFCB argue that core galaxies form by major mergers that are dry because they are so massive that even their progenitors generally have DM masses $M_{\rm DM} \gtrsim M_{\rm crit} \simeq 10^{12}\ M_\odot$ large enough to retain X-ray-emitting gas that heats any cold gas and prevents star formation ($M_{\rm crit}$ quenching). Further evidence for dry mergers is discussed in Sections 6.7.2 and 8.4. And mergers with mass ratios that are not too different from 1:1 are preferred in order to life enough stars to explain observed cores (Merritt 2006). Then, over a large range in luminosity and mass, the only plausible present-day progenitors whose mergers could produce the global properties of core ellipticals are slightly fainter ellipticals and disk galaxies with large bulges. Coreless ellipticals are like NGC 4459: their profiles have extra light near the center with respect to the inward extrapolation of outer Sérsic profiles. It is conceivable that the progenitors of core ellipticals were nothing like any galaxy now in the universe. If so, it would be necessary to use them all up. This seems unlikely. So NGC 4459 is representative of known galaxies that could plausible merge to make core ellipticals.
3. **Figure 29** shows that, over the radius range of the core of NGC 4472, the profile of NGC 4459 is similar to the inward extrapolation of the outer Sérsic fit to NGC 4472. In addition:
4. The profile of a dry-merger remnant is similar to that of the (say: equal-mass) progenitors, with little change in density but a shift of the profile to larger radii (Hopkins et al. 2009c). **Figure 29** includes the profile of NGC 4459 shifted outward in radius by a factor of 2 (a fourfold increase in luminosity). Except at large r, this resembles the profile of NGC 4472, including the inward extrapolation of the outer Sérsic fit. So numerical simulations support our assumption that remergers of realistic progenitors produce remnant profiles such that we can estimate the missing light that defines cores by comparing observed profiles (we assume: after BH scouring) with the inward extrapolation of Sérsic functions fitted to the outer profiles.

5a. More specifically, n-body simulations show that the remnants of dry major mergers – that is, remnants of mergers of two, approximately equal-mass galaxies – are approximately Sérsic at all radii that are not compromised by resolution effects (e. g., Hopkins et al. 2009b).

5b. Moreover, simulations of wet mergers (Mihos & Hernquist 1994; Hopkins et al. 2009a) produce remnants that closely resemble extra-light ellipticals, with a Sérsic outer component that is the product of violent relaxation of the pre-existing stars and a separate, dense central component that is the result of the starburst. This has been emphasized by Kormendy (1999), Côté et al. (2007), Hopkins et al. (2009a), and KFCB.

Thus, within our picture of the merger formation of ellipticals, it is reasonable to expect that the near-central profile of a giant elliptical would not show a core. Rather, the central profile should be a steep continuation of the outer profile if it formed by violent relaxation in dry mergers and in the absence of BHs. This is the motivation behind our procedure to estimate $L_{\rm def}$.

Hopkins & Hernquist (2010) suggest a nonparametric way to estimate $L_{\rm def}$ that is is similar in spirit to what we do. They use lower-mass galaxies that are plausible $z \simeq 0$ progenitors to provide template profiles against which to measure missing light (not) in the cores of higher-mass ellipticals. We prefer our approach, because it relies on the robustness (KFCB) of Sérsic fits over large dynamic ranges in the core galaxies under study. Using template profiles is inherently more uncertain, (1) because relatively few profiles get averaged into the templates, as Hokpkins & Hernquist emphasize, and (2) because progenitors at high z may differ from those at low z. So we use low-z galaxies as a guide in our argument, but we depend on well determined Sérsic fits to the actual galaxies under study to make what is, after all, a tricky differential measurement of $L_{\rm def}$. Nevertheless, the Hopkins & Hernquist (2010) approach should give results that are similar to ours, and it does so.

Using the above prescription, KFCB and Kormendy & Bender (2009) measure central light and mass excesses and deficits as illustrated in **Figure 30**. BH masses for core galaxies are updated to include DM in the dynamical models. We confirm previous results (Milosavljević & Merritt 2001; Milosavljević et al. 2002; Ravindranath, Ho & Filippenko 2002; Graham 2004; Ferrarese et al. 2006; Merritt 2006) that $M_{\rm def} \propto M_\bullet$. Averaging in the log, $<M_{\rm def}/M_\bullet> = 4.1^{+0.8}_{-0.7}$. Our $M_{\rm def}$ measures are larger than previous published values. However, BH masses are revised upward also (**Table 2**). As a result, the ratio $<M_{\rm def}/M_\bullet>$ is in the range given by previous papers.

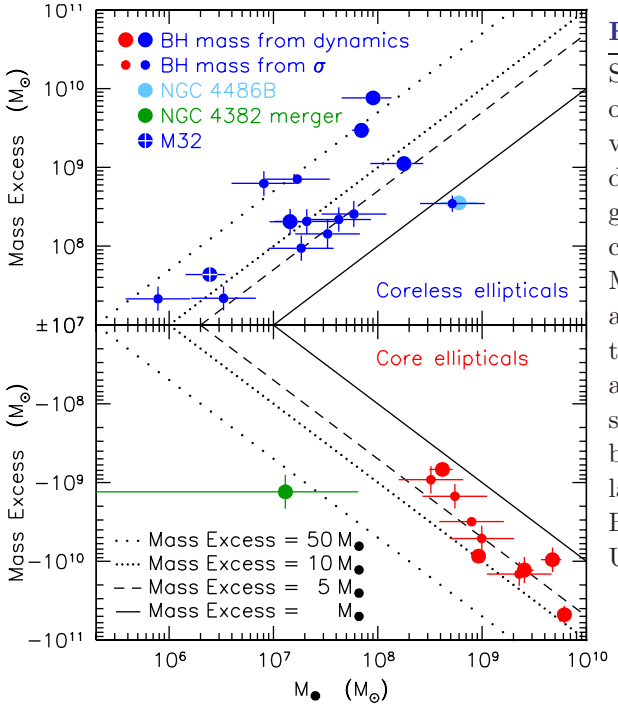

Figure 30

Stellar mass "missing" in cores (*lower panel*) or "extra" in coreless galaxies (*upper panel*) vs. BH mass. Large symbols are for galaxies with dynamical $M_\bullet$ measurements; small ones use $M_\bullet$ given by the $M_\bullet - \sigma$ relation. Core mass deficits correlate tightly with BH mass: $M_{\rm def} \simeq 4\,M_\bullet$. Mass excesses tend to be larger than mass deficits and to show more scatter with $M_\bullet$. It is imporant to note that the merger in progress NGC 4382 has a normal core for its luminosity but deviates to small $M_{\rm def}/M_\bullet$. If cores are excavated by BH binaries, this suggests that the galaxy does not lack a big BH (or BH binary) but rather that this BH (or BH binary) is not resident at the center. Updated from Kormendy & Bender (2009).

The mean ratio $<M_{\rm def}/M_\bullet> = 4.1^{+0.8}_{-0.7}$ is larger than the Merritt (2006) prediction that $M_{\rm def}/M_\bullet \simeq 0.5$ per major merger. However, there are reasons to believe that $M_{\rm def}/M_\bullet$ can be larger than 0.5 per merger event. First, more accurate simulations of the late stages of BH mergers suggest that $M_{\rm def}/M_\bullet$ can be as large as ~ 4 per merger (Merritt, Mikkola & Szell 2007). Second, an additional process has been found that is likely to make large-$M_{\rm def}$ cores (Merritt et al. 2004; Boylan-Kolchin, Ma & Quataert 2004; Gualandris & Merritt 2008). Coalescing binary BHs emit gravitational radiation anisotropically and therefore recoil at velocities that are comparable to galaxy escape velocities. If they do not escape, they decay back to the center by dynamical friction. In the process, they further heat the core. Gualandris & Merritt (2008) estimate that they can excavate as much as $M_{\rm def}/M_\bullet \sim 5$ in addition to the mass that was already scoured by the pre-coalescence binary. **Figure 30** appears at least roughly consistent with the suggestion that cores are made by a combination of BH scouring mechanisms acting over the course of one or more successive dry mergers. Our picture of core formation by BH binary scouring is thereby strengthened.

In particular, Kormendy & Bender (2009) discuss two correlations that provide a "smoking gun" connection between BHs and cores. Their Figure 2 shows that observed BH mass fractions scatter substantially around their mean value (this mean has since been revised upward in our **Figure 18**). But the scatter is not random: it correlates tightly with the ratio of $L_{\rm def}$ to galaxy luminosity. Also, their Figure 4 shows that $L_{\rm def}$ (expressed as a magnitude) corrrelates tightly with σ, which we know is an $M_\bullet$ surrogate for elliptical galaxies. This correlation has the advantage that no dynamical modeling is involved. It is purely a correlation between observables. Both figures support the idea that BHs and cores are closely connected.

At the same time, **Figures 28 – 30** remind us that smaller ellipticals have extra, not missing, light near their centers. Why? KFCB emphasize that BHs are detected in extra-light ellipticals; examples in **Table 2** include M 32, NGC 3377, and NGC 4459. Extra-light ellipticals satisfy the $M_\bullet$ – σ correlation. We believe that they formed in mergers, and these mergers cannot all have involved only pure-disk, BH-less galaxies. Why did core scouring by BH binaries fail?

KFCB and Kormendy & Bender (2009) suggest that this is a consequence of the formation of extra-light galaxies in wet mergers. Like Kormendy (1999) and Côté et al. (2007), they suggest that the extra light was formed by the starburst that results naturally from the dissipation and central concentration of cold gas in a wet merger. This is universally seen in n-body simulations (e. g., Mihos & Hernquist 1994; Springel & Hernquist 2005; Cox et al. 2006; Hopkins et al. 2009a) and observed in young merger remnants (Rothberg & Joseph 2004, 2006). We do not suggest that scouring did not happen, although gas may help BH binaries to merge quickly (Gould & Rix 2000; Armitage & Natarajan 2002, 2005). Rather, the observation that extra mass generally is larger than missing mass (**Figure 30**) suggests that the starburst swamped any core scouring. Thus, extra-light ellipticals present no problem for our picture of core formation by BH binary scouring.

6.14 BH fundamental plane: the correlation with galaxy binding energy

Correlations between $M_\bullet$ and two of r_e, I_e, and σ are slightly tighter than correlations between $M_\bullet$ and any one of these variables (Aller & Richstone 2007; Hopkins et al. 2007a, b; Snyder et al. 2011). These correlations are commonly referred to as the BH "fundamental plane" (not to be confused with a correlation between $M_\bullet$ and the X-ray and radio luminosities of AGNs [Merloni et al. 2003] which has the same name). The existence of a fundamental plane (not a line) for ellipticals (Djorgovski & Davis 1987; Faber et al. 1987; Dressler et al. 1987; Djorgovski et al. 1988; Djorgovski 1992; Bender et al. 1992, 1993; Saglia et al. 1993; Jörgensen et al. 1996) means that the correlation of $M_\bullet$ with the E-galaxy fundamental plane variables is also multivariate.

This result is related to a demonstration by Kormendy & Gebhardt (2001) that galaxies which have abnormally large $M_\bullet$ for their stellar masses tend to have abnormally large σ and small r_e; i. e., to have dissipated and collapsed to smaller radii. And indeed, the above papers find that BH mass correlates well with the binding energy of the spheroidal component. This is yet another connection between BH growth and the details of the formation of classical bulges and ellipticals. In particular, it involves the physics of wet mergers and not just the overall depth of the potential well (which can be large even for pure-disk galaxies that contain no or only small BHs). We do not pursue these correlations further because of length constraints.

6.15 Other correlations?

We also do not pursue a number of additional correlations that have been proposed between $M_\bullet$ and various structural parameters of host galaxies. Graham et al. (2001) discuss a correlation with a concentration index that is a mixture of galaxy stellar mass and structural properties such as Sérsic index n. It could be related to the result in the previous section that more compact ellipticals have higher BH masses at the same M_*. However, we prefer to correlate $M_\bullet$ with M_*, n, and other parameters separately.

Graham & Driver (2007) find a tight correlation between $M_\bullet$ and n. Beifiori et al. (2012) and Vika et al. (2012) do not confirm a tight correlation, and neither do we.

Erwin, Graham & Caon (2004) review the subjects of this subsection.

6.16 Summary – Which components co-evolve with BHs?

BH masses correlate tightly enough to imply coevolution with the properties of classical bulges and elliptical galaxies and with no other galaxy components.

7. CENTRAL BLACK HOLES IN BULGELESS GALAXIES AND GLOBULAR CLUSTERS

In the early days of work on this subject, it appeared that 10^6 to $10^{9.5}$ $M_\odot$ BHs are almost universally associated with bulges and elliptical galaxies (e. g., KR95; Magorrian et al. 1998). Then the exclusion of a BH with $M_\bullet > 1500$ $M_\odot$ in M 33 (Gebhardt et al. 2001; Merritt, Ferrarese & Joseph 2001), which has neither a classical nor a pseudo bulge (Kormendy & Kennicutt 2004), led to the impression that BHs do not exist in pure-disk galaxies. However, the hints from AGNs always were that some pure-disk galaxies do contain BHs (see Ho 2008 for a recent review). Since then, it has been convincingly demonstrated that bulges are not necessary equipment for the formation of BHs. Here we review these and related results.

7.1 A new population of AGNs in late-type galaxies

The most secure example of an AGN BH in a pure-disk galaxy is NGC 4395. The galaxy is classified Sd III-IV in the Revised Shapley-Ames Catalog (Sandage & Tammann 1981) and SA(s)m? in the RC3. At a distance of $D = 4.61$ Mpc (Kennicutt et al. 2008), it has absolute magnitudes of $M_B = -17.75$ and $M_V = -18.20$. **Figure 31** emphasizes how enormously different NGC 4395 is from a bulge-dominated spiral or elliptical. It is a dwarf spiral with no classical bulge, no significant pseudobulge, and only a nuclear star cluster with an absolute magnitude of $M_B \simeq -11.0$ and a velocity dispersion of $\sigma \lesssim 30 \pm 5$ km s^{-1} (Filippenko & Ho 2003; Ho et al. 2009).

NGC 4395 is the nearest Seyfert 1 galaxy known and one of the least luminous (Filippenko & Ho 2003). It has all the hallmark signatures of BH accretion, including prominent optical and UV broad emission lines (Filippenko, Ho & Sargent 1993), highly variable X-ray emission (Shih, Iwasawa, & Fabian 2003), and a compact, flat-spectrum radio core (Wrobel & Ho 2006). Peterson et al. (2005) measured $M_\bullet = (3.6 \pm 1.1) \times 10^5\, M_\odot$ by reverberation mapping of C IV λ1549 using HST STIS. This is the smallest $M_\bullet$ measured by reverberation mapping. The low AGN luminosity corresponds to a small Eddington ratio of $\sim 1.2 \times 10^{-3}$. Filippenko & Ho argue that NGC 4395's BH mass may be as low as $M_\bullet \approx 10^4\, M_\odot$, consistent with the estimate of $M_\bullet = (4.9 \pm 2.6) \times 10^4\, M_\odot$ by Edri et al. (2012) based on a novel approach using broad-band photometric reverberation mapping. All of these masses are larger than $M_\bullet \lesssim 1500\, M_\odot$ in the brighter pure-disk galaxy M 33 ($M_V = -19.0$).

Eddington luminosity: the maximum luminosity that an AGN can have without blowing away its accretion disk via its own radiation pressure.

Eddington ratio: The ratio of an AGN's luminosity to its Eddington luminosity.

Figure 31

The Sd – Sm galaxy NGC 4395 (SDSS *gri* image from NED). The low surface brightness, the lack of a bulge, and the presence of a nuclear star cluster are characteristic of dwarf, late-type galaxies. M 33 and M 101 are more luminous and higher-surface-brightness analogs (Kormendy et al. 2010).

No less remarkable is POX 52 (Barth et al. 2004; Thornton et al. 2008). It is an almost identical twin to NGC 4395 in terms of its AGN properties and BH mass, except that it radiates at a higher fraction 0.2 – 0.5 of its Eddington rate. The galaxy is very dwarfish ($M_V = -17.6$) but completely devoid of a disk. Barth et al. (2004) measured a central stellar velocity dispersion of $36 \pm 5\,\mathrm{km\,s^{-1}}$, which, together with its structural parameters, led them tentatively to classify this as a "dE galaxy." That is, they concluded that its parameters are consistent with the fundamental plane sequence for faint Sph galaxies like Draco, UMi, and Sculptor and bright Sph galaxies like NGC 147, NGC 185, and NGC 205 (see Kormendy 1985, 1987; KFCB). Kormendy & Bender (2011) call these "Sph galaxies" to differentiate them from the disjoint fundamental plane parameter sequence of ellipticals shown in the above papers and in Bender, Burstein, & Faber (1992, 1993).

Galaxies like NGC 4395 and POX 52 are very rare but not unique. The large spectroscopic database from SDSS provides a perfect resource to uncover statistically significant numbers of such hard-to-find objects. Greene & Ho (2004, 2007c) performed a systematic search for AGNs with low-mass BHs from a detailed characterization of the broad-line (type 1) AGN population at $z < 0.35$ (Greene & Ho 2007b). They used the telltale broad Hα line as a signpost for AGN activity and estimated BH masses using the virial mass estimator for this feature calibrated by Greene & Ho (2005b). From a parent sample of nearly 600,000 galaxies, Greene & Ho found ~ 200 type 1 AGNs with $M_\bullet < 2 \times 10^6\,M_\odot$. This is rare indeed but still a hundred-fold increase from the previous sample of two! The sensitivity threshold of the selection method strongly biases the sample toward luminous objects. As a consequence, the majority of the sample has relatively high accretion rates, with a median $L_{\rm bol}/L_{\rm Edd} = 0.4$. Dong et al. (2012) revisited the SDSS database with slightly different selection criteria and increased the sample by another $\sim 30\%$. Consistent with their AGN nature, most of the objects emit X-rays (Greene & Ho 2007a; Desroches, Greene, & Ho 2009; Ai et al. 2011; Dong, Greene, & Ho 2012), but, interestingly, the vast majority are extremely radio-quiet. Greene, Ho, & Ulvestad (2006) attribute this to their high accretion rates.

bolometric luminosity: $L_{\rm bol}$ = total luminosity integrated over all wavelengths

In a complementary effort, Barth, Greene, & Ho (2008) used SDSS to identify candidate low-mass BHs in type 2 Seyferts. Although BH virial masses cannot be estimated for these narrow-line sources, one can maximize the probability of discovering low-mass BHs by selecting AGNs with low-luminosity host galaxies, to the extent that BH mass scales roughly with total galaxy mass. Follow-up Keck spectroscopy confirms that the hosts indeed have low masses and likely very late morphological types: a significant number have $\sigma < 60$ km s^{-1}, some as low as $\sigma \approx 40$ km s^{-1}. If these objects obeyed the $M_\bullet - \sigma$ relation, they would have masses and Eddington ratios comparable with those of the Greene-Ho type 1 objects. Consistent with the type 2 classification, their X-ray properties suggest moderately high obscuration (Thornton et al. 2009).

Apart from the systematic optical searches, there have been a number of reports of AGN activity in late-type galaxies based on detections with Spitzer of the mid-infrared [Ne V] 14.3 μm and/or 24.3 μm line (Satyapal et al. 2007, 2008). With an ionization potential of 97 eV, Ne^{+4} is usually considered to be an unambiguous indicator of nonstellar processes, and the mid-infrared fine-structure transitions are especially insensitive to dust extinction. Follow-up X-ray observations, where available, support the AGN interpretation; heavy obscuration is implied (Gliozzi et al. 2009; McAlpine et al. 2011; Secrest et al. 2012). Despite initial suspicions that a large population of AGNs may lie undiscovered in late-type galaxies, a dedicated Spitzer survey of 18 nearby Sd/Sdm spirals detected [Ne V] in only one galaxy (NGC 4178: Satyapal et al. 2009; Secrest et al. 2012). Thus, while some bulgeless spirals definitely harbor AGNs, most do not. Interestingly, all four secure cases of AGNs in pure-disk spirals contain a nuclear star cluster (NGC 4395: Filippenko & Ho 2003; NGC 1042: Shields et al. 2008; NGC 3621: Barth et al. 2009; NGC 4178: Satyapal et al. 2009). But not all nuclear star clusters host AGNs (e. g., M 33; see also Shields et al. 2012).

X-ray variability is another way to find dwarf AGNs. Kamizasa, Terashima, & Awaki (2012) used the XMM-Newton Serendipitous Source Catalogue to identify 15 AGNs with candidate low-mass BHs on the basis of strong X-ray variability whose amplitude is known to correlate inversely with BH mass. NGC 4395 and the Greene-Ho objects, for example, are among the most highly variable X-ray AGNs known (Miniutti et al. 2009). The empirical correlation between X-ray variability amplitude and BH mass implies $M_\bullet \approx (1-7) \times 10^6\,M_\odot$ for the new candidates, and the most extreme case may be as tiny as $M_\bullet \lesssim 10^5\,M_\odot$ (Ho, Kim, & Terashima 2012; Terashima et al. 2012).

Most of the low-mass BHs discovered to date may be strongly biased toward high Eddington ratios. Are we seeing just the tip of an iceberg? Or are there many more low-mass BHs with low accretion rates yet to be found? X-ray observations again provide tantalizing clues. Taking advantage of Chandra's high angular resolution, which is crucial for isolating faint sources in crowded fields, Desroches & Ho (2009; see also Zhang et al. 2009) report that $\sim$25 % of nearby Scd–Sm spirals contain a central X-ray core consistent with low-level AGN emission at the level of $L_{\rm bol}/L_{\rm Edd} \approx 10^{-6}$ to 10^{-3}, comparable to the lowest accretion rates seen in nearby supermassive BHs (Ho 2009a, b, c, 2002). Some of the sources have 2 –10 keV luminosities no larger than $L_{\rm X} \approx 10^{37} - 10^{38}$ erg s^{-1}, but the authors argue that stellar contamination by X-ray binaries or supernova remnants is unlikely. If the nonstellar origin of these sources can be confirmed, then this would imply that a sizable fraction of bulgeless spirals host central BHs.

7.2 Host galaxy properties

The observations described in Section 7.1 serve as a proof of concept that Nature can and does manufacture BHs in the mass range $M_\bullet \approx 10^4 - 10^6\,M_\odot$. This extends the dynamic range of BH masses below the threshold of $M_\bullet \approx 10^6\,M_\odot$ of most spatially resolved dynamical searches. Importantly, these low-mass BHs apparently can form without the aid of a bulge of any kind. Truly bulgeless hosts such NGC 4395 or spheroidal hosts like POX 52 are, however, relatively rare. The majority of the Greene-Ho sample has been imaged with HST (Greene, Ho & Barth 2008; Jiang et al. 2011b). Fewer than $\sim$ 10% of these objects are qualitatively consistent with being spheroidals. Among the galaxies that have extended, late-type disks, only $\sim$ 5% appear to be truly bulgeless. The vast majority contain resolved central components that resemble pseudobulges on the photometric projections of the fundamental plane. That is, low-mass BHs have not been found in genuine ellipticals or classical bulges. Given their late-type morphologies and low luminosities ($\sim$ 1 mag below L^*; Greene & Ho 2004, 2007b), it is not surprising that these host galaxies tend to have relatively low gas-phase metallicities (Ludwig et al. 2012).

Dwarf hosts and their low-mass BHs let us probe the BH–host-galaxy scaling relations in a regime that previously was poorly constrained by dynamically detected objects. A weak $M_\bullet - \sigma$ relation for AGNs continues to hold down to $M_\bullet \approx 10^5\,M_\odot$ and $\sigma \approx 30$ km s^{-1} (Barth, Greene & Ho 2005; Greene & Ho 2006b; Xiao et al. 2011; **Figure 32**, *left*). There is some tension between these results and **Figure 21** (*upper-right*). Here, the scatter is larger than in inactive galaxies or more massive AGNs, but it is difficult to disentangle the intrinsic scatter from the contribution due to the inherently larger systematic uncertainty of the virial mass estimators extrapolated to low masses. The correlation between BH mass and (pseudo)bulge luminosity is more complicated to interpret. The Greene-Ho objects lie significantly below the fiducial $M_\bullet - L_{\rm bulge}$ relation for inactive galaxies: (pseudo)bulges are overluminous at a fixed BH mass (Greene et al. 2008; Jiang et al. 2011a) or the BHs are undermassive at fixed (pseudo)bulge mass (Section 6.9). Part of this offset can be ascribed to younger stellar populations in pseudobulges. But that is not the whole story. A significant offset remains after applying an M/L correction and even after replacing the (pseudo)bulge luminosity with its dynamical mass computed using the measured velocity dispersion and effective radius (Jiang et al. 2011a; **Figure 32**, right). Therefore **Figure 32** (*right*) is consistent with Section 6.9.

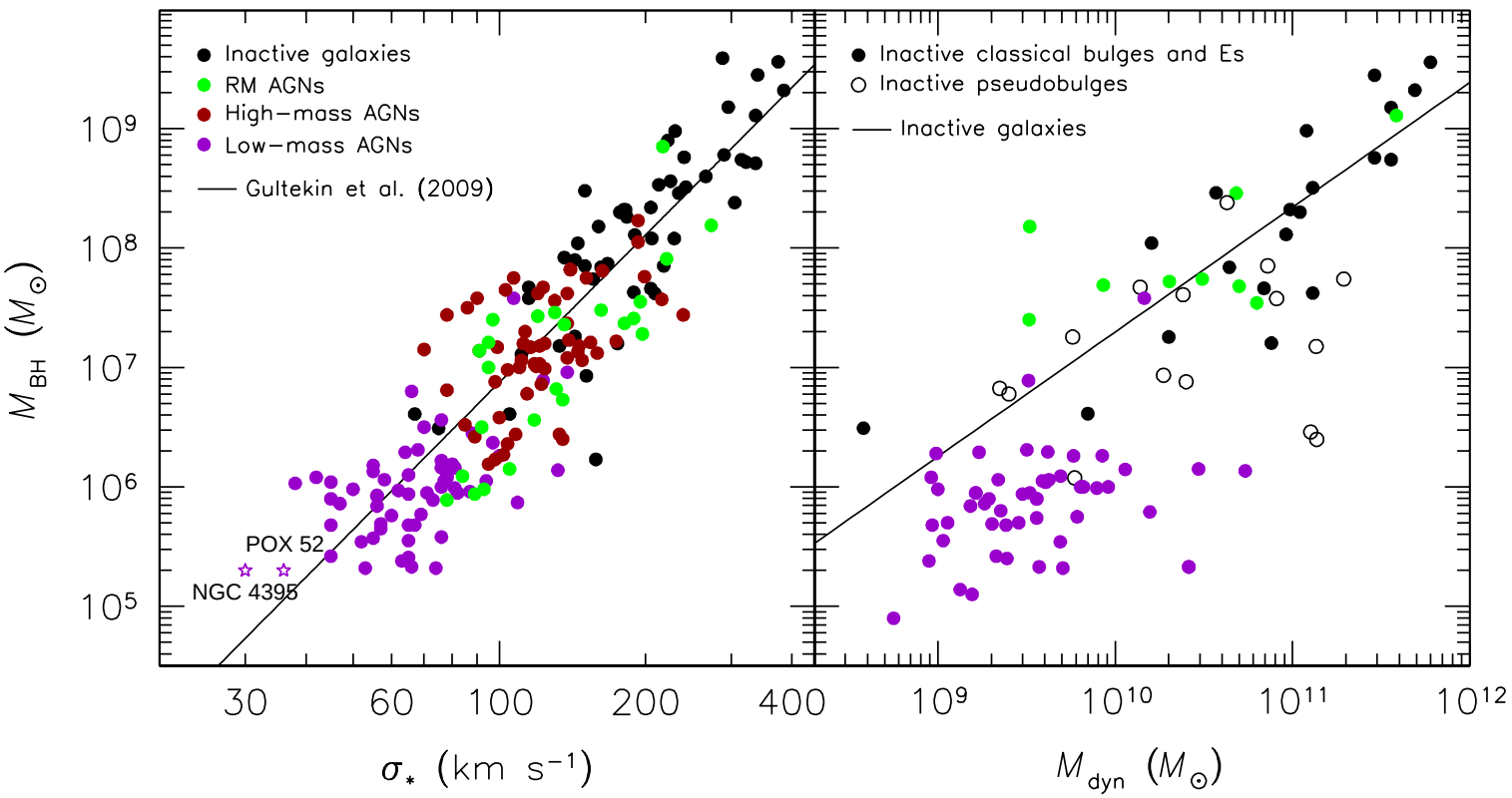

Figure 32

BH–host-galaxy correlations for AGNs with BH masses derived from reverberation mapping (RM) and from single-epoch spectroscopy of broad AGN emission lines. (*left*) AGNs (*colored points*) show considerably larger scatter in the $M_\bullet - \sigma$ relation than inactive galaxies (*black points*). Moreover, the scatter increases toward lower BH masses; most of these galaxies contain pseudobulges. Adapted from Xiao et al. (2011). (*right*) Inactive BHs in classical bulges and ellipticals obey a well-defined relation between $M_\bullet$ and dynamical mass $M_{\rm dyn}$; the same holds for reverberation-mapped AGNs with $M_\bullet \gtrsim 10^7\,M_\odot$ (*green points*). Low-mass AGNs, on the other hand, along with inactive BHs in pseudobulges, fall notably below the correlation for classical bulges and ellipticals. Adapted from Jiang et al. (2011a).

7.3 A BH in the starbursting dwarf galaxy Henize 2-10

The "poster child" for BH discovery using the radio–X-ray–$M_\bullet$ fundamental plane (Merloni, Heinz, & Di Matteo 2003) is Henize 2-10, illustrated in **Figure 33**. Reines et al. (2011) present a good case that the galaxy contains a BH, based on the observation of an X-ray point source with 2 – 10 keV luminosity $L_X \sim 10^{39.4}$ erg s^{-1} and a radio core with 4.9 GHz and 8.5 GHz luminosities of $L_R \approx 10^{35.9}$ erg s^{-1}. Careful astrometry implies that they are the same source. It lies far from the distribution of points for X-ray binary stars and inside the distribution of AGN points in the X-ray–radio-luminosity correlation. The compactness of the radio source ($\lesssim$ 3 pc × 1 pc) and its high brightness temperature ($> 3 \times 10^5$ K) point to a nonthermal origin (Reines & Deller 2012). Therefore the case for an intermediate-mass or supermassive BH is strong.

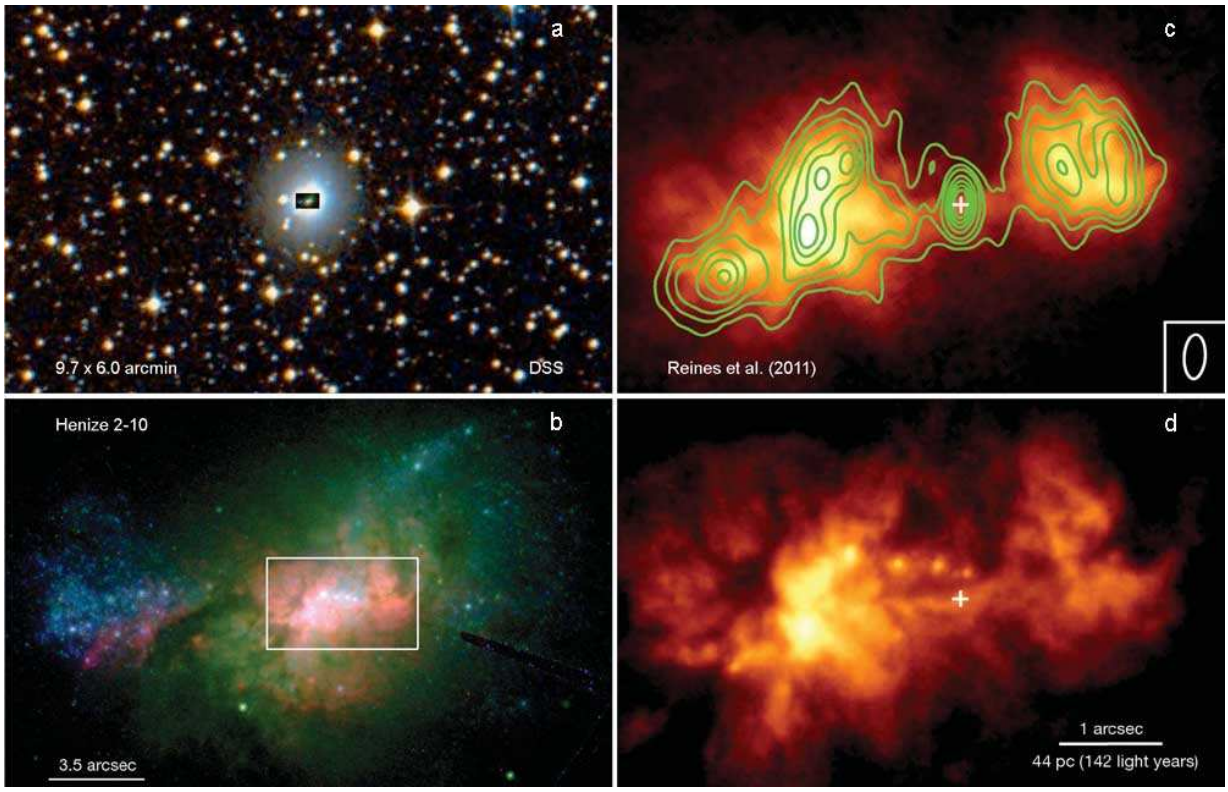

Figure 33

The starbursting blue compact dwarf galaxy Henize 2-10. *(a)* An optical color image from the Digital Sky Survey (DSS, courtesy **http://www.wikisky.org**) shows that the outer parts of the galaxy are blue but have a smooth light distribution. This proves to have an exponential profile. The burned-out central parts contain the ongoing starburst. The tiny rectangle in *(a)* shows a scaled version of panel *(b)* from Reines et al. (2011). It is an HST image showing Hα emission in red, the I-band stellar continuum in green, and U band in blue. The white box shows the field of panels *(c)* and *(d)*, also from Reines et al. (2011). *(c)* Shows radio emission contours (*green*) superposed on a continuum-subtracted, HST Hα image. Radio and Hα emission from ionized gas regions match. The radio point source (beam size in the inset) is coincident with the X-ray source (not shown). Panel *(d)* is an HST Hα image that does not have continuum subtracted; it shows that the AGN (+) is not coincident with any of the super star clusters that are part of the ongoing starburst.

However, determining $M_\bullet$ is tricky. Reines et al. (2011) estimate $M_\bullet$ using the Merloni, Heinz & Di Matteo (2003) correlation between BH mass, radio luminosity, and X-ray luminosity. They get $\log(M_\bullet/M_\odot) = 6.3 \pm 1.1$ for $D = 9$ Mpc. But the error estimate comes from the uncertainty in the coefficients of a linear fit to the above correlation, not from the scatter of BHs around that correlation. Also, the radio and X-ray observations were made two years apart in time, and variations in radio luminosity can easily be factors of several over this time (Gültekin, private communication). For example, a variation in radio luminosity of a factor of 3 would change the derived $\log M_\bullet$ by ± 0.41. Overall, $M_\bullet$ derivations from the above correlation are at best uncertain.

Still, the case for an AGN-mass BH in Henize 2-10 is strong. A mass $M_\bullet \sim 10^6\ M_\odot$ is surprisingly large for a dwarf galaxy. Reines et al. (2011) estimate that the accretion rate is $\sim 5 \times 10^{-6}\ M_\odot\ \mathrm{yr}^{-1}$ and that the Eddington ratio is $L/L_{\rm Edd} \simeq 10^{-4}$. Given the uncertainties, $M_\bullet$ could be 10 times smaller. But this is unlikely to be a stellar-mass BH.

What do we learn from Henize 2-10? The answer depends on the mass of Henize 2-10 and on what kind of galaxy it is evolving into. Both are uncertain:

The mass and BH mass fraction are easier. Noeske et al. (2003) find a total K_s magnitude of 8.89 and 2MASS gets $K_s = 9.004 \pm 0.024$. We adopt the mean, $K_s \simeq 8.95$. With $D = 9$ Mpc and a Galactic absorption of $A_K = 0.041$, the total absolute magnitude is $M_K \simeq -20.86$. This corresponds to a luminosity of $L_K \simeq 5 \times 10^9\ L_{K\odot}$. The galaxy is undergoing a starburst, so the mass-to-light ratio is uncertain, and it probably varies with radius. But it seems safe to assume that $M/L_K \simeq 0.3$ with an uncertainty of a factor of 3. Then the stellar mass is $M_* \sim 1.4 \times 10^9\ M_\odot$ with an uncertainty of a factor of 3. The mass in atomic and molecular gas is $M_{\rm gas} \sim 0.9 \times 10^9\ M_\odot$ (Kobulnicky et al. 1995; cf. Meier et al. 2001). This gives a total mass of $M \sim 2.3 \times 10^9\ M_\odot$ to within a factor of ~ 3. Consistent with the above, the H I rotation curve implies a dynamical mass $M \sim (2.7 \times 10^9\ M_\odot)/\sin^2 i$, where i is the inclination (Kobulnicky et al. 1995). So the BH mass fraction is $M_\bullet/M \sim 0.0006$ to within a combined uncertainty of a factor of 10. This is an order of magnitude smaller than our revised canonical mass fraction of ~ 0.005 (§ 6.6.1). Henize 2-10 is consistent with the pattern that is emerging for other low-mass BHs in late-type galaxies (Greene et al. 2008; Jiang et al. 2011a).

7.4 Intermediate-mass black holes in globular clusters?

The subject of BHs in globular clusters is important, interesting, and controversial. Reviews are provided by van der Marel (2004) and by Miller & Colbert (2004). The evidence is not yet compelling that BHs have been found in any "real" globular clusters. A BH has probably been found in G1 and may have been found in ω Cen. But these may be defunct galactic nuclei. If this is correct, then these BHs are like the ones in NGC 4395 and in other bulgeless galaxies.

Based on HST STIS measurements of an inward-rising σ profile, it has been suggested that the post-core-collapse globular cluster M 15 (Gebhardt et al. 2000c; Gerssen et al. 2002; van der Marel et al. 2002) and the M 31 globular cluster G1 (Gebhardt, Rich & Ho 2002, 2005) contain IMBHs with masses of ~ 4000 and 20000 $M_\odot$, respectively. Similarly, Gemini GMOS integral-field spectroscopy of ω Cen leads to the conclusion that it contains an IMBH of mass $4.0^{+0.75}_{-1.0} \times 10^4\ M_\odot$ (Noyola, Gebhardt & Bergmann 2008). These conclusions have been – and remain – controversial:

First, have central dark masses reliably been detected? Sollima et al. (2009) and van der Marel & Anderson (2010) argue against the detection in ω Cen. Noyola et al. (2010) obtain further kinematic data with VLT-FLAMES and confirm their earlier result. But their dispersion profile and van der Marel's disagree, and the reason is not known. For M 15, Gerssen et al. (2003) correct an error in their 2002 modeling paper; the result is that a BH-less model fits the data to $\sim 1\,\sigma$.

Second, if the dark mass detections are correct, do they see single IMBHs or central clusters of dark stellar remnants? All the above globulars are very old; any stars that initially were massive

enough to leave behind stellar-mass BHs or neutron stars have long since died. Dynamical evolution times for globular clusters are moderately short; any remnants that get retained by the clusters should to sink to the center. In defense of the BH detections, two arguments are cited: (1) the relaxation time of M 15 is short enough to have allowed core collapse, so mass segregation of remnants is plausible (this test was involved in the above error). But the central relaxation time in G1 and ω Cen as given by the observed stellar density and velocity dispersion profiles is longer than the age of the Universe. (2) The supernovae that leave behind stellar mass BHs and neutron stars are frequently asymmetric (Wang & Wheeler 2008). Remnants recoil. Free-flying neutron stars are observed in the Galaxy with peculiar velocities of hundreds of km s^{-1}. If heavy remnants are not retained, then they cannot mimic an IMBH. In contrast, white dwarf remnants – which are now being manufactured in all three clusters – are lighter than the highest-mass main sequence stars that remain; they actually migrate out of the core (albeit slowly).

Both arguments are only somewhat persuasive. Argument (1) is weaker than it sounds. When there is a large mass range, mass segregation is rapid compared to relaxation times calculated for single-mass systems. Lee (1995, 1996, 1998) emphasizes that a cluster of remnants separates dynamically from lower-mass, visible stars and quickly ends up with a short relaxation time. Then the apparent relaxation time of the visible stars is not a good estimate of the evolution timescale for a central cluster of massive remnants. Thus remnants can core-collapse even when the visible stars imply a long relaxation time. Argument 2's uncertainty is that we don't know the distribution of recoil velocities. But the detection of two stellar-mass BHs in the globular cluster M 22 (Strader et al. 2012a) is evidence that BH stellar remnants can be retained in globular clusters. And it is well known that globular clusters retain many neutron stars in the form of millisecond pulsars (e. g., Kulkarni, Hut, & McMillan 1993; Phinney & Kulkarni 1994; Phinney 1996; D'Amico et al. 2001) including at least as many as 20 in 47 Tuc (Camilo et al. 2000; Bogdanov et al. 2006) and 21 in Terzan 4 (Ransom et al. 2005).

We are uncomfortable with the fact that this subject has not shown steady progress toward becoming more convincing. In particular, it would be very compelling to find independent evidence for IMBHs in the same way that the detection of AGNs in dwarf, bulgeless galaxies points to BHs even when they cannot be found dynamically. Finding AGN-like sources in globular clusters would be persuasive. Kong et al. (2010) discuss a central X-ray source in G1 but cannot differentiate between IMBH accretion and a stellar X-ray binary. More generally, X-ray detections of globular clusters appear most consistent with stellar-mass BHs (Maccarone et al. 2007, 2010).

This uncomfortably uncertain situation has not improved. The radio source in G1 reported by Ulvestad, Greene & Ho (2007) was welcome news. Together with an X-ray source detection, it helped to lend confidence to the IMBH interpretation. Unfortunately, a recent observation with much improved sensitivity failed to confirm the earlier radio measurement (Miller-Jones et al. 2012). This does not invalidate the dynamical constraint, but it certainly does not help to build a case that this is an IMBH. Additional deep X-ray and radio searches of globular clusters – particularly bright ones that might be defunct galactic nuclei – would be helpful. So far the news has not been good (Ho, Terashima & Okajima 2003; Wrobel, Greene & Ho 2011; Strader et al. 2012b).

If the IMBHs in ω Cen and G1 prove to be real, there remains the complication that both hosts may be nuclei of defunct dwarf spheroidal galaxies and not globular clusters. We already know that some bulgeless galaxies contain nuclear star clusters that host BHs whereas others (M 33) do not. Work on this subject is continuing (e. g., Lützgendorf et al. 2013).

Whether or not these possible IMBHs lie on the extrapolation of the $M_\bullet - \sigma$ relation, it is unlikely that the same physics is responsible as at high BH masses. This is especially true since supermassive BHs with $M_\bullet \sim 10^6$ to 10^7 $M_\odot$ do not correlate tightly with disks or pseudobulges.

7.5 BHs in ultraluminous X-ray sources?

Ultraluminous X-ray sources (ULXs) in starbursting galaxies are often suggested to be IMBHs. Their interpretation as accreting BHs is not much in doubt, but the BH masses are controversial. Zhang et al. (2009) provide an excellent review and arguments that "the majority of [these sources] are nuclear BHs, rather than X-ray binaries." In contrast, Roberts (2007) concludes that "New observational evidence is now pointing away from the interpretation of ULXs as $\sim 1000\,M_\odot$ black holes." These differences are symptomatic of the fact that application of the $M_\bullet$–X-ray-luminosity–radio-luminosity correlation and other indirect techniques such as variability timescales can fail. We find it suspicious that most ULXs are associated with starbursts and not with galactic nuclei (e. g., Kong et al. 2007). The closeness of that association argues for short lifetimes and stellar-mass BHs (Roberts 2007). This subject deserves further work. High-resolution observations to look for compact radio sources are the biggest need. Körding, Colbert, & Falcke (2005) is a step in this direction and further illustrates the difficulty in distinguishing AGN BHs from stellar-mass BHs and BH alternatives.

The solution is important for an accurate census of low-mass BHs, but it is not crucial to the conclusions of this paper. We already know that bulgeless galaxies can contain AGN BHs with $M_\bullet \sim 10^{5\pm1}\ M_\odot$ and that these can serve as seeds for higher-mass BHs grown in galaxy mergers.

8. COEVOLUTION (OR NOT) OF BHs AND HOST GALAXIES

The discovery of the $M_\bullet - \sigma$ relation enormously energized work on AGN feedback and its effects on galaxy evolution. Two circumstances together make a case that is widely regarded as compelling (Section 8.2). First, many observations and astrophysical arguments provide motivation: they can be tied together into a multiply connected tapestry of the sort that we associate with successful and mature ideas. Second, if a tunable amount of energy is available – source unspecified – several longstanding problems of galaxy formation can be "solved". Hundreds of papers attempt to combine these circumstances to suggest that galaxy formation and BH growth regulate each other.

However, the observations reviewed in this paper lead us to a qualitatively different picture. The evidence for close coevolution – for mutual growth of bulges and BHs in lockstep – is less compelling than we thought. In the present universe, any high-z era of coevolution is over. At $z \sim 0$, no process significantly engineers tight $M_\bullet$–host correlations. Indeed, while some processes help to maintain the correlations, others erode them. Even out to $z \sim 1.5 - 2$, the observations suggest that most BHs do not grow in lockstep with their host bulges. To be sure, some observations do show that AGN activity affects galaxy formation. This convincingly solves some problems of galaxy formation, such as heating hot gas to prevent cooling flows. Nevertheless, the physics that seems most responsible for establishing the $M_\bullet$–host-galaxy correlations is not some magic aspect of AGN feedback. Rather, it is at least partly and perhaps mostly the averaging of BH masses that is inherent in galaxy and BH mergers. These ideas are heretical, so we develop them in Sections 8.3 – 8.6 as carefully as space allows.

8.1 Four Regimes of AGN Feedback: An Introduction

The conclusion that BHs correlate differently with different galaxy components allows us to refine our ideas on coevolution. Section 8 reviews evidence for the "punch line" conclusions of this paper. We present the case that there are four regimes of AGN feedback in three different kinds of galaxies.

(1) **Galaxies that lack dominant classical bulges** can contain BHs, but these grow by low-level AGN activity that involves too little energy to affect the host galaxy (Section 8.3). Decisively at $z \sim 0$ and probably out to $z \sim 1.5 - 2$, most AGNs are of this kind.

(2) Feedback may help to establish $M_\bullet$–host relations during dissipative ("wet") major mergers that make **classical bulges and low- to moderate-luminosity elliptical galaxies**. The jury is still out and the physics remains obscure. But if this is to work, it must work mostly at high z (Section 8.6).

(3) **The highest-mass ellipticals have cores** and otherwise are recognizably different from their lower-mass counterparts. We review evidence that they form in dissipationless ("dry") mergers. These giant ellipticals inherit any feedback effects from (2). In them, AGN feedback plays the essentially negative role of keeping galaxy formation from "going to completion" by keeping baryons locked up in hot gas. Here the controlling point is that these galaxies are massive enough to hold onto hot, X-ray-emitting gas. "Maintenance-mode AGN feedback" helps to keep the hot gas hot and to prevent late star formation and BH accretion (Section 8.4).

(4) **Averaging inherent in galaxy and BH mergers may be the most important effect that leads to BH–host-galaxy correlations.** Then the central limit theorem ensures that the scatter in BH correlations with their hosts decreases as $M_\bullet$ increases (Section 8.5).

The AGN population is dominated by (1) at all redshifts for which we have data. However, the highest-mass BHs and the total mass in BHs are dominated by processes (2) – (4).

8.2 Feedback from AGNs (and Star Formation): Motivation

Before we indulge in heresy, we review the motivation for the idea that BHs and bulges coevolve.

(1) The tightness of the $M_\bullet$ correlations with bulge velocity dispersion, mass, numbers of globular clusters, and core properties suggests that BH growth and galaxy formation are connected. Especially compelling is the conclusion that the scatter in the $M_\bullet - \sigma$ correlation is consistent with (Ferrarese & Merritt 2000; Gebhardt et al. 2000a) or only moderately larger than (Tremaine et al. 2002; Gültekin et al. 2009c; this paper) the measurement errors. However, seeing a tight correlation is not enough to ensure that coevolution happens because of AGN feedback. For example, we argued in Section 6.13 that the correlations with core properties are produced by dynamical processes that are purely gravitational.

(2) The binding energy $\sim 0.1 M_\bullet c^2$ of a BH (assuming a radiative efficiency of 10 %) is much larger than the binding energy $\sim M_{\rm bulge}\sigma^2$ of its host bulge,. For $M_\bullet \approx 5.3 \times 10^{-3} M_{\rm bulge}$ (Section 6.6), the ratio of binding energies is $5.3 \times 10^{-4}(c/\sigma)^2$, or $\gtrsim 500$ for $\sigma \lesssim 300$ km s^{-1}. If only one percent of the AGN energy output couples to gas in the forming galaxy, then all of the gas can be blown away (Silk & Rees 1998; Ostriker & Ciotti 2005). AGN feedback can be radiative (acting via photons) or mechanical (acting via energetic particles or a wind or a jet). Thus, BH growth may be self-limiting, and AGNs may quench star formation.

(3) The histories of BH growth and star formation in the universe are similar (**Figure 34**). Quasars and starbursts appear, at least superficially, to be closely linked. The most luminous starbursts always show signs of buried AGNs, even if these do not dominate the bolometric output (Genzel et al. 1998), and the host galaxies of AGNs often show concurrent or recent star formation (e. g., Kauffmann et al. 2003; Shi et al. 2009). Heckman et al. (2004) note that the volume-averaged ratio of BH accretion rate to star formation rate today is $\sim 10^{-3}$, eerily close to $M_\bullet/M_{\rm bulge}$. Is this just a remarkable coincidence, or does it signify a profound causal connection between BH and galaxy growth?

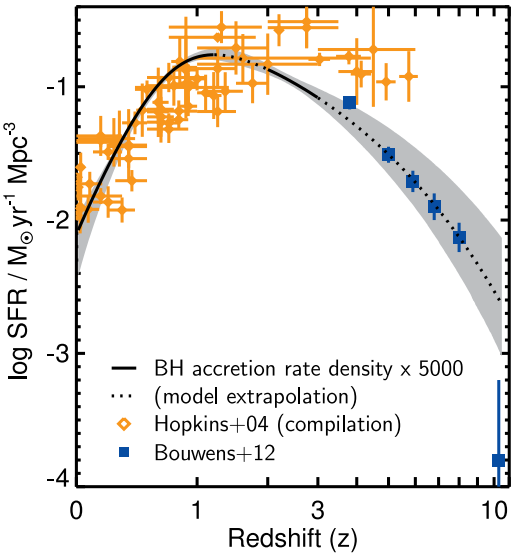

Figure 35

Evolution with redshift of the volume density of black hole accretion rate (*black line with grey band*), scaled up by a factor of 5000. This closely tracks the evolution of cosmic star formation rate compiled by Hopkins (2004; *orange points*) and by Bouwens et al. (2012; *blue squares*). Adapted and updated from Aird et al. (2010).

(4) The observed, zero-redshift volume density of BH mass agrees with the density of the fuel that is required to power quasars for plausible values of the radiative efficiency of BH accretion (Sołtan 1982; Yu & Tremaine 2002; Marconi et al. 2004). The uncertainty is a factor of ~ 2. Unless this agreement is a coincidence, most BH mass must have been acquired through radiatively efficient gas accretion while the galaxy hosted an AGN. BH growth by radiatively inefficient accretion and by swallowing of stars without disruption (at $M_\bullet \gg 10^8\ M_\odot$) must play a small enough role to not invalidate Sołtan's argument. This applies to intermediate masses $M_\bullet \sim 10^{8\pm1}\ M_\odot$. No argument based on energetics constrains the behavior of the smallest BHs, because they contribute negligibly to the mass density. And no dark mergers of BHs of any mass can affect the Sołtan argument, as long as their progenitors grew by radiatively efficient gas accretion. The point is that a large amount of AGN energy is available as input to arguments (1) – (3).

Points (1) to (4) are suggestive but indirect. Direct observations that are consistent with feedback in action (see Alexander & Hickox 2012 for a general review) include the following:

(5) Individual giant ellipticals and groups and clusters of galaxies contain large amounts of hot, X-ray-emitting gas. This gas often shows X-ray cavities or "bubbles" that are believed to be inflated by AGN jets. Plausibly, this is AGN feedback in action (Section 8.4). This subject is reviewed by McNamara & Nulsen (2007, 2012), Cattaneo et al. (2009), and Fabian (2012).

(6) Some bright quasars show blue-shifted X-ray spectral absorption lines interpreted as coming from winds with velocities $v \gtrsim 0.1c$ and with mass loss rates of one to tens of $M_\odot\ \mathrm{yr}^{-1}$ (e. g., Pounds & Page 2006; Reeves et al. 2009; Tombesi et al. 2012). Nonrelativistic outflows are also seen (Cano-Díaz et al. 2012 and references therein). Maiolino et al. (2012) report on a quasar at $z = 6.4$ with an inferred outflow rate of $> 3500\ M_\odot\ \mathrm{yr}^{-1}$. Such an outflow can clean a galaxy of cold gas in a single AGN episode.

(7) Some powerful radio galaxies at $z \sim 2$ show ionized gas outflows with velocities of $\sim 10^3\ \mathrm{km\,s}^{-1}$ and gas masses of $\sim 10^{10}\ M_\odot$. Kinetic energies of $\sim 0.2\,\%$ of BH rest masses are one argument among several that the outflows are driven by the radio sources and not by star formation (Nesvadba et al. 2006, 2008). Molecular gas outflows are also seen (Nesvadba et al. 2010).

(8) We focus on AGN energy feedback in this section, but we emphasize that it may very generally cooperate with starburst-driven feedback. A number of nearby ultraluminous infrared galaxies (ULIRGs), all composite starburst/AGN systems, show strong neutral and molecular outflows with velocities $\gtrsim 10^3\ \mathrm{km\ s}^{-1}$ and outflow rates of several hundred to more than a thousand $M_\odot\ \mathrm{yr}^{-1}$ (Rupke & Veilleux 2011; Sturm et al. 2011). After the fireworks subside and the dust clears, these systems transform to post-starbust systems still enveloped in outflowing gas detectable as $10^3\ \mathrm{km\ s}^{-1}$ Mg II absorbers (Tremonti, Moustakas & Diamond-Stanic 2007). However, winds are not restricted to the most extreme starbursts. Rather, they seem to be generic features of star-forming galaxies at $z \sim 1 - 2$ (Weiner et al. 2009; Genzel et al. 2011; Newman et al. 2012). Nevertheless, their relation to AGN feedback in such objects is unclear.

AGN feedback is also popular because it may resolve longstanding problems in galaxy formation:

(9) Episodic AGN feedback is believed to solve the "cooling flow" problem (Fabian 1994) that, in the absence of energy input, X-ray halos in giant galaxies and in clusters of galaxies would cool quickly, but cool gas and star formation are not seen in the predicted large amounts (e. g., Ostriker & Ciotti 2005). Related issues are the origin of the entropy floor and the steeper-than-expected temperature scaling of the X-ray luminosity of the intracluster and intragroup medium (see Cattaneo et al. 2009 for a review). This "maintenance-mode AGN feedback" is discussed in Section 8.4.

(10) At high masses, the galaxy mass function drops more steeply than the mass function of dark halos that is predicted by our standard cosmology. The proposed solution is that higher-$M_\bullet$ AGNs are more efficient at preventing late galaxy growth, again through the action of radio jets that keep baryons suspended in hot gas (e. g., Bower et al. 2006; Croton et al. 2006).

(11) The star formation histories of the biggest ellipticals are not trivially consistent with galaxy formation by hierarchical clustering (Faber, Worthey, & Gonzalez 1992). Stellar populations in the biggest ellipticals are very old and very enhanced in α elements compared to the Sun. This implies that essentially all star formation was completed, respectively, at high z and in $\lesssim 10^9$ yr (e. g., Worthey, Faber, & Gonzalez 1992; Matteucci 1994; Bender 1996). In general, more massive galaxies formed their stars earlier and more rapidly (Thomas et al. 1999, 2005). In contrast, hierarchical clustering implies that the biggest ellipticals were assembled late via the longest histories of successive mergers. If each merger involved star formation, then neither the old ages nor the α-element enhancement could be preserved. The solution is the realization that star formation and galaxy assembly could easily have happened separately and at different times. In particular, the above and other properties of giant ellipticals require that the last mergers that formed them were mostly dry (Faber et al. 2007; KFCB; Sections 6.7, 6.13, and 8.4 here). AGN feedback is one way to quench late star formation by maintaining hot gas halos (points 9, 10) (Bower et al. 2006; Croton et al. 2006).

(12) Mergers convert spiral galaxies into classical bulges and ellipticals (Toomre & Toomre 1972; Toomre 1977; Schweizer 1990). Since the former are gas-rich and star-forming whereas the latter are gas-poor and "red and dead", something connected with mergers presumably removes gas and quenches star formation. The observed bimodality in the color-magnitude correlation (Strateva et al. 2001; Baldry et al. 2004) can be explained, at least in part, by rapid quenching of star formation (cf. point 11). Expulsion or heating of residual cold gas may be accomplished by AGN feedback (Springel, Di Matteo & Hernquist 2005a; Schawinski et al. 2007). One sign of this may be the close association of high-luminosity AGNs with post-starburst stellar populations (Kauffmann et al. 2003). Another is the detection of fast ($\gtrsim 10^3$ km s^{-1}) outflows in post-starburst systems (Tremonti, Moustakas & Diamond-Stanic 2007). However, the jury is still out as to whether AGNs drive these winds (Diamond-Stanic et al. 2012). Also, feedback from starbursts may play an integral and necessary part in the removal of (most) cold gas from moderate-luminosity elliptical galaxies (point 8).

Galaxy formation studies that incorporate AGN feedback include semi-analytic models (Kauffmann & Haehnelt 2000; Granato et al. 2004; Bower et al. 2006; Croton et al. 2006; Sijacki et al. 2007; Somerville et al. 2008), hydrodynamic models (Quilis, Bower, & Balogh 2001; Dalla Vecchia et al. 2004; Brüggen & Scannapieco 2009; Ciotti, Ostriker, & Proga 2010), and analytical models (Cattaneo et al. 2011). They explain some observations (luminosity functions of galaxies; see Silk & Mamon 2012 for a review) but fail to explain others (bulgeless galaxies; see Abadi et al. 2003 for a model discussion and Kormendy et al. 2010 for the observations). An advantage of such models is that they efficiently explore how various physical effects are helpful.

A disadvantage is that they do not uncover new physics. And, even when they seem to work (e. g., solving the cooling flow problem in clusters), they do not tell us which of several competing mechanisms is responsible. Are hot gas halos that protect giant ellipticals from late star formation kept hot by AGN feedback, by cosmological gas infall, or by gas recycled from dying stars?

We therefore turn to observations for guidance. The following sections summarize what the observations tell us about the four regimes of coevolution (or not) between BHs and host galaxies. We start with the $z \sim 0$ universe, where answers are more clearcut, and then move out to higher redshifts, where conclusions are more tentative. Evidence for coevolution will not be overwhelming.

8.3 BH Growth in Disk Galaxies: No Coevolution at Low $M_\bullet$

The observation that $M_\bullet$ correlates closely with classical bulges and ellipticals but not with pseudobulges and disks motivated Kormendy et al. (2011) to suggest that there are two different BH feeding mechanisms. (1) BHs in bulges and ellipticals grow rapidly when mergers drive gas infall that feeds quasar-like events (e. g., Hopkins et al. 2006). (2) In contrast, small BHs in largely disk-dominated galaxies, most of which host pseudobulges, grow as low-level Seyferts; their feeding is driven locally and stochastically, and they do not coevolve with any part of their host galaxy. This suggestion was made independently by Greene et al. (2008) based on the observation that BH masses in low-luminosity Seyfert 1s (Greene & Ho 2004) are smaller than predicted by the $M_\bullet - L_{\rm bulge}$ relation. Greene et al. (2008; updates in Jiang et al. 2011a, b) had less information about the bulges of their galaxies but argued that most of them are pseudo. Related pictures are suggested by Hopkins & Hernquist (2009) and by Kauffmann & Heckman (2009). BH growth without host coevolution is the subject of this section. It applies to most AGNs at $z \sim 0$, and possibly also to many out to $z \sim 1.5$ (Section 8.6).

Most AGNs in $z \sim 0$ galaxies are weak (Ho 2008). BHs that accrete at significant fractions of their Eddington rates are rare (Heckman et al. 2004; Ho 2009a). Almost all are low-mass, 10^5–10^7-$M_\odot$ BHs that live in low-mass, Sbc – Sd spirals (Greene & Ho 2004, 2007c) that contain pseudobulges (Greene et al. 2008). **Figure 35** illustrates how, among $z \lesssim 0.35$ Seyfert 1 galaxies and quasars

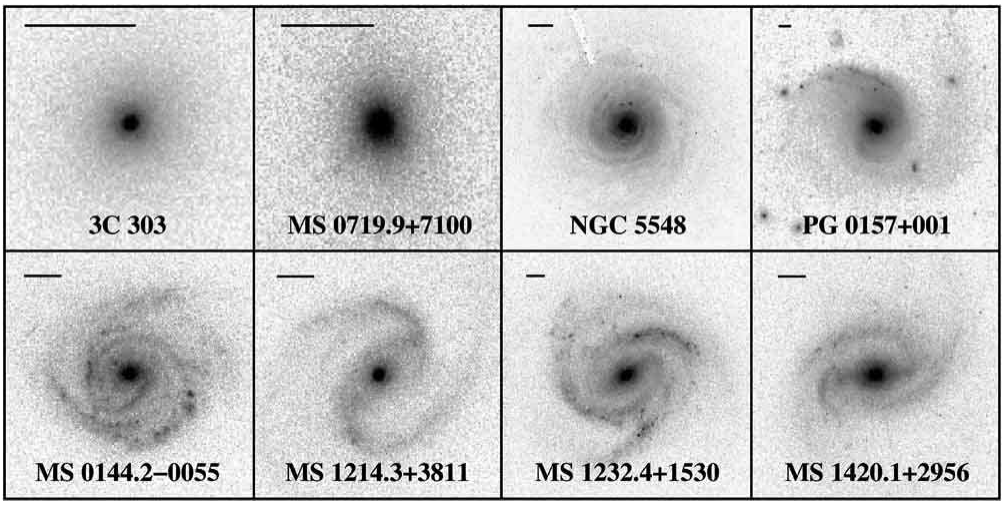

Figure 35

Optical R-band HST images of $\langle z \rangle \sim 0.1$ Seyfert 1 galaxies and quasars. Some of these nearby AGNs have elliptical hosts (the two leftmost objects on the top row), but most have hosts that are spirals with smallish bulge-to-disk luminosity ratios. At least 1/3 are barred (bottom row). The horizontal bar in each panel represents a scale of $2''$. Adapted from Kim et al. (2013).

that have been studied with HST, $\sim 1/3$ of the hosts contain bars (Jiang et al. 2011b; Kim et al. 2013; **Figure 35** here). This fraction is not higher than the already-large bar fraction in local spirals (Eskridge et al. 2000). Bars, oval disks, and tidal torques help to transport gas to the central $\sim 0.1-1$ kpc. Most gas that is accumulated there forms stars and builds pseudobulges, but some can – at least in principle – feed the BH. Numerous observational papers are devoted to this popular idea, but evidence for any enhancement of AGN activity by bars or environmental perturbations is murky (see Ho 2008 for review), in part because most papers on this subject ignore the effects of oval disks in unbarred galaxies (**Figure 10**). Also, the global supply of H I gas in the hosts seems to have no impact on the level of AGN activity (Ho, Filippenko & Sargent 2003; Ho, Darling & Greene 2008; Fabello et al. 2011). The apparent insensitivity of $z \sim 0$ AGN activity to galaxy gas content and to the mechanisms that can deliver it to the center reflects two facts: (1) BH feeding and AGN activity are episodic and not always switched on, and (2) feeding rates of low-mass BHs are very modest. Even if accretion occurs at the maximum Eddington rate, $\dot{M}_{\rm Edd} = 2.2 \times 10^{-8}\,(\eta/0.1)\,(M_\bullet/M_\odot)\,M_\odot\,{\rm yr}^{-1}$, where η is the radiative efficiency, the accretion rate for a 10^6-$M_\odot$ BH is only $0.02\,M_\odot\,{\rm yr}^{-1}$. This is tiny. A variety of stochastic processes driven by local, circumnuclear "weather" can supply the necessary fuel. In fact, the paradox for local BHs is not whether there is enough fuel to light them up. Rather, the puzzle is how to keep them so dim despite the ready abundance of *in situ* gas (Kormendy & Richstone 1995; Ho 2008, 2009a).

BHs are pervasive across much of the Hubble sequence, but is there any evidence that AGNs directly affect galaxy properties? For small BHs in nearby disk galaxies, the answer is: "Not much." The most powerful AGNs do seem to pump up the velocities in associated ionized gas (Greene & Ho 2005a; Ho 2009b), but it is unclear whether this has an impact beyond the relatively compact narrow-line region. Empirical evidence for a connection between AGN activity and star formation is, admittedly, compelling. Local Seyferts often show ongoing or recent star formation (e. g., Cid Fernandes et al. 2001), and stronger starbursts are associated with more powerful AGNs (Kauffmann et al. 2003; Wild et al. 2007). Nevertheless, this evidence is largely circumstantial and does not prove that BHs *cause* the starbursts. A link between BH accretion and star formation arises naturally because both depend on gas from the same reservoir and on the same, largely secular processes that drive gas inward (Kormendy & Kennicutt 2004). Wild, Heckman, & Charlot (2010) find that the peak accretion rate onto the BH typically occurs ~ 250 Myr *after* the onset of the starburst. The two processes are not strictly coeval, as Ho (2005) had suggested independently based on the apparent reduction of star formation efficiency in type 1 AGNs.

The tendency for AGN galaxies to inhabit the "green valley" of the color-magnitude relation (Martin et al. 2007; Nandra et al. 2007; Schawinski et al. 2007, 2009, 2010; but see Xue et al. 2010 for complications due to selection effects) has helped to promote the idea that AGN feedback quenches star formation and drives the color transformation of galaxies from the blue cloud to the red sequence. However, as in the case of star formation, it is dangerous to infer a direct, physical connection between AGN activity and galaxy color. We are unaware of any concrete proof that AGNs orchestrate the star formation histories of disk galaxies at any epoch from $z \sim 0$ (Wild et al. 2010) to $z \sim 1$ (Aird et al. 2012) or higher (Bongiorno et al. 2012).

In summary, most local AGNs accrete at very sub-Eddington rates. Very few galaxies are still growing their BHs at a significant level. Rapid BH growth by radiatively efficient accretion took place mostly in more massive galaxies that are largely quenched today. That is, the era of BH growth by radiatively efficient accretion is now mostly over. The era of major mergers is mostly over, too. We suggest that today's BHs grow mainly by secular processes that involve too little energy to result in structural coevolution with their host galaxies. BHs and host galaxies have stopped coevolving. If coevolution happened at all, it happened at high z. Section 8.6 reviews this subject.

8.4 Maintenance-Mode AGN Feedback at z ∼ 0

Still focusing on AGN feedback at $z \sim 0$, we turn next to the opposite extreme from Section 8.3, i. e., the highest-mass BHs in giant elliptical galaxies with cores. Then Section 8.5 reviews how BH – BH mergers affect the $M_\bullet$ correlations. In these sections, the big-picture physics is moderately well understood, although it remains a challenge to engineer the details. More uncertain is the situation at high z (Section 8.6), where AGN feedback may be substantially different.

The differences between core and coreless ellipticals are reviewed in Sections 6.7 and 6.13; they are part of an "E – E dichotomy" of many physical properties that are diagnostic of galaxy evolution. The physics that creates these differences is summarized there, but the motivating observations are the subject of this section and are illustrated in **Figure 36**. The suggestion is that coreless ellipticals form via wet mergers in which cold-gas dissipation feeds a central starburst that builds a dense "extra light" component that fills in any core (**Figure 28**). **Figure 36** shows that these coreless or "power-law", disky ellipticals generally lack hot gas. In contrast, giant, core-boxy ellipticals contain hot, X-ray-emitting gas. It is the essential agent that evaporates any cold gas and prevents the dissipation that leads to star formation (Nipoti & Binney 2007). The dividing line between galaxies with and without hot gas is at $\sim 1/2$ of the luminosity of the faintest core galaxies. Above this luminosity and corresponding mass, even merger progenitors should have had enough hot gas to keep mergers dry and allow core scouring by BH binaries. Moreover (**Figure 36**), core ellipticals contain radio sources that help, via "maintenance-mode AGN feedback", to keep the hot gas hot.

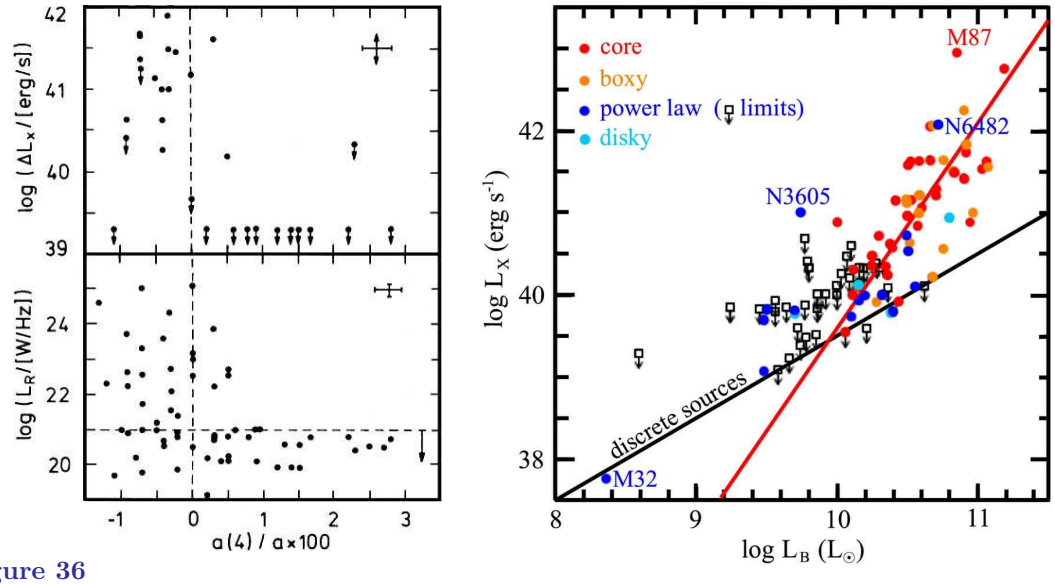

Figure 36

(*left*) From Bender et al. (1989), the correlation with isophote shape parameter a_4 of (*top*) X-ray emission from hot gas and (*bottom*) radio emission. Boxy ellipticals ($a_4 < 0$) contain X-ray-emitting gas and strong radio sources; disky ellipticals ($a_4 > 0$) do not. (*right*) KFCB update of the X-ray correlation: This plot shows total X-ray emission versus galaxy B-band luminosity, adapted from Ellis & O'Sullivan (2006). Detections are color-coded according to the E – E dichotomy. The emission from discrete sources (X-ray binary stars) is estimated by the black line (O'Sullivan et al. 2001) and was already subtracted before constructing the left figure. The red line is a bisector fit to the core-boxy ellipticals. They statistically reach $L_X = 0$ from hot gas at $\log L_B \simeq 9.94$. This corresponds to $M_V \simeq -20.4$, 1 magnitude fainter than the luminosity that divides the two kinds of ellipticals. Similar results were derived by Pellegrini (1999, 2005) and by Ellis & O'Sullivan (2006).

"Radio-mode" or "maintenance-mode" AGN feedback requires a working surface against which the feedback can act (Begelman 2004; Best 2006; McNamara & Nulsen 2007). This is provided by the X-ray gas. It also serves as an energy storage medium that smooths out the episodic energy input from the AGN and ensures that hot gas is always available whenever cold gas is accreted. A galaxy's ability to hold onto this gas depends on the depth of its gravitational potential well, so in this case, the velocity dispersion σ is the fundamental parameter that controls the physics. The transition between galaxies without and with hot gas occurs roughly at a critical halo mass $M_{\rm crit} \simeq 10^{12}\,M_\odot$ at which the gas cooling time is equal to the collapse time (Rees & Ostriker 1977; Dekel & Birnboim 2006; Kereš et al. 2005; Cattaneo et al. 2006, 2008; Dekel & Birnboim 2006, 2008; Faber et al. 2007). Faber et al. (2007) and KFCB get a corresponding stellar mass of $(1-2)\times10^{11}$ $M_\odot$ or $M_{V,\rm crit} \simeq -21.3$. This disagrees slightly with the DM-to-visible-matter calibration in **Figure 25** (*right*). If that calibration is wrong by 1/2 dex, the argument made there is unaffected. Here, we note that hot gas does not disappear suddenly and completely at $M_{\rm crit}$. Some lower-mass halos contain smaller amounts of hot gas (e. g., Bogdán et al. 2012, 2013), and still lower-mass halos likely contain warm-hot gas (Davé et al. 2001). KFCB emphasize the big-picture conclusion that there is remarkably good agreement between (1) the observations of which galaxies contain enough hot gas to be seen in **Figure 36** and which do not and (2) the absolute magnitude $M_V \simeq -21.6$ that divides core and coreless ellipticals. At the more detailed level that takes into account the gradual decrease in amount and temperature of gas as $M_{\rm DM}$ decreases, we suggest that the practical way to approach our engineering problem is this: Formation of extra-light components in dissipative mergers is easily switched off by even a modest amount of feedback (e. g., Cox et al. 2006). So the change at $M_V \sim -21.6$ from extra light to cores tells us how much hot gas and how much AGN activity is needed for feedback to be effective. The answer agrees with what **Figure 35** shows. In summary, KFCB suggest that $M_{\rm crit}$ quenching is the origin of the E – E dichotomy. The corollary is that maintenance-mode radio AGN feedback plausibly can operate in core ellipticals but not in coreless ellipticals or in most classical bulges.

McNamara & Nulsen (2007, 2012) and Fabian (2012) review observations of feedback in action. X-ray gas often shows cavities or bubbles that are connected to and – we believe – inflated by jets. The story is most convincing in galaxy clusters such as Perseus (Fabian et al. 2003, 2006, 2011). X-ray cavities are also seen in individual galaxies such as M 87 (Forman et al. 2005, 2007). The observations make a compelling case that heating is relatively isotropic even though jets are strongly collimated. However, we emphasize: The physics that makes this happen is not well understood. The biggest puzzle is how to confine at least some effects of well-collimated jets within their galaxies. Firing a rifle in a room does not much heat the air in the room. Maybe – as in protostellar jets (Shu et al. 1994, 1995) – the AGN jets are not as one-dimensional as they look. After all, a BH can more easily accrete gas if an outflow carries away some angular momentum. Maybe most of the impact comes not from the infrequent, episodic, well-collimated, extended jets, but from the accumulated effects of steady, slower outflows associated with the pervasive compact cores. Diehl & Statler (2008a, 2008b) find widespread evidence that even weak AGNs can create significant disturbances in the spatial distribution and thermal structure of X-ray-emitting gas in normal ellipticals. Ho (2009b) saw hints of this, too, based on analysis of the kinematics of the warm (10^4 K) gas. Is this level of "stirring" by compact radio sources enough to keep even field ellipticals quenched?

Also, it is not certain that every giant elliptical can host a powerful radio jet, either periodically, as required to keep hot gas hot, or even occasionally. While $\sim 30\%$ of galaxies with $M_\star \sim 10^{11.5}\,M_\odot$ host a radio source with power above $P_{1.4\ \rm GHz} = 10^{23}$ W Hz^{-1} (cf. **Figure 36**, *lower-left*); this could be consistent either with the hypothesis that jets are switched on $\sim 1/3$ of the time or with the (for present purposes) less benign hypothesis that only $\sim 1/3$ of giant ellipticals can make jets.

Could jet production require special conditions such as rapid BH spin (Sikora, Stawarz & Lasota 2007; Fabian 2013) that exist in only a subset of giant ellipticals? If so, then it gets harder to understand how hot gas is kept hot.

However the detailed physics turns out, AGN feedback has enthusiastically been embraced by the galaxy formation community. In one fell swoop, maintenance-mode feedback and $M_{\rm crit}$ quenching seem to offer a solution to many thorny problems that have plagued our picture of galaxy evolution: (1) how to prevent cooling flows, (2) how to shape the upper end of the galaxy luminosity function, (3) how to quench star formation in massive galaxies and keep them red, dead, and α-element-enhanced, and (4) how to explain the dichotomy into core and extra light elliptical galaxies. The effect of maintenance-mode feedback is largely negative. It stops the completion of galaxy formation by keeping baryons suspended in hot gas. Observations and theory lead to a picture in which heating and cooling are, on average, finely balanced but in which relaxation oscillations occur: accretion lights up the AGN; its feedback heats gas and drives it away; the BH is starved of further fuel and switches off; and cooling resumes until new cool gas revives the AGN. Supporting observations include (1) that the estimated AGN energy output is similar to the radiative losses in the hot gas, (2) that weak AGNs are found in the majority of clusters that have short cooling times, and (3) that low-density bubbles are younger than the cooling time of the hot gas through which they are rising, so AGNs recur quickly enough to prevent runaway cooling. This picture is developed or reviewed in Binney & Tabor (1995), Ostriker & Ciotti (2005), Croton et al. (2006), Rafferty et al. (2006, 2008), Sijacki & Springel (2006), Ciotti & Ostriker (2007), McNamara & Nulsen (2007, 2012), Cattaneo et al. (2009), Fabian (2012), and many other papers.

Notwithstanding the popularity of radio-mode AGN feedback, we should not forget that there are other sources of heating. Ostriker & Ciotti (2005) discuss the role of radiative heating. Gravitational heating from cosmological accretion (Dekel & Birnboim 2006, 2008) and satellite infall in dense environments (Khochfar & Ostriker 2008) should also be important. Even internal stellar processes such as stellar mass loss and Type 1a supernovae may contribute. The important point is this: The ingredient that is necessary to solve the above problems is hot gas in giant galaxies. Observations of those galaxies tell us that the gas is present, and temperature measurements tell us that the gas is not cooling catastrophically. The rest is engineering. We include the subject because AGN feedback is relevant to this review. But, as KFCB emphasize, any combination of the above and possibly other heating mechanisms suffices provided that it keeps the gas in the state in which we observe it.

8.5 Making the $M_\bullet - M_{\rm bulge}$ Correlation by Mass Averaging in Mergers

A radical alternative to making the $M_\bullet - M_{\rm bulge}$ relation by AGN feedback emerges from the statistics of mass averaging in galaxy mergers. This idea was first articulated clearly and explicitly by Peng (2007), although elements of it were implicit in previous work (e. g., Croton et al. 2006), and it has been emphasized independently by Gaskell (2010, 2011). The original Monte Carlo experiments of Peng have now been elaborated using more realistic semi-analytic models of galaxy formation properly embedded in ΛCDM merger trees (Hirschmann et al. 2010; Jahnke & Macciò 2011). As illustrated in **Figure 37** (*left*), if the $i^{\rm th}$ progenitor galaxy of mass $M_{*,i}$ contains one BH of mass $M_{\bullet,i}$ that may or (as in the figure) may not correlate with $M_{*,i}$, then building bigger galaxies by a succession of N major mergers in which the galaxy masses and BH masses separately add ("Σ") builds a correlation $\Sigma M_{\bullet,i} \propto (\Sigma M_{*,i})^\beta$ with $\beta \simeq 1$ and a fractional scatter that decreases with increasing mass as $1/\sqrt{N}$. This is a consequence of the Law of Large Numbers and arises completely independently of any input astrophysics that couples the BH and the galaxy.

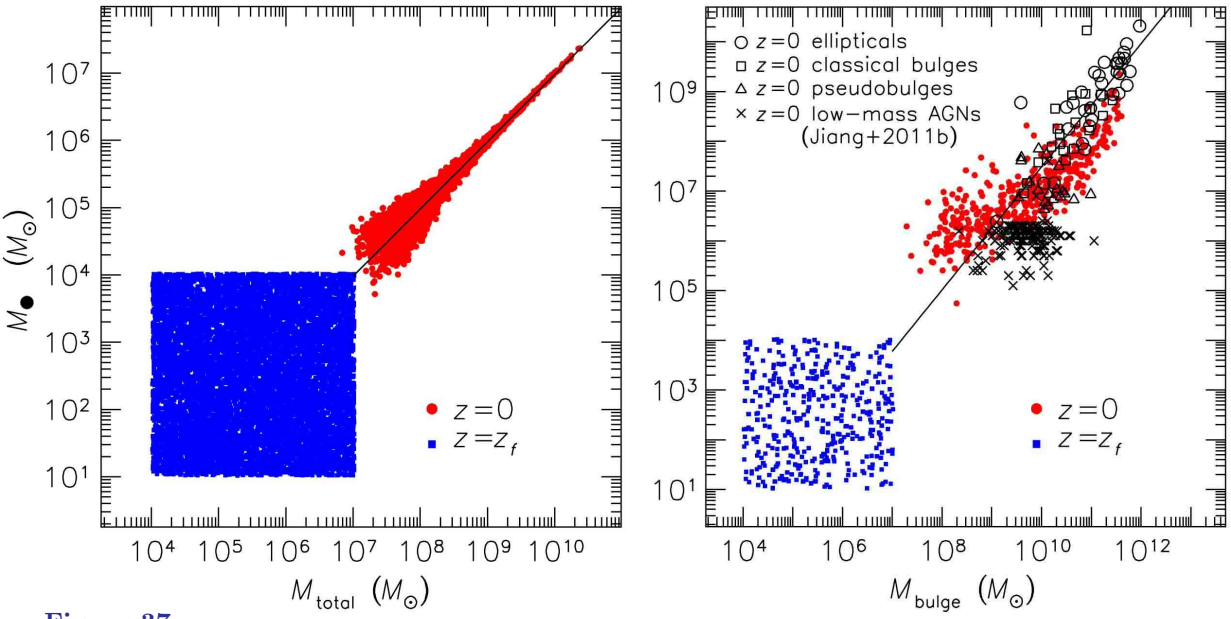

Figure 37

(*left*) Numerical experiment to show how a correlation (*red points*) between BH mass and bulge stellar mass is produced from an initially uncorrelated distribution (*blue points*) by a succession of dry mergers. A tight linear correlation emerges, and the scatter decreases toward higher masses. The solid line has a slope of 1. (*right*) Here, a subset of 400 randomly selected merger trees include simple prescriptions for star formation, BH accretion, population of dark matter halos with stars, and conversion of disks to bulges during major mergers. Overplotted in black is the Section 5 database of dynamically measured BH masses supplemented by low-mass BHs from Greene & Ho (2004, 2007c) that have bulge photometry in Jiang et al. (2011b). The line is the best-fit $M_\bullet - M_{\rm bulge}$ relation from Section 6.6.1 (Equation 10). Simulations adapted from Jahnke & Macciò (2011).

If the mean and dispersion $\equiv \sqrt{\rm variance}$ of the mass distribution of the progenitors galaxies are $\overline{m_g}$ and s_g, and the mean and dispersion of the mass distribution of seed BHs are $\overline{m_\bullet}$ and $s_\bullet$, then, for a large number N of mergers, the galaxy mass tends toward $N\overline{m_g}$ with dispersion $Ns_g/\sqrt{N}$ and the BH mass independently tends toward $N\overline{m_\bullet}$ with dispersion $Ns_\bullet/\sqrt{N}$. Thus the fractional dispersions in $N\overline{m_g}$ and $N\overline{m_\bullet}$ both decrease as $1/\sqrt{N}$. Since $d(\log_{10} x) \simeq 0.434\, dx/x$ for small dx/x, the scatter in a $\log_{10}$-$\log_{10}$ plot decreases as $1/\sqrt{N}$ in both coordinates, again for large N. The Central Limit Theorem further tells us that, independent of the forms of the initial distributions, the distributions of final galaxy and BH masses converge to Gaussians.

This result is broadly consistent with the observation that the scatter in the $M_\bullet$ – host-galaxy correlations decreases with increasing mass. We say "broadly consistent" because N is not extremely large. To better reproduce the normalization, slope, and scatter seen in local galaxies, the simulations shown in **Figure 37** (*right*) incorporate physically motivated recipes which describe how DM halo mass relates to stellar mass, how star formation rates vary with redshift, and how AGN accretion rates vary with redshift. Jahnke & Macciò further adopt a simple recipe guided by simulations to convert disks to bulges during major mergers. The numerical results roughly reproduce our BH database, including the decrease in scatter toward higher masses. There is a minor offset in normalization, but this is not surprising, because the simulations were not fine-tuned to our data. In particular, they were made prior to the change in $M_\bullet$ zeropoint derived in this review. Gaskell (2010) reports a similar trend for AGNs; it is further amplified in Section 8.6 (**Figure 38**).

It is possible that merger averaging is at least as important as feedback-driven coevolution in creating the observed BH – host correlations. The observation that points to this possibility is the result that $M_\bullet$ correlates tightly with the properties of bulges and ellipticals but not with those of pseudobulges and disks. These are not remnants of major mergers. Merger averaging is not relevant for them. In contrast, we concluded that at least several dry, major mergers are required to excavate realistic cores. And these can easily have been preceeded by one or more wet mergers.

We do not know the relative importance of merger averaging and AGN feedback in setting up the BH–host correlations. If feedback plays a major role, then – we suggest in Section 8.6 – it is quasar-mode feedback that happens at large z. It is poorly understood. However, as summarized in the next section, observations of high-z quasars and submillimeter galaxies (SMGs) suggest that a nascent correlation between $M_\bullet$ and $M_{\rm host}$ was already in place at $z \approx 2-6$. Given the prodigious accretion and star formation rates of these gas-rich systems, it seems likely that some form of energy feeback – from the AGN, from the starburst, or (most likely) from both – *did* help to establish the BH – host correlations during the quasar era. The intrinsic scatter of the correlations, on the other hand, appears to be larger than at $z \sim 0$. Moreover, the observations suggest that BH accretion and star formation were not precisely coeval. Thus the BH – host correlations seen in nearby galaxies may have been tightened by hierarchical merging at intermediate-to-late times.

One caveat is inherent in the downsizing of both AGNs and star formation as $z \to 0$. As discussed in Section 6.4, it involves giant, pure-disk galaxies at $z \sim 0$. Prototypes are galaxies like M 101, NGC 6946, and IC 342 (Kormendy et al. 2010). Their gas content and BH masses are small. When two such pure-disk galaxies merge, their stars get scrambled up into a bulge or elliptical, and their cold gas presumably feeds a modest starburst that helps to make the resulting bulge dense enough to satisfy the fundamental plane structural parameter correlations. But the sum of the BH masses remains too small for the newly converted bulge mass, and there is uncomfortably little gas in $z \sim 0$ progenitors to feed up the BH mass in proportion to how much disk mass got converted into bulge mass. Mergers of pure-disk galaxies have become somewhat rare at $z \sim 0$, but the observation in Section 6.4 of undermassive BHs in mergers in progress may be a sign that merger averaging can actually erode the BH – host correlations in the nearby universe.

Clearly we need more work to determing the evolving relative importance of AGN feedback and merger averaging as functions of cosmic time.

8.6 Quasar-Mode AGN Feedback in Wet Mergers

8.6.1 The formation of coreless ellipticals in wet mergers is relatively well understood. It is reviewed in detail in KFCB; some of the present discussion is abstracted from that review. Galaxy collisions lead to mergers that scramble disks into ellipticals (Toomre & Toomre 1972; Toomre 1977); numerical simulations (see Barnes & Hernquist 1992; Barnes 1998 for reviews and Steinmetz & Navarro 2002 for a case study) and observations of mergers-in-progress (see Schweizer 1990, 1998 for reviews) make a definitive case. When the progenitors contain gas, gravitational torques drive it to the center and feed starbursts. These build a distinct, extra stellar component that is recognizably smaller and denser than the Sérsic-function main body of the remnant (Mihos & Hernquist 1994; Springel & Hernquist 2005, Fig. 43 in KFCB; Cox et al. 2006; Hopkins et al. 2008, 2009a). Kormendy (1999) was the first to observe and recognize the extra component; he interpreted it as the "smoking gun" result which shows that coreless ellipticals formed in wet mergers. Further observational confirmation followed, both for mergers-in-progress (Rothberg & Joseph 2004, 2006) and for old, relaxed ellipticals (Côté et al. 2007; KFCB; **Figure 28** here). KFCB emphasize that the extra light often has properties such as disky structure and rapid rotation that further point to dissipative formation.

Classical bulges and coreless ellipticals make up $\gtrsim 2/3$ of the dynamic range in the BH correlations of Section 6. Knowing how they got their tight scatter is the key to understanding coevolution. They bequeath their tight scatter to core ellipticals via dry mergers; no further coevolution is needed for core galaxies beyond the need to preserve the tight correlations.

8.6.2 ULIRGs are prototypes of the formation of coreless ellipticals. ULIRGs are enormous starbursts that are almost completely shrouded by dust. By definition, they have infrared luminosities greater than $10^{12}\ L_\odot$. In the nearby universe, almost all of them are observed to be mergers in progress (Joseph & Wright 1985; Sanders et al. 1988a, 1988b; Sanders & Mirabel 1996; Rigopoulou et al. 1999; Dasyra et al. 2006a). They are local prototypes of the formation of ellipticals by very wet mergers.

What kind of ellipticals are they forming? Their structural parameters are consistent with the fundamental plane (Kormendy & Sanders 1992; Doyon et al. 1994; Genzel et al. 2001; Tacconi et al. 2002; Veilleux et al. 2006; Dasyra et al. 2006a, 2006b), so they are making normal ellipticals. The crucial observation is that ULIRGs have stellar velocity dispersions of $\sigma \simeq 100-230$ km s^{-1} (Genzel et al. 2001; Tacconi et al. 2002; Dasyra et al. 2006b, 2006c). Therefore they make moderate-mass ellipticals; i. e., the disky-coreless-rotating side of the E – E dichotomy discussed in Section 6.7.

8.6.3 ULIRGs are prototypes of BH–host coevolution driven by quasar-mode feedback. Remnants of major mergers show tight $M_\bullet$ correlations whereas disks and pseudobulges do not, even over a substantial range where they overlap in σ (**Figure 21**). Therefore σ as a measure of the depth of the gravitational potential well does not control whether coevolution happens or not. That is, the lowest-mass objects that coevolve with BHs (small ellipticals like M 32 and NGC 4486A and small classical bulges like the one in NGC 4258) are much lower in mass than the highest-mass disks and pseudobulges that do not coevolve (e. g., M 101, IC 342, and NGC 1068). It is important to increase the numbers of objects on which these conclusions are based. Meanwhile, the observations imply that coevolution is controlled by the process that makes coreless ellipticals and not just by galaxy mass. That process is dissipative mergers with starbursts, as exemplified by ULIRGs. We now enlarge on these suggestions, starting with observed connections between ULIRGs and AGNs.

8.6.4 The ULIRG – AGN connection: What is the energy source that powers ULIRGs? A connection between ULIRGs and AGNs emerged very early. Sanders et al. (1988a, b) suggested that "ultraluminous infrared galaxies represent the initial, dust-enshrouded stages of quasars". ULIRGs and quasars have similar number densities at $z \lesssim 0.08$ (ULIRGs are slightly more common) and luminosities (the ULIRG Mrk 231 is as luminous as the brightest nearby quasars). Both show frequent signs of mergers (essentially always, in the case of ULIRGs). And ULIRG spectra range from completely starburst-dominated (Arp 220) through many Seyfert 1 objects to quasars. Sanders et al. (1988a) state, "The discovery of several more distant (and presumably rarer) optical quasars with substantial infrared excess, as illustrated by the energy distributions for 3C 48 and Mrk 1014, strengthens the case for an orderly progression from ultraluminous infrared galaxy to optical quasar" (3C 273: their Figure 17). Similar suggestions were made by Sanders et al. (1988b) and Mirabel et al. (1989). Recent papers along the same line include – among many others – Urrutia et al. (2008), Wang et al. (2010), Simpson et al. (2012), and Xia et al. (2012). They find large amounts of molecular gas in quasars of all redshifts and support the case that the transition from starburst-dominated to AGN-dominated evolution is rapid.

These suggestions led to an enduring debate about whether starbursts or AGNs power ULIRGs (Joseph 1999; Sanders 1999). It is now clear that both are important but that starbursts usually dominate energetically (e. g., Genzel et al. 1998; see KFCB for a review). ULIRGs are rare locally, but they get more common rapidly with increasing redshift (Sanders & Mirabel 1996; Le Floc'h

et al. 2005) as do quasars. Many theoretical papers pursue and develop this picture; a review is beyond the scope of this review. We mention only one paper: Hopkins et al. (2006) develop "a unified, merger-driven model of the origin of starbursts, quasars, the cosmic X-ray background, supermassive black holes, and galaxy spheroids". Importantly, while the early starburst and associated, dust-obscured quasar phase last longer, "the total mass growth and radiated energy are dominated by the final blowout stage visible as a bright optical quasar". This is necessary by the Sołtan (1982) argument.

At the same time, nothing in the preceding discussion tells us whether AGN feedback or starburst-driven feedback engineers the BH – host-galaxy correlations. Both may be important.

8.6.5 Morphologies of AGN hosts at high redshifts. We saw in Section 8.3 that, in the nearby universe, most AGN host galaxies are not mergers in progress. This is consistent with what we know about mass functions of different kinds of galaxies: the most numerous galaxies are small ones, and overwhelmingly, they are disk galaxies. The fraction of galaxies or galaxy components that are merger remnants increases with increasing mass. The highest-mass galaxies are core-boxy-nonrotating ellipticals, and are all remnants of major mergers. This is mirrored in the distribution of BH masses: the lowest-mass BHs are in secularly evolving disks, whereas the highest-mass BHs are all in merger remnants. Observations suggest that this same picture holds at least out to $z \sim 2$.

Classifying quasar hosts at high z is difficult, but a consensus is emerging. Most AGNs of moderate luminosity (X-ray luminosity $L_X \simeq 10^{43\pm1}$ erg s^{-1}) live in disk galaxies, even when they are optically obscured (Cisternas et al. 2011a, b; Schawinski et al. 2011, 2012; Kocevski et al. 2012; Treister et al. 2012; Böhm et al. 2013; Schramm & Silverman 2013). On the other hand, the highest-bolometric-luminosity AGNs, true quasars with $L_X > 10^{44}$ erg s^{-1} and $L_{\rm bol} > 10^{45}$ erg s^{-1}, commonly are in mergers-in-progress and specifically in dust-shrouded, merger-induced starbursts (e. g., Urrutia et al. 2008; Treister et al. 2010, 2012). As noted earlier, observations indicate that a substantial fraction ($\sim 1/2$) of the growth of the largest BHs happens in this dust-shrouded phase.

We emphasize that these different results are not inconsistent. They address different questions:

(1) How do typical AGNs behave? For any realistic mass or energy function, typical objects are the smallest ones that can be found by the detection limits. Observations indicate – as many authors concluded – that BH growth by secular evolution of disk galaxies is more important at large z than we thought. In contrast:

(2) How do ellipticals form, how do big BHs grow, and how do the answers conspire to produce tight BH–host correlations? Our answer is the subject of this section: We suggest that ellipticals form by major mergers of the above disks and their small BHs, coevolution happens in the context of dissipative events and dust-shrouded starbursts, and statistical averaging via mergers finishes the job by tightening the BH-host correlations. At $z < 0.3$, the few remaining optically luminous quasars are already predominantly in ellipticals or in objects that are about to become ellipticals (e. g., Bahcall et al. 1997).

A similar distinction between high-luminosity AGNs fed by wet mergers and lower-luminosity AGNs fed by long-duration secular processes is discussed by Hopkins & Hernquist (2009). It is important to note that classical bulges and ellipticals are a moderately small fraction of all galaxy components. Giant ellipticals are particularly rare. Thus the results on AGN host galaxies at high redshifts appear to be consistent with the picture of coevolution that we suggest.

The new result that we did not anticipate is that well-formed disk galaxies already exist at $z \sim 2$ and that these have had time and opportunity to evolve secularly and to feed their BHs by local processes. We have no concrete reason to believe that these low-luminosity AGN BHs correlate tightly with any property of their host galaxy.

8.6.6 Evolution of $M_\bullet/M_{\rm bulge}$ at higher redshifts

The complexity of the BH-host correlations at $z \sim 0$ and the uncertain role of AGN feedback in shaping them compel us to turn to observations at high z for guidance. Here we briefly summarize this very active field, concentrating on the aspects that most affect our preceding discussion.

Any attempt to map out the origin and evolution of the BH-host correlations beyond the local universe faces two major obstacles. BH masses cannot yet be measured directly for distant galaxies; this forces us to resort to less-accurate, single-epoch virial mass estimators based on broad AGN emission lines (Supplemental Information). Moreover, the glare of the bright nucleus compounded by the large distances of the sources severely limits our ability to measure host galaxies, especially bulges and especially in the systems for which we must rely on broad emission lines to get $M_\bullet$.

Progress on this subject has therefore depended on high-resolution images to separate the host from the AGN and the bulge from the rest of the galaxy. Most of this work uses HST, with important recent contributions from 8-meter-class, ground-based telescopes (e. g., McLeod & Bechtold 2009; Targett, Dunlop & McLure 2012). Deblending the host from the AGN is feasible for relatively nearby sources with modest AGN-to-host brightness constrasts (e. g., Kim et al. 2008; Bennert et al. 2010), but systematic errors due to PSF mismatch become increasingly problematic for more luminous, distant quasars (Kukula et al. 2001; Ridgway et al. 2001). At the highest redshifts, no detection is possible at all (Mechtley et al. 2012), except for rare cases in which strong gravitational lenses stretch the host into an Einstein ring (Peng et al. 2006b). To circumvent blinding by the AGN, some authors have resorted to sources where line-of-sight obscuration creates a natural coronograph (e. g., McLure et al. 2006; Sarria et al. 2010). However, even when the host can be detected, we still need to convert measurements of light into estimates of stellar mass. This requires at least some color information or assumptions about the star formation history. Only a handful of studies have attempted to do this (Jahnke et al. 2009; Bennert et al. 2010, 2011; Decarli et al. 2010; Merloni et al. 2010; Sarria et al. 2010; Cisternas et al. 2011b; Schramm & Silverman 2013).

Photometry is hard, but kinematic measurements are harder. The AGN not only dilutes the stellar features but corrupts them with a plethora of emission lines that can result in systematic errors in the inferred central stellar velocity dispersions σ (Greene & Ho 2006a). Several studies have used AGN samples that were chosen to minimuze these complications, but so far, efforts to quantify the $M_\bullet - \sigma$ relation have been restricted to $z \lesssim 0.3 - 0.4$ (Treu, Malkan & Blandford 2004; Barth, Greene & Ho 2005; Greene & Ho 2006b; Woo et al. 2006; Shen et al. 2008; Xiao et al. 2011; Canalizo et al. 2012; Harris et al. 2012; Hiner et al. 2012), with just one venturing out to $z \sim 0.6$ (Woo et al. 2008). AO assisted by laser guide stars appears well poised to contribute to this subject soon (Inskip et al. 2011). In the meantime, some have used the widths of narrow emission lines to estimate σ (e. g., Shields et al. 2003; Salviander et al. 2007), while others advocate the use of radio emission lines to probe the rotation velocities of the hosts on larger scales (e. g., Walter et al. 2004; Shields et al. 2006; Ho 2007b; Ho et al. 2008; Riechers et al. 2008; Wang et al. 2010).

Broad-brush summary: Provided that the above caveats concerning $M_\bullet$ and $M_{\star,\rm bulge}$ are not too serious, the zero point and possibly the intrinsic scatter of the $M_\bullet-$host relations appear to evolve strongly with redshift. At higher redshifts, BHs appear to be more massive with respect to their hosts than they are in $z \sim 0$ galaxies of the same mass or gravitational potential. This suggests that BHs grew faster than their hosts formed stars or were assembled.

This conclusion is illustrated in **Figure 38**. It summarizes all available observations of AGNs at $z \approx 0.1 - 7.1$ that have reliable estimates of $M_\bullet$, of the stellar masses of the host galaxies, and of bulge-to-disk ratios determined from photometric component decompositions (low-z objects only). We compare these to the $z \sim 0$, $M_\bullet - M_{\rm bulge}$ relation from Häring & Rix (2004), because the AGN BH masses are zeropointed to that relation. This is discussed further below.

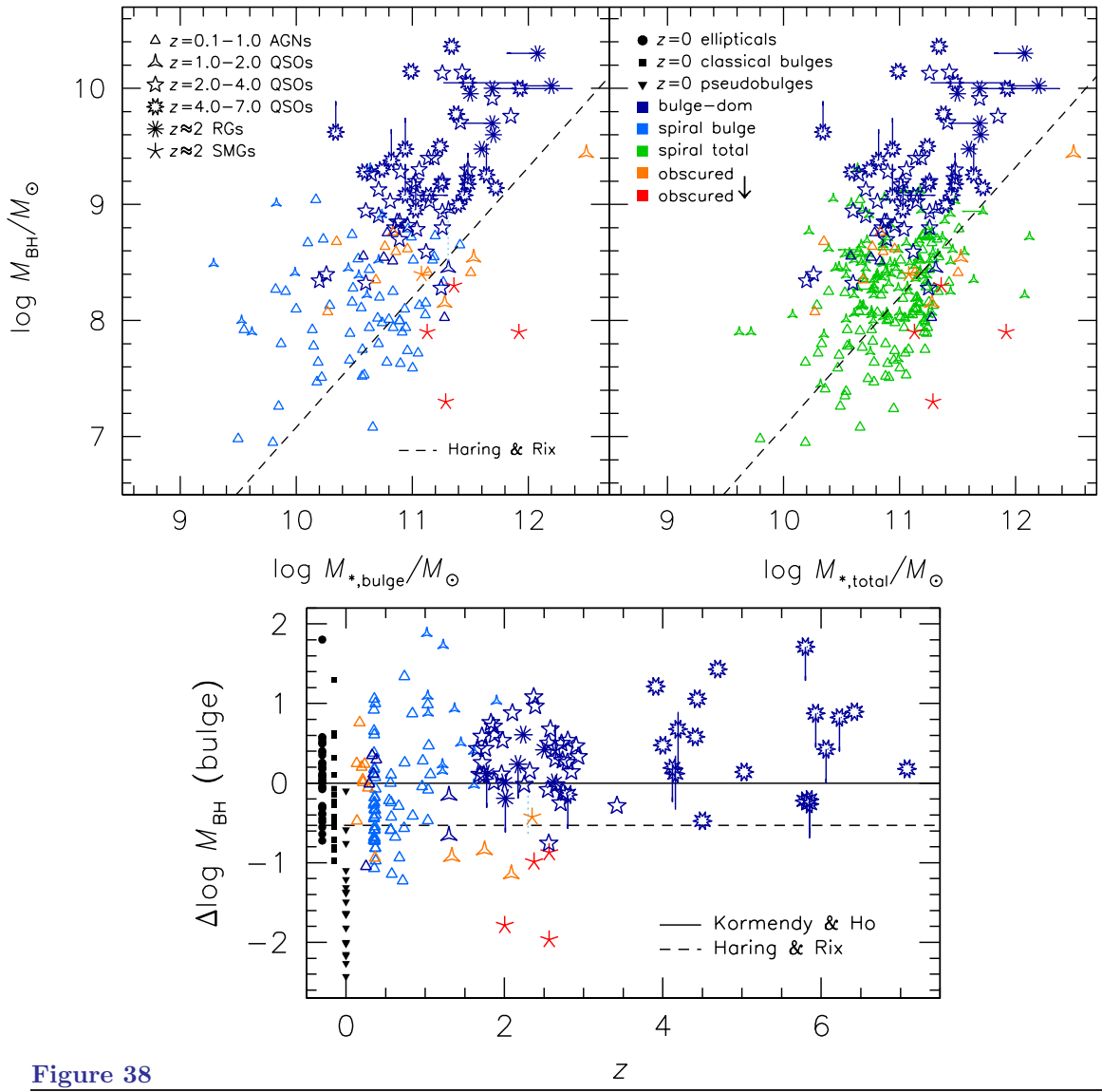

Figure 38

Correlation between $M_\bullet$ and host galaxy stellar mass (explicitly: M_*) of AGNs from $z \sim 0.1$ to 7.1, shown separately (*upper left*) for the bulge only and (*upper right*) for the entire galaxy. The dashed line is the Häring & Rix (2004) correlation between $M_\bullet$ and $M_{\star,\rm bulge}$ at $z \sim 0$ for inactive galaxies, which is roughly consistent with the zeropoint calibration of AGN BH masses. Dark blue points denote hosts that are known to be ellipticals or that contain classical bulges or that are massive enough so that they must be bulge-dominated by $z \sim 0$. They obey a moderately strong correlation. Dust-reddened quasars and other obscured AGNs appear to have preferentially undermassive BHs, the most extreme being the submm galaxies (SMGs). Less massive hosts are mostly disk-like, spiral galaxies at $z \lesssim 2$; they show a larger scatter in $M_\bullet - M_{\star,\rm bulge}$ like that of pseudobulges at $z \sim 0$. (*bottom*) Offset of $\log M_\bullet$ with respect to the local $M_\bullet - M_{\star,\rm bulge}$ relation derived by Häring & Rix (2004; *dashed line*) and here in Section 6.6 (*solid line*). The black points at $z \simeq 0$ are our sample of (*left to right*) classical bulges, ellipticals, and pseudobulges with dynamically detected BHs (**Tables 2** and **3**; objects are slightly offset from $z = 0$ for clarity). Adapted from Ho (2013).

Figure 38 show that, on average, $M_\bullet/M_{\star,\rm bulge}$ is larger than the local value from Häring & Rix (2004) by factors of ~ 2 at $z \approx 0.2 - 0.6$ (Treu et al. 2004; Woo et al. 2006, 2008; Canalizo et al. 2012) to factors of ~ 4 at $z \approx 2$ (e. g., Peng et al. 2006a, 2006b; Shields et al. 2006; Ho 2007b), or more at $z \approx 4 - 6$ (Walter et al. 2004; Wang et al. 2010; Targett et al. 2012). Parameterizing the evolution as $M_\bullet/M_{\star,\rm bulge} \propto (1+z)^\beta$, published values span the range $\beta \approx 0.7 - 2$ (McLure et al. 2006; Bennert et al. 2010, 2011; Decarli et al. 2010; Merloni et al. 2010). Taken at face value, these results imply that BH growth preceded or outpaced the growth of the bulge. However, it is tricky to interpret the observed distribution of points. Selection efffects are difficult to quantify (Lauer et al. 2007c; Shen & Kelly 2010; Schulze & Wisotzki 2011), and current samples of high-z AGNs may be biased toward the most luminous quasars. We cannot exclude the possibility that the points in **Figure 38** are the upper envelope of a distribution that extends to smaller BH masses. Still, two conclusions seem robust. First, the population of actively growing BHs at high z contains members with higher $M_\bullet/M_{\star,\rm bulge}$ ratios than are seen in most present-day massive galaxies. **Section 6.5** and **Figure 18** illustrate a few local examples of BH monsters that are much more massive with respect to their host bulges than the well-defined scatter shown by other galaxies. As noted there, these may be fossils of high-z quasars with higher-than-normal $M_\bullet/M_{\star,\rm bulge}$. And second, whatever its true distribution, the observed scatter in $M_\bullet/M_{\star,\rm bulge}$ at high z is almost certainly larger than it is at low z. Coevolution may take place, but it does not look finely coordinated.

The most undermassive BHs are seen in $z \sim 2$ SMGs (*red points*). SMGs are the high-z analogs of ULIRGs (Sections 8.6.2 – 8.6.4). Like ULIRGs, SMGs are dusty, gas-rich mergers powered simultaneously by a massive starburst and often by a heavily buried AGN (Tacconi et al. 2008). Importantly, SMGs are not just run-of-the-mill, high-z star-forming galaxies. Borys et al. (2005) find that $z \sim 2$ SMGs have a median stellar mass of $\sim 2 \times 10^{11}\,M_\odot$, fully compatible with being the precursors of most $z \sim 2$ quasars and perhaps of present-day coreless ellipticals (the masses are too large to be entirely comfortable). Within this backdrop, it is noteworthy that SMGs have $M_\bullet/M_{\star,\rm bulge}$ values that are at least an order of magnitude smaller than the fiducial local value (Borys et al. 2005; Alexander et al. 2008; Coppin et al. 2008; Carrera et al. 2011). A weaker but similar effect is seen in less extreme obscured systems (orange points). Given their already substantial stellar masses, SMGs clearly have been forming stars already for some time. And they are still at it. Their central BH, then, has *a lot* of catching up to do. How does it know how to control itself so that it ends up with the "right" value of $M_\bullet/M_{\star,\rm bulge}$ at $z \simeq 0$?

It may be a coincidence with a different explanation, but we note that our mergers in progress (Section 6.4), while not ULIRG-like starbursts, similarly contain undermassive BHs.

Curiously, any sign that BH-to-host mass ratios evolve with z weakens or disappears at $z \lesssim 2$ if we consider not the bulge component but the whole of the host galaxy (*green points*, **Figure 38**, *right*). At intermediate redshifts, the samples shift to moderate-luminosity, Seyfert-like AGNs, which tend to have lower-mass BHs ($M_\bullet \approx 10^7 - 10^8\,M_\odot$) that live in spiral disk galaxies (Section 8.6.6). The vast majority show no signs of morphological peculiarity (Cisternas et al. 2011a; Schawinski et al. 2011, 2012; Kocevski et al. 2012; Treister et al. 2012; Böhm et al. 2013; Schramm & Silverman 2013). Internal processes, not mergers, govern the evolution of these galaxies. If, at these intermediate redshifts, the bulge lies off the local correlation but the galaxy as a whole does not, then, over the next $7 - 10$ Gyr, the galaxy must find a way to redistribute the stars from its disk to its bulge. The obvious possibility is major mergers, but a serious caveat is that present data suggest that too many mergers are required and that they make too many big bulges and ellipticals. Alternatively, recent studies frequently invoke minor mergers and bulge formation through disk instabilities (Jahnke et al. 2009; Merloni et al. 2010; Bennert et al. 2011; Cisternas et al. 2011b; Schramm & Silverman 2013). Here, it is important to note that violent disk instabilities that make

$10^8 - 10^9$-$M_\odot$, kpc-size star-forming clumps which then sink to the center and merge (Elmegreen et al. 2005, 2007, 2008a, 2009a, b; Bournaud et al. 2007; Genzel et al. 2008; Förster Schreiber et al. 2009; Tacconi et al. 2010) are not secular processes (Kormendy & Kennicutt 2004; Kormendy 2012). Rather, this is a variant of the merger picture. It makes classical bulges (Elmegreen et al. 2008b). Connections between these processes and AGN BH growth remain to be explored, though it is reasonable to expect that they more nearly resembles major mergers than they do the secular growth of pseudobulges. Also, more accurate observations – especially to determine mass-to-light rations – and more rigorous calculations are needed to check whether the results seen in **Figure 38** are robust and to see what physical processes link high-z progenitors to $z \simeq 0$ descendants.

Our inference above that $M_\bullet/M_{\star,\rm bulge}$ evolves with z is based on single-epoch BH mass estimates for AGNs zeropointed to $z \simeq 0$ $M_\bullet$–host-galaxy relations published before the present work (e. g., the *dashed line* in **Figure 38**). A major, unanticipated development in this review has been that the zeropoint and, to a lesser extent, the slope of the BH-host correlations need to be revised (Section 6.6). Therefore the zeropoint for AGN $M_\bullet$ estimates must be revised, too. This work is in progress but has not yet been completed. If we provisionally use our present $M_\bullet - M_{\rm bulge}$ relation (*solid line* in the bottom panel of **Figure 38**), then the amount of evolution inferred for the $z > 0$ AGN population is significantly reduced. The $\sim 0.3 - 0.5$ dex evolution reported above for the $z < 1$ objects essentially vanishes, and the offset inferred for the $z \gtrsim 2$ quasars reduces to a comfortable factor of $2 - 3$.

It seems entirely reasonable that BHs in $z \gtrsim 2$ quasars were overmassive by the above factor compared to their remnants today. In fact, this is expected. Our understanding of the growth and assembly histories of galaxies is that high-mass galaxies at $z \approx 2 - 3$ – i. e., candidate quasar hosts when their BHs were deactivated – roughly double in stellar mass and quadruple in size by $z = 0$ (e. g., Buitrago et al. 2008; van Dokkum et al. 2010; Szomoru et al. 2012). If the stellar mass of these systems grows mainly by dry, minor mergers (e. g., Oser et al. 2010, 2012; Huang et al. 2013b; Naab 2013), we expect that $M_\bullet$ was more-or-less "locked in" at the value that it had at $z \approx 2 - 3$. Then, by the time massive ellipticals arrive at $z = 0$, the factor-of-two difference in $M_\bullet/M_{\star,\rm bulge}$ is erased. In support of this scenario, Targett et al. (2012) find that the host galaxies of $z \sim 4$ quasars were not only undermassive but also too compact by a factor of ~ 5 with respect to local ellipticals. In other words, the hosts of high-z quasars are closely related to red nuggets. And perhaps not coincidentally, to the hosts of BH monsters today (Section 6.5).

How much our recalibration of the $M_\bullet/M_{\rm bulge}$ distribution affects the above conclusions remains to be seen. Many objects used to calibrate AGN BH masses (Onken et al. 2004; Park et al. 2012) have low-mass BHs that live in pseudobulges. For these, $M_\bullet$ revisions are modest. Stay tuned.

While the absolute masses are still unsettled, the relative masses of the AGN BHs and those of their hosts should be more secure. As a summary of the above discussion, the take-away points on what we learn from **Figure 38** are as follows:

(1) Quasars at $z \gtrsim 2$ (*dark blue points*) populate a reasonably well-defined locus that lies above and parallels the sequence of BHs at $z = 0$. These quasars generally have $M_\bullet \gtrsim 10^{8.5}\,M_\odot$ and $M_{\star,\rm total} \gtrsim 10^{10.5}\,M_\odot$.

(2) The observed distribution of points has a maximum perpendicular spread of $\gtrsim 1$ dex. While the measurements of $M_\bullet$ and $M_{\star,\rm total}$ are both uncertain, it seems likely that the intrinsic scatter for the high-z points is larger than the local value of 0.29 dex (Section 6.6).

(3) If SMGs are any guide, it appears that high-z BHs initially grow more slowly than their galaxies. The BHs quickly "catch up," so that, by the time the dust is cleared away, they achieve $M_\bullet/M_{\star,\rm total}$ ratios seen in optically selected quasars. If quasar-mode feedback

moderates star formation and accretion, it presumably happens in this context. The details, however, are murky. Who is in control?

(4) Whatever the initial distribution of $M_\bullet/M_{\star,\rm total}$, it evidently settles to a relatively restricted range of values quite early on. A log-linear trend between $M_\bullet$ and $M_{\star,\rm total}$ is already recognizable in the quasar population between $z \sim 2$ and 6 with no obvious change in scatter across this redshift range (**Figure 38**, *lower panel*). To attain their enormous masses by these early times, we know that quasars had to grow by a combination of gas-rich mergers and near-Eddington-limited accretion (e. g., Li et al. 2007). The nascent $M_\bullet - M_{\star,\rm total}$ relation at these high redshifts could not have been established entirely through merger averaging.

(5) In Section 6.7, we suggested that coreless ellipticals are made in wet mergers in which quasar-mode feedback takes place. We now identify these events with the high-z SMG population. SMGs are analogs of nearby ULIRGs, and like ULIRGs, most SMGs are gas-rich mergers (e. g., Tacconi et al. 2008). These highly dissipative systems naturally produce the high central densities and globally disky structure that are characteristic of coreless ellipticals. Because major, wet mergers are quasi-spherical train wrecks, their gas and dust distributions may achieve a high enough covering factor to effectively couple the AGN radiation field with the interstellar medium of the host galaxy. This is a generic requirement for any AGN feedback mechanism to work (Silk & Rees 1998; Fabian 1999; King 2003; Murray, Quataert & Thompson 2005). Later, the remnants of these early SMGs presumably get converted to core ellipticals by dry mergers.

(6) Evolution in the $M_\bullet - M_{\star,\rm bulge}$ correlation for high-z quasars slows down dramatically at $z \lesssim 2$ when star formation and AGN activity cease. AGNs persist in massive, quiescent galaxies (Olsen et al. 2013), but at low levels that do not much grow $M_\bullet$. By contrast, we believe that high-mass galaxies roughly double their stellar mass from $z \sim 2$ to 0 through a series of dry, mostly minor mergers that are necessary to add their low-Sérsic-index halos (e. g., van Dokkum et al. 2010). By $z \sim 0$, this presumably lowers the zero point in the $M_\bullet - M_{\star,\rm bulge}$ correlation as stellar mass is driven from disks into bulges.

(7) Given that little $M_\bullet$ growth happens in dry mergers beyond the merging of BH binaries, core ellipticals inherit the $M_\bullet$–host correlations from smaller (and ultimately coreless) bulges and ellipticals. Then merger averaging is essentially the only effect that tights the correlations (Section 8.5). Radio-mode AGN feedback protects the galaxies from late star formation. These BHs coast on into the future quite unrelated to the BHs in point (8).

(8) At $z \lesssim 1.5$, BHs with $M_\bullet \lesssim 10^{8.5}\,M_\odot$ are generally hosted by disk galaxies (*light blue points* in **Figure 38**). The scatter of these points in the $M_\bullet - M_{\star,\rm bulge}$ plane flares up, and they show little correlation. Ironically, for these objects, the total stellar mass of the galaxy correlates better with $M_\bullet$ than the bulge mass (*green points* in **Figure 38**, *upper right*). This is not entirely unexpected, in view of the complex mass growth history of spiral galaxies, which is governed by a combination of internal, secular processes and external factors such as gas accretion and minor mergers (e. g., Martig et al. 2012; Sales et al. 2012). Disks settle (Kassin et al. 2012), bars and spiral arms develop (Kraljic, Bournaud & Martig 2012), and material gradually drains toward the center to build pseudobulges (Kormendy & Kennicutt 2004). Some minute fraction of the gas gets accreted by the BH. This is enough to sustain modest AGN activity and continued BH growth that persists to the present day. Given the essentially stochastic and local nature of these processes, it would be remarkable if BH accretion and star formation had much to do with each other. We suggest that this accounts for the poor BH-host correlations seen in pseudobulges.

9. CONCLUSIONS

9.1 Summary of our Picture of BH and Host Galaxy Coevolution

We have reviewed observations which tell us that BH masses correlate tightly only with classical bulges and ellipticals. In contrast, they correlate weakly enough with pseudobulges and dark halos to imply no relationship closer than the fact that it is easier to grow bigger BHs in bigger galaxies that contain more fuel. And BHs do not correlate with disk properties at all. We conclude that the physics that engineers tight $M_\bullet - \sigma$ and other correlations happens in the context of dissipative mergers that build disky-coreless-rotating bulges and elliptical galaxies. We use these constraints to navigate through a variety of sometimes-conflicting theory and observational results to construct a consensus picture of the relationships between BHs and host galaxies.

This picture is most uncertain at $z \simeq 2-4$ in the quasar era. Most growth of large BHs happens then by radiatively efficient gas accretion. Any coevolution that engineers the $M_\bullet - \sigma$ relation mostly happens then, too. Observations of the host galaxies of high-z quasars are fraught with challenges because of the enormous distances of these sources and the bright glare of their AGNs. Nevertheless, the evidence suggests that, even at these early times, the BHs already "knows about" the gravitational potential wells of the host galaxies, although the $M_\bullet$ zeropoint of the correlation may be a factor of $2-3$ higher and the scatter may be larger than at $z \sim 0$. The progenitors of high-z quasars appear to be gas-rich systems possibly involved in major mergers and possibly related to submillimeter galaxies. In light of the substantial stellar masses and star formation rates of submillimeter galaxies and the evidence for subdominant AGN activity and moderate BH masses, this scenario implies that gas-rich major mergers convert most gas into stars before they much build their BHs. When the BHs reach a critical threshold, "quasar-mode energy feedback" balances outward radiation or mechanical pressure against gravity. Then the AGNs and starbursts together limit galaxy growth by blowing away (or preventing the accretion of) a larger fraction of baryon mass from bigger galaxies. This quenches star formation and leaves the galaxies red and dead soon after their AGNs become visible.

The $z \sim 0$ situation is clearer. "Downsizing" means that most star formation and most AGN $M_\bullet$ growth now happen in relatively low-mass galaxies. By and large, these galaxies lack classical bulges. NGC 1068 and NGC 4151 are prototypical Seyfert (1943) galaxies that contain high-mass pseudobulges (Kormendy 2012). We suggest that BHs in such galaxies are fed by local processes and that the resulting AGNs produce too little energy to affect their hosts. The AGN activity is episodic but intrinsically secular; not much changes over long time periods. BHs that now live in classical bulges and ellipticals continue to correlate tightly with their hosts, but the physics that engineered this has mostly stopped happening. The highest-mass BHs at $z \sim 0$ live in giant, boxy-core-nonrotating elliptical galaxies that, at late times, grow mostly by dry mergers. They inherit coevolution magic from smaller galaxies. AGN feedback is different from that at high z: it is "maintenance-mode feedback" in which radio jets help to heat hot, X-ray-emitting gas halos in the biggest galaxies and in clusters of galaxies. This solves the "cooling flow problem" by keeping baryons locked up in hot gas. The result is to arrest star formation in the biggest galaxies. BH mass growth in this phase is relatively small.

At all z, major mergers concurrently grow larger BHs and larger elliptical hosts. The averaging that is inherent in mergers helps to decrease the scatter in BH-host correlations. Judging by the observed large scatter of the $M_\bullet - M_{\star,\rm host}$ relation for high-z quasars, any viable model for BH-galaxy coevolution must explain how it converges to the tight local relation. The relative importance of merger averaging and feedback magic in engineering tight correlations is not known. Merger averaging probably dominates the largest $M_\bullet$ and may be significant at all BH masses.

The era in which major mergers help to build BH correlations is already ending. Low-$M_\bullet$ outliers to the $M_\bullet$ – host-galaxy correlations are – we suggest – being created at $z \sim 0$ by mergers that convert disk mass into bulge mass without much BH growth beyond the mergers of BH binaries. Then mergers-in-progress have undermassive BHs if their progenitor disks had low-mass BHs. Major mergers are becoming rarer. They must largely have stopped happening in clusters, because these have velocity dispersions that are too large compared to galaxy velocity dispersions. In sparser environments, major mergers can make exceptions to the BH correlations at $z \sim 0$ whereas they help to create the correlations at large z because gas fractions in progenitor galaxies are small in the nearby universe but large at large z. ULIRGs that resemble our picture of large-z BH growth still occur today, but a growing fraction of major mergers in the nearby universe involve only modest star formation (Schweizer 1990) and necessarily only modest BH growth. Thus the coevolution era has largely ended and we have entered a time when the correlations slowly erode as mergers transform stellar disks into bulges without concurrent BH feeding.

In contrast, a few $z \sim 0$ exceptions to $M_\bullet - \sigma$ have unusually high BH masses in unusually compact host galaxies. These may be the rare remnants of galaxies in which BH growth spurted ahead of galaxy growth at high z. I. e., they may be remnants of a time when an $M_\bullet - \sigma$ relation either was not yet established or was offset from today's relation in the direction of high BH masses. They are most likely to survive in rich, dynamically relaxed clusters of galaxies, where remnant gas is too hot and galaxies move too rapidly to grow. In such environments, the rich get richer and the poor get poorer – giant ellipticals tend to grow via minor mergers, whereas small galaxies get starved of cold gas infall and whittled by dynamical harrassment. It seems no accident that the BH monsters are found in small galaxies that live near the centers of rich clusters

9.2 Burning Issues Regarding AGN Feedback

Remaining tensions involve a recurring theme: Supporting observations – even "smoking gun" observations such as relativistic outflows in quasars – are essentially circumstantial. We need to develop a more rigorous theoretical understanding that coevolution works as we suggest. Or not. Burning issues include the following:

(1) What processes clean cold gas out of early-type galaxies? For coreless-disky-rotating elliptical galaxies and classical bulges, we suggest that the fundamental initial cleaning process is an unknown combination of starburst-driven and quasar-mode AGN feedback. Is this correct? Which is more important? And what keeps these galaxies clean? Is it AGN activity that recurs when gas builds up?

(2) For core-boxy-nonrotating ellipticals, we suggest that radio, maintenance-mode feedback is responsible for keeping hot gas hot in individual giant ellipticals and in clusters of galaxies. The microphysics of this process is not well understood. Can radio jet energy be confined within individual galaxies and can it be thermalized?

(3) A broader issue about X-ray gas is whether AGN feedback is the main energy source that keeps it hot. Alternatives include (i) continued infall of gas from the cosmological web, which feeds a shock at the boundary to the quasistatic halo and keeps hot gas hot (Dekel & Birnboim 2006, 2008), and (ii) gas recycled from dying stars; this is injected into the gas halo at the kinetic temperature of stellar motions, which, by the virial theorem, is necessarily just right to maintain hot gas temperatures. It is not critical for our coevolution picture to know the relative importance of these (and possibly other) heating mechanisms; it is sufficient to observe that the gas is hot enough in all objects observed. But the balance between heating mechanisms affects conclusions about AGN duty cycles and about the amount of BH mass growth by gas accretion that happens during the maintenance-mode feedback phase.

9.3 Open Issues That We Have Not Reviewed

9.3.1. How do BHs grow so quickly at high redshifts? The highest-redshift ($z = 7.085$) quasar known already had $M_\bullet \sim (2.0^{+1.5}_{-0.7}) \times 10^9\ M_\odot$ only 770 million years after the Big Bang (Mortlock et al. 2011). The BH mass is based on the quasar's luminosity and on its Mg II $\lambda 2798$ Å line width. It is uncertain. But this is only the latest and most extreme of a growing number of known giant BHs at early times whose rapid growth, within the (somewhat squishy) constraint of the Eddington limit, is difficult to understand. The best bet is that these BHs get a head start on radiatively efficient growth by merging many small seed BHs, possibly Population III remnants. The point worth making is this: Such objects are so rare that any attempt to find a "natural" explanation is probably wrong. If the suggested process that makes these objects is not extremely unusual, it is probably the wrong process. This subject is reviewed by Volonteri (2010).

9.3.2 Why do we not see many BH binaries near galaxy centers? BH binaries formed in galaxy merges shrink in separation by several processes. At moderate separations, the tendency toward energy equipartition causes binaries to fling stars away, thereby – we believe – excavating cores. At small separations, they emit gravitational radiation. In between, there can be a bottleneck at separations of ~ 1 pc where decay processes are slow. This "final parsec problem" is discussed or reviewed in Begelman, Blandford, & Rees (1980); Yu (2002); Milosavljević & Merritt (2003); Makino & Funato (2004), and Merritt & Milosavljević (2005). The subject is complicated; we have neither the space nor the expertise to review it. Komossa (2006) reviews the observations. The "bottom line" is that BH binaries with separations ~ 1 pc are surprisingly rare, especially in big classical bulges and ellipticals. Additional decay processes are discussed in the above papers. We bring this subject up because it leads to interesting expectations:

9.3.3 Why do we not see BHs that are not at galaxy centers? If a second merger supplies a third BH to a BH binary, the resulting three-BH interactions generally fling all BHs away from the center. Even if the most massive BHs make a binary that ejects the third BH, the binary recoils. This leads to expectations that we have not observed: Where are the BH-less bulges and ellipticals? And where are the free-flying BHs and their very compact cloaks of stars?

An important corollary is this: BHs that have been evicted from the centers of their galaxies by multiple-BH interactions should decay back to the center by dynamical friction, but not instantly. So we expect that some BHs are located near but not at the centers of their host galaxies. Except in M 31 (Kormendy & Bender 1999), it is not realistic to expect that we see this in galaxies with dynamical BH detections. But radio observations can measure AGN positions very accurately. An astrometric survey to look for offcenter AGNs could pay interesting dividends. The problem is hard, because radio and optical observations are made at different times, and the stars whose astrometry is needed to tie radio frames of reference to optical ones have poorly known proper motions.

An even more important corollary involves observations of early-type galaxies at $z \sim 2 \pm 1$ that reveal high-mass red nuggets that are factors of ~ 4 smaller than similar-mass ellipticals at $z \sim 0$ (e. g., Daddi et al. 2005; Trujillo et al. 2006, 2007; van Dokkum et al. 2008; Buitrago et al. 2008; Damjanov et al. 2009; Szomoru et al. 2012). They are sometimes also described as denser and higher in velocity dispersion than $z \sim 0$ ellipticals, but this is misleading. These quantities look high when measured at or averaged inside small half-light radii r_e. But their central brightness profiles are very similar to those of nearby giant ellipticals when corrected for cosmological dimming and stellar population age (Hopkins et al. 2009; Bezanson et al. 2009; van Dokkum et al. 2010). So puffing up is not needed. Instead, giant ellipticals at $z \sim 0$ and $z \sim 2$ are similar near their centers; they differ at large radii because nearby core-boxy-nonrotating ellipticals have high-Sérsic-index outer halos (KFCB) that are not present in their high-z counterparts. These red nuggets are usually

interpreted as the ancestors of today's core-boxy-nonrotating ellipticals. The favored evolution scenario is inside-out growth in which outer halos are added onto already-formed centers mostly by minor mergers (Khochfar & Silk 2006; Naab et al. 2009; Hopkins et al. 2010; Feldmann et al. 2010; van Dokkum et al. 2010; Oser et al. 2010, 2012; Hilz, Naab & Ostriker 2013; see Naab 2013 for a review of this subject).

How does this story affect our picture of BH – host coevolution? The whole answer is not known. However, one suggestion follows immediately from looking at typical merger trees. In most minor mergers, the small galaxies are not vanishingly small. Many should bring their own BHs – probably not ones that coevolved, but nevertheless ones with $M_\bullet \gtrsim 10^5\ M_\odot$ – to the burgeoning large galaxy. Cold gas is not available to speed mergers, and dynamical friction is slower for smaller objects. Many minor mergers occur. We suggest that the result could often be a swarm of smallish but still supermassive BHs surrounding the central giant BH. They should reveal themselves as a cluster of AGNs during phases when the central BH is most active. The devil is in the details. But it is worth considering whether sensitive radio searches should already have found AGN clusters in the many radio galaxies that have been surveyed. This may constrain the histories of minor mergers.

Finally, it seems inevitable that some BHs with masses $M_\bullet \sim 10^4$ to $10^7\ M_\odot$ in bulgeless galaxies will be accreted by much bigger spirals. For example, imagine that a giant galaxy like M 31 inhales a fluffy dwarf like NGC 4395 (**Figure 31**). Its stars and gas will be deposited at large radii in the bigger galaxy. After that, the BH, probably still cloaked in its nucleus, should fly free in the halo potential. Dynamical friction is slow. This suggests that there should be low-level AGNs in the disks and (more often) the halos of galaxies like M 31 and our own. Can we find them?

9.4 Conclusion

Our inward journey to observe closer to the Schwarzschild radius and to observe relativistic effects such as BH spin is progressing rapidly. We are optimistic that spectacular advances are just around the corner. Our optimism is also based on a concurrent outward journey – the increasingly broad and convincing connections between the $M_\bullet$ demographics that are the subjects of this paper and a variety of aspects of galaxy physics. Robust connections between disparate research fields are a sign of the developing maturity of this subject. The observation that BH masses correlate differently with different galaxy components increases the richness of this subject and opens the door to a more nuanced and reliable understanding of BH–host-galaxy coevolution.

DISCLOSURE STATEMENT

The authors are not aware of any affiliations, memberships, funding, or financial holdings that might be perceived as affecting the objectivity of this review. Indeed, they are conscious of a deplorable lack of financial holdings that might be perceived as affecting anything at all.

ACKNOWLEDGEMENTS

Scott Tremaine has been associated with this paper since the beginning, and we have benefited enormously from his advice and constructive criticism. His comments on most sections of this paper have been invaluable and have influenced both the science and its presentation. We do not mean to imply that he agrees with all of our conclusions; any results that prove to be wrong are, of course, our responsibility. We sincerely thank Scott for all his help.

We acknowledge with pleasure our many years of productive collaboration with the Nuker team (Sandy Faber and Doug Richstone, past and present PIs). Some of our ideas on BHs and BH-galaxy coevolution matured in the intense and enjoyable environment of this collaboration. For conversations or emails that were specifically helpful to this paper, we thank Ralf Bender, Andrew Benson, Andi Burkert, Michele Cappellari, Ken Freeman, Reinhard Genzel, Kayhan Gültekin, John

Mulchaey, Doug Richstone, and Mark Sarzi. We are also grateful to Ralf Bender for letting us use his symmetric least-squares fitting code and the sm macro that makes 1σ shading around plots of those fits. And JK thanks Martin Gaskell for helpful conversations and comments on AGNs.

This paper would be much weaker without the generosity of people who provided data before publication. We are most sincerely grateful to Karl Gebhardt, Stephanie Rusli, and Roberto Saglia for allowing us to use their BH discoveries and $M_\bullet$ measurements. We thank Michele Cappellari for providing ATLAS3D σ_e measurements of some of our BH host galaxies. The following colleagues provided figures or data that contributed to some of the figures: James Aird, Reinhard Genzel, Knud Jahnke, Yan-Fei Jiang, Minjin Kim, Andrea Macciò, and Ting Xiao.

It is a particular pleasure to thank our Scientific Editor, Sandy Faber, for her thorough reading of the paper and for detailed comments that led to significant improvements both in science and in presentation. We thank Production Editor Roselyn Lowe-Webb and the production team at Annual Reviews for their masterful handling of a difficult paper. Also, we note that we have been greatly influenced by **http://www.annualreviews.org/page/infooverload**, an Annual Reviews White paper about "The Role of the Critical Review Article in Alleviating Information Overload". We recommend this paper to all ARA&A authors.

JK warmly thanks Mary Kormendy for her editorial help and for her support and understanding during the many years when this paper dominated his thinking and controlled our schedule.

This work would not have been practical without extensive use of NASA's Astrophysics Data System bibliographic services and the NASA/IPAC Extragalactic Database (NED). NED is operated by the Jet Propulsion Laboratory and the California Institute of Technology under contract with NASA. We also used the HyperLeda electronic database (Paturel et al. 2003) at **http://leda.univ-lyon1.fr** and the WIKISKY image database (**www.wikisky.org**). And we made extensive use of images from the *Hubble Space Telescope* archive and from the Two Micron All Sky Survey (2MASS: Skrutskie et al. 2006). 2MASS is a joint project of the University of Massachusetts and the Infrared Processing and Analysis Center/California Institute of Technology, funded by NASA and the NSF.

JK's research was supported in part by NSF grant AST-0607490. Also, this multi-year research project would not have been possible without the long-term support provided to JK by the Curtis T. Vaughan, Jr. Centennial Chair in Astronomy. We are most sincerely grateful to Mr. and Mrs. Curtis T. Vaughan, Jr. for their continuing support of Texas astronomy. LCH's work is supported by the Carnegie Institution for Science and by NASA grants from the Space Telescope Science Institute (operated by AURA, Inc., under NASA contract NAS5-26555). LCH thanks the Chinese Academy of Sciences and the hospitality of the National Astronomical Observatories, where part of this review was written.

LITERATURE CITED

Abadi, M. G., Navarro, J. F., Steinmetz, M., & Eke, V. R. 2003, ApJ, 591, 499
Ai, Y. L., Yuan, W., Zhou, H. Y., Wang, T. G., & Zhang, S. H. 2011, ApJ, 727, 31
Aird, J., Coil, A. L., Moustakas, J., et al. 2012, ApJ, 746, 90
Aird, J., Nandra, K., Laird, E. S., et al. 2010, MNRAS, 401, 2531
Alexander, D. M., Brandt, W. N., Smail, I., et al. 2008, AJ, 135, 1968
Alexander, D. M., & Hickox, R. C. 2012, NewAR, 56(4), 93
Aller, M. C., & Richstone, D. O. 2007, ApJ, 665, 120
Argon, A. L., Greenhill, L. J., Reid, M. J., Moran, J. M., & Humphreys, E. M. L. 2007, ApJ, 659, 1040
Arkhipova, V. P., & Saveleva, M. V. 1984, Trudy Gosudarstvennogo Astronomicheskogo Instituta P. K. Sternberga, 54, 33
Armitage, P. J., & Natarajan, P. 2002, ApJ, 567, L9

Armitage, P. J., & Natarajan, P. 2005, ApJ, 634, 921
Ashman, K. M., & Zepf, S. E. 1992, ApJ, 384, 50
Atkinson, J. W., Collett, J. L., Marconi, A., et al. 2005, MNRAS, 359, 504
Bacon, R., Emsellem, E., Combes, F., et al. 2001, A&A, 371, 409
Bacon, R., Emsellem, E., Monnet, G., & Nieto, J.-L. 1994, A&A, 281, 691
Baes, M., Buyle, P., Hau, G. K. T., & Dejonghe, H. 2003, MNRAS, 341, L44
Bahcall, J. N., Kirhakos, S., Saxe, D. H., & Schneider, D. P. 1997, ApJ, 479, 642
Bahcall, J. N., & Wolf, R. A. 1976, ApJ, 209, 214
Bajaja, E., van der Burg, G., Faber, S. M., et al. 1984, A&A, 141, 309
Baldry, I. K., Glazebrook, K., Brinkmann, J., et al. 2004, ApJ, 600, 681
Barbosa, F. K. B., Storchi-Bergmann, T., Cid Fernandes, R., Winge, C., & Schmitt, J. 2006, MNRAS, 371, 170
Barnes, J. E. 1989, Nature, 338, 123
Barnes, J. E. 1992, ApJ, 393, 484
Barnes, J. E. 1998, in 26$^{\rm th}$ Advanced Course of the Swiss Society of Astronomy and Astrophysics, Galaxies: Interactions and Induced Star Formation, ed. D. Friedli, L. Martinet, & D. Pfenniger (New York: Springer), 275
Barnes, J. E., & Hernquist, L. 1992, ARA&A, 30, 705
Barth, A. J., Greene, J. E., & Ho, L. C. 2005, ApJ, 619, L151
Barth, A. J., Greene, J. E., & Ho, L. C. 2008, AJ, 136, 1179
Barth, A. J., Ho, L. C., Rutledge, R. E., & Sargent, W. L. W. 2004, ApJ, 607, 90
Barth, A. J., Sarzi, M., Rix, H.-W., et al. 2001, ApJ, 555, 685
Barth, A. J., Strigari, L. E., Bentz, M. C., Greene, J. E., & Ho, L. C. 2009, ApJ, 690, 1031
Bastian, N., Covey, K. R., & Meyer, M. R. 2010, ARA&A, 48, 339
Batcheldor, D., Axon, D., Merritt, D., et al. 2005, ApJS, 160, 76
Baumgardt, H., Makino, J., Hut, P., McMillan, S., & Portegies Zwart, S. 2003, ApJ, 589, L25
Beckers, J. M. 1993, ARA&A, 31, 13
Begelman, M. C. 2004, in Carnegie Observatories Astrophysics Series, Vol. 1: Coevolution of Black Holes and Galaxies, ed. L. C. Ho (Cambridge: Cambridge Univ. Press), 375
Begelman, M. C., Blandford, R. D., & Rees, M. J. 1980, Nature, 287, 307
Begelman, M. C., Blandford, R. D., & Rees, M. J. 1984, Rev. Mod. Phys., 56, 255
Behroozi, P. S., Conroy, C., & Wechsler, R. H. 2010, ApJ, 717, 379
Behroozi, P. S., Wechsler, R. H., & Conroy, C. 2012, arXiv:1207.6105
Beifiori, A., Courteau, S., Corsini, E. M., & Zhu Y. 2012, MNRAS, 419, 2497
Beifiori, A., Sarzi, M., Corsini, E. M., et al. 2009, ApJ, 692, 856
Bell, E. F., & de Jong, R. S. 2001, ApJ, 550, 212
Bell E. F., McIntosh D. H., Katz N., & Weinberg M. D., 2003, ApJ, 585, L117
Bender, R. 1996, in IAU Symposium 171, New Light on Galaxy Formation, ed. R. Bender & R. L. Davies (Dordrecht: Kluwer), 181
Bender, R., Burstein, D., & Faber, S. M. 1992, ApJ, 399, 462
Bender, R., Burstein, D., & Faber, S. M. 1993, ApJ, 411, 153
Bender, R., Kormendy, J., et al. 2013, in preparation
Bender, R., Kormendy, J., Bower, G., et al. 2005, ApJ, 631, 280
Bender, R., Kormendy, J., & Dehnen, W. 1996, ApJ, 464, L123
Bender, R., Pierce, M. J., Tully, R. B., & Kormendy, J. 2008, unpublished
Bender, R., Surma, P., Döbereiner, S., Möllenhoff, C., & Madejsky, R. 1989, A&A, 217, 35
Benedict, G. F. 1976, AJ, 81, 799
Bennert, N., Schulz, H., & Henkel, C. 2004, A&A, 419, 127
Bennert, V. N., Auger, M. W., Treu, T., Woo, J.-H., & Malkan, M. A. 2011, ApJ, 742, 107
Bennert, V. N., Treu, T., Woo, J.-H., et al. 2010, ApJ, 708, 1507
Bessell, M. S. 2005, ARA&A, 43, 293
Best, P. N. 2006, Paper Presented at the Workshop on The Role of Black Holes in Galaxy Formation and Evolution, Potsdam, Germany, 2006 September 10 – 13 (see Cattaneo et al. 2009)

Bezanson, R., van Dokkum, P. G., Tal, T., et al. 2009, ApJ, 697, 1290
Binggeli, B., & Cameron, L. M. 1991, A&A, 252, 27
Binggeli, B., Sandage, A., & Tammann, G. A. 1985, AJ, 90, 1681
Binggeli, B., Sandage, A., & Tammann, G. A. 1988, ARA&A, 26, 509
Binggeli, B., Sandage, A., & Tarenghi, M. 1984, AJ, 89, 64
Binggeli, B., Tammann, G. A., & Sandage, A. 1987, AJ, 94, 251
Binney, J. 1978a, Comments Astrophys., 8, 27
Binney, J. 1978b, MNRAS, 183, 501
Binney, J., & de Vaucouleurs, G. 1981, MNRAS, 194, 679
Binney, J., & Mamon, G. A. 1982, MNRAS, 200, 361
Binney, J., & Tabor, G. 1995, MNRAS, 276, 663
Binney, J., & Tremaine, S. 1987, Galactic Dynamics (Princeton: Princeton Univ. Press)
Binney, J., & Tremaine, S. 2008, Galactic Dynamics, 2nd Edition (Princeton: Princeton Univ. Press)
Blakeslee, J. P., Cantiello, M., Mei, S., et al. 2010, ApJ, 724, 657
Blakeslee, J. P., Jordán, A., Mei, S., et al. 2009, ApJ, 694, 556
Blitz, L., & Spergel, D. N. 1991, ApJ, 379, 631
Bogdán, A., David, L. P., Jones, C., Forman, W. R., & Kraft, R. P. 2012, ApJ, 758, 65
Bogdán, A., Forman, W. R., Vogelsberger, M., et al. 2013, ApJ, in press (arXiv:1212.0541)
Bogdanov, S., Grindlay, J. E., Heinke, C. O., Camilo, F., Freire, P. C. C., & Becker, W. 2006, ApJ, 646, 1104
Böhm, A., Wisotzki, L., Bell, E. F., et al. 2013, A&A, 549, A46
Böker, T. 2010, in IAU Symposium 266, Star Clusters: Basic Galaxy Building Blocks, ed. R. de Grijs, & J. R. D. Lépine (Cambridge: Cambridge Univ. Press), 58
Böker, T., Laine, S., van der Marel, R. P., et al. 2002, AJ, 123, 1389
Böker, T., Sarzi, M., McLaughlin, D. E., et al. 2004, AJ, 127, 105
Böker, T., van der Marel, R. P., & Vacca, W. D. 1999, AJ, 118, 831
Bond, J. R., Arnett, W. D., & Carr, B. J. 1984, ApJ, 280, 825
Bongiorno, A., Merloni, A., Brusa, M., et al. 2012, MNRAS, 427, 3103
Booth, C. M., & Schaye, J. 2010, MNRAS, 405, L1
Borys, C., Smail, I., Chapman, S. C., et al. 2005, ApJ, 635, 853
Bosma, A. 1981, AJ, 86, 1825
Bournaud, F., Elmegreen, B. G., & Elmegreen, D. M. 2007, ApJ, 670, 237
Bouwens, R. J., llingworth, G. D., Oesch, P. A., et al. 2012, ApJ, 754, 83
Bower, G. A., Green, R. F., Bender, R., et al. 2001, ApJ, 550, 75
Bower, G. A., Green, R. F., Danks, A., et al. 1998, ApJ, 492, L111
Bower, G. A., Heckman, T. M., Wilson, A. S., & Richstone, D. O. 1997, ApJ, 483, L33
Bower, G. A., Wilson, A. S., Heckman, T. M., et al. 2000, BAAS, 32, 1566
Bower, R. G., Benson, A. J., Malbon, R., et al. 2006, MNRAS, 370, 645
Boylan-Kolchin, M., Ma, C.-P., & Quataert, E. 2004, ApJ, 613, L37
Boylan-Kolchin, M., Ma, C.-P., & Quataert, E. 2005, MNRAS, 362, 1184
Boylan-Kolchin, M., Ma, C.-P., & Quataert, E. 2006, MNRAS, 369, 1081
Braatz, J. A., Reid, M. J., Humphreys, E. M. L, et al. 2010, ApJ, 718, 657
Brodie, J. P., & Strader, J. 2006, ARA&A, 44, 193
Brüggen, M., & Scannapieco, E. 2009, MNRAS, 398, 548
Buitrago, F., Trujillo, I., Conselice, C. J., et al. 2008, ApJ, 687, L61
Burkert, A., & Tremaine, S. 2010, ApJ, 720, 516
Burkhead, M. S. 1986, AJ, 91, 777
Buta, R., Corwin, H. G., & Odewahn, S. C. 2007, The de Vaucouleurs Atlas of Galaxies (Cambridge: Cambridge Univ. Press)
Camilo, F., Lorimer, D. R., Freire, P., Lyne, A. G., & Manchester, R. N. 2000, ApJ, 535, 975
Canalizo, G., Wold, M., Hiner, K. D., et al. 2012, ApJ, 760, 38
Cano-Díaz, M., Maiolino, R., Marconi, A., et al. 2012, A&A, 537, L8
Caon, N., Capaccioli, M., & D'Onofrio, M. 1994, A&AS, 106, 199

Cappellari, M., Bacon, R., Bureau, M., et al. 2006, MNRAS, 366, 1126
Cappellari, M., Bacon, R., Davies, R. L., et al. 2008, in IAU Symposium 245, Formation and Evolution of Galaxy Bulges, ed. M. Bureau, E. Athanassoula, & B. Barbuy (Cambridge: Cambridge Univ. Press), 215
Cappellari, M., Emsellem, E., Bacon, R., et al. 2007, MNRAS, 379, 418
Cappellari, M., Emsellem, E., Krajnović, D., et al. 2011, MNRAS, 416, 1680
Cappellari, M., Neumayer, N., Reunanen, J., et al. 2009, MNRAS, 394, 660
Cappellari, M., Scott, N., Alatalo, K., et al. 2013, MNRAS, in press (arXiv:1208.3522)
Cappellari, M., Verolme, E. K., van der Marel, R. P., et al. 2002, ApJ, 578, 787
Carollo, C. M. 1999, ApJ, 523, 566
Carpenter, J. M. 2001, AJ, 121, 2851
Carrera, F. J., Page, M. J., Stevens, J. A., et al. 2011, MNRAS, 413, 2791
Cattaneo, A., Dekel, A., Devriendt, J., Guiderdoni, B., & Blaizot, J. 2006, MNRAS, 370, 1651
Cattaneo, A., Dekel, A., Faber, S. M., & Guiderdoni, B. 2008, MNRAS, 389, 567
Cattaneo, A., Faber, S. M., Binney, J., et al. 2009, Nature, 460, 213
Cattaneo, A., Mamon, G. A., Warnick, K., & Knebe, A. 2011, A&A, 533, A5
Cecil, G., Greenhill, L. J., De Pree, C. G., et al. 2000, ApJ, 536, 675
Cecil, G., Wilson, A. S., & De Pree, C. 1995, ApJ, 440, 181
Centrella, J., Baker, J. G., Kelly, B. J., & van Meter, J. R. 2010, Rev. Mod. Phys., 82, 3069
Chakrabarty, D., & Saha, P. 2001, AJ, 122, 232
Chemin, L., Carignan, C., & Foster, T. 2009, ApJ, 705, 1395
Cherepashchuk, A. M., Afanas'ev, V. L., Zasov, A. V., & Katkov, I. Yu. 2010, Astr. Reports, 54, 578
Cho, J., Sharples, R. M., Blakeslee, J. P., et al. 2012, MNRAS, 422, 3591
Cid Fernandes, R., Heckman, T. M., Schmitt, H. R., et al. 2001, ApJ, 558, 81
Ciotti, L., & Ostriker, J. P. 2007, ApJ, 665, 1038
Ciotti, L., Ostriker, J. P., & Proga, D. 2010, ApJ, 718, 708
Cisternas, M., Jahnke, K., Bongiorno, A., et al. 2011a, ApJ, 741, L11
Cisternas, M., Jahnke, K., Inskip, K. J., et al. 2011b, ApJ, 726, 57
Coccato, L., Sarzi, M., Pizzella, A., et al. 2006, MNRAS, 366, 1050
Combes, F., & Sanders, R. H. 1981, A&A, 96, 164
Conroy, C., & van Dokkum, P. G. 2012, ApJ, 760, 71
Cooke, A. J., Baldwin, J. A., Ferland, G. J., Netzer, H., & Wilson, A. S. 2000, ApJS, 129, 517
Coppin, K. E. K., Swinbank, A. M., Neri, A., et al. 2008, MNRAS, 389, 45
Côté, P., Ferrarese, L., Jordán, A., et al. 2007, ApJ, 671, 1456
Côté, P., McLaughlin, D. E., Hanes, D. A., et al. 2001, ApJ, 559, 828
Côté, P., Piatek, S., Ferrarese, L., et al. 2006, ApJS, 165, 57
Courteau, S., Widrow, L. M., McDonald, M., et al. 2011, ApJ, 739, 20
Cox, T. J., Jonsson, P., Primack, J. R., & Somerville, R. S. 2006, MNRAS, 373, 1013
Crane, P., Stiavelli, M., King, I. R., et al. 1993, AJ, 106, 1371
Cretton, N., de Zeeuw, P. T., van der Marel, R. P., & Rix, H.-W. 1999a, ApJS, 124, 383
Cretton, N., & van den Bosch, F. C. 1999b, ApJ, 514, 704
Croton, D. J., Springel, V., White, S. D. M., et al. 2006, MNRAS, 365, 11
Daddi, E., Renzini, A., Pirzkal, N.,et al. 2005, ApJ, 626, 680
Dalla Bontà, E., Ferrarese, L., Corsini, E. M., et al. 2009, ApJ, 690, 537
Dalla Vecchia, C., Bower, R. G., Theuns, T., et al. 2004, MNRAS, 355, 995
D'Amico, N., Lyne, A. G., Manchester, R. N., Possenti, A., & Camilo, F. 2001, ApJ, 548, L171
Damjanov, I., McCarthy, P. J., Abraham, R. G., et al. 2009, ApJ, 695, 101
Dasyra, K. M., Tacconi, L. J., Davies, R. I., et al. 2006a, ApJ, 638, 745
Dasyra, K. M., Tacconi, L. J., Davies, R. I., et al. 2006b, ApJ, 651, 835
Dasyra, K. M., Tacconi, L. J., Davies, R. I., et al. 2006c, New Astron. Rev., 50, 720
Davé, R., Cen, R., Ostriker, J. P., et al. 2001, ApJ, 552, 473
Davies, R., & Kasper, M. 2012, ARA&A, 50, 305
Davies, R. I., Thomas, J., Genzel, R., et al. 2006, ApJ, 646, 754

Davies, R. L., Efstathiou, G., Fall, S. M., Illingworth, G., & Schechter, P. L. 1983, ApJ, 266, 41
Davis, T. A., Bureau, M., Cappellari, M., Sarzi, M., & Blitz, L. 2013, Nature, 494, 328
Decarli, R., Falomo, R., Treves, A., et al. 2010, MNRAS, 402, 2453
De Francesco, G., Capetti, A., & Marconi A. 2006, A&A, 460, 439
De Francesco, G., Capetti, A., & Marconi A. 2008, A&A, 479, 355
Dehnen, W. 1993, MNRAS, 265, 250
Dehnen, W. 1995, MNRAS, 274, 919
Dekel, A., & Birnboim, Y. 2006, MNRAS, 368, 2
Dekel, A., & Birnboim, Y. 2008, MNRAS, 383, 119
Dekel, A., & Silk, J. 1986, ApJ, 303, 39
De Rijcke, S., Prugniel, P., Simien, F., & Dejonghe, H. 2006, MNRAS, 369, 1321
Desroches, L.-B., & Ho, L. C. 2009, ApJ, 690, 267
Desroches, L.-B., Greene, J. E., & Ho, L. C. 2009, ApJ, 698, 1515
de Vaucouleurs, G. 1948, Ann. Astrophys., 11, 247
de Vaucouleurs, G. 1961, ApJS, 6, 213
de Vaucouleurs, G., de Vaucouleurs, A., Corwin, H. G., et al. 1991, Third Reference Catalogue of Bright Galaxies (Berlin: Springer) (RC3)
Devereux, N., Ford, H., Tsvetanov, Z., & Jacoby, G. 2003, AJ, 125, 1226
Diamond-Stanic, A. M., Moustakas, J., Tremonti, C. A., et al. 2012, ApJ, 755, L26
Diehl, S., & Statler, T. S. 2008a, ApJ, 680, 897
Diehl, S., & Statler, T. S. 2008b, ApJ, 687, 986
Djorgovski, S. 1992, in Morphological and Physical Classification of Galaxies, ed. G. Longo, M. Capaccioli, & G. Busarello (Dordrecht: Kluwer), 337
Djorgovski, S., & Davis, M. 1987, ApJ, 313, 59
Djorgovski, S., de Carvalho, R., & Han, M.-S. 1988, in The Extragalactic Distance Scale, ed. S. van den Bergh & C. J. Pritchet (San Francisco: ASP), 329
Dong, R., Greene, J. E., & Ho, L. C. 2012, ApJ, 761, 73
Dong, X.-B., Ho, L. C., Yuan, W., et al. 2012, ApJ, 755, 167
Doyon, R., Wells, M., Wright, G. S., Joseph, R. D., Nadeau, D., & James, P. A. 1994, ApJ, 437, L23
Dressler, A. 1989, in IAU Symposium 134, Active Galactic Nuclei, ed. D. E. Osterbrock & J. S. Miller (Dordrecht: Kluwer), 217
Dressler, A., Lynden-Bell, D., Burstein, D., et al. 1987, ApJ, 313, 42
Dressler, A., & Richstone, D. O. 1988, ApJ, 324, 701
Dressler, A., & Richstone, D. O. 1990, ApJ, 348, 120
Dressler, A., & Sandage, A. 1983, ApJ, 265, 664
D'Souza, R., & Rix, H.-W. 2013, MNRAS, 429, 1887
Duncan, M. J., & Wheeler, J. C. 1980, ApJ, 237, L27
Dutton, A. A., Conroy, C., van den Bosch, F. C., Prada, F., & More, S. 2010, MNRAS, 407, 2
Dutton, A. A., Conroy, C., van den Bosch, F. C., et al. 2011, MNRAS, 416, 322
Dwek, E., Arendt, R. G., Hauser, M. G., et al. 1995, ApJ, 445, 716
Ebisuzaki, T., Makino, J., & Okamura, S. K. 1991, Nature, 354, 212
Eckart, A., & Genzel, R. 1997, MNRAS, 284, 576
Edri, H., Rafter, S. E., Chelouche, D., Kaspi, S., & Behar, E. 2012, ApJ, 756, 73
Ellis, S. C., & O'Sullivan, E. 2006, MNRAS, 367, 627
Elmegreen, B. G., Bournaud, F., & Elmegreen, D. M. 2008a, ApJ, 684, 829
Elmegreen, B. G., Bournaud, F., & Elmegreen, D. M. 2008b, ApJ, 688, 67
Elmegreen, B. G., & Elmegreen, D. M. 2005, ApJ, 627, 632
Elmegreen, B. G., Elmegreen, D. M, Fernandez, M. X., & Lemonias, J. J. 2009a, ApJ, 692, 12
Elmegreen, D. M., Elmegreen, B. G, Marcus, M. T., et al. 2009b, ApJ, 701, 306
Elmegreen, D. M., Elmegreen, B. G, Ravindranath, S., & Coe, D. A. 2007, ApJ, 658, 763
Emsellem, E., Bacon, R., & Monnet, G. 1995, in IAU Colloquium 149, Tridimensional Optical Spectroscopic Methods in Astrophysics, ed. G. Comte & M. Marcelin (San Francisco: ASP), 282
Emsellem, E., Cappellari, M., Krajnović, D., et al. 2007, MNRAS, 379, 401

Emsellem, E., Cappellari, M., Krajnović, D., et al. 2011, MNRAS, 414, 888
Emsellem, E., Cappellari, M., Peletier, R. F., et al. 2004, MNRAS, 352, 721
Emsellem, E., & Combes, F. 1997, A&A, 323, 674
Emsellem, E., Dejonghe, H., & Bacon, R. 1999, MNRAS, 303, 495
Emsellem, E., Monnet, G., Bacon, R., & Nieto, J.-L. 1994, A&A, 285, 739
Erwin, P., Graham, A. W., & Caon, N. 2004, in Carnegie Observatories Astrophysics Series, Vol. 1: Coevolution of Black Holes and Galaxies, ed. L. C. Ho (Cambridge: Cambridge Univ. Press), 12
Erwin, P., Vega Beltrán, J. C., Graham, A. W., & Beckman, J. E. 2003, ApJ, 597, 929
Eskridge, P. B., Frogel, J. A., Pogge, R. W., et al. 2000, AJ, 119, 536
Evans, N. W., & de Zeeuw, P. T. 1994, MNRAS, 271, 202
Fabello, S., Kauffmann, G., Catinella, B., et al. 2011, MNRAS, 416, 1739
Faber, S. M., Balick, B., Gallagher, J. S., & Knapp, G. R. 1977, ApJ, 214, 383
Faber, S. M., Dressler, A., Davies, R. L., et al. 1987, in Nearly Normal Galaxies: From the Planck Time to the Present, ed. S. M. Faber (New York: Springer), 175
Faber, S. M., & Jackson, R. E. 1976, ApJ, 204, 668
Faber, S. M., Tremaine, S., Ajhar, E. A., et al. 1997, AJ, 114, 1771
Faber, S. M., Willmer, C. N. A., Wolf, C., et al. 2007, ApJ, 665, 265
Faber, S. M., Worthey, G., & Gonzalez, J. J. 1992, in IAU Symposium 149, The Stellar Populations of Galaxies, ed. B. Barbuy & A. Renzini (Dordrecht: Kluwer), 255
Fabian, A. C. 1994, ARA&A, 32, 277
Fabian, A. C. 1999, MNRAS, 308, L39
Fabian, A. C. 2012, ARA&A, 50, 455
Fabian, A. C. 2013, in IAU Symposium 290, Feeding Compact Objects: Accretion on All Scales, ed. C. M. Zhang, T. Belloni, M. Mendez & S. N. Zhang (Cambridge: Cambridge Univ. Press), 3 (arXiv:1211.2146)
Fabian, A. C., Sanders, J. S., Allen, S. W., et al. 2003, MNRAS, 344, L43
Fabian, A. C., Sanders, J. S., Allen, S. W., et al. 2011, MNRAS, 418, 2154
Fabian, A. C., Sanders, J. S., Taylor, G. B., et al. 2006, MNRAS, 366, 417
Faltenbacher, A., Finoguenov, A., & Drory, N. 2010, ApJ, 712, 484
Feldmann, R., Carollo, C. M., Mayer, L., et al. 2010, ApJ, 709, 218
Ferrarese, L. 2002, ApJ, 578, 90
Ferrarese, L., Côté, P., Dalla Bontà, E., et al. 2006, ApJ, 644, L21
Ferrarese, L., & Ford, H. 2005, SSRev, 116, 523
Ferrarese, L., & Ford, H. C. 1999, ApJ, 515, 583
Ferrarese, L., Ford, H. C., & Jaffe, W. 1996, ApJ, 470, 444
Ferrarese, L., & Merritt, D. 2000, ApJ, 539, L9
Filippenko, A. V., & Ho, L. C. 2003, ApJ, 588, L13
Filippenko, A. V., Ho, L. C., & Sargent W. L. W. 1993, ApJ, 410, L75
Fisher, D. 1997, AJ, 113, 950
Fisher, D. , Illingworth, G., & Franx, M. 1995, ApJ, 438, 539
Fisher, D. B., & Drory, N. 2008, AJ, 136, 773
Fisher, D. B., & Drory, N. 2010, ApJ, 716, 942
Forbes, D. A., Brodie, J. P., & Grillmair, C. J. 1997, AJ, 113, 1652
Ford, H. C., Harms, R. J., Tsvetanov, Z. I., et al. 1994, ApJ, 435, L27
Forman, W., Jones, C., Churazov, E., et al. 2007, ApJ, 665, 1057
Forman, W., Nulsen, P., Heinz, S., et al. 2005, ApJ, 635, 894
Förster Schreiber, N. M., Genzel, R., Bouché, N., et al. 2009, ApJ, 706, 1364
Freeman, K. C. 1970, ApJ, 160, 811
Freeman, K. C. 2008, in Formation and Evolution of Galaxy Disks, ed. J. G. Funes, & E. M. Corsini (San Francisco, CA: ASP), 3
Fryer, C. L., Woosley, S. E., & Heger, A. 2001, ApJ, 550, 372
Gallimore, J. F., Baum, S. A., O'Dea, C. P., Brinks, E., & Pedlar, A. 1996, ApJ, 462, 740
Gaskell, C. M. 2010, in The First Stars and Galaxies: Challenges for the Next Decade, ed. D. J. Whalen,

V. Bromm, & N. Yoshida (Melville, NY: AIP), 261
Gaskell, C. M. 2011, in SF2A-2011: Proceedings of the Annual Meeting of the French Society of Astronomy and Astrophysics, ed. G. Alecian, K. Belkacem, R. Samadi, & D. Valls-Gabaud (Paris: SF2A), 577
Gebhardt, K. 2004, in Carnegie Observatories Astrophysics Series, Vol. 1: Coevolution of Black Holes and Galaxies, ed. L. C. Ho (Cambridge: Cambridge Univ. Press), 37
Gebhardt, K., Adams, J., Richstone, D., et al. 2011, ApJ, 729, 119
Gebhardt, K., Bender, R., Bower, G., et al. 2000a, ApJ, 539, L13
Gebhardt, K., Kormendy, J., Ho, L. C., et al. 2000b, ApJ, 543, L5
Gebhardt, K., Lauer, T. R., Kormendy, J., et al. 2001, AJ, 122, 2469
Gebhardt, K., Lauer, T. R., Pinkney, J., et al. 2007, ApJ, 671, 1321
Gebhardt, K., Pryor, C., O'Connell, R. D., Williams, T. B., & Hesser, J. E. 2000c, AJ, 119, 1268
Gebhardt, K., Rich, R. M., & Ho, L. C. 2002, ApJ, 578, L41
Gebhardt, K., Rich, R. M., & Ho, L. C. 2005, ApJ, 634, 1093
Gebhardt, K., Richstone, D., Ajhar, E. A., et al. 1996, AJ, 112, 105
Gebhardt, K., Richstone, D., Kormendy, J., et al. 2000d, AJ, 119, 1157
Gebhardt, K., Richstone, D., Tremaine, S., et al. 2003, ApJ, 583, 92
Gebhardt, K., & Thomas, J. 2009, ApJ, 700, 1690
Gebhardt, K., et al. 2013, in preparation
Genzel, R., Burkert, A., Bouché, N., et al. 2008, ApJ, 687, 59
Genzel, R., Eckart, A., Ott, T., & Eisenhauer, F. 1997, MNRAS, 291, 219
Genzel, R., Eisenhauer, F., & Gillessen, S. 2010, Rev. Mod. Phys., 82, 3121 (GEG10)
Genzel, R., Hollenbach, D., & Townes, C. H. 1994, Rep. Prog. Phys., 57, 417
Genzel, R., Lutz, D., Sturm, E., et al. 1998, ApJ, 498, 579
Genzel, R., Newman, S., Jones, T., et al. 2011, ApJ, 733, 101
Genzel, R., Pichon, C., Eckart, A., Gerhard, O. E, & Ott T. 2000, MNRAS, 317, 348
Genzel, R., Tacconi, L. J., Rigopoulou, D., Lutz, D., & Tecza, M. 2001, ApJ, 563, 527
Genzel, R., Thatte, N., Krabbe, A., Kroker, H., & Tacconi-Garman, L. E. 1996, ApJ, 472, 153
Genzel, R., & Townes, C. H. 1987, ARA&A, 25, 377
Gerhard, O. 2013, in IAU Symposium 295, The Intriguing Live of Massive Galaxies, ed. D. Thomas, A. Pasquali, & I. Ferreras (Cambridge: Cambridge University Press), in press (arXiv:1212.2768)
Gerhard, O. E., & Binney, J. 1985, MNRAS, 216, 467
Gerssen, J., van der Marel, R. P., Gebhardt, K., et al. 2002, AJ, 124, 3270.
Gerssen, J., van der Marel, R. P., Gebhardt, K., et al. 2003, AJ, 125, 376
Ghez, A. M., Becklin, E., Duchêne, G., et al. 2003, AN Suppl. 1, 324, 527
Ghez, A. M., Klein, B. L., Morris, M., & Becklin, E. E. 1998, ApJ, 509, 678
Ghez, A., Morris, M., Lu, J., et al. 2009, Astro2010, 89 (arXiv:0903.0383)
Ghez, A. M., Salim, S., Hornstein, S. D., et al. 2005, ApJ, 620, 744
Ghez, A. M., Salim, S., Weinberg, N. N, et al. 2008, ApJ, 689, 1044
Gillessen, S., Eisenhauer, F., Fritz, T. K., et al. 2009a, ApJ, 707, L114
Gillessen, S., Eisenhauer, F., Trippe, S., et al. 2009b, ApJ, 692, 1075
Gliozzi, M., Satyapal, S., Eracleous, M., Titarchuk, L., & Cheung, C. C. 2009, ApJ, 700, 1759
Goodman, J., & Binney, J. 1984, MNRAS, 207, 511
Gould, A., & Rix, H.-W. 2000, ApJ, 532, L29
Graham, A. W. 2004, ApJ, 613, L33
Graham, A. W. 2007, MNRAS, 379, 711
Graham, A. W. 2008a, ApJ, 6580, 143
Graham, A. W. 2008b, PAS Australia, 25, 167
Graham, A. W. 2012, MNRAS, 422, 1586
Graham, A. W., Colless, M.M., Busarello, G., Zaggia, S., & Longo, G. 1998, A&AS, 133, 325
Graham, A. W., & Driver, S. P. 2007, ApJ, 655, 77
Graham, A. W., Erwin, P., Caon, N., & Trijillo, I. 2001, ApJ, 563, L11
Graham, A. W., & Li, I.-H. 2009, ApJ, 698, 812
Graham, A. W., Onken, C. A., Athanassoula, E., & Combes, F. 2011, MNRAS, 412, 2211

Graham, A. W., & Scott, N. 2013, ApJ, 764, 151
Graham, A. W., & Spitler, R. L. 2009, MNRAS, 397, 2148
Granato, G. L., De Zotti, G., Silva, L., Bressan, A., & Danese, L. 2004, ApJ, 600, 580
Graves, G. J., & Faber, S. M. 2010, ApJ, 717, 803
Greene, J. E. 2012, Nature Communications, 3, 1304
Greene, J. E., & Ho, L. C. 2004, ApJ, 610, 722
Greene, J. E., & Ho, L. C. 2005a, ApJ, 627, 721
Greene, J. E., & Ho, L. C. 2005b, ApJ, 630, 122
Greene, J. E., & Ho, L. C. 2006a, ApJ, 641, 117
Greene, J. E., & Ho, L. C. 2006b, ApJ, 641, L21
Greene, J. E., & Ho, L. C. 2007a, ApJ, 656, 84
Greene, J. E., & Ho, L. C. 2007b, ApJ, 667, 131
Greene, J. E., & Ho, L. C. 2007c, ApJ, 670, 92
Greene, J. E., Ho, L. C, & Barth, A. J. 2008, ApJ, 688, 159
Greene, J. E., Ho, L. C, & Ulvestad, J. S. 2006, ApJ, 636, 56
Greene, J. E., Peng, C. Y., Kim, M., et al. 2010, ApJ, 721, 26
Greenhill, L. J. 2007, in IAU Symposium 242, Astrophysical Masers and their Environments, ed. J. M. Chapman, & W. A. Baan (Cambridge: Cambridge Univ. Press), 381
Greenhill, L. J., Booth, R. S., Ellingsen, S. P., et al. 2003, ApJ, 590, 162
Greenhill, L. J., & Gwinn, C. R. 1997, ApSS, 248, 261
Greenhill, L. J., Gwinn, C. R, Antonucci, R., & Barvainis, R. 1996, ApJ, 472, L21
Greenhill, L. J., Kondratko, P. T., Moran, J. M., & Tilak, A. 2009, ApJ, 707, 787
Greenhill, L. J., Moran, J. M., & Herrnstein, J. R. 1997, ApJ, 481, L23
Gualandris, A., & Merritt, D. 2008, ApJ, 678, 780
Gültekin, K., Cackett, E. M., Miller, J. M., et al. 2009a, ApJ, 706, 404
Gültekin, K., Richstone, D. O., Gebhardt, K., et al. 2009b, ApJ, 695, 1577
Gültekin, K., Richstone, D. O., Gebhardt, K., et al. 2009c, ApJ, 698, 198
Gültekin, K., Richstone, D. O., Gebhardt, K., et al. 2011, ApJ, 741, 38
Gunn, J. E. 1987, in IAU Symposium 117, Dark Matter in the Universe, ed. J. Kormendy & G. R. Knapp (Dordrecht: Reidel), 537
Guo, Q., White, S., Li, C., & Boylan-Kolchin, M. 2010, MNRAS, 404, 1111
Haller, J. W., Rieke, M. J., Rieke, G. H., et al. 1996, ApJ, 456, 194
Hansen, S. M., Sheldon, E. S., Wechsler, R. H., & Koester, B. P. 2009, ApJ, 699, 1333
Häring, N., & Rix, H.-W. 2004, ApJ, 604, L89
Häring-Neumayer, N., Cappellari, M., Rix, H.-W., et al. 2006, ApJ, 643, 226
Harms, R. J., Ford, H. C., Tsvetanov, Z. I., et al. 1994, ApJ, 435, L35
Harris, C. E., Bennert, V. N., Auger, M. W., et al. 2012, ApJS, 201, 29
Harris, G. L. H., & Harris, W. E. 2011, MNRAS, 410, 2347
Harris, W. E. 1991, ARA&A, 29, 543
Harris, W. E, Whitmore, B. C., Karakla, D., et al. 2006, ApJ, 626, 90
Haschick, A. D., Baan, W. A., & Peng, E. W. 1994, ApJ, 437, L35
Heckman, T. M., Kauffmann, G., Brinchmann, J., et al. 2004, ApJ, 613, 109
Heger, A., Fryer, C. L., Woosley, S. E., Langer, N., & Hartmann, D. H. 2003, ApJ, 591, 288
Henkel, C., Braatz, J. A., Greenhill, L. J., & Wilson, A. S. 2002, A&A, 394, L23
Héraudeau, Ph., Simien, F., Maubon, G., & Prugniel, Ph. 1999. A&AS, 136, 509
Herrnstein, J. R., Moran, J. M., Greenhill, L. J., et al. 1999,Nature, 400, 539
Herrnstein, J. R., Moran, J. M., Greenhill, L. J., & Trotter, A. S. 2005, ApJ, 629, 719
Hicks, E. K. S., & Malkan, M. A. 2008, ApJS, 174, 31
Hilz, M., Naab, T., & Ostriker, J. P. 2013, MNRAS, 429, 2924
Hilz, M., Naab, T., Ostriker, J. P., et al. 2012, MNRAS, 425, 3119
Hiner, K. D., Canalizo, G., Wold, M., Brotherton, M. S., & Cales, S. L. 2012, ApJ, 756, 162
Hinshaw, G., Larson, D., Komatsu, E., et al. 2013, ApJS, in press (arXiv:1212.5226)
Hirschmann, M., Khochfar, S., Burkert, A., et al. 2010, MNRAS, 407, 1016

Ho, L. C. 1999a, in Observational Evidence for Black Holes in the Universe, ed. S. K. Chakrabarti (Dordrecht: Kluwer), 157
Ho, L. C. 1999b, ApJ, 510, 631
Ho, L. C. 1999c, ApJ, 516, 672
Ho, L. C. 2002, ApJ, 564, 120
Ho, L. C, ed. 2004a, Carnegie Observatories Astrophysics Series, Vol. 1: Coevolution of Black Holes and Galaxies (Cambridge: Cambridge Univ. Press)
Ho, L. C. 2004b, in Carnegie Observatories Astrophysics Series, Vol. 1: Coevolution of Black Holes and Galaxies, ed. L. C. Ho (Cambridge: Cambridge Univ. Press), 293
Ho, L. C. 2005, ApJ, 629, 680
Ho, L. C. 2007a, ApJ, 668, 94
Ho, L. C. 2007b, ApJ, 669, 821
Ho, L. C. 2008, ARA&A, 46, 475
Ho, L. C. 2009a, ApJ, 699, 626
Ho, L. C. 2009b, ApJ, 699, 638
Ho, L. C. 2013, ApJ, in preparation
Ho, L. C., Darling, J., & Greene, J. E. 2008, ApJ, 681, 128
Ho, L. C., & Filippenko, A. V. 1996, ApJ, 472, 600
Ho, L. C., Filippenko, A. V., & Sargent, W. L. W. 1997a, ApJS, 112, 315
Ho, L. C., Filippenko, A. V., & Sargent, W. L. W. 1997b, ApJ, 487, 568
Ho, L. C., Filippenko, A. V., & Sargent, W. L. W. 2003, ApJ, 583, 159
Ho, L. C., Greene, J. E., Filippenko, A. V., & Sargent, W. L. W. 2009, ApJS, 183, 1
Ho, L. C., Kim, M., & Terashima, Y. 2012, ApJ, 759, L16
Ho, L. C., Sarzi, M., Rix, H.-W., et al. 2002, PASP, 114, 137
Ho, L. C., Terashima, Y., & Okajima, T. 2003, ApJ, 587, L35
Holley-Bockelmann, K., & Richstone, D. 1999, ApJ, 517, 92
Holley-Bockelmann, K., & Richstone, D. 2000, ApJ, 531, 232
Hopkins, A. M. 2004, ApJ, 615, 209
Hopkins, P. F., Bundy, K., Hernquist, L., Wuyts, S., & Cox, T. J. 2010, MNRAS, 401, 1099
Hopkins, P. F., Bundy, K., Murray, N., et al. 2009a, MNRAS, 398, 898
Hopkins, P. F., Cox, T. J., Dutta, S. N., et al. 2009b, ApJS, 181, 135
Hopkins, P. F., & Hernquist, L. 2009, ApJ, 694, 599
Hopkins, P. F., & Hernquist, L. 2010, MNRAS, 407, 447
Hopkins, P. F., Hernquist, L., Cox, T. J., Dutta, S. N., & Rothberg, B. 2008, ApJ, 679, 156
Hopkins, P. F., Hernquist, L., Cox, T. J., Robertson, B., & Krause, E. 2007a, ApJ, 669, 45
Hopkins, P. F., Hernquist, L., Cox, T. J., Robertson, B., & Krause, E. 2007b, ApJ, 669, 67
Hopkins, P. F., Hernquist, L., Cox, T. J., et al. 2006, ApJS, 163, 1
Hopkins, P. F., Lauer, T. R., Cox, T. J., Hernquist, L., & Kormendy, J. 2009c, ApJS, 181, 486
Houghton, R. C. W., Magorrian, J., Sarzi, M., et al. 2006, MNRAS, 367, 2
Howard, C. D., Rich, R. M., Clarkson, W., et al. 2009, ApJ, 702, L153
Hoyle, F., & Fowler, W. A. 1963, Nature, 197, 533
Hu, J. 2008, MNRAS, 386, 2242
Huang, S., Ho, L. C., Peng, C. Y., Li, Z.-Y., & Barth, A. J. 2013a, ApJ, 766, 47
Huang, S., Ho, L. C., Peng, C. Y., Li, Z.-Y., & Barth, A. J. 2013b, ApJL, in press (arXiv:1304.2299)
Hubble, E. 1930, ApJ, 71, 231
Hughes, M. A., Axon, D., Atkinson, J., et al. 2005, AJ, 130, 73
Humphreys, E. M. L., Reid, M. J., Greenhill, L. J., Moran, L. M., & Argon, A. L. 2008, ApJ, 672, 800
Huré, J.-M. 2002, A&A, 395, L21
Huré, J.-M., Hersant, F., Surville, C., Nakai, N., & Jacq, T. 2011, A&A, 530, 145
Illingworth, G. 1977, ApJ, 218, L43
Inskip, K. J., Jahnke, K., Rix, H.-W., & van de Ven, G. 2011, ApJ, 739, 90
Into, T., & Portinari, L. 2013, MNRAS, 430, 2715
Ishihara, Y., Nakai, N., Iyomoto, N., et al. 2001, PASJ, 53, 215

Jahnke, K., Bongiorno, A., Brusa, M., et al. 2009, ApJ, 706, L215
Jahnke, K., & Macciò, A. V. 2011, ApJ, 734, 92
Jalali, B., Baumgardt, H., Kissler-Patig, M., et al. 2011, A&A, 538, A19
Jardel J., Gebhardt, K., Shen, J., et al. 2011, ApJ, 739, 21
Jarrett, T. H., Chester, T., Cutri, R., Schneider, S. E., & Huchra, J. P. 2003, AJ, 125, 525
Jarvis, B. J., & Freeman, K. C., 1985, ApJ, 295, 324
Jiang, Y.-F., Greene, J. E., & Ho, L. C. 2011a, ApJ, 737, L45
Jiang, Y.-F., Greene, J. E., Ho, L. C., Xiao, T., & Barth, A. J. 2011b, ApJ, 742, 68
Johnson, H. L. 1962, ApJ, 135, 69
Jones, D. H., Mould, J. R., Watson, A. M., et al. 1996, ApJ, 466, 742
Jørgensen, I., Franx, M., & Kjærgaard, P. 1996, MNRAS, 280, 167
Joseph, C. L., Merritt, D., Olling, R., et al. 2001, ApJ, 550, 668
Joseph, R. D. 1999, Ap&SS, 266, 321
Joseph, R. D., & Wright, G. S. 1985, MNRAS, 214, 87
Kamizasa, N., Terashima, Y., & Awaki, H. 2012, ApJ, 751, 39
Karachentsev, I. D., Karachentseva, V. E., Huchtmeier, W. K., & Makarov, D. I. 2004, AJ, 127, 2031
Kassin, S. A., Weiner, B. J., Faber, S. M., et al. 2012, ApJ, 758, 106
Kauffmann, G., & Haehnelt, M. 2000, MNRAS, 311, 576
Kauffmann, G.,& Heckman, T. M. 2009, MNRAS, 397, 135
Kauffmann, G., Heckman, T. M., Tremonti, C., et al. 2003, MNRAS, 346, 1055
Kennicutt, R. C. 1989, ApJ, 344, 685
Kennicutt, R. C. 1998a, ARA&A, 36, 189
Kennicutt, R. C. 1998b, in 26$^{\rm th}$ Advanced Course of the Swiss Society of Astronomy and Astrophysics, Galaxies: Interactions and Induced Star Formation, ed. D. Friedli, L. Martinet, & D. Pfenniger (New York: Springer), 1
Kennicutt, R. C, Lee, J. C., Funes, J. G., Sakai, S., & Akiyama, S. 2008, ApJS, 178, 247
Kent, S. M. 1990, AJ, 100, 377
Kent, S. M. 1992, ApJ, 387, 181
Kent, S. M, Dame, T. M., & Fazio, G. 1991, ApJ, 378, 131
Kent, S. M, & Gunn, J. E. 1982, AJ, 87, 945
Kereš, D., Katz, N., Weinberg, D. H., & Davé, R. 2005, MNRAS, 363, 2
Khochfar, S., & Ostriker, J. P. 2008, ApJ, 680, 54
Khochfar, S., & Silk, J., 2006, ApJ, 648, L21
Kim, E., Lee, M. G., & Geisler, D. 2000, MNRAS, 314, 307
Kim, M., Ho, L. C., Peng, C. Y., Barth, A. J., & Im, M. 2008, ApJS, 179, 283
Kim, M., Ho, L. C., Peng, C. Y., & Im, M. 2013, ApJ, in preparation
King, A. 2003, ApJ, 596, L27
Kinney, A. L., Schmitt, H. R., Clarke, C. J., et al. 2000, ApJ, 537, 152
Kobulnicky, H. A., Dickey, J. M., Sargent, A. I., Hogg, D. E., & Conti, P. S. 1995, AJ, 110, 116
Kocevski, D. D., Faber, S. M., Mozena, M., et al. 2012, ApJ, 744, 148
Komatsu, E., Dunkley, J., Nolta, M. R., et al. 2009, ApJS, 180, 330
Komossa, S. 2006, MemSAI, 77, 733
Kondratko, P. T., Greenhill, L. J., & Moran, J. M. 2005, ApJ, 618, 618
Kondratko, P. T., Greenhill, L. J., & Moran, J. M. 2006, ApJ, 652, 136
Kondratko, P. T., Greenhill, L. J., & Moran, J. M. 2008, ApJ, 678, 87
Kong, A. K. H., Heinke, C. O., di Stefano, R., et al. 2010, MNRAS, 407, L84
Kong, A. K. H., Yang, Y. J., Hsieh, P.-Y., Mak, D. S. Y., & Pun, C. S. J. 2007, ApJ, 671, 349
Körding, E., Colbert, E., & Falcke, H. 2005, A&A, 436, 427
Kormendy, J. 1977, ApJ, 217, 406
Kormendy, J. 1982, in Morphology and Dynamics of Galaxies, 12th Advanced Course of the Swiss Society of Astronomy and Astrophysics, ed. L. Martinet & M. Mayor (Sauverny: Geneva Obs.), 113
Kormendy, J. 1984, ApJ, 287, 577
Kormendy, J. 1985, ApJ, 295, 73

Kormendy, J. 1987, in Nearly Normal Galaxies: From the Planck Time to the Present, ed. S. M. Faber (Berlin: Springer), 163
Kormendy, J. 1988a, ApJ, 325, 128
Kormendy, J. 1988b, ApJ, 335, 40
Kormendy, J. 1992a, Testing the AGN Paradigm, ed. S. S. Holt, S. G. Neff, & C. M. Urry (New York: AIP), 23
Kormendy, J. 1992b, in High Energy Neutrino Astrophysics, ed. V. J. Stenger, J. G. Learned, S. Pakvasa, & X. Tata (Singapore: World Scientific), 196
Kormendy, J. 1993a, in The Nearest Active Galaxies, ed. J. Beckman, L. Colina, & H. Netzer (Madrid: Consejo Superior de Investigaciones Científicas), 197
Kormendy, J. 1993b, in IAU Symposium 153, Galactic Bulges, ed. H. Dejonghe & H. J. Habing (Dordrecht: Kluwer), 209
Kormendy, J. 1999, in Galaxy Dynamics: A Rutgers Symposium, ed. D. Merritt, J. A. Sellwood, & M. Valluri (San Francisco: ASP), 124
Kormendy, J. 2004, in Carnegie Observatories Astrophysics Series, Vol. 1: Coevolution of Black Holes and Galaxies, ed. L. C. Ho (Cambridge: Cambridge Univ. Press), 1
Kormendy, J. 2009, in Galaxy Evolution: Emerging Insights and Future Challenges, ed. S. Jogee, I. Marinova, L. Hao, & G. A. Blanc (San Francisco: ASP), 87
Kormendy, J. 2012, in XXIII Canary Islands Winter School of Astrophysics, Secular Evolution of Galaxies, ed. J. Falcón-Barroso & J. H. Knapen (Cambridge: Cambridge Univ. Press), in press
Kormendy, J. 2013, in IAU Symposium 295, The Intriguing Life of Massive Galaxies, ed. D. Thomas, A. Pasquali, & I. Ferreras (Cambridge: Cambridge University Press), in press
Kormendy, J., & Bender, R. 1999, ApJ, 522, 772
Kormendy, J., & Bender, R. 2009, ApJ, 691, L142
Kormendy, J., & Bender, R. 2011, Nature, 469, 377
Kormendy, J., & Bender, R. 2012, ApJS, 198, 2
Kormendy, J., & Bender, R. 2013a, ApJL, submitted
Kormendy, J., & Bender, R. 2013b, ApJS, in preparation
Kormendy, J., Bender, R., Ajhar, E. A., et al. 1996a, ApJ, 473, L91
Kormendy, J., Bender, R., & Cornell, M. E. 2011, Nature, 469, 374
Kormendy, J., Bender, R., Evans, A. S., & Richstone, D. 1998, AJ, 115, 1823
Kormendy, J., Bender, R., Magorrian, J., et al. 1997, ApJ, 482, L139
Kormendy, J., Bender, R., Richstone, D., et al. 1996b, ApJ, 459, L57
Kormendy, J., Byun, Y.-I., Ajhar, E. A., et al. 1996c, in IAU Symposium 171, New Light on Galaxy Evolution, ed. R. Bender & R. L. Davies (Dordrecht: Kluwer), 105
Kormendy, J., Drory, N., Bender, R., & Cornell, M. E. 2010, ApJ, 723, 54
Kormendy, J., Fisher, D. B., Cornell, M. E., & Bender, R. 2009, ApJS, 182, 216 (KFCB)
Kormendy, J., & Gebhardt, K. 2001, in 20$^{\rm th}$ Texas Symposium on Relativistic Astrophysics, ed. J. C. Wheeler & H. Martel (Melville, NY: AIP), 363
Kormendy, J., Gebhardt, K., Fisher, D. B., et al. 2005, AJ, 129, 2636
Kormendy, J., Gebhardt, K., & Richstone, D. 2000, BAAS, 32, 702
Kormendy, J., & Illingworth, G. 1982, ApJ, 256, 460
Kormendy, J., & Kennicutt, R. C. 2004, ARA&A, 42, 603
Kormendy, J., & McClure, R. D. 1993, AJ, 105, 1793
Kormendy, J., & Richstone, D. 1992, ApJ, 393, 559
Kormendy, J., & Richstone, D. O. 1995, ARA&A, 33, 581 (KR95)
Kormendy, J., & Sanders, D. B. 1992, ApJ, 390, L53
Krabbe, A., Genzel, R., Eckart, A., et al. 1995, ApJ, 447, L95
Krajnović, D., McDermid, R. M., Cappellari, M., & Davies, R. L. 2009, MNRAS, 399, 1839
Krajnović, D., Sharp, R., & Thatte, N. 2007, MNRAS, 374, 385
Kraljic, K., Bournaud, F., & Martig, M. 2012, ApJ, 757, 60
Kroupa, P. 2001, MNRAS, 322, 231
Kukula, M. J., Dunlop, J. S., McClure, R. J., et al. 2001, MNRAS, 326, 1533

Kulkarni, S. R., Hut, P., & McMillan, S. 1993, Nature, 364, 421
Kumar, P. 1999, ApJ, 519, 599
Kundu, A., Whitmore, B. C., Sparks, W. B., et al. 1999, ApJ, 513, 733
Kuo, C. Y., Braatz, J. A., Condon, J. J., et al. 2011, ApJ, 727, 20
Laor, A. 2001, ApJ, 553, 677
Larsen, S. S., Brodie, J. P., Huchra, J. P., Forbes, D. A., & Grillmair, C. J. 2001, AJ, 121, 2974
Larson, R. B. 2000, in ESLAB Symposium 33, Star Formation from the Small to the Large Scale, ed. F. Favata, A. Kaas, & A. Wilson (Noordwijk: European Space Agency), 13
Lauer, T. R. 1999, PASP, 111, 227
Lauer, T. R. 2012, ApJ, 759, 64
Lauer, T. R., Ajhar, E. A., Byun, Y.-I., et al. 1995, AJ, 110, 2622
Lauer, T. R., Bender, R., Kormendy, J., Rosenfield, P., & Green, R. F. 2012, ApJ, 745, 121
Lauer, T. R., Faber, S. M., Ajhar, E. A., Grillmair, C. J., & Scowen, P. A. 1998, AJ, 116, 2263
Lauer, T. R., Faber, S. M., Currie, D. G., et al. 1992, ApJ, 104, 522
Lauer, T. R., Faber, S. M., Gebhardt, K., et al. 2005, AJ, 129, 2138
Lauer, T. R., Faber, S. M., Groth, E. J., et al. 1993, AJ, 106, 1436
Lauer, T. R., Faber, S. M., Lynds, D. R., et al. 1992, AJ, 103, 703
Lauer, T. R., Faber, S. M., Richstone, D., et al. 2007a, ApJ, 662, 808
Lauer, T. R., Gebhardt, K., Faber, S. M., et al. 2007b, ApJ, 664, 226
Lauer, T. R., Gebhardt, K., Richstone, D.,et al. 2002, AJ, 124, 1975
Lauer, T. R., Tremaine, S., Richstone, D., & Faber, S. M. 2007c, ApJ, 670, 249
Launhardt, R., Zylka, R., & Mezger, P. G. 2002, A&A, 384, 112
Leauthaud, A., Tinker, J., Bundy, K., et al. 2012, ApJ 744, 159
Lee, H. M. 1995, MNRAS, 272, 605
Lee, H. M. 1996, in IAU Symposium 174, Dynamical Evolution of Star Clusters: Confrontation of Theory and Observations, ed. P. Hut & J. Makino (Dordrecht: Kluwer), 293
Lee, H. M. 1998, J. Korean Physical Society, 33, S549
Le Floc'h, E., Papovich, C., Dole, H., et al. 2005, ApJ, 632, 169
Lemaître, G. E. 1931, quoted in IAU Symposium 92, Objects of High Redshift, ed. G. O. Abell & P. J. E. Peebles (Dordrecht: Reidel), Frontispiece
Li, Y., Hernquist, L., Robertson, B., et al. 2007, ApJ, 665, 187
Liebling, S. L., & Palenzuela, C. 2012, Living Reviews in Relativity, 15, No. 6, cited 2012 October 4, **http://relativity.livingreviews.org/Articles/lrr-2012-6/**
Light, E. S., Danielson, R. E., & Schwarzschild, M. 1974, ApJ, 194, 257
Lin, Y.-T., & Mohr, J. J. 2004, ApJ, 617, 879
Lodato, G., & Bertin, G. 2003, A&A, 398, 517
Ludwig, R. R., Greene, J. E., Barth, A. J., & Ho, L. C. 2012, ApJ, 756, 51
Lützgendorf, N., Kissler-Patig, M., Gebhardt, K., et al. 2013, A&A, 552, A49
Lynden-Bell, D. 1969, Nature, 223, 690
Lynden-Bell, D. 1978, Physica Scripta, 17, 185
Lynden-Bell, D., & Rees, M. J. 1971, MNRAS, 152, 461
Maccarone, T. J., Bergond, G., Kundu, A., et al. 2007, in IAU Symposium 246, Dynamical Evolution of Dense Stellar Systems, ed. E. Vesperini, M. Giersz, & A. Sills (Cambridge: Cambridge Univ. Press), 336
Maccarone, T. J., Kundu, A., Zepf, S. E., & Rhode, K. L. 2010, MNRAS, 409, L84
Macchetto, F., Marconi, A., Axon, D. J., et al. 1997, ApJ, 489, 579
Maciejewski, W., & Binney, J. 2001, MNRAS, 323, 831
Madau, P., & Rees, M. J. 2001, ApJ, 551, L27
Magorrian, J., Tremaine, S., Richstone, D., et al. 1998, AJ, 115, 2285
Maiolino, R., Gallerani, S., Neri, R., et al. 2012, MNRAS, 425, L66
Maiolino, R., Krabbe, A., Thatte, N., & Genzel, R. 1998, ApJ, 493, 650
Makino, J., & Ebisuzaki, T. 1996, ApJ, 465, 527
Makino, J., & Funato, Y. 2004, ApJ, 602, 93
Mamyoda, K., Nakai, N., Yamauchi, A., Diamond, P., & Huré, J.-M. 2009, PASJ, 61, 1143

Maoz, E. 1995, ApJ, 447, L91
Maoz, E. 1998, ApJ, 494, L181
Marconi, A., Axon, D. J., Capetti, A., Maciejewski, W., & Atkinson, J. 2003, ApJ, 586, 868
Marconi, A., Capetti, A., Axon, D. J., et al. 2001, ApJ, 549, 915
Marconi, A., & Hunt, L. K. 2003, ApJ, 589, L21
Marconi, A., Pastorini, G., Pacini, F., et al. 2006, A&A, 448, 921
Marconi, A., Risaliti, G., Gilli, R., et al. 2004, MNRAS, 351, 169
Martig, M., Bournaud, F., Croton, D. J., Dekel, A., & Teyssier, R. 2012, ApJ, 756, 26
Martin, D. C., Wyder, T. K., Schiminovich, D., et al. 2007, ApJ, 173, 342
Marziani, P., & Sulentic, J. 2012, NewAR, 56, 49
Matković, A., & Guzmán, R. 2005, MNRAS, 362, 289
Matteucci, F. 1994, A&A, 288, 57
McAlpine, W., Satyapal, S., Gliozzi, M., et al. 2011, ApJ, 728, 25
McConnell, N. J., & Ma, C.-P. 2013, ApJ, 764, 184
McConnell, N. J., Ma, C.-P., Gebhardt, K., et al. 2011a, Nature, 480, 215
McConnell, N. J., Ma, C.-P., Graham, J. R., et al. 2011b, ApJ, 728, 100
McConnell, N. J., Ma, C.-P., Murphy, J. D., et al. 2012, ApJ, 756, 179
McDermid, R. M., Emsellem, E., Shapiro, K. L. et al. 2006, MNRAS, 373, 906
McLeod, K. K., & Bechtold, J. 2009, ApJ, 704, 415
McLure, R. J., & Dunlop, J. S. 2002, MNRAS, 331, 795
McLure, R. J., Jarvis, M. J., Targett, T. A., Dunlop, J. S., & Best, P. N. 2006, MNRAS, 368, 1395
McNamara, B. R., & Nulsen, P. E. J. 2007, ARA&A, 45, 117
McNamara, B. R., & Nulsen, P. E. J. 2012, New J. Phys., 14, 055023
Mechtley, M., Windhorst, R. A., Ryan, R. E., et al. 2012, ApJ, 756, L38
Mei, S., Blakeslee, J. P., Côté, P., et al. 2007, ApJ, 655, 144
Meier, D. S., Turner, J. L., Crosthwaite, L. P., & Beck, S. C. 2001, AJ, 121, 740
Melia, F. 2007, The Galactic Supermassive Black Hole (Princeton: Princeton Univ. Press)
Melia, F., & Falcke, H. 2001, ARA&A, 39, 309
Méndez-Abreu, J., Aguerri, J. A. L., Corsini, E. M., & Simonneau, E. 2008, A&A, 478, 353
Merloni, A., Bongiorno, A., Bolzonella, M., et al. 2010, ApJ, 708, 137
Merloni, A., Heinz, S., & Di Matteo, T. 2003, MNRAS, 345, 1057
Merritt, D. 1999, PASP, 111, 129
Merritt, D. 2006, ApJ, 648, 976
Merritt, D., & Cruz, F. 2001, ApJ, 551, L41
Merritt, D., & Ferrarese, L. 2001, MNRAS, 320, L30
Merritt, D., Ferrarese, L., & Joseph, C. J. 2001, Science, 293, 1116
Merritt, D., Mikkola, S., & Szell, A. 2007, ApJ, 671, 53
Merritt, D., & Milosavljević, M. 2005, Living Reviews in Relativity, 8, No. 8, cited 2012 October 23, **http://www.livingreviews.org/lrr-2005-8**
Merritt, D., Milosavljević, M., Favata, M., Hughes, S. A., & Holz, D. E. 2004, ApJ, 607, L9
Merritt, D., & Quinlan, G. D. 1998, ApJ, 498, 625
Meyer, L., Ghez, A. M., Schödel, R., et al. 2012, Science, 338, 84
Mihalas, D., & Routly, P. M. 1968, Galactic Astronomy (San Francisco: Freeman)
Mihos, J. C., & Hernquist, L. 1994, ApJ, 437, L47
Miller, M. C., & Colbert, E. J. M. 2004, International J. Mod. Phys. D, 13, 1
Miller-Jones, J. C. A., Wrobel, J. M., Sivakoff, G. R., et al. 2012, ApJ, 755, L1
Milosavljević, M., & Merritt, D. 2001, ApJ, 563, 34
Milosavljević, M., & Merritt, D. 2003, in AIP Conference Proceedings No. 686, The Astrophysics of Gravitational Wave Sources, ed. J. M. Centrella (Melville, NY: AIP), 201
Milosavljević, M., Merritt, D., Rest, A., & van den Bosch, F. C. 2002, MNRAS, 331, L51
Miniutti, G., Ponti, G., Greene, J. E., et al. 2009, MNRAS, 394, 443
Mirabel, I. F., Sanders, D. B., & Kazès, I. 1989, ApJ, 340, L9
Miyoshi, M., Moran, J., Herrnstein, J., et al. 1995, Nature, 373, 127

Möllenhoff, C., Matthias, M., & Gerhard, O. E. 1995, A&A, 301, 359
Monachesi, A., Trager, S. C., Lauer, T. R., et al. 2011, ApJ, 727, 55
Moore, B., Ghigna, S., Governato, F., et al. 1999, ApJ, 524, L19
Moran, J. M. 2008, in Frontiers of Astrophysics: A Celebration of NRAO's 50$^{\rm th}$ Anniversary, ed. A. H. Bridle, J. J. Condon, & G. C. Hunt (San Francisco: ASP), 87
Mortlock, D. J., Warren, S. J., Venemans, B. P., et al. 2011, Nature, 474, 616
Moster, B. P., Naab, T., & White, S. D. M. 2013, MNRAS, 428, 3121
Moster, B. P., Somerville, R. S., Maulbetsch, C., van den Bosch, F. C., Macciò, A. V., Naab, T., & Oser, L. 2010, ApJ, 710, 903
Mouhcine, M., Ferguson, H. C., Rich, R. M., Brown, T. M., & Smith, T. E. 2005, ApJ, 633, 810
Mould, J., & Sakai, S. 2008, ApJ, 686, L75
Müller-Sánchez, F., Davies, R. I., Eisenhauer, F., et al. 2006, A&A, 454, 481
Mundell, C. G., Pedlar, A., Axon, D. J., Meaburn, J., & Unger, S. W. 1995, MNRAS, 277, 641
Murray, N., Quataert, E., & Thompson, T. A. 2005, ApJ, 618, 569
Naab, T., 2013, in IAU Symposium 295, The Intriguing Life of Massive Galaxies, ed. D. Thomas, A. Pasquali, & I. Ferreras (Cambridge: Cambridge University Press), in press (arXiv:1211.6892)
Naab, T., Johansson, P. H., & Ostriker, J. P. 2009, ApJ, 699, L178
Nagino, R., & Matsushita, K. 2009, A&A, 501, 157
Nandra, K., Georgakakis, A., Willmer, C. N. A., et al. 2007, ApJ, 660, L11
Navarro, J. F., Frenk, C. S., & White, S. D. M. 1997, ApJ, 490, 493
Nesvadba, N. P. H., Boulanger, F., Salomé, P., et al. 2010, A&A, 521, A65
Nesvadba, N. P. H., Lehnert, M. D., De Breuck, C., Gilbert, A. M., & van Breugel, W. 2008, A&A, 491, 407
Nesvadba, N. P. H., Lehnert, M. D., Eisenhauer, F., et al. 2006, ApJ, 650, 693
Neumayer, N., Cappellari, M., Reunanen, J., et al. 2007, ApJ, 671, 1329
Neumayer, N., & Walcher, C. J. 2012, Adv. Astron., 2012, 709038
Newman, S. F., Genzel, R., Förster-Schreiber, N. M., et al. 2012, ApJ, 761, 43
Nipoti, C., & Binney, J. 2007, MNRAS, 382, 1481
Noel-Storr, J., Baum, S. A., & O'Dea, C. P. 2007, ApJ, 663, 71
Noel-Storr, J., Baum, S. A., Verdoes Kleijn, G. A., et al. 2003, ApJS, 148, 419
Noeske, K. G., Papaderos, P., Cairós, L. M., & Fricke, K. J. 2003, A&A, 410, 481
Noordermeer, E., van der Hulst, J. M., Sancisi, R., Swaters, R. S., & van Albada, T. S. 2007, MNRAS, 276, 1513
Norman, C. A., May, A., & van Albada, T. S. 1985, ApJ, 296, 20
Nowak, N., Saglia, R. P., Thomas, J., et al. 2008, MNRAS, 391, 1629
Nowak, N., Saglia, R. P., Thomas, J., et al. 2007, MNRAS, 379, 909
Nowak, N., Thomas, J., Erwin, P., et al. 2010, MNRAS, 403, 646
Noyola, E., Gebhardt, K., & Bergmann, M. 2008, ApJ, 676, 1008
Noyola, E., Gebhardt, K., Kissler-Patig, M., et al. 2010, ApJ, 719, L60
Oegerle, W. R., & Hoessel, J. G. 1991, ApJ, 375, 15
Oliva, E., Origlia, L., Kotilainen, J. K., & Moorwood, A. F. W. 1995, A&A, 301, 55
Olsen, K. P., Rasmussen, J., Toft, S., & Zirm, A. W. 2013, ApJ, 764, 4
Onken, C. A., Ferrarese, L., Merritt, D., et al. 2004, ApJ, 615, 645
Onken, C. A., Valluri, M., Peterson, B. M., et al. 2007, ApJ, 670, 105
Oser, L., Naab, T., Ostriker, J. P., & Johansson, P. H. 2012, ApJ, 744, 63
Oser, L., Ostriker, J. P., Naab, T., Johansson, P. H., & Burkert, A. 2010, ApJ, 725, 2312
Ostriker, J. P., & Ciotti, L. 2005, Phil. Trans. R. Soc. London, 363, A667
O'Sullivan, E., Forbes, D. A., & Ponman, T. J. 2001, MNRAS, 328, 461
Park, D., Woo, J.-H., Treu, T., et al. 2012, ApJ, 747, 30
Pastorini, G., Marconi, A., Capetti, A., et al. 2007, A&A, 469, 405
Paturel, G., Fang, Y., Petit, C., Garnier, R., & Rousseau, J. 2000, A&AS, 146, 19
Paturel, G., Petit, C., Prugniel, Ph., et al. 2003, A&A, 412, 45
Peebles, P. J. E. 1972, ApJ, 178, 371
Peiris, H. V., & Tremaine, S. 2003, ApJ, 599, 237

Peletier, R. F., Davies, R. L., Illingworth, G. D., Davis, L. E., & Cawson, M. 1990, AJ, 100, 1091
Pellegrini, S. 1999, A&A, 351, 487
Pellegrini, S. 2005, MNRAS, 364, 169
Peng, C. Y. 2007, ApJ, 671, 1098
Peng, C. Y., Impey, C. D., Ho, L. C., Barton, E. J., & Rix, H.-W. 2006a, ApJ, 640, 114
Peng, C. Y., Impey, C. D., Rix, H.-W., et al. 2006b, ApJ, 649, 616
Peng, E. W., Jordán, A., Côté, P., et al. 2006c, ApJ, 639, 95
Peng, E. W., Jordán, A., Côté, P., et al. 2008, ApJ, 681, 197
Peterson, B. M. 2008, NewAR, 52, 240
Peterson, B. M., Bentz, M. C., Desroches, L.-B., et al. 2005, ApJ, 632, 799; Erratum. 2005, ApJ, 641, 638
Phinney, E. S. 1996, in ASP Conference Series, Vol. 90, The Origins, Evolution, and Destinies of Binary Stars in Clusters, ed. E. F. Milone & J.-C. Mermilliod (San Francisco: ASP), 163
Phinney, E. S., & Kulkarni, S. R. 1994, ARA&A, 32, 591
Pignatelli, E., Salucci, P., & Danese, L. 2001, MNRAS, 320, 124
Pinkney, J., Gebhardt, K., Bender, R., et al. 2003, ApJ, 596, 903
Portinari, L., & Into, T. 2011, in ASP Conference Series, Vol. 445, Why Galaxies Care About AGB Stars II: Shining Examples and Common Inhabitants, ed. F. Kerschbaum, T. Lebzelter, & R.F. Wing (San Francisco: ASP), 403
Pounds, K. A., & Page, K. L. 2006, MNRAS, 372, 1275
Qian, E. E., de Zeeuw, P. T., van der Marel, R. P., & Hunter, C. 1995, MNRAS, 274, 602
Quilis, V., Bower, R. G., & Balogh, M. L. 2001, MNRAS, 328, 1091
Quinlan, G. D., & Hernquist, L. 1997, NewA, 2, 533
Rafferty, D. A., McNamara, B. R., & Nulsen, P. E. J. 2008, ApJ, 687, 899
Rafferty, D. A., McNamara, B. R., Nulsen, P. E. J., & Wise, M. W. 2006, ApJ, 652, 216
Ransom, S. M., Hessels, J. W. T., Stairs, I. H., et al. 2005, Science, 307, 892
Ravindranath, S., Ho, L. C., & Filippenko, A. V. 2002, ApJ, 566, 801
Read, J. I., & Trentham, N. 2005, Phil. Trans. R. Soc. London, A363, 2693
Reddick, R. M., Wechsler, R. H., Tinker, J. L., & Behroozi, P. S. 2012, arXiv:1207.2160
Rees, M. J. 1984, ARA&A, 22, 471
Rees, M. J., & Ostriker, J. P. 1977, MNRAS, 179, 541
Reeves, J. N., O'Brien, P. T., Braito, V., et al. 2009, ApJ, 701, 493
Reid, M. J., Braatz, J. A., Condon, J. J., et al. 2009, ApJ, 695, 287
Reines, A. E, & Deller, A. T. 2012, ApJ, 750, L24
Reines, A. E., Sivakoff, G. R., Johnson, K. E., & Brogan, C. L. 2011, Nature, 470, 66
Renzini, A. 1999, in The Formation of Galactic Bulges, ed. C. M. Carollo, H. C. Ferguson, & R. F. G. Wyse (Cambridge: Cambridge Univ. Press), 9
Rhode, K. L. 2012, AJ, 144, 154
Richstone, D., Ajhar, E. A., Bender, R., et al. 1998, Nature, 395, A14
Richstone, D., Bower, G., & Dressler, A. 1990, ApJ, 353, 118
Richstone, D., Gebhardt, K., Aller, M., et al. 2004, arXiv:astro-ph/0403257
Richstone, D. O., & Tremaine, S. 1984, ApJ, 286, 27
Richstone, D. O., & Tremaine, S. 1985, ApJ, 296, 370
Richstone, D. O., & Tremaine, S. 1988, ApJ, 327, 82
Ridgway, S. E., Heckman, T. M., Calzetti, D., & Lehnert, M. 2001, ApJ, 550, 122
Riechers, D. A., Walter, F., Brewer, B. J., et al. 2008, ApJ, 686, 851
Rigopoulou, D., Spoon, H. W. W., Genzel, R., Lutz, D., Moorwood, A. F. M., & Tran, Q. D. 1999, AJ, 118, 2625
Rix, H.-W. 1993, in IAU Symposium 153, Galactic Bulges, ed. H. Dejonghe, & H. J. Habing (Dordrecht: Kluwer), 423
Rix, H.-W., Kennicutt, R. C., Braun, R., & Walterbos, R. A. M. 1995, ApJ, 438, 155
Roberts, T. P. 2007, ApSS, 311, 203
Rossa, J., van der Marel, R. P., Böker, T., et al. 2006, AJ, 132, 1074
Rothberg, B., & Joseph, R. D. 2004, AJ, 128, 2098

Rothberg, B., & Joseph, R. D. 2006, AJ, 131, 185
Rupke, D. S., & Veilleux, S. 2011, ApJ, 729, L27
Rusli, S. P., Thomas, J., Erwin, P., et al. 2011, MNRAS, 410, 1223
Rusli, S. P., Thomas, J., Saglia, R. P., et al. 2013, preprint
Ryden, B. S., & Gunn, J. E. 1987, ApJ, 318, 15
Sadoun, R., & Colin, J. 2012, MNRAS, 426, L51
Saglia, R. P, Bender, R., & Dressler, A. 1993, A&A, 279, 75
Sales, L. V., Navarro, J. F., Theuns, T., et al. 2012, MNRA, 423, 1544
Salpeter, E. E. 1964, ApJ, 140, 796
Salviander, S., Shields, G. A., Gebhardt, K., & Bonning, E. W. 2007, ApJ, 662, 131
Samurović, S., & Danziger, I. J. 2005, MNRAS, 363, 769
Sánchez-Portal, M., Díaz, ''A., Terlevich, E., & Terlevich, R. 2004, MNRAS, 350, 1087
Sancisi, R., & van Albada T. S. 1987, in IAU Symposium 117, Dark Matter in the Universe, ed. J. Kormendy & G. R. Knapp (Dordrecht: Reidel), 67
Sandage, A. 1961, The Hubble Atlas of Galaxies (Washington: Carnegie Institution of Washington)
Sandage, A., & Bedke, J. 1994, The Carnegie Atlas of Galaxies (Washington, DC: Carnegie Institution of Washington)
Sandage, A., & Binggeli, B. 1984, AJ, 89, 919
Sandage, A., Binggeli, B., & Tammann, G. A. 1985, AJ, 90, 1759
Sandage, A., Freeman, K. C., & Stokes, N. R. 1970, ApJ, 160, 831
Sandage, A., & Tammann, G. A. 1981, A Revised Shapley-Ames Catalog of Bright Galaxies (Washington: Carnegie Institution of Washington)
Sanders, D. B. 1999, Ap&SS, 266, 331
Sanders, D. B., & Mirabel, I. F. 1996, ARA&A, 34, 749
Sanders, D. B., Soifer, B. T., Elias, J. H., et al. 1988a, ApJ, 325, 74
Sanders, D. B., Soifer, B. T., Elias, J. H., Neugebauer, G., & Matthews, K. 1988b, ApJ, 328, L35
Sani, E., Marconi, A., Hunt, L. K., & Risaliti, G. 2011, MNRAS, 413, 1479
Sargent, W. L. W., Young, P. J., Boksenberg, A., Shortridge, K., Lynds, C. R., & Hartwick, F. D. A. 1978, ApJ, 221, 731
Sarria, J. E., Maiolino, R., La Franca, F., et al. 2010, A&A, 522, L3
Sarzi, M., Rix, H.-W., Shields, J. C., et al. 2001, ApJ, 550, 65
Sarzi, M., Rix, H.-W., Shields, J. C., et al. 2002, ApJ, 567, 237
Satyapal, S., Böker, T., Mcalpine, W., et al. 2009, ApJ, 704, 439
Satyapal, S., Vega, D., Dudik, R. P., Abel, N. P., & Heckman, T. 2008, ApJ, 677, 926
Satyapal, S., Vega, D., Heckman, T., O'Halloran, B., & Dudik, R. 2007, ApJ, 663, L9
Schawinski, K. 2012, in 2011 Frank N. Bash Symposium, New Horizons in Astronomy, ed. S. Salviander, J. Green, & A. Pawlik, Proc. Sci., **http://pos.sissa.it/cgi-bin/reader/conf.cgi?confid=149**
Schawinski, K., Dowlin, N., Thomas, D., Urry, C. M., & Edmondson, E. 2010, ApJ, 714, L108
Schawinski, K., Simmons, B. D., Urry, C. M., Treister, E., & Glikman, E. 2012, MNRAS, 425, L61
Schawinski, K., Thomas, D., Sarzi, M., et al. 2007, MNRAS, 382, 1415
Schawinski, K., Treister, E., Urry, C. M., et al. 2011, ApJ, 727, L31
Schawinski, K., Virani, S., Simmons, B., et al. 2009, ApJ, 692, L19
Schechter, P. 1976, ApJ, 203, 297
Schlafly, E. F., & Finkbeiner, D. P. 2011, ApJ, 737, 103
Schlegel, D. J., Finkbeiner, D. P., & Davis, M. 1998, ApJ, 500, 525
Schmidt, M. 1959, ApJ, 129, 243
Schmidt, M. 1963, Nature, 197, 1040
Schödel, R., Merritt, D., & Eckart, A. 2009, A&A, 502, 91
Schödel, R., Ott, T., Genzel, R., et al. 2002, Nature, 419, 694
Schramm, M., & Silverman, J. D. 2013, ApJ, 767, 13
Schulze, A., & Gebhardt, K. 2011, ApJ, 729, 21
Schulze, A., & Wisotzki, L. 2011, A&A, 535, A87
Schunck, F. E., & Mielke, E. W. 2003, Classical and Quantum Gravity, 20, 301

Schwarzschild, M. 1979, ApJ, 232, 236
Schwarzschild, M. 1993, ApJ, 409, 563
Schweizer, F. 1990, in Dynamics and Interactions of Galaxies, ed. R. Wielen (New York: Springer), 60
Schweizer, F. 1998, in 26th Advanced Course of the Swiss Society of Astronomy and Astrophysics, Galaxies: Interactions and Induced Star Formation, ed. D. Friedli, L. Martinet, & D. Pfenniger (New York: Springer), 105
Scorza, C., & Bender, R. 1995, A&A, 293, 20
Scott, N., & Graham, A. W. 2013, ApJ, 763, 76
Secrest, N., Satyapal, S., Gliozzi, M., et al. 2012, ApJ, 753, 38
Seigar, M. S., Barth, A. J., & Bullock, J. S. 2008, MNRAS, 389, 1911
Sellgren, K., McGinn, M. T., Becklin, E. E., & Hall, D. N. B. 1990, ApJ, 359, 112
Sérsic, J. L. 1968, Atlas de Galaxias Australes (Córdoba: Obs. Astron. Univ. Nacional de Córdoba)
Seth, A. C., Agüeros, M., Lee, D., & Basu-Zych, A. 2008, ApJ, 678, 116
Seth, A. C., Cappellari, M., Neumayer, N., et al. 2010, ApJ, 714, 713
Seyfert, C. K. 1943, ApJ, 97, 28
Shapiro, K. L., Cappellari, M., de Zeeuw, T., et al. 2006, MNRAS, 370, 559
Shen, J., & Gebhardt, K. 2010, ApJ, 711, 484
Shen, J., Rich, R. M., Kormendy, J., et al. 2010, ApJ, 720, L72
Shen, J., Vanden Berk, D. E., Schneider, D. P., & Hall, P. B. 2008, AJ, 135, 928
Shen, Y., & Kelly, B. C. 2010, ApJ, 713, 41
Shi, Y., Rieke, G. H., Ogle, P., Jiang, L., & Diamond-Stanic, A. M. 2009, ApJ, 703, 1107
Shields, G. A., Gebhardt, K., Salviander, S., et al. 2003, ApJ, 583, 124
Shields, G. A., Menezes, K. L., Massart, C. A., & Vanden Bout, P. 2006, ApJ, 641, 683
Shields, J. C., Böker, T., Ho, L. C., et al. 2012, AJ, 144, 12
Shields, J. C., Rix, H.-W., Sarzi, M., et al. 2007, ApJ, 654, 125
Shields, J. C., Walcher, C. J., Böker, T., et al. 2008, ApJ, 682, 104
Shih, D. C., Iwasawa, K., & Fabian, A. C. 2003, MNRAS, 341, 973
Shostak, G. S. 1987, A&A, 175, 4
Shu, F., Najita, J., Ostriker, E., et al. 1994, ApJ, 429, 781
Shu, F. H., Najita, J., Ostriker, E. C., & Shang, H. 1995, ApJ, 455, L155
Sijacki, D., & Springel, V. 2006, MNRAS, 366, 397
Sijacki, D., Springel, V., Di Matteo, T., & Hernquist, L. 2007, MNRAS, 380, 877
Sikora, M., Stawarz, L., & Lasota, J.-P. 2007, ApJ, 658, 815
Silge, J. D., Gebhardt, K., Bergmann, M., & Richstone, D. 2005, AJ, 130, 406
Silk, J., & Mamon, G. A. 2012, Res. Astron. Ap., 12, 917
Silk, J., & Rees, M. J. 1998, A&A, 331, L1
Simien, F., & Prugniel, Ph. 2000, A&AS, 145, 263
Simien, F., & Prugniel, P. 2002, å, 384, 371
Simpson, J. M., Smail, I., Swinbank, A. M., et al. 2012, MNRAS, 426, 3201
Siopis, C., Gebhardt, K., Lauer, T. R., et al. 2009, ApJ, 693, 946
Skrutskie, M. F., Cutrie, R. M., Stiening, R., et al. 2006, AJ, 131, 1163
Snyder, G. F., Hopkins, P. F., & Hernquist, L. 2011, ApJ, 728, L24
Sollima, A., Bellazzini, M., Smart, R. L., et al. 2009, MNRAS, 396, 2183
Sołtan, A. 1982, MNRAS, 200, 115
Somerville, R. S., Hopkins, P. F., Cox, T. J., Robertson, R. E., & Hernquist, L. 2008, MNRAS, 391, 481
Spitler, L. R., Forbes, D. A., Strader, J., Brodie, J. P., & Gallagher, J. S. 2008, MNRAS, 385, 361
Springel, V., Di Matteo, T., & Hernquist, L. 2005a, MNRAS, 361, 776
Springel, V., & Hernquist, L. 2005, ApJ, 622, L9 (see arXiv:astro-ph/041379)
Springel, V., White, S. D. M., Jenkins, A., et al. 2005b, Nature, 435, 629
Steinmetz, M., & Navarro, J. F. 2002, NewA, 7, 155
Strader, J., Brodie, J. P. , Spitler, L., & Beasley, M. A. 2006, AJ, 132, 2333
Strader, J., Chomiuk, L., Maccarone, T. J., Miller-Jones, J. C. A., & Seth, A. C. 2012a, Nature, 490, 71
Strader, J., Chomiuk, L., Maccarone, T. J., et al. 2012b, ApJ, 750, L27

Strateva, I. V., Ivezić, Ž., Knapp, G. R., et al. 2001, AJ, 122, 1861
Sturm, E., González-Alfonso, E., Veilleux, S., et al. 2011, ApJ, 733, L16
Szebehely, V., & Peters, C. F. 1967, AJ, 72, 876
Szomoru, D., Franx, M., & van Dokkum, P. G. 2012, ApJ, 749, 121
Tacconi, L. J., Genzel, R., Lutz, D., et al. 2002, ApJ, 580, 73
Tacconi, L. J., Genzel, R., Neri, R., et al. 2010, Nature, 463, 781
Tacconi, L. J., Genzel, R., Smail, I., et al. 2008, ApJ, 680, 246
Tadhunter, C., Marconi, A., Axon, D., et al. 2003, MNRAS, 342, 861
Tanaka, Y., Nandra, K., Fabian, A. C., et al. 1995, Nature, 375, 659
Targett, T. A., Dunlop, J. S., & McLure, R. J. 2012, MNRAS, 420, 3621
Tempel, E., Tamm, A., & Tenjes, P. 2010, A&A, 509, A91
Terashima, Y., Kamizasa, N., Awaki, H., Kubota, A., & Ueda, Y. 2012, ApJ, 752, 154
Terlevich, E., Díaz, A. I., & Terlevich, R. 1990, MNRAS, 242, 271
Thomas, D., Greggio, L., & Bender , R. 1999, MNRAS, 302, 537
Thomas, D., Maraston, C., Bender, R., & Mendes de Oliveira, C. 2005, ApJ, 621, 673
Thomas, J. 2010, arXiv:1007.3591
Thomas, J., Saglia, R. P., Bender, R., et al. 2004, MNRAS, 353, 391
Thomsen, B., Baum, W. A., Hammergren, M., & Worthey, G. 1997, ApJ, 483, L37
Thornton, C. E., Barth, A. J., Ho, L. C., & Greene, J. E. 2009, ApJ, 705, 1196
Thornton, C. E., Barth, A. J., Ho, L. C., Rutledge, R. E., & Greene, J. E. 2008, ApJ, 686, 892
Thornton, R. J., Stockton, A., & Ridgway, S. E. 1999, AJ, 118, 1461
Tombesi, F., Cappi, M., Reeves, J. N., & Braito, V. 2012, MNRAS, 422, L1
Tonry, J. L. 1984, ApJ, 283, L27
Tonry, J. L. 1987, ApJ, 322, 632
Tonry, J. L., Dressler, A., Blakeslee, J. P., et al. 2001, ApJ, 546, 681
Toomre, A. 1977, in The Evolution of Galaxies and Stellar Populations, ed. B. M. Tinsley & R. B. Larson (New Haven: Yale University Observatory), 401
Toomre, A., & Toomre, J. 1972, ApJ, 178, 623
Torres, D. F., Capozziello, S., & Lambiase, G. 2000, Phys. Rev. D, 62, 10012
Treister, E., Natarajan, P., Sanders, D. B., et al. 2010, Science, 328, 600
Treister, E., Schawinski, K., Urry, C. M., & Simmons, B. D. 2012, ApJ, 758, L39
Tremaine, S. 1995, AJ, 110, 628
Tremaine, S. 1997, in Unsolved Problems in Astrophysics, ed. J. N. Bahcall & J. P. Ostriker (Princeton: Princeton University Press), 137
Tremaine, S, Gebhardt, K., Bender, R., et al. 2002, ApJ, 574, 740
Tremaine, S., Richstone, D. O., Byun, Y.-I., et al. 1994, AJ, 107, 634
Tremblay, B., & Merritt, D. 1996, AJ, 111, 2243
Tremonti, C. A., Moustakas, J., & Diamond-Stanic, A. M. 2007, ApJ, 663, L77
Treu, T., Malkan, M. A., & Blandford, R. D. 2004, ApJ, 615, L97
Trujillo, I., Conselice, C. J., Bundy, K., et al. 2007, MNRAS, 382, 109
Trujillo, I., Förster Schreiber, N. M., Rudnick, G., et al. 2006, ApJ, 650, 18
Turner, M. L., Côté, P., Ferrarese, L., et al. 2012, ApJS, 203, 5
Ulvestad, J. S., Greene, J. E., & Ho, L. C. 2007, ApJ, 661, L151
Urrutia, T., Lacy, M., & Becker, R. H. 2008, ApJ, 674, 80
Valluri, M., Ferrarese, L., Merritt, D., & Joseph, C. L. 2005, ApJ, 628, 137
Valluri, M., Merritt, D., & Emsellem, E. 2004, ApJ, 602, 66
van Albada, G. D. 1980, A&A, 90, 123
van Albada, T. S., & Sancisi, R. 1986, Phil. Trans. R. Soc. London A, 320, 447
van den Bergh, S., Li, W., & Filippenko, A. V. 2002, PASP, 113, 820
van den Bosch, R. C. E., & de Zeeuw, P. T. 2010, MNRAS, 401, 1770
van den Bosch, R. C. E., Gebhardt, K., Gültekin, K., et al. 2012, Nature, 491, 729
van den Bosch, R. C. E., van de Ven, G., Verolme, E. K., & de Zeeuw, P. T. 2008, MNRAS, 385, 647
van der Kruit, P. C., & Freeman, K. C. 2010, ARA&A, 49, 301

van der Kruit, P. C., Oort, J. H., & Mathewson, D. S. 1972, A&A, 21, 169
van der Marel, R. P. 1994a, MNRAS, 270, 271
van der Marel, R. P. 1994b, ApJ, 432, L91
van der Marel, R. P. 1995, Highlights of Astronomy, 10, 527
van der Marel, R. P. 2004, in Carnegie Observatories Astrophysics Series, Vol. 1: Coevolution of Black Holes and Galaxies, ed. L. C. Ho (Cambridge: Cambridge Univ. Press), 37
van der Marel, R. P., & Anderson, J. 2010, ApJ, 710, 1063
van der Marel, R. P., Cretton, N., de Zeeuw, P. T., & Rix, H.-W. 1998, ApJ, 493, 613
van der Marel, R. P., de Zeeuw, P. T., & Rix, H.-W. 1997a, ApJ, 488, 119
van der Marel, R. P., de Zeeuw, P. T., Rix, H.-W., & Quinlan, G. D. 1997b, Nature, 385, 610
van der Marel, R. P., Evans, N. W., Rix, H.-W., White, S. D. M., & de Zeeuw, T. 1994a, MNRAS, 271, 99
van der Marel, R. P., Gerssen, J., Guhathakurta, P., Peterson, R. C., & Gebhardt, K. 2002, AJ, 124, 3255
van der Marel, R. P., Rix, H.-W., Carter, D., et al. . 1994b, MNRAS, 268, 521
van der Marel, R. P., & van den Bosch, F. C. 1998, AJ, 116, 2220
van de Ven, G., van den Bosch, R. C. E., Verolme, E. K., & de Zeeuw, P. T. 2006, A&A, 445, 513
van Dokkum, P. G., Franx, M., Kriek, M., et al. 2008, ApJ, 677, L5
van Dokkum, P. G., Whitaker, K. E., Brammer, G., et al. 2010, ApJ, 709, 1018
van Driel, W., & van Woerden, H. 1991, A&A, 243, 71
Veilleux, S., Kim, D.-C., Peng, C. Y., et al. 2006, ApJ, 643, 707
Verdoes Kleijn, G. A., van der Marel, R. P., Carollo, C. M., & de Zeeuw, P. T. 2000, AJ, 120, 1221
Verdoes Kleijn, G. A., van der Marel, R. P., de Zeeuw, P. T., Noel-Storr, J., & Baum, S. A. 2002, AJ, 124, 2524
Verdoes Kleijn, G. A., van der Marel, R. P., & Noel-Storr, J. 2006, AJ, 131, 1961
Verolme E. K., Cappellari M., Copin Y., et al. 2002, MNRAS, 335, 517
Vika, M., Driver, S. P., Cameron, E., Kelvin, L., & Robotham, A. 2012, MNRAS, 419, 2264
Volonteri, M. 2010, A&AR, 18, 279
Volonteri, M., & Ciotti, L. 2013, ApJ, 768, 29
Volonteri, M., Haardt, F., & Madau, P. 2003, ApJ, 582, 559
Volonteri, M., & Natarajan, P. 2009, MNRAS, 400, 1911
Volonteri, M., & Rees, M. J. 2005, ApJ, 633, 624
Walcher, C. J., van der Marel, R. P., McLaughlin, D., et al. 2005, ApJ, 618, 237
Walsh, J. L., Barth, A. J., & Sarzi, M. 2010, ApJ, 721, 762
Walsh, J. L., van den Bosch, R. C. E., Barth, A. J., & Sarzi, M. 2012, ApJ, 753, 79
Walter, F., Carilli, C., Bertoldi, F., et al. 2004, ApJ, 615, L17
Walterbos, R. A. M., & Kennicutt, R. C. 1987, A&AS, 69, 311
Wang, L., & Jing, Y. P. 2010, MNRAS, 402, 1796
Wang, L., & Wheeler, J. C. 2008, ARA&A, 46, 433
Wang, R., Carilli, C. L., Neri, R., et al. 2010, ApJ, 714, 699
Watson, W. D., & Wallin, B. K. 1994, ApJ, 432, L35
Wehner, E. H., & Harris, W. E. 2006, ApJ, 644, L17
Weiland, J. L., Arendt, R. G., Berriman, G. B., et al. 1994, ApJ, 425, L81
Weiner, B. J., Coil, A. L., Prochaska, J. X., et al. 2009, AJ, 692, 187
Weinzirl, T., Jogee, S., Khochfar, S., Burkert, A., & Kormendy, J. 2009, ApJ, 696, 411
Weller, J., Ostriker, J. P., Bode, P., & Shaw, L. 2005, MNRAS, 364, 823
Wild, V., Heckman, T., & Charlot, S. 2010, MNRAS, 405, 933
Wild, W., Kauffmann, G., Heckman, T., et al. 2007, MNRAS, 668, 543
Williams, M. J., Bureau, M., & Cappellari, M. 2009, MNRAS, 400, 1665
Wilson, A. S., Braatz, J. A., & Henkel, C. 1995, ApJ, 455, L127
Wirth, A., & Gallagher, J. S. 1984, ApJ, 282, 85
Wold, M., Lacy, M., Käufl, H. U., & Siebenmorgen, R. 2006, A&A, 460, 449
Wolf, J., Martinez, G. D., Bullock, J. S., et al. 2010, MNRAS, 406, 1220
Woo, J.-H., Treu, T., Malkan, M. A., & Blandford, R. D. 2006, ApJ, 645, 900
Woo, J.-H., Treu, T., Malkan, M. A., & Blandford, R. D. 2008, ApJ, 681, 925

Worthey, G., Faber, S. M., & Gonzalez, J. J. 1992, ApJ, 398, 69
Wrobel, J. M., Greene, J. E., & Ho, L. C. 2011, AJ, 142, 113
Wrobel, J. M., & Ho, L. C. 2006, ApJ, 646, L95
Wyithe, J. S. B. 2006a, MNRAS, 365, 1082
Wyithe, J. S. B. 2006b, MNRAS, 371, 1536
Xia, X. Y., Gao, Y., Hao, C.-N., et al. 2012, ApJ, 750, 92
Xiao, T., Barth, A. J., Greene, J. E., et al. 2011, ApJ, 739, 28
Xue, Y. Q., Brandt, W. N., Luo, B., et al. 2010, ApJ, 720, 368
Yamauchi, A., Nakai, N., Ishihara, Y., Diamond, P., & Sato, N. 2012, PASJ, 64, 103
Yang, X., Mo, H. J., & van den Bosch, F. C. 2009, ApJ, 695, 900
Yang, X., Mo, H. J., van den Bosch, F. C., Zhang, Y., & Han, J. 2012, ApJ, 752, 41
Yang, Y., Li, B., Wilson, A. S., & Reynolds, C. S. 2007, ApJ, 660, 1106
Yelda, S., Ghez, A. M., Lu, J. R., et al. 2011, in The Galactic Center: A Window to the Nuclear Environment of Disk Galaxies, ed. M. R. Morris, Q. D. Wang, & F. Yuan (San Francisco: ASP), 167
Yoon, S.-J., Lee, S.-Y., Blakeslee, J. P., et al. 2011, ApJ, 743, 150
Young, P. J. 1980, ApJ, 242, 1232
Young, P. J., Westphal, J. A., Kristian, J., Wilson, C. P., & Landauer, F. P. 1978, ApJ, 221, 721
Yu, Q. 2002, MNRAS, 331, 935
Yu, Q, & Tremaine, S. 2002, MNRAS, 335, 965
Zel'dovich, Ya. B. 1964, Soviet Physics – Doklady, 9, 195
Zepf, S. E., & Ashman, K. M. 1993, MNRAS, 264, 611
Zhang W. M., Soria R., Zhang S. N., Swartz D. A, & Liu J. 2009, ApJ, 699, 281
Zheng, Z., Coil, A. L., & Zehavi, I. 2007, ApJ, 667, 760